The properties of mixed crystals of zinc-cadmium-sulphide(Zn(_x)Cd(_1-x)S)

Saidin, Mohamad Khairi B.

THE PROPERTIES OF MIXED CRYSTALS OF ZINC-CADMIUM-SULPHIDE

($Zn_xCd_{1-x}S$)

by

MOHAMAD KHAIRI B. SAIDIN

(GRADUATE SOCIETY)

Presented in candidature for the degree of

Doctor of Philosophy

in the

University of Durham

March 1987

For Abdullah, God loves you more than we do.

ACKNOWLEDGEMENTS

I would like to express my gratitude to my supervisor, Prof. J.Woods for his continuous guidence and encouragement throughout the course of the research and writting up of this thesis. I am particularly indebted to Dr. G.J.Russell for his help in use of the SEM and proof reading this thesis thoroughly and setting it up to rights.

I would like to thank Professor G.G.Robert for the use of the departmental facilities, and the workshop staff headed by Mr.F.Spence for their skill and advices.

I also wish to thank Dr. A.W.Brinkman and other members of the group who render me their help during the course of this work in one way or another.

I also owe a special thank to Norman Thompson for the growth of the crystals and technical assistance, and to Allen Thomas for the help at the begining of the work.

Help from Mr.R.Coult of Chemistry Department for composition analysis and technical assistance from Ron Hardy of Geology Department are fully acknowledge.

The financial support and study leave provided by Universiti Teknologi Malaysia, Jalan Gurney, Kuala Lumpur is greatfully acknowledge.

Finally, special thanks to my parents, my wife, Rusmidah and my daughter, Haryani for their understanding and support.

ABSTRACT

CdS and ZnS are two binary compounds of II-VI semiconductors which form a continuous series of solid-solutions throughout the whole range of composition ($Zn_xCd_{1-x}S$). The main purpose of the work reported in this thesis was to characterise some electrical properties of $Zn_xCd_{1-x}S$ crystals grown in the department.

Atomic Absorption Spectroscopy (AAS) was used to determine the actual composition of the solid solutions to compare with Energy Dispersive Analysis by X-Ray (EDAX) measurements. A calibration curve of ratio intensity versus composition can then be used to estimate the composition of $Zn_xCd_{1-x}S$ non-destructively. From the X-Ray diffraction studies, all $Zn_xCd_{1-x}S$ crystals with $x \leqslant 0.85$ were found to have the hexagonal, wurtzite form while ZnS crystals have the cubic, zinc blende phase.

Conductivity and Hall coefficient measurements were also carried out. At 300K, conductivities up to about $1x10^{-3}$ $ohm^{-1}cm^{-1}$ could be achieved for composition up to $x=0.45$. The Hall mobility was found to decrease drastically at $x=0.2$. Scattering due to a combination of polar optical and piezoelectric processes was thought to

control the carrier mobility for crystals with $x<0.2$. With $x>0.2$, scattering due to ionised impurities, space charge or alloy processes is probably more important.

The barrier heights of Au-$Zn_xCd_{1-x}S$ ($x<0.5$) Schottky diodes were calculated from forward I-V characteristics, C-V and photoelectric measurements were also carried out. A quite linear relationship with composition was observed for barrier heights measured by photoelectric method. Barrier heights calculated by the other methods was very much dependent on the nature of the barrier.

From steady state photocapacitance studies, a level situated at about 1.1-1.2eV above the valence band is the dominant feature for copper doped samples and crystals grown by the Piper-Polich method. This centre was pinned to the valence band. A second deep centre situated at about 1.4-1.5eV below the conduction band was also observed in some samples and was pinned to the conduction band. The existence of this centre is thought to depend very much on the history of the individual sample.

CONTENTS

CHAPTER I

INTRODUCTION TO II-VI COMPOUNDS

1.1 Introduction

II-VI compounds are compounds formed by reaction of elements of groups II and VI of the periodic table. Among them are the sulphides, selenides and tellurides of zinc, cadmium and mercury. Due to the variety of uses of these compounds, they have been and still are the subject of much intensive investigation, along with elemental semiconductor and III-V compounds. For a better understanding of their properties, it is important that good quality single crystals of high purity should be readily available. Some of the important aspects of the crystal growth of these compounds are to control the stoichiometry, native defects and introduction of impurities. As far as electrical and optical properties are concerned, differences in growth technique will produce crystals with different properties. In fact, the presence of native defects and certain impurities give these materials their interesting properties.

Apart from the binary compounds, such as CdS, ZnS, ZnSe etc., there are at least 10 ternary compounds which can be made from this group of materials, for example $Zn_xCd_{1-x}S$, ZnS_ySe_{1-y} etc. which are miscible with each

other (1). Work on these ternary compounds is very interesting because varying the composition is a natural way of tuning the parameters of the material, for example to achieve the required lattice parameter, band gap or electron affinity for particular applications.

Because of the various uses of ternary compounds, much work on these materials has been done throughout the world. On the whole, the dependence of band gap (E_g) on composition is the only property to have been investigated in any depth, but the experimental results are not in good agreement since both linear and non-linear dependences of band gap on composition are reported. The non-linear dependences reported follow a quadratic relationship described by a bowing parameter b (1) as follows:-

$$E_g(x) = xE_gAC + (1-x)E_gBC - x(1-x)b \qquad 1.1$$

where E_gAC is the energy gap of the binary compound AC and E_gBC the energy gap of the binary compound BC in $A_xB_{1-x}C$. An analogous relationship holds for mixed anion compounds, of the type MF_yG_{1-y}, so that

$$E_g(y) = yE_gMF + (1-y)E_gMG - y(1-y)b \qquad 1.2$$

Some of the reported experimental values of these parameters are given in table 1.1.

Compound	b	Band Gap range(eV)
$Zn_xCd_{1-x}S$	0.61	2.42-3.66
$Zn_xCd_{1-x}Te$	0.20	1.58-2.25
ZnS_ySe_{1-y}	0.41	2.67-3.66
ZnS_yTe_{1-y}	3.0	2.25-3.66
$ZnSe_yTe_{1-y}$	1.27	2.25-2.67
CdS_ySe_{1-y}	0.31	1.73-2.42
CdS_yTe_{1-y}	1.7	1.58-2.42
$CdSe_yTe_{1-y}$	0.85	1.58-1.73

Table 1.1. Bowing parameter b of some II-VI ternary compounds(1).

1.2 Structure

Almost all II-VI compounds (MX), crystallise in either the zinc blende or the wurtzite structure (3). In some compounds, for example ZnS, the structure is dependent on the growth temperature. The wurtzite structure (figure 1.1b) consists of two interpenetrating hexagonal lattices displaced with respect to one other by a distance of 3c/8 along the c axis. The nearest neighbour distance, with ideal tetrahedral sites is 3c/8 for the hexagonal crystal. The zinc blende structure is derived from the diamond structure and it composed of two interpenetrating face centred cubic lattices translated with respect to each other by 1/4 of the body diagonal of the unit cell (figure 1.1a). In this case the nearest neighbour distance is $\sqrt{3}/4$ a where a is the lattice parameter for cubic structure.

There is a close relationship between the wurtzite and zinc blende structures. The lattice parameters of the hexagonal unit cell are almost exactly related to the cubic parameter of the same compound by:-

$$a_{hex} = \frac{1\sqrt{2}}{2} a_{cub} \quad \text{and} \quad c_{hex} = \frac{2\sqrt{3}}{3} a_{cub} \qquad 1.3$$

A quite useful description for the structural relations is based on the stacking sequence along the lowest indices for polar directions i.e <0001> and <111>. For the zinc blende structure the sequence along this

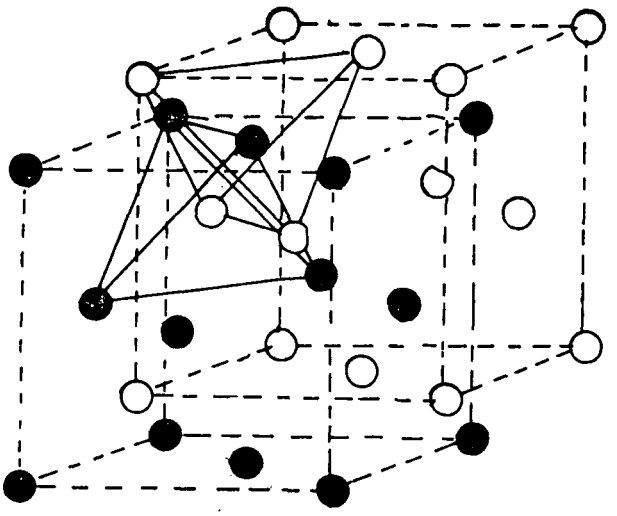

(a)

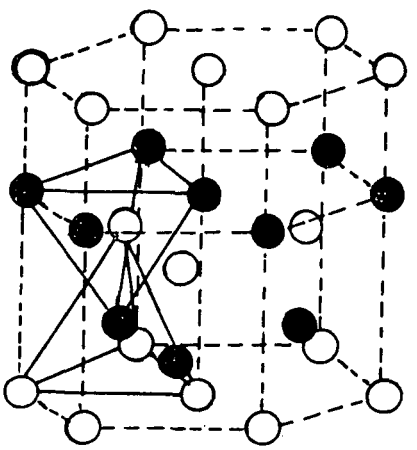

(b)

Figure 1.1. a) The zinc blende structure and b) The wurtzite structure.

direction is of the form

$$A\alpha B\beta C\gamma A\alpha B\beta C\gamma A\alpha$$

where A, B, C and α, β, γ represent the metal (M) and non-metal (X) of the compound layers respectively. Using the same notation, the stacking of atomic layers in the wurtzite structure is of the form

$$A\alpha B\beta A\alpha B\beta A\alpha B\beta A\alpha$$

The stacking sequence of the closed-packed planes in wurtzite is different from that in zinc blende in that the positions of atoms are repeated after every double atomic layer instead of after every two double atomic layers.

1.3 Scope of The Present Study

The work described in this thesis is concerned with the properties of ternary crystals of $Zn_xCd_{1-x}S$ grown in Durham. The crystals grown were all n-type material as in the previous work of Oktik (2).

The earlier work on $Zn_xCd_{1-x}S$ solid solutions is described in the next chapter. Some applications and problems related to these materials are also discussed in that chapter. In chapter III, the theoretical background to the work is presented, and this is followed by the

experimental chapter which includes the methods of growing the crystals and the preparation of samples. The results on the structural and compositional studies are given in chapter V. Chapter VI is concerned with the measurements of electrical conductivity and Hall effect in order to evaluate the transport properties of the mixed crystals and their variation with composition. Chapter VII is devoted to measurements made on Au-$Zn_xCd_{1-x}S$ Schottky diodes, particularly of barrier heights determined in three different ways. Measurements of steady state photocapacitance (PHCAP), and infra red quenching of photocapacitance (IRQPHCAP) on as-grown and intentionally copper doped samples are discussed in chapter VIII.

Finally, chapter IX provides a summary of the results obtained in this study.

Reference for chapter I

1) H.Hartmann, R.Mach and B.Selle, **Current Topics in Material Science**, (North Holland Publ., 1982) edited by E.Kaldis.

2) S.Oktik, **PhD Thesis**, Durham University, 1982.

3) B.Ray, **II-VI Compounds**, (Pergamon Press, 1969)

CHAPTER II

PROPERTIES OF $Zn_xCd_{1-x}S$ SOLID SOLUTIONS

2.1 Introduction

In this chapter, the properties of $Zn_xCd_{1-x}S$ solid solutions are discussed. The preparation, growth and structure of the solid solutions are described in section 2.2. This is followed by an account of their electrical properties in section 2.3. The optical properties of the solid solutions are discussed in section 2.4, and some applications and related problems are discussed in section 2.5.

2.2 Preparation, Growth and Structure.

Crystals of CdS, ZnS and $Zn_xCd_{1-x}S$ are frequently grown from the vapour phase because of the large dissociation pressure developed near the stoichiometric melting points which makes growth from the melt experimentally more difficult (1). Nevertheless single crystals of ZnS (2), CdS (3) and $Zn_xCd_{1-x}S$ (4) have been obtained by controlled cooling from the melt but very expensive, high temperature, high pressure equipment is required. In this department, the vapour phase technique originally developed here to grow crystals of CdS (7) has been successfully used by Oktik et al (8) to grow single

crystals of $Zn_xCd_{1-x}S$ for compositions with $x<0.4$. The details of the growth arrangements will be given in chapter 4 section 2. The growth of single crystals of $Zn_xCd_{1-x}S$ was first carried out by Vitrikhovskii and Mizetskaya (5). They synthesised the compounds directly from zinc, cadmium and sulfur heated in separate closed quartz boats. It was claimed that the composition of invidual crystals with a mean dimension of 15x1.5x0.04 mm^3 was uniform. The structure of the crystals was hexagonal and the lattice constants were found to increase monotonically with increasing concentration of cadmium sulfide.

Using chemical transport with iodine as the transporting agent, Cherin et al (6) grew single crystals of $Zn_xCd_{1-x}S$ over the entire range of x. The crystals had a uniform composition and were relatively free from strain. The crystals had a hexagonal structure, although at x=0.95, a cubic component was detected. The variation of the lattice parameters with composition was found to follow Vegard´s law (linear relation).

In earlier times, thin films of $Zn_xCd_{1-x}S$ were prepared by vacuum evaporation by Kane et al (9). CdS and ZnS powders placed in two separate boats were heated simultaneously to produce films with uniform composition over the whole range of x. The structure of the films was found to be hexagonal up to x=0.6, and the transition from hexagonal to cubic took place between x=0.6 and x=0.85.

Films with $x>0.85$ were of the cubic form. Among other work on thin films produced by vacuum evaporation (11, 12, 13, 14), Vankar et al (11) studied the dependence of the crystallographic structure on depositional conditions in some detail. They found that the lattice parameter exhibited a strong dependence on the temperature of deposition.

Another method which has been used quite extensively to prepare films of $Zn_xCd_{1-x}S$ is the spray-pyrolysis technique (15-19). Generally, this method involves spraying suitable solution mixtures on to heated substrates. The solution used combinations of $ZnCl_2$, $CdCl_2$ and thiourea, according to the chemical composition required:

$$(1-x)CdCl_2 + xZnCl_2 + CS(NH_2)_2 + 2H_2O \longrightarrow$$

$$Zn_xCd_{1-x}S + 2NH_4Cl + CO_2$$

A quite detailed study of the structure of films produced by the spray technique has been made by Banerjee et al (16). The crystallographic structure does not depend upon the deposition temperature as in vacuum evaporated films. The films were normally produced on glass substrates at deposition temperatures which varied from 250-400^{o}C. Their structure was found to be hexagonal for $x<0.6$ and the transition to cubic occurred at $0.6<x<0.8$. Films with

$x>0.8$ were cubic. According to recent work by Duchemin et al (20), the structure of their sprayed films was more dependent on the type of substrate used rather than the zinc content. With higher zinc content ($x>0.05$), degradation of the crystallinity of the layers was observed with the formation of cracks.

Another method of producing solid solutions of $Zn_xCd_{1-x}S$ by epitaxial growth of $Zn_xCd_{1-x}S$ on ZnS substrates has been described by Sakurai et al (21). This method made use of zinc diffusion from the substrate during the deposition of CdS by sublimation. The CdS vapour was transported to the substrate in a stream of argon while the substrate (ZnS) temperature was varied between $800^{o}C$ and $950^{o}C$. The temperature of the evaporation zone was held at $1100^{o}C$. From an x-ray examination, they were able to show that the grown layers were single crystalline but no details of the structure were given. Using this technique, single crystal layers of $Zn_xCd_{1-x}S$ with $0<x<0.3$ could be obtained. With large x ($x>0.3$), the zinc component had to be added externally into the layers during the growth.

Powders of $Zn_xCd_{1-x}S$ doped with various activators such as copper, etc., have been studied for a long time past. A comprehensive review of the early work on phosphors can be found in the book by Leverenz (37). Phosphors of $Zn_xCd_{1-x}S$ were normally prepared by mixing the binary CdS and ZnS powders in the desired ratio.

Copper was added as an aqueous solution of $Cu(C_2H_3O_2)_2$, and the halogens Cl, Br, I as the Zn or Cd halide dissolved in water. The resulting slurries were stirred to ensure uniformity and dried. The samples were then fired in small capped quartz tubes in argon or H_2S or in evacuated and sealed quartz tubes (38,39).

Uchida (35) also prepared phosphors of $Zn_xCd_{1-x}S$ by mixing the binary CdS and ZnS powders in a sealed evacuated quartz tube which was then heated at 950°C for five hours. X-ray analysis indicated that the samples produced had the hexagonal structure over the entire range of composition.

2.3 Electrical Properties

As far as we are aware, not much work has been done on the electrical properties of solid solutions of $Zn_xCd_{1-x}S$. With their single crystals, Vitrikhovskii and Mizetskaya (5) reported that the electrical resistivity of all their samples varied between 10^{10} and 10^{13} ohm-cm but no compositional dependence of resistivity was given. A more detailed study by Davis and Lind (22) on single crystals grown by the iodine transport technique showed that the dark conductivity of their crystals was about 0.01 $ohm^{-1}cm^{-1}$ in the range of lower x ($x<0.15$). The incorporation of about 15% zinc into CdS reduced this dark conductivity by a little over one order of magnitude, but

over the next 5-10% increase in zinc content, the dark conductivity decreased by about 7-8 orders of magnitude, in spite of the fact that a similar concentration of iodine donors was probably present in all the crystals. From 25-60% zinc, the dark conductivity was about 10^{-10} $ohm^{-1}cm^{-1}$. A further decrease of about three orders of magnitude was observed when 60-100% zinc was added. From Hall effect studies, it was concluded that the conduction was n-type and that the mobility did not vary significantly with temperature. The increase in resistivity as the zinc content was increased was explained by the fact that the shallow donor ionization energy of 0.03eV, normally found in halogen doped CdS, increased to about 0.32eV in $Zn_xCd_{1-x}S$ at x=0.2. Using thermally stimulated current measurements, Davis and Lind also detected two dominant traps with energies below the conduction band which varied monotonically with composition.

In contrast, Oktik et al (8) grew single crystals from the vapour phase, and showed that the conductivity of their as-grown crystals at room temperature ranged from 0.5 to 2.0 $ohm^{-1}cm^{-1}$ for $0<x<0.4$ and was independent of illumination. This high conductivity was associated with a non-stiochiometric excess of the metallic component.

Using a spray pyrolysis technique, Fiegelson et al (15) showed that the resistivity of their films was a very strong function of composition, x. They divided their

observations into three catagories: 1) With $0<x<0.1$ the resistivity was relatively independent of x. 2) With $0.1<x<0.2$ a rapid rise in resistivity was observed. 3) With $0.2<x<1$ the resistivity increased exponentially with x. Using the same technique Banerjee et al (16), showed that the resistivity of their films could be decreased by annealing them at about $300^{o}C$ for 30 minutes in vacuum. This treatment was found to be effective for films with a low zinc content (maximum for $x=0$) and neglible for $x>0.8$.

Low resistivity $Zn_xCd_{1-x}S$ films have been reported by Romeo et al (14) but unfortunately no other details of measurements of their electrical properties have been given. They showed that at $x=0.3$, the resistivity is still limited at 2 ohm-cm and as x further increased, the resistivity increased exponentially. The Hall mobility for films with $0<x<0.3$ varied between 100 and 20 $cm^2V^{-1}s^{-1}$.

By using thermoelectric power measurements, Chynoweth and Bube (17) showed that the electron density decreased exponentially with x in their as-deposited films. The electron mobility was also found to decrease as x increased. Heat tretment in hydrogen at $300^{o}C$ for about 10 minutes was effective in reducing the resistivity and a value of $4.0x10^2$ ohm-cm was obtained for $x=0.35$.

Domens et al (23) showed that, the plane resistivity of their films produced by thermal evaporation

increased slightly with x for $x<0.1$, and then drastically for $x>0.15$. The Hall mobility also decreased dramatically but the electron density determined by three independent methods increased with x initially and tended to saturate for $x>0.1$.

Using films of two different thicknesses (2.2μm and 4.5μm), Kwok et al (32) demonstrated that the carrier density increased with increasing zinc concentration initially, but the trend reversed beyond a certain zinc concentration. The inflection point was different for the two types of film. For the thinner one, it occurred at about $x=0.05$ and in the thicker film, it occurred at $x=0.35$.

Electrical measurements of epitaxial layers of $Zn_xCd_{1-x}S$ on ZnS grown by Sakurai et al (21) showed that the resistivity was around 1 ohm-cm for layers with $x<0.25$. With $x>0.4$ the resistivity increased to 10^5 ohm-cm. The carrier concentration increased as x increased but the trend was reversed at about $x=0.15$. The Hall mobility varied from sample to sample and was independent of the composition. Generally the mobility was less then 60 $cm^2V^{-1}s^{-1}$ but a maximum value of 190 $cm^2V^{-1}s^{-1}$ was observed in one sample.

2.4 Optical Properties

Photoconductivity measurements by Vitrikhovskii and

Mizetskaya (5) on single crystals of $Zn_xCd_{1-x}S$ showed that the peak in the spectral response of the photoconductivity shifted gradually towards higher photon energy with increasing x. The band gap estimated by observing the spectral peak of photoconductivity was found to increase monotonically as x increased.

Work by Ballentyne and Ray (24) on the electroluminescent and photoluminescent properties of $Zn_xCd_{1-x}S$ crystals showed that alloys containing 0.1% of copper were strongly electroluminescent for compositions with a high concentration of zinc ($0.8<x<1$), while in photoluminescence, emission in the visible region occurred when $0.4<x<1$.

By observing the peak of photoconductivity, Davis and Lind (22) also found that the band gap increased monotonically with x (from ~ 2.4eV at x=0 to~3.7eV at x=1). A decrease in photoconductivity as x increased was also reported. From measurements of the infra red quenching of photoconductivity, the energy position of the sensitizing centre which is observed in CdS and ZnS was found to be almost invariant with composition at about 1.1eV above the valence band.

Oktik et al (8) and Das et al (33) working on Cu_2S-$Zn_xCd_{1-x}S$ photovoltaic cells showed that the photon energy of the photothreshold increased with the zinc

content (the photothreshold was measured by observing the photoresponse at long wavelengths).

From their DLTS studies on Schottky diodes, Pande et al (25) revealed that the ionisation energy of the 0.45eV electron trap in CdS increased monotonically with composition up to a value of 0.58eV at x=0.2. The trap appeared to be pinned to the valence band. From a photocapacitance study of their Cu_2S-$Zn_{0.2}Cd_{0.8}S$ heterojunctions, Pande et al (25) also claimed to have found a new recombination centre at 1.27eV above the valence band, which was formed during junction preparation. It was suggested that this centre led a reduction in the short circuit current in the devices. More work on space charge spectroscopic techniques (such as ODLTS and DLOS) applied to Au-$Zn_xCd_{1-x}S$ Schottky diodes was carried out by Claybourn (34).

The optical properties of $Zn_xCd_{1-x}S$ films were first reported by Kane et al (9), who determined the energy gap from transmission measurements and found a linear dependence on composition. The photoconductivity of such films has also been reported by Banerjee et al (16) who showed that the photoconductivity decreased as x increased. The photoconductivity was also found to depend on the temperature of deposition. A decrease in photosensitivity as x increased was also reported by Domens et al (23). They also showed that the band gap determined

by means of spectral variation of the optical absorption coefficient increased with x but not linearly.

The photoluminescence at 77K investigated by Sakurai et al (21) showed two emission lines, which were associated with excitons varying from blue-green to near ultra violet depending on the composition, while the self activated luminescence varied from red to blue depending on the composition.

The optical properties of powdered $Zn_xCd_{1-x}S$ were first studied a long time ago. Cathodluminescence of these materials showed that the single blue emission band in ZnS is displaced gradually towards longer wavelengths on increasing the proportion of CdS until the infra-red emitting band at 100% CdS (37) is reached.

Emission spectra of $Zn_xCd_{1-x}S$ phosphors activated by Cu, Cl (38) and Ag, Cl (39) showed that copper produces two emission bands in ZnS and that both bands known as the blue and the green shift monotonically to lower energy as x decreases. Silver activated phosphors showed a gradual shift of the blue emission band of ZnS:Ag as x decreased towards the red and into the near infrared at x=0.

Work on powdered $Zn_xCd_{1-x}S$ by means of a photoluminescence study with different coactivators has been reported by Uchida (35). Determination of the band gap

energy from transmission curves showed that the linear relationship was obeyed.

2.5 Applications and Problems

The use of $Zn_xCd_{1-x}S$ phosphors in CRT screens in black & white tv, colour tv, radar and viewing oscilloscopes is well established (37).

A major advantage of $Zn_xCd_{1-x}S$ solid solutions in these and other opto-electronic applications is that the direct band gap varies from 2.4eV at x=0 to 3.7eV at x=1, ranging therefore from the visible spectrum to the ultra violet. Some of the required parameters for particular applications can be changed by simply varying the composition of the solid solutions. Before this can be done effectively, complete charactarisation of electrical and optical properties should obviously be established and thoroughly understood.

$Zn_xCd_{1-x}S$ has been used as a window material for thin film heterojunction solar cells, see for example reference 14. A heterojunction is required because $Zn_xCd_{1-x}S$ cannot be made p-type. The variation of band gap meets the requirement that a suitable collector should allow a maximum fraction of the solar radiation to be transmitted. Furthermore $Zn_xCd_{1-x}S$ can be produced quite cheaply in thin film form. Apart from this, the

resistivity of the film should be low, in order to limit series resistance losses and to shift the junction field region into the absorber material. Efforts to reduce the resistivity of $Zn_xCd_{1-x}S$ have dominated most of the work and still form a major part of continuing studies (14, 15, 17, 18).

In heterojunction fabrication on n-$Zn_xCd_{1-x}S$, a wide range of p-type materials, to form the absorber can be used, provided that they have low resistivity. There are two important parameters, namely lattice constant and electron affinity which have to be considered:

1) The two materials to be joined to form the heterojunction should have a minimum lattice mismatach to avoid the presence of surface states at the interface. The thermal expansion coefficients should also be as equal as possible to avoid strain-induced interfacial defects, and to allow high temperature processing. With $Zn_xCd_{1-x}S$, the option to vary the lattice constant from CdS to ZnS provides a wide choice for the p-type material.

2) The other feature is that differences in electron affinity of the two materials, can result in additional barriers for the minority carrier flow across the junction, and these should avoided.

Photovoltaic cells of Cu_2S-CdS have been

investigated for quite a long time past. With the present technology, the conversion efficiency of thin film cells is estimated to be about 10% (26). This is thought to be limited by a difference in electron affinities of some 0.2eV and in lattice "a" constant of about 4.5%. The open circuit voltage which is limited to about 0.5 V in the CdS-Cu_2S cells can be increased to about 0.85 V in the absence of such mismatches (27).

The use of $Zn_xCd_{1-x}S$ to achieve better matching of lattice constant and electron affinity was first suggested by Palz et al (10). Unfortunately, matching of the lattice constant and electron affinity does not occur at the same value of x. According to theoretical predictions by Boer (28), a good match with the Cu_2S lattice parameter occurs at $x \sim 0.46$ but this is not the case for the electron affinity. Up to now there is no data available regarding the variation of electron affinity with composition, but it is generally assumed that this parameter decreases as the zinc content is increased (29). The measurements of photothreshold by Oktik et al (8) and Das et al (33), show that (8) the difference of 0.2eV between electron affinity of Cu_2S and CdS is eliminated when the zinc content is increased at about $x \sim 0.2$. An efficiency in excess of 10% has been obtained in thin film Cu_2S-$Zn_xCd_{1-x}S$ cells by Hall et al (30), but in practice it has proved difficult to obtain a sufficiently large short circuit current.

GaAs has also been used as an absorber (31). At x~0.44, a lattice mismatch can be avoided but a difference in the electron affinities of about 0.17eV occurs at this composition. With x~0.18, an effiency of 6.2% has been obtained under AM1 illumination. Romeo et al (36) reported that an efficiency up to 7% can be achieved using p-$CuGa_yIn_{1-y}Se_2$/n-$Zn_xCd_{1-x}S$ (y=0.5, x=0.29).

$Zn_xCd_{1-x}S$ has also proved useful in other opto-electronic applications for example as a photoresistor, a photoconductive detector and in ac and dc electroluminescent thin film displays (31). As far as light emitting diodes (L.E.D) are concerned, high hopes were raised and much effort was put in II-VI compounds. Red, orange and green L.E.D's are commercially available with GaP and $GaAs_xP_{1-x}$, blue emission is almost lacking and this is where ZnS, ZnSe, $Zn_xCd_{1-x}S$ and ZnS_ySe_{1-y} might come into their own. Again, the problems of reducing the resistivity of these materials have to be solved first before p-n junctions, MS or MIS devices can be fabricated on them.

References for chapter II

1) B.Ray, **II-VI Compounds.** (Pergamon Press, 1969)

2) A.Addiamino and M.Aven, J. Appl. Phys., **31** (1960) 736

3) M.E.Medcalf and R.H. Fahrig, J. Electrochem. Soc., **105** (1958) 719

4) M.J.Kozislski, J. Cryst. Growth, **30** (1975) 86

5) N.I.Vitrikhovskii and I.B.Mizetskaya, Soviet Phys., Solid-state, **2** (1961) 2301

6) P.Cherin, E.L.Lind and E.A.Davis, J. Electrochem. Soc., **117** (1970) 233

7) L.Clark and J.Woods, J. Cryst. Growth, **3/4** (1968) 126

8) S.Oktik, G.J.Russell and J.Woods, J. Cryst. Growth, **59** (1982) 414

9) W.M.Kane, J.P.Spratt, L.W.Hershinger and I.H.Khan, J. Electrochem. Soc., **113** (1966) 137

10) W.Palz, J.Besson, T.Nguyen Duy and J.Vedel, **10th. Photovoltaic Specialists Conf.**, Palo Alto, Callifornia Nov. 1973, IEEE, New York, p. 69

11) V.D.Vankar, R.S.Das, P.Nath and K.L.Chopra, Phys. stat. sol(a)., **45** (1978) 665

12) G.Gordillo, Solar Cells, **14** (1985) 219

13) J.Kimmerle, R.Menner, H.W.Shock and A.Valera,Thin Solid Films, **126** (1985) 23

14) N.Romeo, G.Sberveglieri and L.Taricone, Appl. Phys. Lett., **32** (1978) 807

15) R.S.Fiegelson, A.N.Diaye, S.Y.Yin and R.H.Bube, J. Appl Phys., **48** (1977) 3126

16) A.Banerjee, P.Nath, V.D.Vankar and K.L.Chopra, Phys. stat. sol(a)., **46** (1978) 723

17) T.A.Chynoweth and R.H.Bube, J. Appl. Phys., **51**(1980) 1844

18) H.L.Kwok and Y.C.Chau, Thin Solid Films, **66** (1980) 303

19) V.P.Singh and J.F.Jordan, IEEE Elec. Dev. Lett., **EDL-2** (1981) 137

20) S.Duchemin, M.Kaka, J.Bougnot and M.Cadene, Thin Solid Films, **136** (1986) 289

21) Y.Sakurai, Y.Kokubun, H.Watanabe and M.Wada, Jpn. J. Appl. Phys., **16** (1977) 1455

22) E.A.Davis and E.L.Lind, J. Phys. Chem. Sol., **29** (1968) 79

23) P.Domens, M.Cadene, G.W.C.Solal, S.Martinuzzi and C. Brouty, Phys. stat. sol(a), **59** (1980) 201

24) D.G.W.Ballentyne and B.Ray, Physica, **27** (1961) 337

25) P.C.Pande, M.Claybourn, G.J.Russell, A.W.Brinkman and J.Woods, J. Cryst. Growth, 72 (1985) 174

26) A.M.Barnett and A.Rothwarf, IEEE Trans. Elec. Dev., **ED-27** (1980) 615

27) J.A.Bragagnolo, A.M.Barnett, J.E.Phillips, R.B.Hall, A. Rothwarf and J.D.Meakin, IEEE Trans. Elec. Dev., **27** (1980) 645

28) K.W.Boer, J. Appl. Phys., **50** (1979) 5356

29) L.C.Burton, Solar Cells, (1979/80) 159

30) R.B.Hall, R.W.Birkmire, J.E.Meakin, Appl. Phys. Lett., **38** (1981) 925

31) H.Hartmann, R.Mach and B.Selle, **Current Topics in Mat-**

erial Science, (North Holland Publ. 1982), ed E.Kaldis

32) H.H.L.Kwok, M.Y.Leung and Y.W.Lam, J. Cryst. Growth, **59** (1982) 421

33) R.S.Das, A.Banerjee and K.L.Chopra, Sol. St. Elec., **22** (1979) 533

34) M.Claybourn, **PhD Thesis**, Durham University 1985

35) W.Uchida, Phys. stat. sol(a)., **80** (1983) K199

36) N.Romeo, V.Canevari, G.Sberveglie, C.Paorici and L. Zanotti, Phys. stat. sol(a), **60** (1980) K95

37) H.W.Leverenz, **An Introduction to Luminescence of Solid**, (Dover Publ. Inc. New York 1950)

38) W.Lehmann, J. Electrochem. Soc., **113** (1966) 449

39) W.Lehmann, J. Electrochem. Soc., **113** (1966) 788

CHAPTER III

BACKGROUND THEORY

3.1 Introduction

In this chapter, the background theory used in analysing the results obtained in this study are reviewed.

3.2 Introduction to Semiconductors

3.2.1 Intrinsic and extrinsic semiconductors

In semiconductors, only the upper levels of the valence band and the lower levels of the conduction band and the levels existing between them are of importance. The diagram in figure 3.1 represents an intrinsic semiconductor with energy gap E_g. The density of free electrons in the conduction band, n is given by:-

$$n = \int_{E=E_c}^{E_{cT}} S(E)F(E)dE \qquad 3.1$$

where S(E) is the density of available electron states in the conduction band. Close to the bottom of the conduction band, the density of states is given by:-

$$S(E) = \left[\frac{4\pi}{h^3}\right](2m^*_e)^{3/2}(E-E_c)^{1/2} \qquad 3.2$$

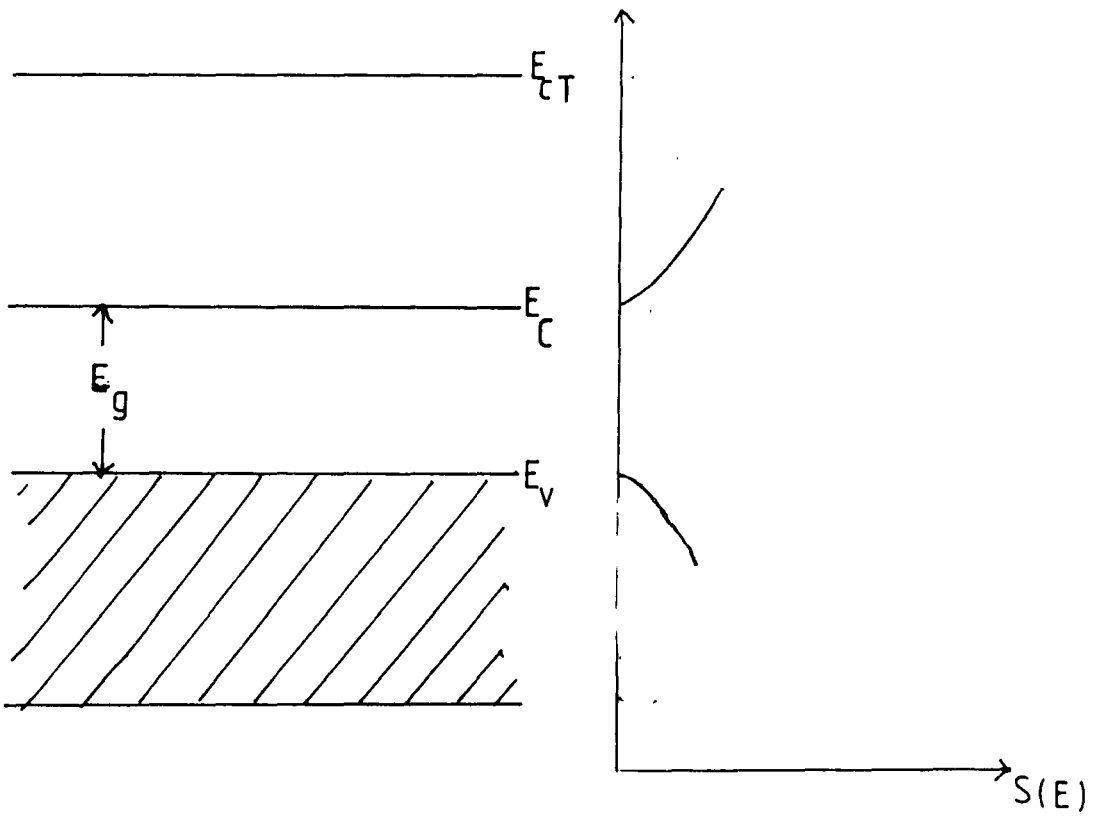

Figure 3.1. Energy band diagram of an intrinsic semiconductor.
E_{CT} is the energy at the top of conduction band

where m^*_e is the effective mass of the electrons and h is Planck's constant. F(E) is the Fermi-Dirac function which determines the probability of a state being filled by an electron,

$$F(E) = \frac{1}{\exp(E-E_f)/kT + 1} \qquad 3.3$$

where k is Boltzmann's constant and E_f is the characteristic Fermi energy. For $(E-E_f)>>kT$, the classical statistical mechanical distribution function of Maxwell and Boltzmann can be used since the exponential term in the denominator of the above equation is large compared with unity and equation 3.3 takes the approximate form of

$$F(E) = \exp\{-(E-E_f)/kT\} \qquad 3.4$$

This function, falls off very rapidly with energy, so the upper limit of integration in 3.1 can be replaced by ∞. Substituting 3.2 and 3.4 in equation 3.1 gives the number of electrons in the conduction band.

$$n = \left[\frac{4\pi}{h^3}\right] (2m^*_e)^{3/2} \int_{E=E_c}^{\infty} \frac{(E-E_c)^{1/2}}{\exp(E-E_f)/kT}\, dE \qquad \text{and}$$

when the integral is evaluated, it is found that

$$n = 2\left[\frac{2\pi m^*_e kT}{h^2}\right]^{3/2} \exp-(E_c-E_f)/kT \qquad 3.5$$

or

$$n_{,} = N_c \exp-(E_c - E_f)/kT$$

where N_c , the effective density of states in the conduction band is

$$N_c = 2\left[\frac{2\bar{\iota}m^*_e kT}{h^2}\right]^{3/2} \qquad 3.6$$

Since F(E) describes the fraction of states occupied by electrons then {1-F(E)} describes the fraction occupied by holes, and then a similar approach can be carried out, to give

$$n_h = 2\left[\frac{2\pi m^*_h kT}{h^2}\right]^{3/2} \exp-(E_f - E_v)/kT$$

and

$$N_v = 2\left[\frac{2\pi m^*_h kT}{h^2}\right]^{3/2} \qquad 3.7$$

Since $n = n_h$ in an intrinsic semiconductor, the equation for the Fermi level can be obtained from 3.5 and 3.7

$$E_f = \left[\frac{E_c + E_v}{2}\right] + \frac{3}{4} kT \log_e\left[\frac{m^*_h}{m^*_e}\right] \qquad 3.8$$

For an extrinsic semiconductor with impurity levels in the band gap, with both donors (N_d) and acceptors (N_a) present, the situation will be more complex. For the compensated case $N_d > N_a$, assuming that all the acceptor

levels are completely filled with electrons, and all the donor levels are ionised, the actual number of carriers available for conduction is given by N_d-N_a for n-type material. Thus the density of occupied donor levels, n_d at temperature T is

$$n_d = \text{density of donors x Fermi function}$$

or

$$n_d = N_d\{(1/g)\exp((E_d-E_f)/kT) + 1\}^{-1} \qquad 3.9$$

where g is the degeneracy factor of that particular donor, usually = 2, and E_d is the position of the donor level below the conduction band. At T=0 there must be N_d-N_a electrons in the donor level and at temperature T when there are n electrons per unit volume in conduction band, we must have

$$N_d - N_a = n + N_d\{(1/2)\exp((E_d-E_f)/kT) + 1\}^{-1}$$

rearranging the above equation gives

$$\frac{N_d}{N_d-N_a-n} - 1 = 1/2\ \exp((E_d-E_f)/kT)$$

$$= \frac{\exp(E_d/kT)}{2\exp(E_f/kT)}$$

$$= \frac{1}{2} \frac{\exp((E_c-E_f)/kT)}{\exp((E_c-E_d)/kT)}$$

from 3.6

$$\frac{N_a+n}{N_d-N_a-n} = \frac{N_c}{2n\exp((E_c-E_d)/kT)}$$

or

$$\frac{n(N_a+n)}{N_d-N_a-n} = (N_c/2)\exp-((E_c-E_d)/kT) \qquad 3.10$$

where (E_c-E_d) is also known as the ionization energy of that particular donor.

If we neglect the $T^{3/2}$ dependence of N_c compared with the exponential dependence in equation 3.10, then a plot of log n versus reciprocal temperature gives a straight line with slope of $-(E_c-E_d)/k$.

3.2.2 **Defects and impurity centres**

When the periodicity of the perfect crystal potential is interrupted by some kind of defect such as a native defect or an impurity atom, new energy levels are realised in a localised region of the crystal near the disturbance. These levels usually lie within the forbidden gap of a semiconductor and hence have important effects on crystal properties. Such defects are given a variety of names such as traps, recombination centres, acceptors,

donors etc., but these names do not necessarily reflect a different kind of species existing in the semiconductor. To give a complete picture of a defect energy level, several parameters such as the ionisation energy, density, thermal, and optical capture and emission constants for electrons and holes have to be determined. The most important of these is the ionisation energy and this parameter is used to classify the defects as either shallow or deep levels.

a) **shallow levels**

Defects or impurity levels located near the valence band or conduction band with an ionisation energy comparable with kT (at 300K, kT~0.026eV), are considered to be shallow levels. Since these are normally ionised at room temperature, their presence determines the type of conduction (i.e n or p type) of the semiconductor.

The theory known as the effective mass theory, introduced by Kohn (1) has been successfully applied to many semiconductors to calculate the ionisation energies of shallow levels (2,3,4). According to this model, a hydrogenic system is embedded within the dielectric medium of a crystal, and the coulombic potential V of the ionised atom is considered to be a self-consistent one-electron potential. Because of the relatively large dielectric constants of II-VI compounds, the binding energy between

the ionised impurity atom and the bound electron is much less than in the free hydrogen atom. This indicates that the bound electron is in a large orbit and the wave function describing the electron is spread out over many lattice atoms and therefore only the long range coulombic interactions are effective.

b) **deep levels**

The energy levels which lie further into the band gap are classified as deep levels. They can act either as traps or recombination centres. If the carrier having been captured has a greater probability of being thermally re-excited to the free state than of recombining with a carrier of opposite sign at the imperfection, the centre is a trapping centre or trap. On the other hand, if the captured carrier has a greater probability of recombining, the imperfection is a recombination centre. A large ionisation energy implies a strong potential which acts to localise the carrier wave function near the site of the defect. The system cannot be described by the hydrogenic model. Deep levels in semiconductors are important because they can control the life time of the free carriers (5).

In II-VI compounds, elements such as copper, silver, and gold are well known as luminescence activators. When they occupy zinc or cadmium lattice sites, deep

acceptors are formed . On the other hand elements of group VII such as chlorine, bromine and iodine occupy anion sites (i.e. S,Se); and group III elements like indium, gallium and aluminium occupy cation sites (Cd,Zn) and form relatively deep donors (11).

3.3 Electrical Conductivity and Hall Effect

3.3.1 Introduction

Measurements of both conductivity and Hall coefficient and hence the carrier concentration can provide a great deal of information about a semiconductor. If the measurements are made as a function of temperature, it is possible to determine the ionization energy for the carriers and to some extent to ascertain the carrier scattering mechanisms.

3.3.2 Electrical conductivity

The dark conductivity of a semiconductor is generally defined as:

$$\sigma = nqu_n + pqu_p \qquad 3.11$$

where n and p are the densities of the free electrons and holes, and u_n and u_p are their mobilities respectively. q is the electronic charge. In II-VI semiconductors the

conductivity is normally dominated by one type of carrier, usually electrons (i.e n-type), except for ZnTe and CdTe which are amphoteric, and equation 3.11 reduces to:

$$\sigma = nqu_n \qquad 3.12$$

As far as the temperature dependence of electrical conductivity is concerned, equation (3.12) involves the carrier concentration and their mobility. By recalling equation 3.5, and substituting into equation 3.12 we have

$$\sigma = qu_n N_c \exp -(E_c - E_f)/kT \qquad 3.13$$

which by taking logs reduces to

$$\log \sigma = \log(N_c q u_n) - (E_c - E_f)/kT \qquad 3.14$$

Assuming that m^*_e is a constant (equation 3.6), the effective density of states in the conduction band is proportional to $T^{1.5}$. For acoustic mode lattice scattering, where the mobility is proportional to $T^{-1.5}$, a plot of $\log(\sigma)$ versus reciprocal temperature should then show a straight line with a slope of $-(E_c-E_f)/k$. When the mobility is controlled by impurity scattering ($u \sim T^{+1.5}$), a plot of $\log(\sigma T^{-3})$ versus reciprocal temperature would be expected to yield a straight line with a slope of $-(E_c-E_f)/k$. In both cases, the slope enables the donor activation energy (E_c-E_f) to be evaluated.

To make the electrical conductivity measurements, a rectangular block as shown in figure 3.2 is used. By measuring the voltage between probes 3 and 4, V_x, the conductivity, σ can be obtained by

$$\sigma = \frac{I_x \ell}{V_x bd} \qquad 3.15$$

where I_x is the current in the x-direction.

3.3.3 **Hall Effect**

The same rectangular block samples with an extra two Hall voltage probes (5,6), in figure 3.2 were used for the Hall effect study by applying a magnetic field in the z-direction, B_z, simultaneously with an electric field in x-direction. The magnetic field causes carriers to be deflected horizontally in the y-direction until an electric field E_y is set up which exactly balances the deflecting Lorentz force and an equilibrium state is then reached. Consider, an n-type semiconductor, when the forces on an electron are equated at equilibrium, then

$$B_z q v = E_y q \qquad 3.16$$

where v is the electron drift velocity.

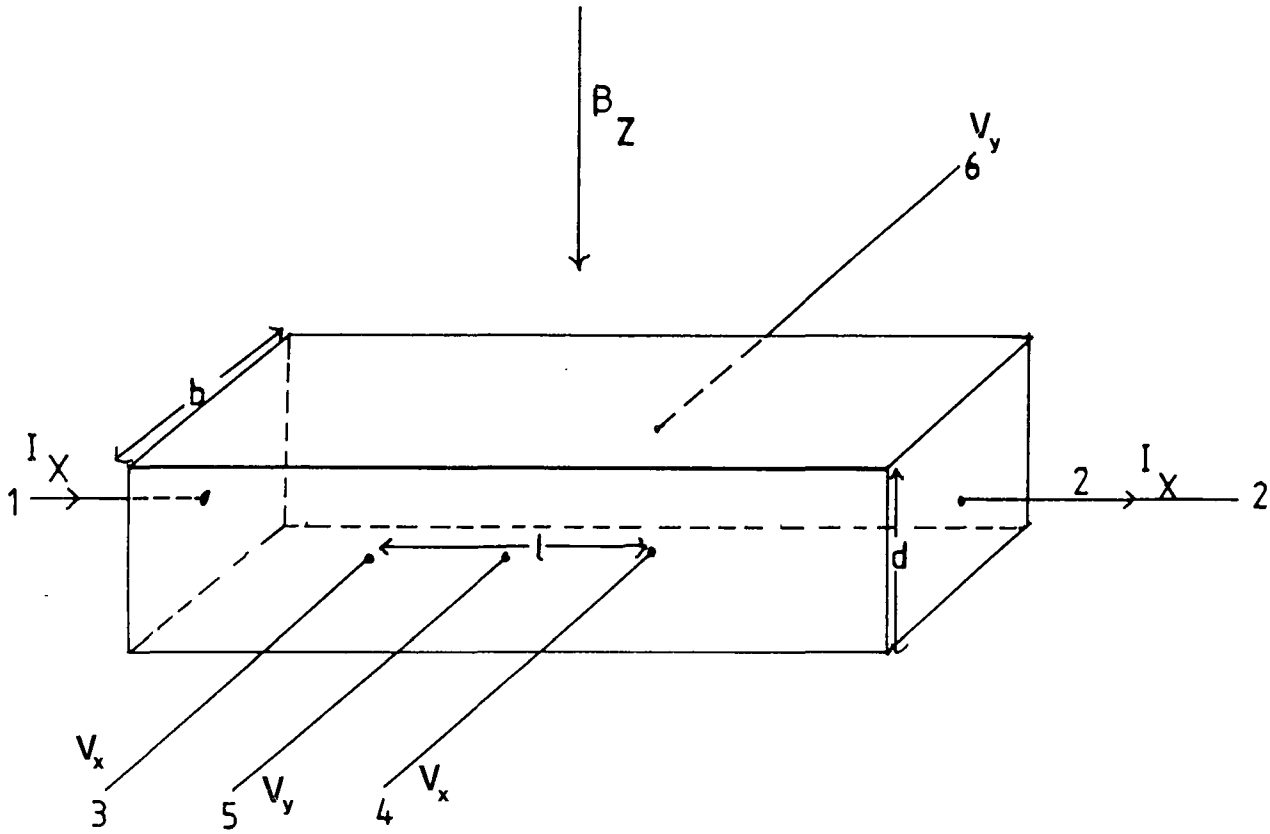

Figure 3.2. Diagrammatic representation of a conductivity and Hall Effect sample.

The current density, J_x is given by

$$J_x = nqv \qquad 3.17$$

and from the two equations (3.16 and 3.17),

$$E_y = \frac{B_z J_x}{nq} \qquad 3.18$$

The Hall coefficient R_H is defined as the ratio of the electric field to the magnetic field per unit current density, i.e,

$$R_H = \frac{E_y}{B_z J_x} = \frac{V_y d}{B_z I_x} \qquad 3.19$$

By comparing 3.18 and 3.19, we get

$$R_H = \frac{1}{nq} \qquad 3.20$$

V_y, the voltage set up between probes 5 and 6 is known as the Hall voltage. Since all others parameters are measurable, R_H and hence carrier concentration (n) can be obtained.

From the equations 3.12 and 3.20,

$$u_H = R_H \sigma \qquad 3.22$$

is called the Hall mobility.

For clover-leaf samples (6,7), 4 ohmic contacts are made at the edge of the sample (see figure 4.3b). If we define the resistance R_{ABCD} to the potential drop across AB perunit current through CD, the resistivity is given by (37):-

$$\rho = \frac{\pi d(R_{ABCD} + R_{BCDA})}{2 \ln 2} \; f\left(\frac{R_{ABCD}}{R_{BCDA}}\right) \qquad 3.23$$

where d is the thickness of the slices and f is the correction function defined by the equation

$$\frac{R_{ABCD} - R_{BCDA}}{R_{ABCD} + R_{BCDA}} = \frac{f}{\ln 2} \text{ arc cosh } \left[\frac{\exp(\ln 2/f)}{2}\right] \qquad 3.24$$

The correction function, f has been shown to follow the approximation (8):-

$$f \sim 1 - \left[\frac{R_{ABCD} - R_{BCDA}}{R_{ABCD} + R_{BCDA}}\right]^2 \ln 2 - \left[\frac{R_{ABCD} - R_{BCDA}}{R_{ABCD} + R_{BCDA}}\right]^4 \left[\frac{(\ln 2)^2}{4} - \frac{(\ln 2)^3}{12}\right] \qquad 3.25$$

shown graphically in figure 3.3.

The Hall mobility is given by

$$u_H = \frac{d \, \Delta R_{DBAC}}{B\rho} \qquad 3.26$$

where the change in resistance R_{BDAC} on application of a

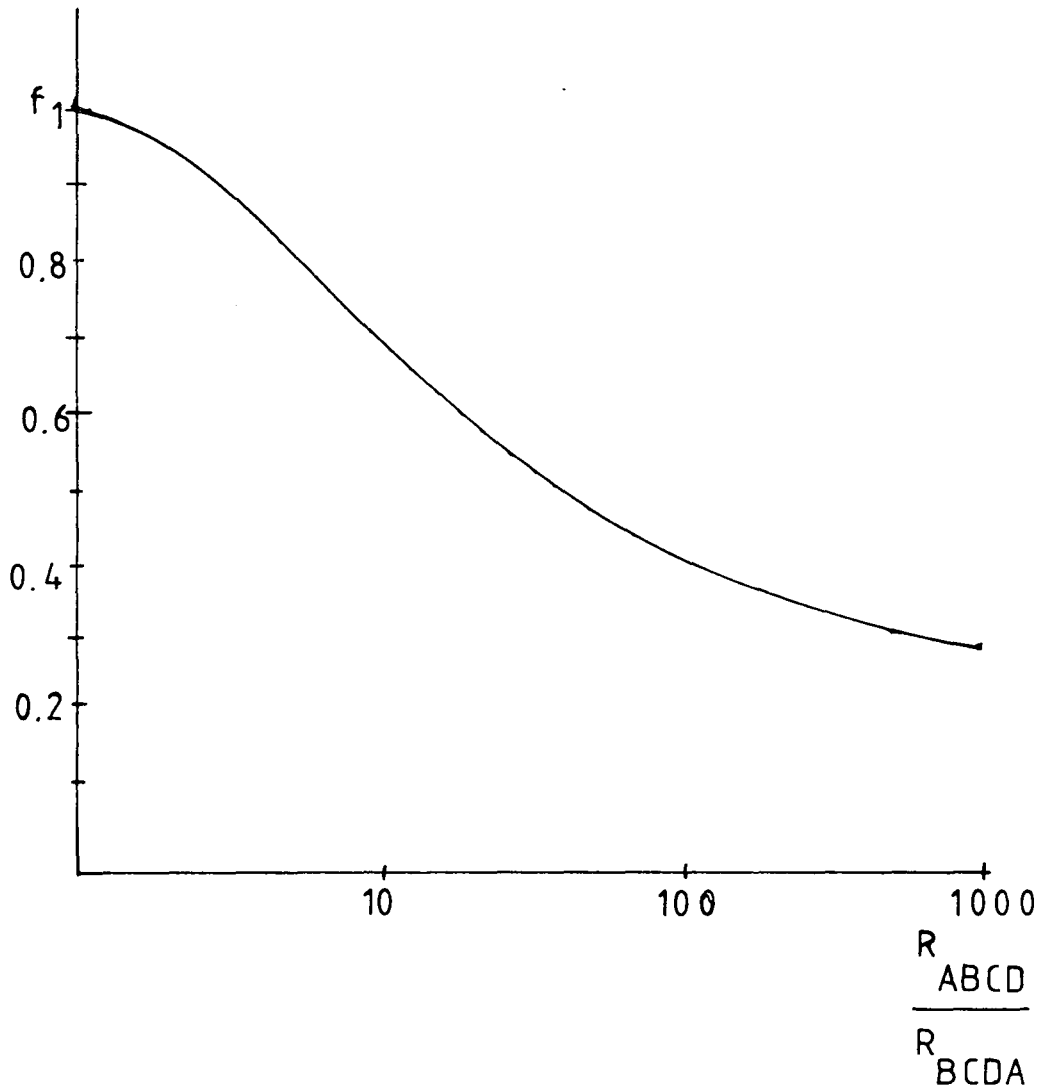

Figure 3.3. Correction function used in calçulation of resistivity in clove-leaf sample.

magnetic field, B is ΔR_{BDAC}. The correction function, according to Allen (8) is correct to four significant figures up to a value of R_{ABCD}/R_{BCDA} of 1.6. Ridpath (9) has shown that at R_{ABCD}/R_{BCDA} = 10, the approximate formula is correct to 5%.

3.3.4 **Carrier mobility**

When a semiconductor is subjected to an electric field E, the additional velocity that the carriers experience is called the drift velocity. If this velocity is small compared to the mean thermal velocity, then

$$v = uE \qquad 3.27$$

where v is the drift velocity and u is a parameter called the drift mobility.

In solids, at high temperatures (> 150K) lattice vibrations and lattice deformation play the dominant role in providing the damping force which prevents unlimited acceleration of an electron and brings it to a steady value. Imperfections due to native defects or substitutional impurities can also dominate the carrier scattering and this normally happens at lower temperatures (i.e < 100K). In heavily doped material, charged impurity scattering may become important at room temperature. Scattering phenomena influence the mean free time, τ ,

between collisions. The mobility is related to the collision time by the equation, $u = q\tau/m^*_e$.

There are several scattering mechanisms which can limit the carrier mobility. A short description follows and only the relevant results will be given here. As stated earlier, carrier mobility in solids is mainly limited by lattice or impurity scattering or perhaps a combination of both.

a) Lattice scattering or electron-phonon interaction

There are three important lattice scattering mechanisms which are optical, deformation potential and piezoelectric scattering.

i) Optical Phonon scattering

Optical phonon scattering is also known as polar optical mode scattering. It is associated with the vibration of two atoms in a unit cell in anti-phase which collectively produces an optical phonon. In compound semiconductors, adjacent atoms are oppositely charged and this allows an electrostatic potential to be associated with an optical phonon. The magnitude of this potential is dependent upon the degrees of ionicity of the bonding and this kind of scattering is therefore important in II-VI

compounds. The effective charges on each ion, and hence the electron-lattice interaction, can be related to the difference between the static and optical dielectric constants. According to Howarth and Sondhemier (10), the strength of the interaction beteween an electron and the optical modes is characterised by a coupling constant α defined by the relation

$$\alpha = \left[\frac{q^2}{\hbar}\right]\left[\frac{m^*_e}{2\hbar w_l}\right]\left[\frac{\epsilon_{s'} - \epsilon_\infty}{\epsilon_{s'}\epsilon_\infty}\right] \qquad 3.29$$

where $\epsilon_{s'}$ and ϵ_∞ are the static and the optical (high frequency) dielectric constants respectively, and $\hbar w_l$ is the energy of the optical mode (L.O) phonon. In non-polar crystals $\epsilon_{s'} - \epsilon_\infty$ is small, and α is small, except for polar crystals where it can assume a value of just less than unity. The expression for the mobility limited by optical mode scattering proposed by Howarth and Sondhemier (10) is

$$u_{OPT} = \left[\frac{1}{2\alpha w_l}\right]\left[\frac{q}{m^*_e}\right]\left[\frac{8}{3\sqrt{\pi}\sqrt{z}}\right]\psi(z)(e^z - 1) \qquad 3.30$$

where z is the ratio of Debye temperature to the lattice temperature (i.e θ_D/T or hw_l/kT), and $\psi(z)$ is a factor, varying as a function of z from 0.6 to 1 over the temperature range involved (11).

ii) Piezoelectric scattering

This mechanism is confined to crystals which lack inversion symmetry. These are usually ionic or partly ionic and so it is also important in II-VI compounds. The interaction arises because acoustic modes generate regions of compression and rarefaction in a crystal. In piezoelectric crystals, this leads to electric fields. All the II-VI compounds are piezoelectric although those with the cubic structure are less than the hexagonal ones. Harrison (12) gives the mobility limited by piezoelectric scattering as

$$u_{PIE} = \frac{0.044\rho C_L^2 \hbar^2 \epsilon_s^2}{qC^2 (m^*_e{}^3 kT)^{1/2}} \qquad 3.31$$

where ρ = density of the semiconductor

C_L = longitudinal acoustic wave velocity, and

C = piezoelectric electrochemical coupling constant

iii) Acoustic phonon scattering

For semiconductors in which the bonding is primarily covalent, electrons are scattered predominantly by longitudinal acoustic (L.A) phonons. These L.A modes produce compressions and dilations which create local deformations in the dielectric constant as well as changes in the width of the band gap. The L.A phonons are the same as those involved in piezoelectric scattering. The

deformation produces a variation in the kinetic energy of an electron as it passes through the crystal and the resultant interaction is known as acoustic phonon scattering. The main parameter involved in this type of scattering is the deformation potential E_1, which gives a measure of the change in position of the conduction band edge due to change in the volume of the unit cell. It is expressed as $-V(dE_c/dV)$. This subject was first introduced by Shockley and Bardeen (13) who proposed the following equation for the mobility limited by acoustic phonons

$$u_A = \left[\frac{8\pi\hbar}{m^*_e{}^5 (kT)^3}\right]^{1/2} \left[\frac{q\hbar^4 \rho C_L{}^2}{3E_1{}^2}\right] \qquad 3.32$$

b) **Impurity scattering**

i) **Ionised impurity scattering**

This type of scattering results from either deliberately introduced impurities or lattice defects generated by non-stoichiometry of the compounds. The defect can be positively or negatively charged and thus deflect the path of a passing electron. Conwell and Weisskopf (14) derived an equation for the mobility limited by this kind of process by following the mathematical arguments used by Rutherford in his model for alpha-particle scattering. However, Brooks and Herring developed an alternative procedure (15) which takes account of screening of the coulomb field of ionised impurities by free electrons.

They proposed the following equation

$$u_I = \left[\frac{2^7(kT)^3}{\pi^3 m^*_e}\right]^{1/2} \frac{\epsilon_s'^2}{q^3 N_i} \left\{\ln\left[\frac{6m^*_e \epsilon_s'(kT)^2}{q^2h^2n'(2-n'/N)}\right]\right\}^{-1} \qquad 3.33$$

for a compensated semiconductor, where $N_i = ZAN_a + ZBN_d$, N_a and N_d being the number of ionised acceptors and donors per unit volume, and ZA and ZB are respective effective charges, n´= number of free carriers per unit volume (i.e n+p) and $N = |N_d - N_a|$

ii) **Neutral impurity scattering**

This type of scattering normally occurs at very low temperature. As the temperature of a semiconductor is lowered, carriers freeze out into impurity centres. The interaction of the electrons with neutral impurities is analogous to electron scattering by hydrogen atoms. Erginsoy (16) proposed the equation for this type of scattering as follows

$$u_N = \frac{m^*_e}{20N\epsilon_s'\hbar}\left[\frac{q}{\hbar}\right]^3 \qquad 3.34$$

where N is the number of neutral impurity atoms per unit volume. However Sclar (17) introduced a rather different approach, but this is only important at very low temperature. Once again the mobility is temperature independent.

3.3.5 **Scattering factor**

In equation 3.16 and 3.17, the velocity involved is and average value for all the electrons. However, since different processes are involved in conduction and in magnetic deflection, the average values are not identical. As the velocity depends on the relaxation time τ, it is the averaging of τ which is of interest. It is found that τ varies with energy

$$\tau = E^{-S} \qquad 3.35$$

where S is a constant depending on the scattering processes involved. Therefore the relaxation time must be averaged over a range of energies. In a metal and degenerate semiconductor, only electrons of a single energy, the fermi energy, take part in the transport processes, and therefore the two averaging processes give the same result and the equations above are then correct. In a non-degenerate semiconductor electrons with various energies can take part in conduction, and a factor r, known as the scattering factor must be introduced. r is the ratio of relaxation times averaged over energy for the two effects

$$r = \frac{\langle \tau(E)^2 \rangle}{\langle \tau(E) \rangle^2} \qquad 3.36$$

where < > is an average over energy.

r is found to be related to S as

$$r = \frac{\Gamma(5/2-2S)\,\Gamma(5/2)}{[\Gamma(5/2-S)]^2} \qquad 3.37$$

For more information concerning the scattering factor, see for example Smith (18). When the scattering factor is taken into account, equations 3.20 and 3.22 are modified to

$$R_H = r/nq \qquad \text{and}$$

$$u = 1/r \times R_H\sigma \qquad 3.38$$

The mobility given by equation 3.22 is known as the Hall mobility and that given by equation 3.38 is the conductivity mobility u, which is obtained from conductivity measurements, since

$$u_H = R_H\sigma \qquad \text{and}$$

$$u = 1/r\, R_H\sigma$$

and we have

$$r = u_H/u \qquad \text{and}$$

$$n = r/R_Hq \qquad 3.39$$

The value of r depends on the scattering processes which are dominant. Values of S and r for different scattering mechanisms are given in table 3.1 together with the temperature dependence of the mobility. It is clear that r is always near unity and quite often it is simply ignored.

3.4 Metal-Semiconductor contacts

3.4.1 Schottky-Mott theory of ideal Metal-Semiconductor contacts

When a metal makes an intimate contact with an n-type semiconductor where the work function of the metal (ϕ_m) is greater than that of semiconductor (ϕ_s), a flow of electrons from the semiconductor to the metal takes place until the fermi levels are in equilibrium. As a result a potential barrier is formed at the surface. Referring to the figure 3.4b, the height of this barrier on the semiconductor side is

$$qV_{diff} = \phi_m - \phi_s \qquad 3.40$$

where V_{diff} is the potential in the interior of the semiconductor known as diffusion potential. The height of the barrier on the metal side is given by

$$\phi_{bn} = (\phi_m - \phi_s) + (\phi_s - X_s) = \phi_m - X_s \qquad 3.41a$$

Mechanism	$u \propto (m^*_e)^x T^y$		r
	x	y	
Acoustic	-5/2	-3/2	$3\pi/8$
Polar	-3/2	exponen-tial	1.00-1.14
Piezoelectric	-3/2	-1/2	$45\pi/128$
Ionised Impurity	-1/2	3/2	$315\pi/512$
Neutral Impurity	1	indepen-dent	1

Table 3.1 Summary of scattering mechanism[37].

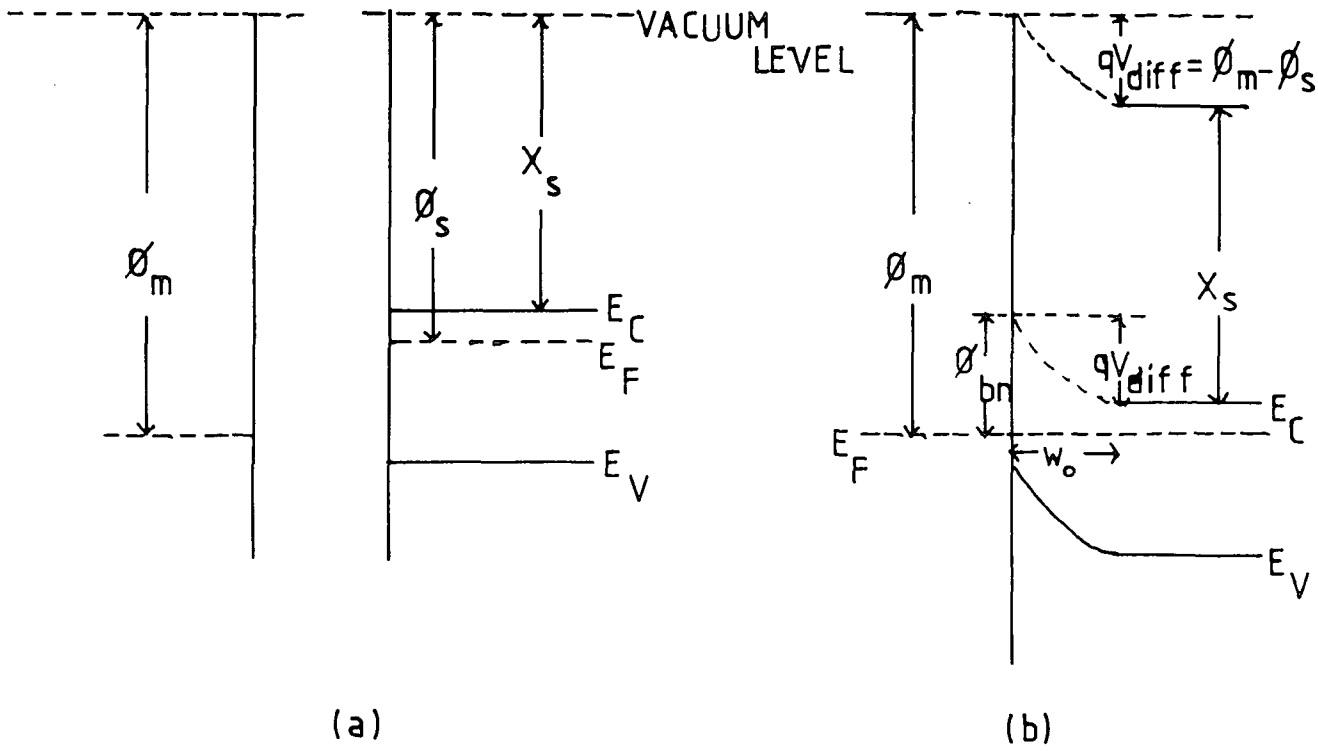

Figure 3.4. Band diagrams of metal contact to n-type semiconductor with $\phi_m > X_s$, a) Before contact b) Situation after contact has been made and reached equilibrium.

or

$$\phi_{bn} = qV_{diff} + (E_c - E_f) \qquad 3.41b$$

where X_s is the electron affinity of the semiconductor. The conduction electrons which cross over into the metal leave a positive charge of ionised donors behind, which is distributed uniformly over a region called the space charge or depletion region (w).

The nature of the electrostatic potential barrier and rectifying mechanism was explained by Schottky (19) and independently by Mott (20) in 1938. According to Schottky the density of charge is constant in the barrier region so that the electric field increases linearly and the potential quadratically as the metal is approached. Mott, on the other hand proposed that there is no ionised impurity in the barrier region, so the electric field is constant and the potential varies linearly (see figure 3.5). The two types of barrier have come to be known as Schottky and Mott barriers.

3.4.2 **Surface states**

The equations in the previous section are valid for an ideal contact between metal and semiconductor. The equation used to calculate the barrier height at the

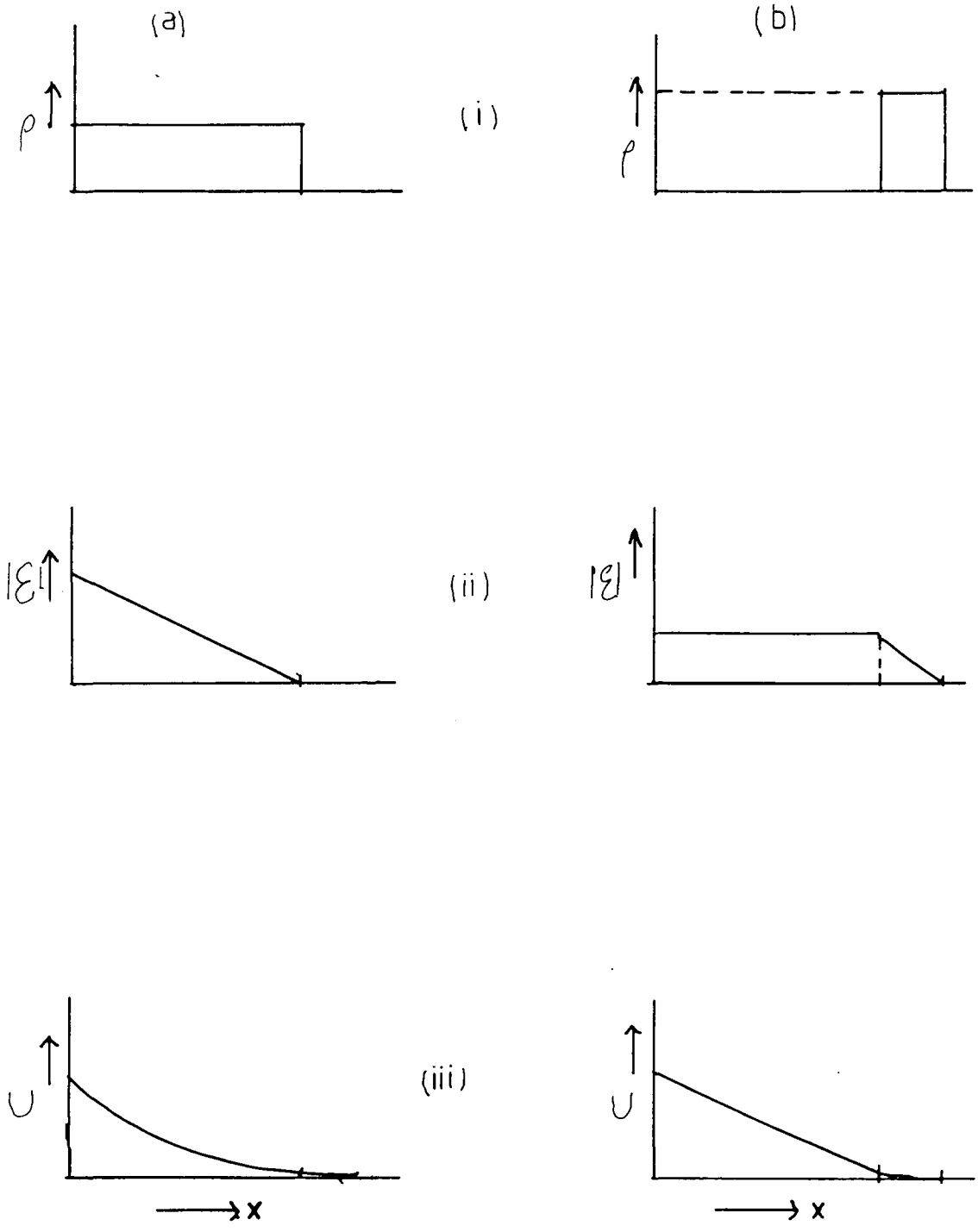

Figure 3.5. Variation of i) Charge density ii) Electric field iii) Electrostatic potential in a) Schottky barrier and b) Mott barrier.

interface (3.41), is simply concerned with the difference between the metal work function (ϕ_m) and the electron affinity of semiconductor (X_s). This situation is not always so simple. Bardeen (21) working on silicon found that ϕ_{bn} is not a linear function of ϕ_m, and later pointed out the importance of surface states at the interface in controlling the barrier height.

Surface states arise because the surface of a crystal interupts the perfect periodicity of the crystal lattice. To see clearly what happens, it is sometimes helpful to look at surface states from the point of view of chemical bonds. At a free surface, in which the atoms have neighbours on one side only, each surface atom therefore has associated with it an unpaired electron in a localised orbital which is directed away from the surface and called a "dangling bond". Energy levels can therefore exist at the surface and are sometimes localised in the band gap. States which are entirely associated with dangling bonds of a perfect crystal are called Tamm states (36). Under some conditions, the binding of impurity atoms to the surface will also give rise to surface states. These are called extrinsic surface states. In both cases, surface states can act as either donors or acceptors. In thermal equilibrium, band bending downwards near the surface indicates donor-like surface states or bending upwards acceptor-like states, even before contact to a metal is made (for n-type material).

Bardeen introduced the concept of a neutral level ϕ_o, for these states, defined as a demarcation level below which the states must be filled in order to achieve an electrically neutral surface. In the absence of surface states the negative charge Q_m on the metal surface must be equal to the positive space-charge in the semiconductor (Q_d). If surface states are present, this neutrality condition will certainly be affected, and $Q_m=-(Q_d + Q_{ss})$ where Q_{ss} is density of the surface states.

The occupancy of the surface states is also determined by the Fermi level, which is constant through the barrier region at zero bias. According to the 'absolute-zero' approximation in which states are assumed to be filled up to Fermi level and empty above it and if the neutral level ϕ_o happens to be above the Fermi level, the surface states contain a net positive charge and Q_d must therefore be smaller than if surface states were absent. This indicates that the width of the depletion region (w) will be correspondingly reduced, and the amount of band bending (propotional to w^2) will also be reduced. On the other hand, if ϕ_o happens to be below the Fermi level, Q_{ss} is negative and Q_d must be greater than if the surface states were absent, which means that w and the amount of band bending will also be increased.

When the density of surface states is sufficiently high, the charge associated with the electrical field

developed across the metal-semiconductor interface can be accommodated by these states without significantly altering the position of the Fermi level. So the height of the metal-semiconductor barrier is then determined mainly by the occupancy of the surface states rather than the metal work function. The Fermi level is then said to be pinned by the high density of surface states. This extreme case is called the Bardeen limit and the barrier height is given by

$$\phi_{bn} = E_g - \phi_o \qquad 3.42$$

However, as has been demonstrated by Crowell and Sze (25), the barrier height is usually a function of both the metal work function and the charge in the interface states. A more general expression (at zero bias) is

$$\phi_{bn} = \beta(\phi_m - X_s) + (1-\beta)(E_g - \phi_o) \qquad 3.43$$

where

$$\beta = \frac{\epsilon_i}{\epsilon_i + dqD_s}$$

D_s is the density of surface states, ϵ_i and d the permittivity and the thickness of the interface layer respectively. If $D_s \longrightarrow 0$ the above equation reduces to the barrier height predicted by the Schottky-Mott theory (equation 3.41).

3.4.2 The Schottky effect

The Schottky effect is the image-force-induced lowering of the potential energy for charge carrier emission when an electric field is applied. Consider a metal-vacuum system. The minimum energy necessary for an electron to escape into vacuum from an initial energy at the fermi level is defined as the work function ϕ_m (figure 3.4).

When an electron is at a distance x from the metal, a positive charge will be induced on the metal surface. The force of attraction between the electron and the induced positive charge is equivalent to the force that would exist between the electron and an equal positive charge located at -x. This positive charge is referred to as the image charge. The attractive force called the image force is given by:-

$$F = \frac{-q^2}{4\pi(2x)^2\epsilon_o} = \frac{-q^2}{16\pi\epsilon_o x^2} \qquad 3.44$$

where ϵ_o is the permittivity of free space. The work done by an electron in the course of its transfer from infinity to the point x is given by:-

$$W(x) = \int F dx = \frac{q^2}{16\pi\epsilon_o x} \qquad 3.45$$

which corresponds to the potential energy of an electron at the distance x from the metal surface (figure 3.6), and is measured downward from the x axis.

When an external field, E is applied, the potential energy is given by:-

$$V = qEx \qquad 3.46$$

and the total potential energy PE as a function of distance (measured downward from the x axis) is the sum of both potential energies

$$PE(x) = \frac{q^2}{16\pi\epsilon_o x} + qEx \qquad 3.47$$

The Schottky barrier lowering (image force lowering) $\Delta\phi_{bn}$ and the location of the lowering xm (see figure 3.6) are given by the condition d[PE(x)]/dx=0 or

$$xm = \sqrt{\frac{q}{16\pi\epsilon_o E}} \quad cm$$

$$\Delta\phi_{bn} = \sqrt{\frac{qE}{4\pi\epsilon_o}} = 2E_{xm}\ V \qquad 3.48$$

This result can also be applied to metal-semiconductor systems. However, the field should be replaced by the

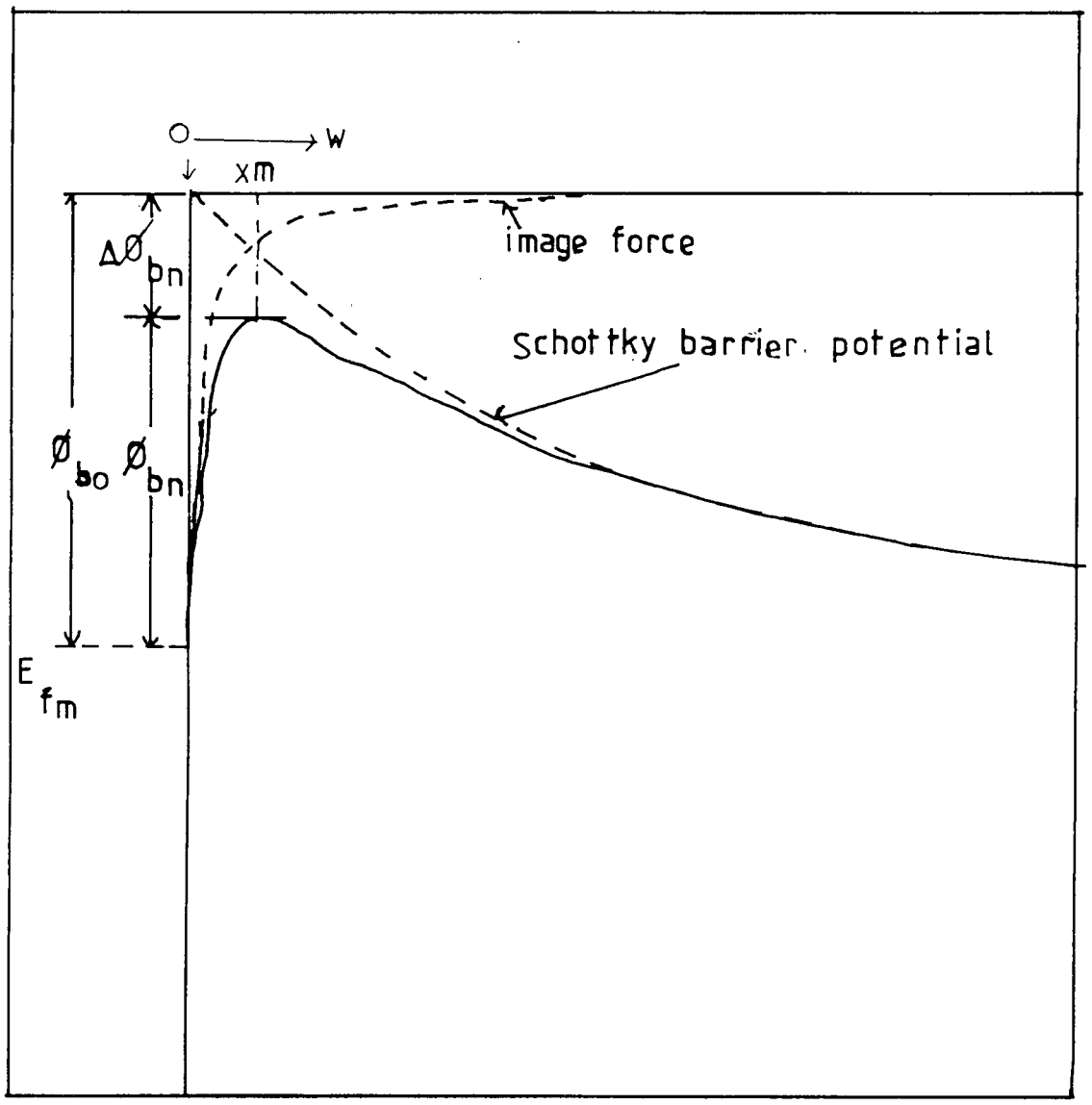

Figure 3.6. Image force lowering in a Schottky barrier

maximum field at the interface, and the free-space permittivity ϵ_o should be replaced by an appropriate permittivity ϵ_s characterising the semiconductor medium.

3.4.4 **Current transport mechanisms**

a) **Forward bias**

When a metal-n-type semiconductor contact (figure 3.4) is biased in the forward direction (i.e. the metal electrode is positive), there are four ways (22) in which charge can be transported across the barrier. The mechanisms are

a) emission of electrons from the semiconductor over the top of the barrier into the metal,
b) quantum mechanical tunnelling through the barrier,
c) recombination in the depletion region,
d) minority carrier injection

These are indicated schematically in figure 3.7.

In an ideal diode only process a is present; b, c, and d lead to a departure from ideal behavior.

Referring to figure 3.7, an electron emitted over the barrier from semiconductor to metal must move through

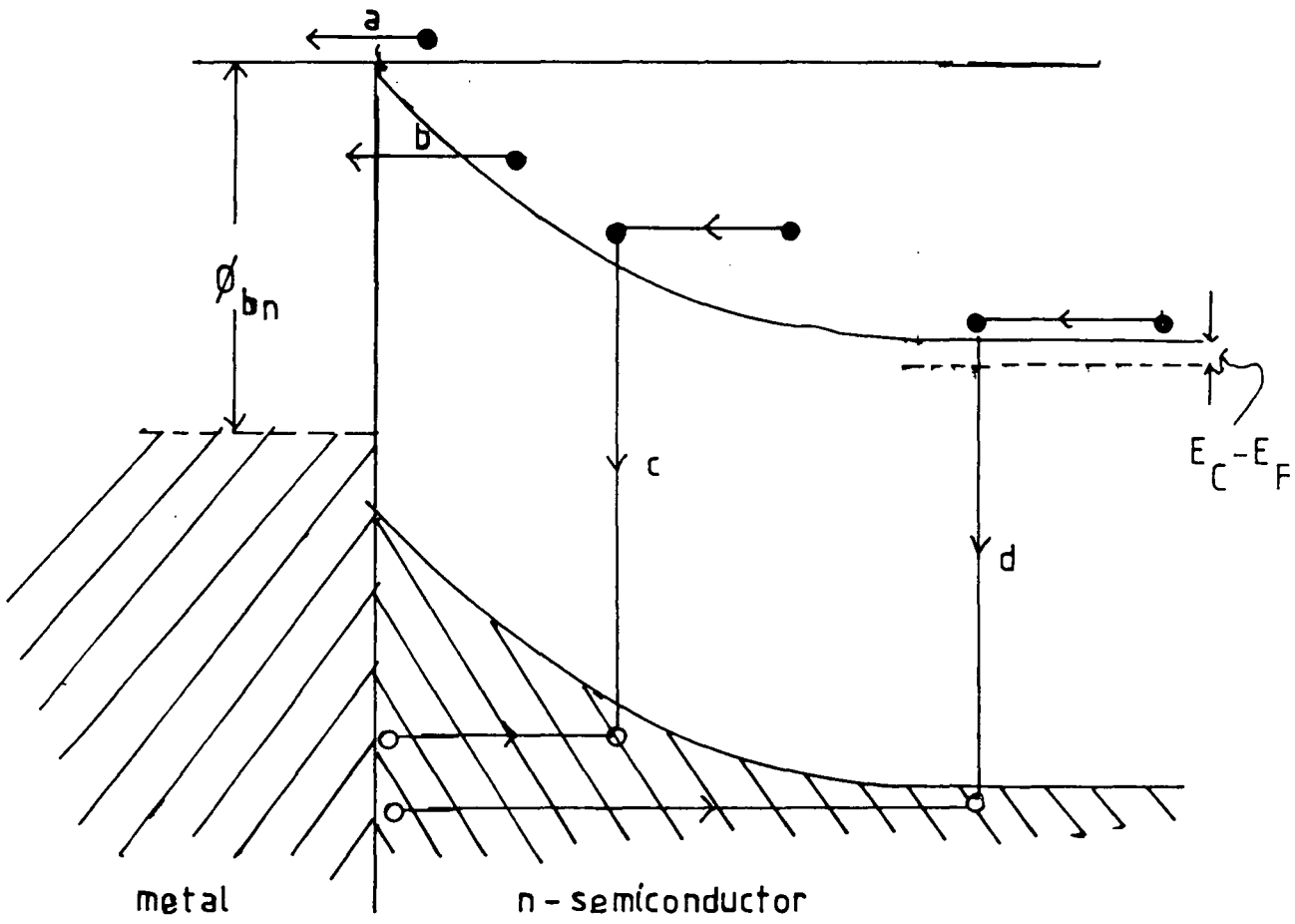

Figure 3.7. Current transport in a forward biased Schottky barrier.

the high field depletion region. In traversing this region the motion of electron is governed by drift and diffusion processes. Schottky and Spenke (23) suggested that the current flow is limited by diffusion processes, whereas Bethe (24) proposed that thermionic emission was the limiting mechanism. In many cases, the current-voltage characteristic is best described by the latter process.

According to the thermionic emission theory, the forward bias current density is:

$$J_f = J_s \{\exp(qV/kT) - 1\} \qquad 3.49$$

provided the width of the space charge region is less than the diffusion length of the electrons. J_s is the reverse saturation current density

$$J_s = R^*T^2\exp(-q\phi_{bn}/kT) \qquad 3.50$$

where R^* is the modified Richardson constant ($R^* = 4\pi m^*_e qk^2/h^3 \approx 120\ m^*_e/m$ amp/cm^{2}K^2).

On the other hand, if the width of the space charge region is greater than the diffusion length, the forward current is limited by the diffusion mechanism, and the current-voltage characteristic becomes(22)

$$J_f = qN_c u_n E_{max} \exp(-q\phi_{bn}/kT)\{\exp((qV/kT)-1)\} \quad 3.51$$

where E_{max} is the maximum electric field at the junction.

Acording to Crowell and Sze (25), a combination of these two mechanisms leads to the expression

$$J_f = \left[\frac{qN_c v_r}{1+v_r/v_d}\right] \exp\left[\frac{-q\phi_{bn}}{kT}\right] \exp\left[\frac{qV}{kT} - 1\right] \quad 3.52$$

where v_r is an effective recombination velocity at the potential energy maximum, and v_d is an effective diffusion velocity for the transport of electrons from the edge of the depletion region to the potential energy maximum.

In practice many Schottky diodes deviate from the ideal behaviour. For instance plots of ln J_f versus V do not exhibit the predicted slope of q/kT. In this event the J-V relationship can be written as

$$J_f = J_s \exp(qV/nkT) \quad 3.53$$

where n is known as the ideality factor and is normally greater than unity. Such behaviour is usually attributed to the bias dependence of the barrier height which results from non-ideal conditions at the surface. In fact, in ideal conditions the barrier height would be slightly bias dependent because of the Schottky effect.

As mentioned earlier, the presence of processes b,

c and d will cause the current-voltage characteristic to deviate from the ideal behaviour. Tunnelling through the barrier may be possible for electrons with energies below the top of the barrier. For example in the case of a very heavily doped semiconductor at low temperature, the current in the forward direction arises from the tunnelling of electrons with energies close to the Fermi level in the semiconductor. This is known as "field emission" (FE). If the temperature is increased, electrons are excited to higher energies and the tunnelling probablity increases very rapidly because the barrier becomes thinner at the top. On the other hand, the number of excited electrons decreases very rapidly with increasing energy, and there will be a maximum contribution to the current from electrons which have an energy E_m above the top of the conduction band. This is known as "thermionic field emission" (TFE). If the temperature is raised still further, a point is eventually reached in which all the electrons have enough energy to go over the top of the barrier, and thermionic emission is now a dominant process and the effect of tunnelling is neglible.

The process of recombination in the depletion region, has been demonstrated by Yu and Snow (38). The recombination normally take place via localised centres and according to Schockley and Read (39) and Hall (40), the most effective centres are those with energy laying near the centre of the gap.

If the height of Schottky barrier on n-type material is greater than half of the band gap, the region of semiconductor adjacent to the metal becomes p-type and contains a high density of holes. These holes could diffuse into the neutral region of the semiconductor under forward bias, and give rise to the injection of holes. Hole injection at metal contacts was extensively studied in the early days of semiconductor research and a summary of the work can be found in the book by Henisch (41).

b) **Effect of interfacial layers**

The effect of an interfacial layer on the current-voltage characteristic has been extensively studied by Card and Rhoderick (26) who showed that the ideality factor (n) is given by

$$n = 1 + \frac{(d/\epsilon_i)(\epsilon_s/w + qD_{sb})}{1 + (d/\epsilon_i)qD_{sa}} \qquad 3.54$$

where ϵ_i and d are the permittivity and the thickness of the interfacial layer respectively. D_{sa} is the density of interface states that are in equilibrium with the metal, while D_{sb} is the density at the interface that are in equilibrium with the semiconductor. If the layer is very thin, $D_{sa} >> D_{sb}$, and the above equation reduces to

$$n = 1 + \frac{d\epsilon_s}{w(\epsilon_i + dqD_{sa})} \qquad 3.55$$

On the other hand, for thicker layers $D_{sb} >> D_{sa}$, then n is given by

$$n = 1 + \frac{d}{\epsilon_i}(\epsilon_s/w + qD_{sb}) \qquad 3.56$$

When the density of surface states of either group is very low, the equation reduces to

$$n = 1 - \frac{d\epsilon_s}{w\epsilon_i} \qquad 3.57$$

3.4.5 **Capacitance of Schottky diodes**

The capacitance of a Schottky barrier diode is associated with its depletion region and its charge state. The capacitance is usually measured by superimposing a small alternating voltage on a d.c bias which yields the differential capacitance C (dQ/dV). The differential capacitance is therefore not constant but decreases as reverse bias V_r is increased. In the absence of surface states there are three sources of charge, which assuming an n-type semiconductor are;

1) Q_d, the charge due to uncompensated donor density

2) Q_m, the charge on the surface of the metal

3) Q_h, the charge due to any hole, which may exist in the semiconductor immediately adjacent to the metal

Because there is no electric field in the bulk of the semiconductor or in the metal

$$Q_d + Q_m + Q_h = 0 \qquad 3.58$$

and if reverse bias is applied to the junction, electrons move into the bulk of semiconductor so Q_d increases and holes move into the metal and Q_h decreases. The capacitance of the Schottky diode, can be calculated either from $C = dQ_d/dV_r$ or $C = -d(Q_h+Q_m)/dV_r$.

Outside the depletion region, the semiconductor is neutral. In the depletion region the charge density is equal to qN_d, using Gauss theorem

$$\frac{dE}{dx} = \frac{Q_d}{\epsilon_s} = \frac{qN_d}{\epsilon_s} \qquad 3.59$$

The magnitude of E , therefore, increases linearly as the metal is approached, rising from 0 at x=w to qN_dw/ϵ_s at the interface. If we take potential as zero in the neutral region (U(w)=0) then the potential at x is given by

$$U(x) = \int_{x}^{w} E\,dx$$

$$= -\int_{x}^{w} \frac{qN_d(w-x)}{\epsilon_s}\,dx$$

$$= -\frac{qN_d(w-x)^2}{2\epsilon_s} \qquad 3.60$$

Thus U increases quadratically as the metal is approached and at the interface (x=0),

$$U(0) = -\frac{qN_d w^2}{2\epsilon_s} \qquad 3.61$$

The magnitude of U(0) at the interface is equal to the diffusion potential V_d,

$$V_d = \frac{qN_d w^2}{2\epsilon_s}$$

$$E_{max} = \frac{qN_d}{\epsilon_s} = \frac{Q_d}{\epsilon_s}$$

V_d can be rewritten in another form as

$$V_d = \frac{\epsilon_s |E_{max}|^2}{2qN_d}$$

$$= \frac{Q_d^2}{2\epsilon_s qN_d} \qquad 3.62$$

and $C = \frac{dQ_d}{dV_d} = \left[\frac{\epsilon_s qN_d}{2V_d}\right]^{0.5}$

where $V_d = V_{diff} + V_r$

so $$C = \frac{dQ_d}{dV_r} = \frac{dQ_d}{dV_d} = \left[\frac{\epsilon_s qN_d}{2V_d}\right]^{0.5} \qquad 3.63$$

From the above equation a plot of C^{-2} versus V_r should give a straight line. N_d can be calculated from the slope and V_d from the intercept on the V axis. In practice the capacitance of a Schottky diode is usually affected by the existence of interfacial layers and deep traps due to native defects or impurities.

a) **Effect of interfacial layer on capacitance**

If an interfacial layer is present at the interface, the effect on total capacitance is quite considerable since the capacitance of this layer is effectively in series with the capacitance of the depletion region. Studies by Cowley (27), Goodman (28) and Crowell and Roberts (29) have shown that the barrier height measured by the capacitance-voltage method is usually larger than that determined from the current-voltage characteristic or by the photoelectric method.

The analysis is easy, if the layer is sufficiently thin for the occupation of any interface states which may exist at the insulator-semiconductor interface to be determined by the Fermi level in the metal (i.e d<30 Å). The interface states are then emptied or filled by the tunnelling electrons from the metal and make no direct contribution to the capacitance. According to analysis by Cowley (27), the plot of C^{-2} against V_r remains linear with a slope of $2/q\epsilon_s N_d$ as in the ideal case, but the intercept

of V' on the V_r axis is modified and is given by

$$V' = V_{diff} - \left[\frac{kT}{q}\right] \alpha \left[\frac{2qN_d}{\epsilon_s}\right]^{1/2} \left[V_{diff} - \frac{kT}{q}\right]^{1/2} + \frac{qN_d\alpha^2}{2\epsilon_s}$$

where $\alpha = \dfrac{d\epsilon_s}{\epsilon_i + qdD_s}$

In deriving this result it was assumed that α remains constant as V_r changes (i.e the density of states D_s is constant), and also the effect of holes can be neglected.

With a thicker interfacial layer (i.e d>30 $\mathring{A}$), some of the interface states are not in equilibrium with the metal and they can be filled from the semiconductor. then the capacitance is given by $d(Q_d+Q_{ss})/dV_r$ which is similar to that of a MOS capacitor and the graph of C^{-2} against V_r is generally not linear.

b) **Effect of deep traps**

The general expression for the capacitance of a Schottky barrier in the presence of deep traps is given by (30)

$$C = A\left[\frac{\epsilon_s qN_d}{2(V_{diff}+V_r)}\right]^{1/2}\left[1 + \frac{N_t}{n}\left[\frac{e_n^2}{e_n^2 + w_s^2}\right]\right] \qquad 3.64$$

where A is the area of the diode, N_t is the density of the

deep traps, and N_d^+ is the total density of ionised donors. If $w_s >> e_n$ the above equation reduces to normal Schottky diode capacitance as in the equation 3.63. The effect of deep traps on junction capacitance has been discussed by Roberts and Crowell (29), Zotha (32), Kimmerling (33) and Noras(34).

3.4.6 **Methods of measuring the barrier height**

The barrier height of a metal-semiconductor contact can be measured in several ways, which are described briefly in this section.

a) **From the current-voltage characteristic**

The forward bias current-voltage characteristic of a near ideal Schottky diode is given by equation 3.5o. As a result, a plot of log J_f against V can be used to determine the Schottky barrier height. Rearranging equation 3.53 gives

$$\phi_{bn} = \frac{kT}{q} \ln \frac{R^*T^2}{J_s} \qquad 3.65$$

and J_s can be determined from the intercept of the plot of log J_f against V at V=0. This will be an accurate value of ϕ_{bn} when the ideality factor is equal to unity, but from a practical point of view $0<n<2$ is often taken as the requirement for a reasonably accurate calculation of ϕ_{bn}.

b) **From capacitance-voltage measurements**

The differential capacitance associated with the depletion region of a Schottky barrier is given by equation 3.63. If N_d is constant in the depletion region, a plot of C^{-2} against reverse voltage V_r should be linear with an intercept $V_i=V_{diff}-kT/q$, on the voltage axis. The barrier height is then given by

$$\phi_{bn} = V_{diff} + (E_c-E_f) \qquad 3.66$$

where

$$E_c-E_f = \frac{kT}{q} \ln \frac{N_c}{N_d}$$

c) **From the Photoelectric method**

When sufficiently energetic monochromatic light is incident upon the metal surface, some electrons excited from the Fermi level of the metal can cross into the semiconductor and contribute to the short circuit photocurrent. Fowler(35) has shown that the photocurrent per absorbed photon, R is given by

$$R \sim \frac{T^2}{\sqrt{(E_s-h\nu)}} \left[\frac{x^2}{2} + \frac{\pi^2}{6} - \left(e^{-x} - \frac{e^{-2x}}{4} + \frac{e^{-3x}}{9} \ldots.\right)\right] \qquad 3.67$$

for $x>0$ and $x = h(\nu-\nu_o)/kT$

The term $h\nu_o$ represents the Schottky barrier height, ϕ_{bn}, and E_s is equal to the sum of ϕ_{bn} and the Fermi energy (measured from the bottom of the metal conduction band). Provided that $E_s >> h\nu$ and $h\nu - h\nu_o > 3kT$, then to a good approximation equation 3.67 reduces to

$$R \sim c(h\nu - h\nu_o)^2 \qquad 3.68$$

where c is a constant. Thus a plot of $R^{1/2}$ against $h\nu$ should be linear over a certain range of energy and the extrapolation of this linear region to the energy axis gives a direct measurement of the reduced barrier height. This method is the most accurate and direct one for the determination of barrier height and it is generally regarded as the definitive measurement (22).

References for chapter III

1) W.Khon, Sol. State Phys., **5** (1957) 257

2) H.H.Woodbury and M.Aven, Phys. Rev., **B9** (1974) 5179

3) D.M.Larson, Phys. Rev., **187** (1969) 1147

4) T.H.Ning and C.T.Sah, Phys. Rev., **B4** (1971) 3468

5) H.G.Grimmeiss, Ann. Rev. Mat. Sci., (1977) 341

6) Van der Pauw, Philips Res. Rep., **13** (1958) 1

7) H.H.Weider in **Non-destructive Evaluation of Semiconductor, Material and Devices**, edited by Jay N. Zemel

8) Allen, **M.Sc Thesis**, Newcastle University 1965

9) D.L. Ridpath, **PhD Thesis**, Durham University 1971

10) D.Howarth and E.H.Sondheimer, Proc. Roy. Soc., **A219** (1953) 53

11) S.S.Devlin in **Physics and Chemistry of II-VI Compounds**, edited by M.Aven and J.S.Prener (North-Holland publ. Co 1967)

12) W.A.Harrison, Phys. Rev., **101** (1956) 903

13) W.Shockley and J.Bardeen, Phys. Rev., **80** (1950) 72

14) E.M.Conwell and V.F.Weisskopf, Phys. Rev., **141** (1950) 388

15) H.Brooks, **Advances in Electronics and Electron Physics** Vol.7 Marton Ed. (Academic Press) p. 85-182

16) C.Erginsoy, Phys. Rev., **79** (1950) 1013

17) N.Sclar, Phys. Rev., **104** (1956) 1559

18) R.A.Smith, **Semiconductor** (Cambridge University Press), second ed. (1978)

19) W.Schottky, Naturwiss., **26** (1938) 843

20) N.F.Mott, Proc. Cambridge Phil. Soc., **34** (1938) 568

21) J.Bardeen, Phys. Rev., **71** (1947) 717

22) E.H.Rhoderick, **Metal-Semiconductor Contacts** (Clarendon Press Oxford) 1980

23) W.Schottky and E.Spenke, Weiss. Verof Siemens-Werken, **18** (1959) 225

24) H.A.Bethe, M.I.T Rad. Lab. Rep., 43-12 (1942)

25) C.R.Crowell and S.M.Sze, Sol. Stat. Elec., **9** (1966) 1035

26) H.C.Card and E.H.Rhoderick, J. Phys. D: Appl. Phys., **4** (1971) 1589

27) A.M.Cowley, J. Appl. Phys., **37** (1966) 3024

28) A.M.Goodman, J. Appl. Phys., **34** (1963) 329

29) C.R.Crowell and G.I.Roberts, J. Appl. Phys., **40** (1969) 3726

30) G.Vincent, D.Bois and P.Pinard, J. Appl. Phys., **46** (1975) 5173

31) G.I.Roberts and C.R.Crowell, J. Appl. Phys., **41** (1970) 1767

32) Y.Zotha, Sol. Stat. Elec., **16** (1973) 1029

33) L.C.Kimmerling, J. Apply. Phys., **45** (1974) 1839

34) J.M.Noras, J. Phys. C: Soild State, **14** (1981) 2341

35) R.H.Fowler, Phys. Rev., **38** (1931) 45

36) **Surface of phosphors and semiconductors.** Academic Press, 1975 London, edited by C.G.Scott and C.E.Reed.

37) K.Seeger, **Semiconductor Physics, An Introduction.** Springer Series in Solid State Sciences.

38) A.Y.C.Yu and E.H.Snow, J. Appl. Phys., **39** (1968) 3008

39) W.Schockley and W.J.Read, Phys. Rev., **87** (1952) 835

40) R.N.Hall, Phys., Rev., **87** (1952) 387

41) K.H.Henisch, **Rectifying Semiconductor Contacts** (1957), Oxford University Press, Oxford.

CHAPTER IV

EXPERIMENTAL PROCEDURE

4.1 Introduction

In this chapter the experimental procedures used to grow the $Zn_xCd_{1-x}S$ crystals in this department and to characterise their properties are described.

4.2 Crystal Growth

4.2.1 Purification of starting material

The starting material (CdS and ZnS) has to be purified before it is loaded into the growth tube, to ensure that the growing crystal is as free as possible from any impurity which might be present in the starting material. CdS Optran grade powder obtained from BDH Chemicals was purified by sublimation in a continuous stream of argon by placing it in a boat in a long silica tube and maintaining it at 600^{o}C for about four hours. This process is designed to remove any volatile impurity which might be present. The temperature was then raised to 1150^{o}C to sublime the CdS, which was transported to the lower temperature region of the tube where it was deposited on a split silica liner leaving the non-volatile impurities behind. This gave rod and platelet crystals which were

used to grow larger single crystals. For ZnS, ZnS powder (also from BDH Chemicals) was outgassed and sublimed in a continuously evacuated tube. This method was used because ZnS required a much high temperature than CdS (about 1400^{o}C).

4.2.2 **The Clark-Woods method**

This method (also called the sealed tube method) was developed by Clark and Woods (1) originally for CdS. The arrangement of the system used is shown in figure 4.1. The charge (a mixture of CdS and ZnS measured by weight) was loaded into the growth ampoule which was evacuated and sealed. The charge was held at 1150^{o}C in the growth ampoule which was connected via a narrow orifice to a long tail containing a reservoir of cadmium or sulfur. The temperature of the tail was adjusted to provide an appropriate vapour pressure over the evaporating charge. Higher reservoir temperatures were required as the zinc content of the final crystal increased. In fact with the mixed crystals the charge was first converted to a solid solution of $Zn_xCd_{1-x}S$ in a reverse temperature gradient. As the capsule was pulled vertically through the furnace the temperature gradient was developed and the various vapour species diffused to the cooler region where supersaturation occurred and the crystal grew. Normally a boule 3cm long and 1cm in diameter took about two weeks to grow.

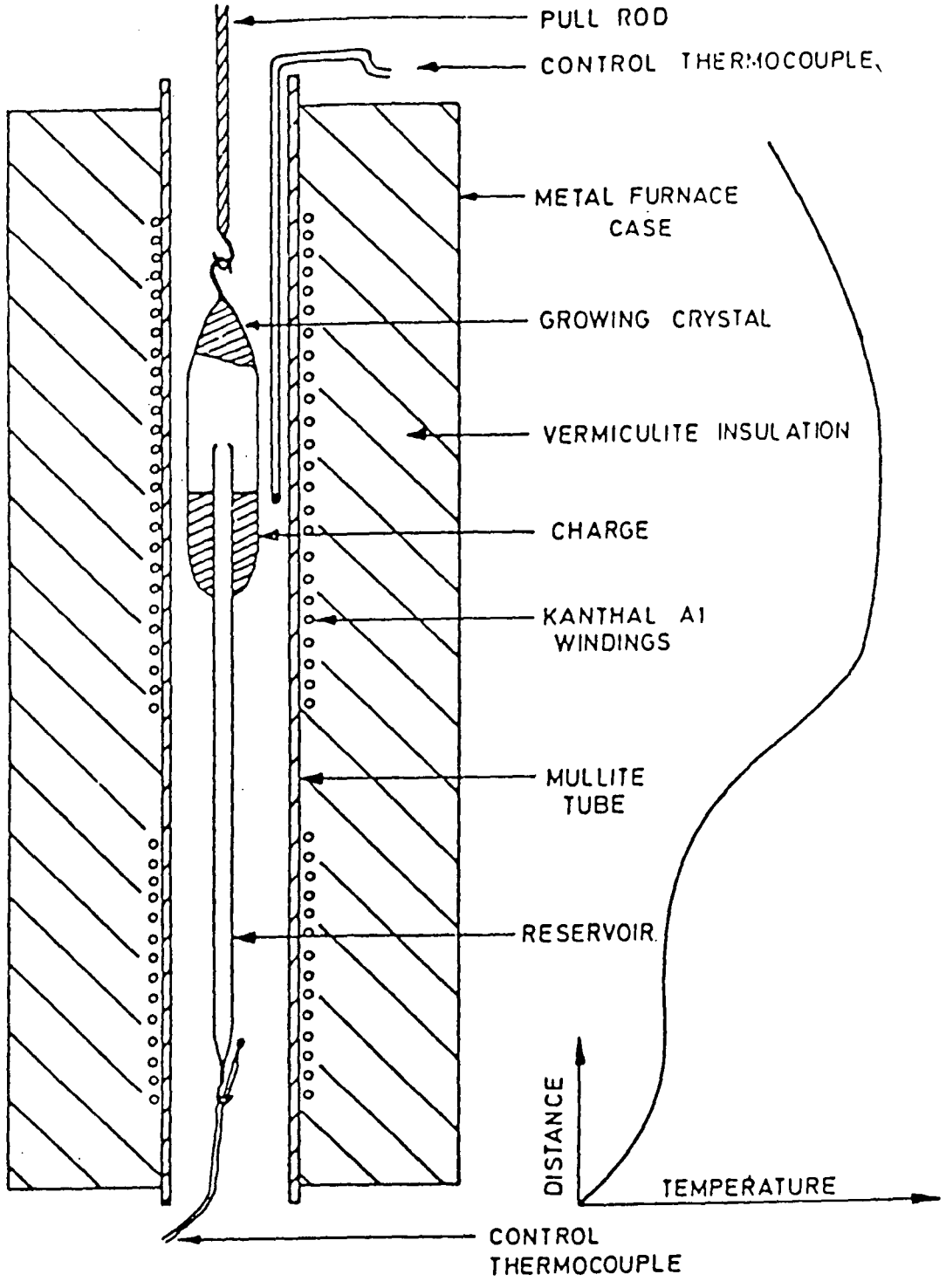

Figure 4.1. The Clark-Woods method for the growth of $Zn_xCd_{1-x}S$ crystals (1).

4.2.3 **The Piper-Polich method**

This method (also called the open ended tube method) was based on a technique developed by Piper and Polich (2). The arrangement of the system used here is shown in figure 4.2. The charge was loaded into an open silica tube and placed in a tubular furnace so that the charge was near the flat region of the temperature profile. Argon was admitted via a needle valve, passing through the system at a rate of 100ml/min. The open end procedure allowed unwanted volatile impurities to escape prior to crystal growth. As the material was transported to the cooler end of the capsule, condensation occurred and the growth chamber was sealed off. Generally a run lasted 2-3 days including a cool down period of 24 hours. Boules produced were 2-4cm long and 1cm in diameter.

4.3 **Sample Preparation**

4.3.1 **Cutting, polishing and etching**

Boules were normally cut into 1mm thick slices and ultimately into dice of required dimensions, using a diamond saw. Both surfaces of a slice were then smoothed by mechanical polishing down to 1μm grit size alumina.

The dice were then etched in cool concentrated

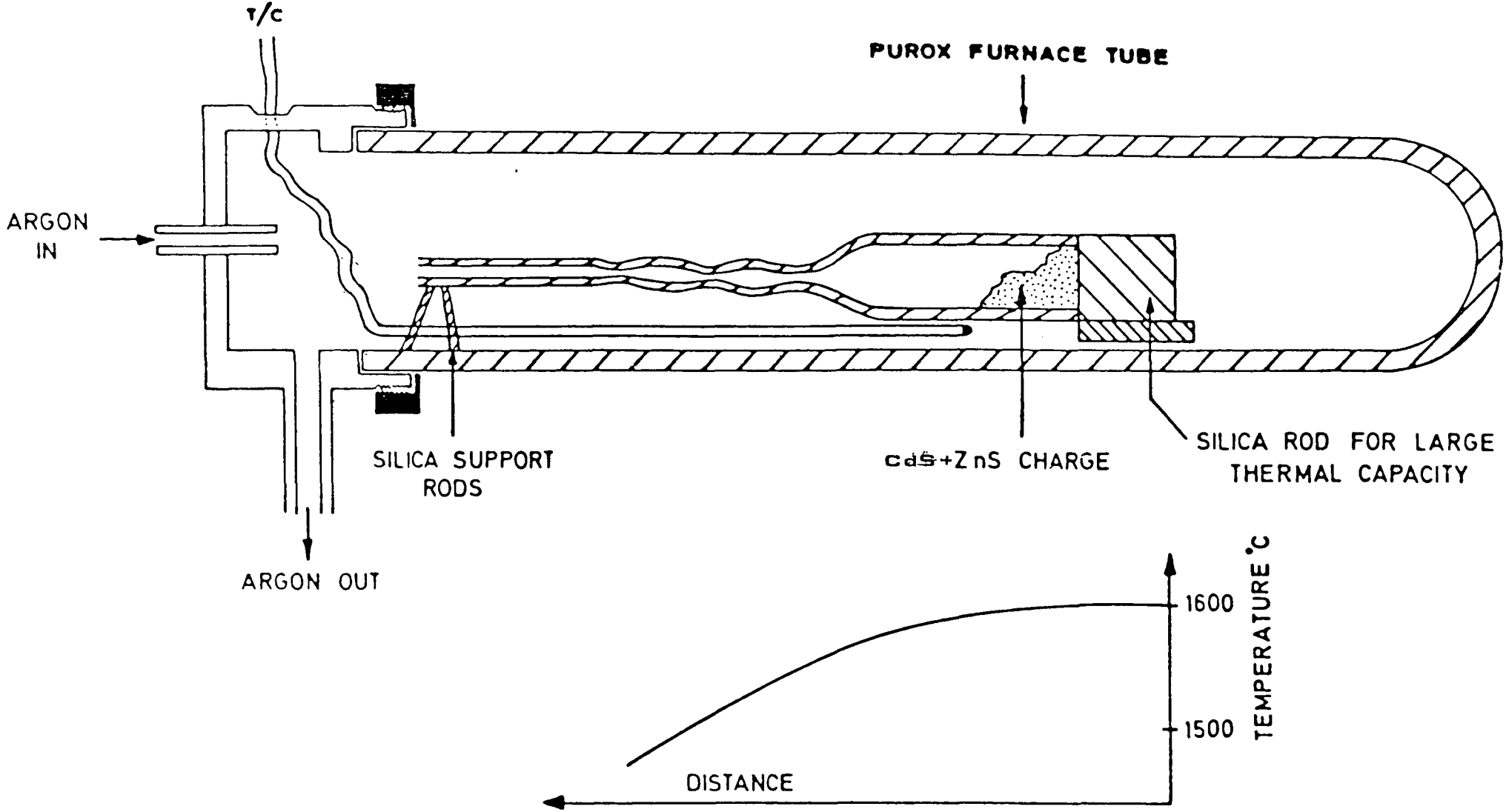

Figure 4.2. The Piper-Polich method for the growth of $Zn_xCd_{1-x}S$.

hydrochloric acid for about 20 seconds (3) to remove the surface damage, and quickly dried in a stream of nitrogen.

4.3.2 **Doping**

Copper doped samples were prepared by evaporating a small amount of metallic copper (99.99%) onto one of the faces of the dice. Dice were then sealed in the evacuated silica tube and underwent heat treatment at 800^{o}C for about 10 hours. This was done to ensure uniform distribution of copper (4). It is quite difficult to obtain a moderate resistivity of the order 10-100 ohm-cm which is necessary if reasonably good Schottky diodes are to be made.

4.3.3 **Hall effect and conductivity**

Retangular bars normally with dimensions of 8x2x1 mm^{3} were cut from the boules. In some cases clover-leaf samples were used. After cleaning and etching (as described previously), In-10% Cd alloy was used to form an ohmic contact. The alloy was brushed with a fine wire onto the face on which it was required. The bars were then heated to around 300^{o}C for about 5-10 minutes in argon. This process gave quite good ohmic contacts with excellent mechanical strength.

The sample was then fixed with varnish to a glass microscope cover slip as shown in figure 4.3a. The sample

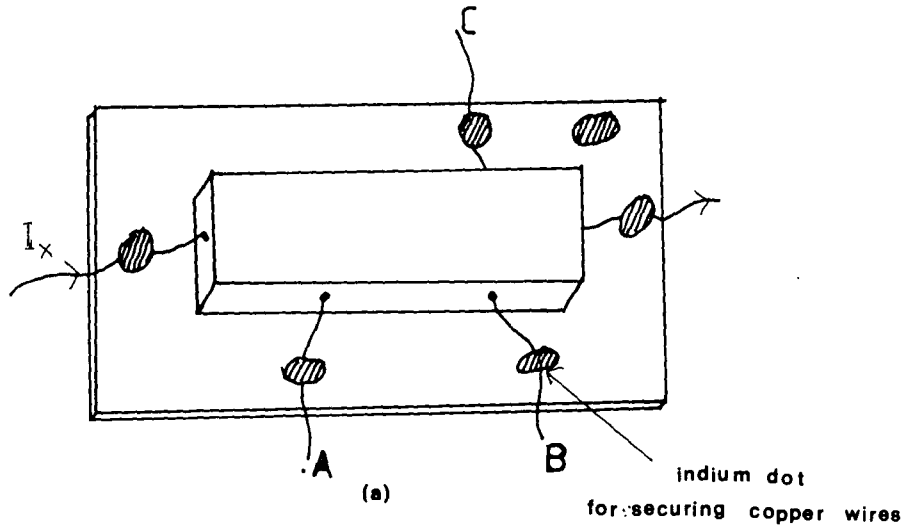

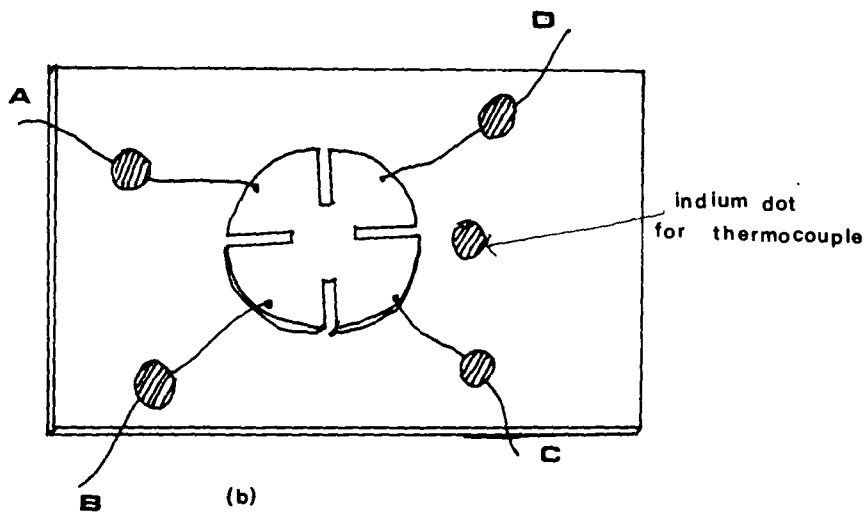

Figure 4.3. Contact arrangement for a) bar sample and b) clover-leaf sample.

was not shorted out as the resistivity of the varnish was several orders of magnitude greater than that of the sample. Good thermal contact was made to the cover slip.

Electrical contact to the specimen was made with fine copper wires soldered to the cover slip with indium (figure 4.3a). The wires were connected to the specimen with quick drying silver paste. A copper-constantan thermocouple was embedded in a separate indium dot, soldered onto the cover slip. The current contacts to the bars were made as large as possible for strength, and uniformity of current flow. The remaining contacts were made as small as possible with a minimum diameter of about 1mm.

The clover-leaf samples were normally 1mm thick slices of 1cm diameter cut from the boule to which four contacts were applied at the edge of the samples (see figure 4.3b). It was easy to make contacts to these specimens compared with the bar samples but the difficulties in growing uniform $Zn_xCd_{1-x}S$ crystals limited the usefulness of this type of sample.

4.3.4 **Schottky diodes**

Normally 3x3x1 mm^3 dice were used to fabricate Schottky diodes following the cleaning and etching procedures (4.3.1). Indium was used to make the ohmic

contact. The indium wire (1 mm in diameter) was first cleaned using concentrated nitric acid and then washed with water. A small piece of indium was pressed on to the surface of the dice and then heated in an argon atmosphere at 200^{o}C for about 10 minutes. The contact was covered by lacomit (acid resistant laquer) and then etched once again to clean the surface before evaporating gold onto the other surface to make the rectifying contact in a high vacuum of about 10^{-5} torr.

4.4 EDAX Examination in The SEM

A Cambridge Stereoscan S 600 SEM operated in the EDAX mode, together with a Link system 860 analyzer was used to measure the relative intensity of CdL1 and ZnKα lines from mixed single crystals of $Zn_xCd_{1-x}S$. The block diagram of the system used is illustrated in figure 4.4. Excitation can be in any form of radiation capable of ejecting electrons from the inner shells of the atoms. In this study, the beam of electrons in the SEM was used, and the incomplete electron shells thus produced were subsequently filled with electrons from more loosely bound states resulting in the emission of characteristic x-rays. The emission spectra of the elements present were accumulated over a period of several minutes and were observed on a monitor. The relative intensities of the emission lines can be measured directly from the print out spectra, taking care to substract the back-ground levels

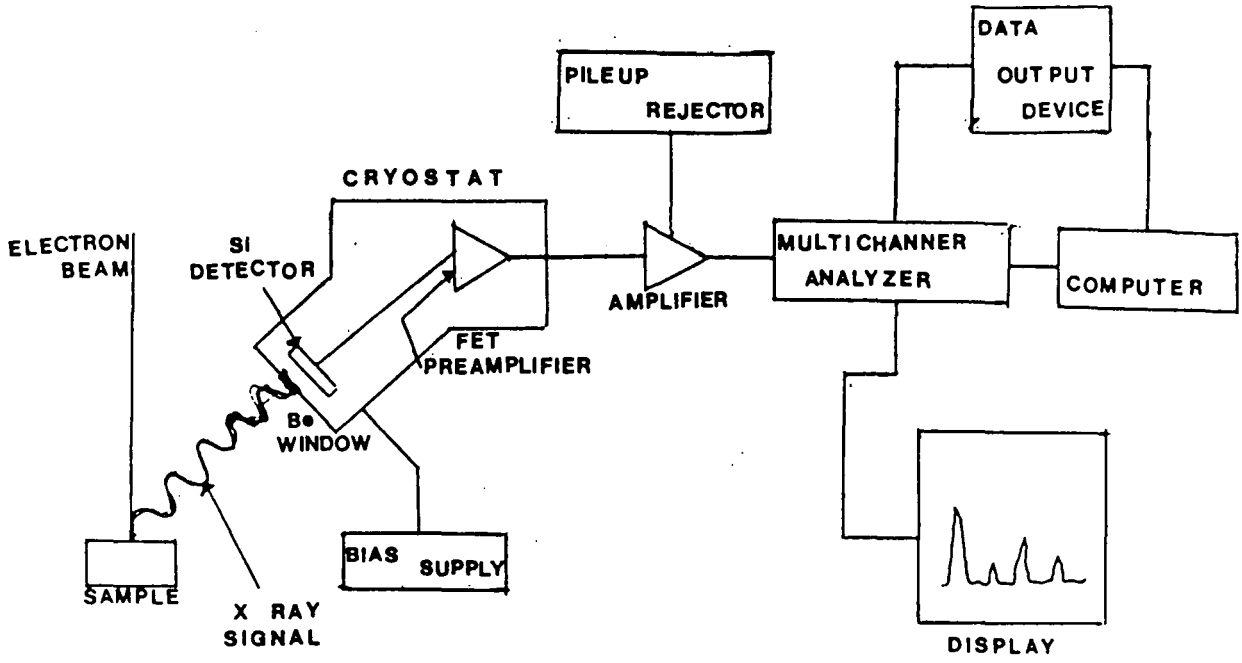

Figure 4.4. Block diagram for EDAX measurement.

from the peak.

4.5 X-Ray Diffraction

A Phillips diffractometer was used to record the diffraction patterns obtained from finely ground powders of the mixed crystals of $Zn_xCd_{1-x}S$. Each sample was prepared by spreading a powder layer of the material on to a glass slide with acetone. The scan was than made across the sample using CoK_α radiation (λ=1.7902Å) with a goniometer scanning rate of one degree per minute.

The equation used to calculate the lattice parameters a_o and c_o is given by (5)

$$\frac{1}{d_{hkl}^2} = \frac{4(h^2+hk+k^2)}{3a_o^2} + \frac{l^2}{c_o^2}$$

where d_{hkl} is the spacing between the planes.

4.6 Chemical Analysis by Atomic Absorption Spectroscopy

Atomic absorption spectroscopy (AAS) measurements to determine the composition of the mixed crystals were made using a Perkin Elmer 5000 Atomic Absorption Spectrometer. Because of the destructive nature of this technique, it was deployed after all other measurements on the samples had been completed. Samples were prepared by

dissolving them in concentrated hydrochloric acid, and then placing them in a container in the machine. The sample solution was converted into atomic vapour and then its absorbance was measured at a selected wavelength which is characteristic for each individual element. The absorbance is proportional to the concentration of the element, so that direct comparison with the reference solutions gives a measure of this quantity.

4.7 Conductivity and Hall Effect Measurements

A cryostat built in the department was used in all the experiments. The cryostat is shown in figure 4.5b. Liquid nitrogen was held in a container of about one litre capacity which was connected to the sample block by a hollow tube enclosing the so called exchange space. This space could be evacuated or filled with gas when necessary so that it acted as a thermal switch. A silica window was provided opposite the sample and if required the sample could be illuminated via a mirror mounted at 45^{o} on one of the pole pieces of the magnet. The window was kept covered during the measurements unless otherwise stated. A heater was mounted directly onto the sample block and the copper-constantan thermocouple on the cover slip was used to monitor the temperature. The reference junction of the thermocouple was held at liquid nitrogen temperature. The sample holder was pressed onto the block with a mechanical clamp. All electrical connections were made via ten wires

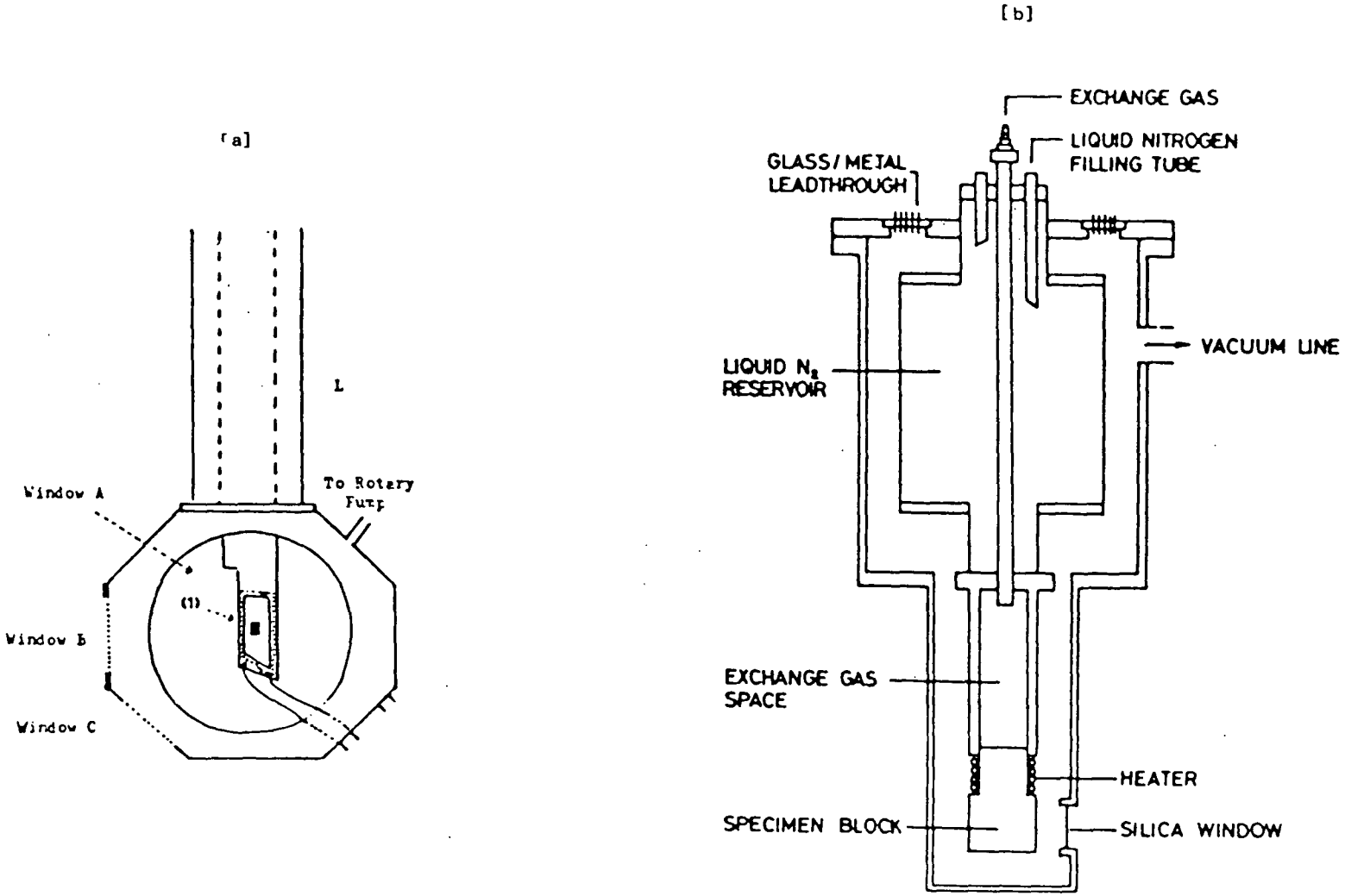

Figure 4.5. a) Cold finger cryostat used for spectral response and photocapacitance and b) Gas exchange cryostat for conductivity and Hall Effect measurements.

passing through the top of the cryostat. The pressure around the cryostat was maintained at 10^{-4} torr using a small oil diffusion pump.

The five probe method was used for many Hall effect measurements (figure 4.3a). This was done with samples which were too small for six probes to be applied successfully. The electrical supply to the sample was a constant current power supply built in the department. Measurements were carried out from room temperature to about 100K. When measurements were to be made, the temperature was controlled by evacuating the exchange space so that the temperature could be kept steady. The magnet used in the experiment was also built in the department and provided a flux density of 0.225 Tesla at 1.75 A. The Hall effect was measured in a constant field (0.225T) for every sample. The conductivity was found by measuring the current I_x and the voltage between A and B (figure 4.3a). By using a Hewlett Packard multimeter type 3465B which has a high input impedance ($\sim 10^9$ ohm), the measurements were independent of contact resistance at A or B. To minimise any errors in the conductivity measurements, the voltage between A and B was determined by reversing the current and averaging the two values.

The Hall voltage was obtained by measuring the potential between B and C when the magnetic field was applied. In the absence of the magnetic field, there was

often an out-of-balance voltage between B and C because of their imperfect alignment. This was eliminated by reversing the magnetic field and remeasuring the potential between C and D. To minimise possible error because of temperature gradients, another pair of readings was taken with the magnetic field normal and reversed. Averaging the four values gave the final measured value of Hall voltage.

4.8 Spectral Response Measurements

Measurements of the spectral response of the short circuit current from the Schottky diodes, were carried out using monochromatic radiation from the exit slit of a Barr and Stroud double prism monochromator type VL2 fitted with spectrosil A quality prisms. The light source was a 250 watt quartz halogen lamp driven by a 200 V a.c stabilised power supply. A schematic diagram of the apparatus is shown in figure 4.6. The monochromator was periodically calibrated using a sodium lamp to avoid any effects of wavelength drift. The spectral response measurements could be performed at both room and liquid nitrogen temperatures. The device under test was mounted in a cryostat (figure4.5a) where its temperature was monitored using a copper-constantan thermocouple.

Almost all the spectral measurements were taken starting from a long wavelength of about 2μm (0.5eV) to short wavelengths depending on the composition of the

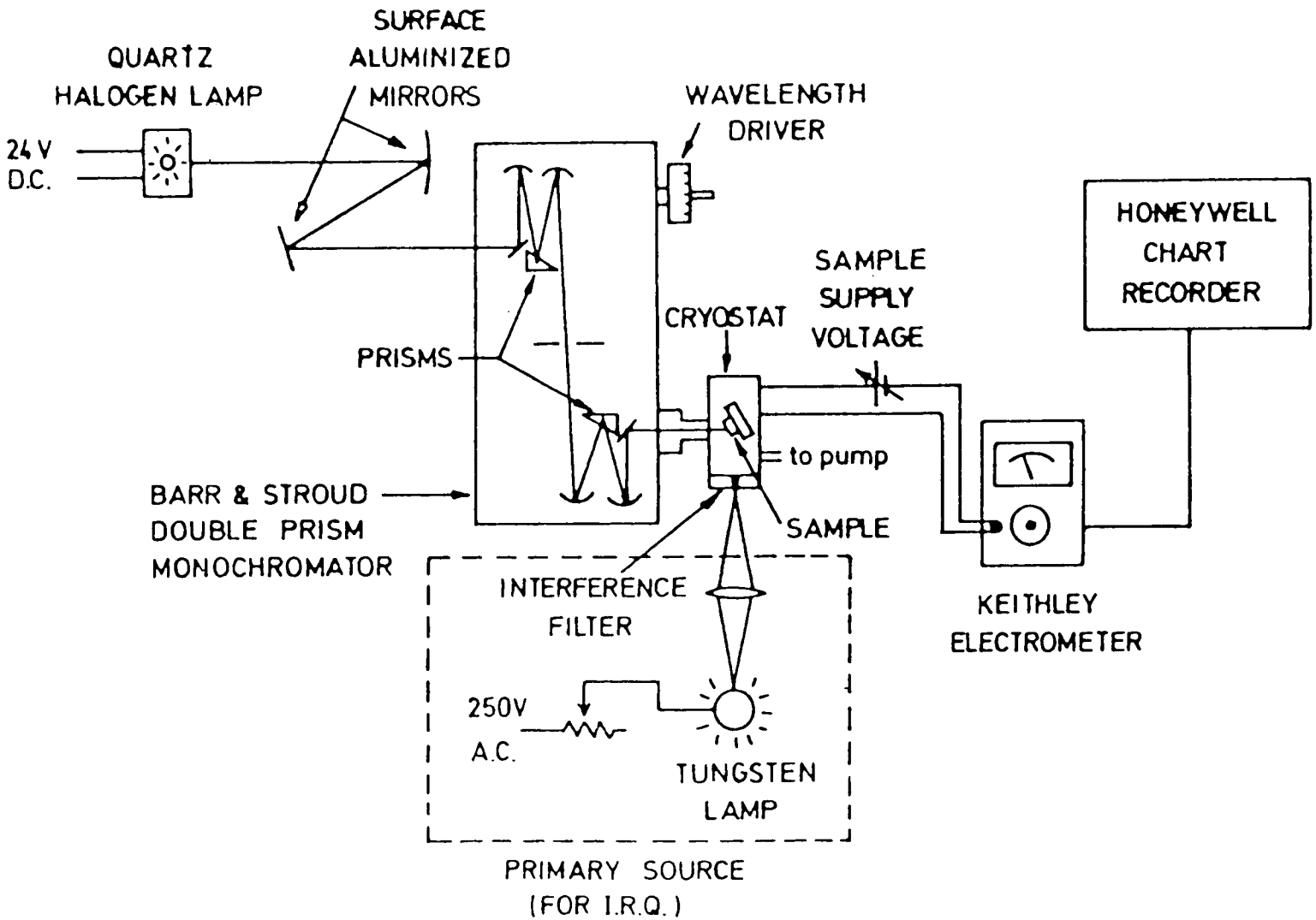

Figure 4.6. Experimental set up for spectral response measurements.

$Zn_xCd_{1-x}S$.

The bias voltage applied across the sample was provided by a DC Voltage calibrator, while the current was measured with a Keithley 602 electrometer and recorded on a Honeywell electronic 196 chart recorder.

4.9 Current-Voltage Measurenents

Current voltage characteristics were recorded in the dark using a high impedance Bradley voltmeter (type 173B) and a low impedance Hewlett Packard ammeter (type 3465B). Bias voltage was provided by a D.C voltage calibrator type 2003S (Time Electronics Ltd.).

4.10 Capacitance Measurements

4.10.1 Capacitance-voltage

Capacitance-voltage characteristics of the Schottky diode were determined using a Boonton 72B capacitance meter which operates at 1MHz. The bias voltage was obtained from the D.C voltage calibrator.

4.10.2 Steady state photocapacitance

The same monochromator was used as for the spectral response measurements to provide monochromatic radiation

for the photocapacitance measurements (see figure 4.7). As mentioned before, the capacitance was monitored with a Boonton capacitance meter. The diode capacitance was normally compensated with an external capacitance to allow small changes induced by the monochromatic radiation to be recorded. The output of the capacitance meter was connected to a Honeywell chart recorder and the bias voltage could be applied directly when necessary. Measurements were made at both room temperature and about 90K using the cryostat shown in figure 4.5a. Sufficient time was left to allow steady state to be reached before the scan was made very slowly from long to short wavelengths.

For infra red quenching of photocapacitance, the second source was provided by a quartz halogen lamp powered by a 24 Vd.c supply with appropriate band pass and infra red absorbing filters at the window while the samlpes were being scanned with monochromatic light from the monochromator.

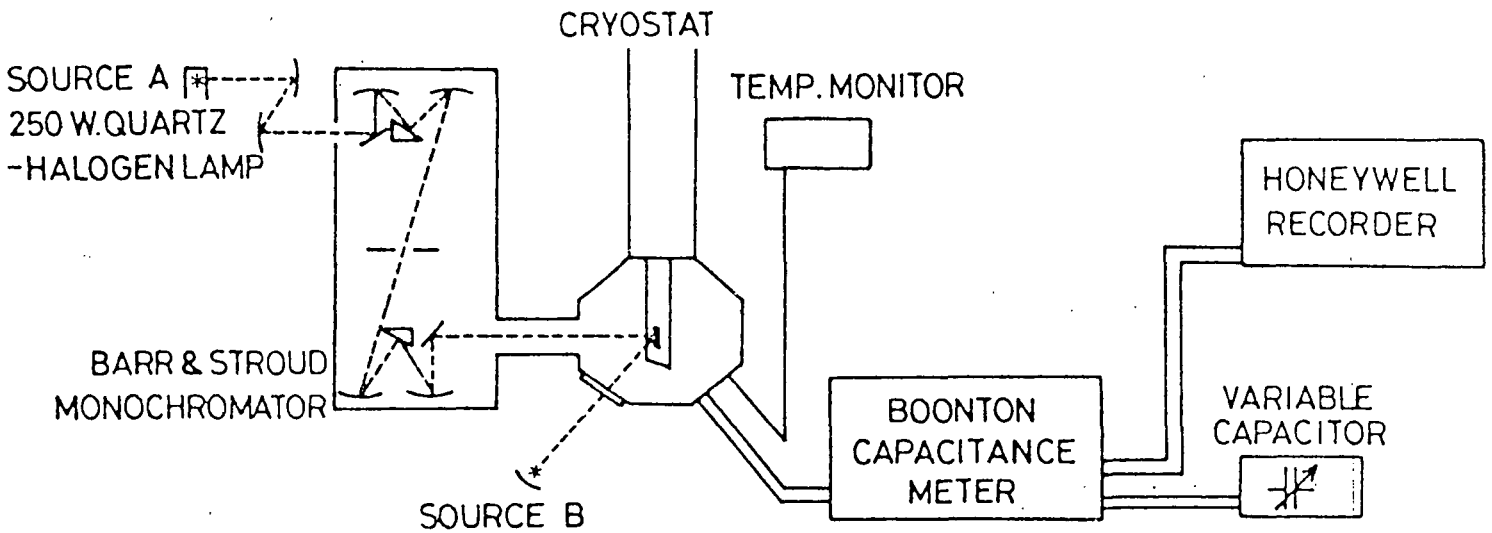

Figure 4.7. Experimental arrangement used for photocapacitance measurements.

References for chapter IV

1) L.Clark and J.Woods, J. Cryst. Growth, **14** (1968) 126

2) W.W.Piper and S.J.Polich, J. Appl. Phys., **32** (1961) 1278

3) S.Oktik, **PhD Thesis**, 1982, Durham University

4) H.G.Grimmeiss, N.Kullendorf and R.Broser, J. Appl. Phys., **52** (1981) 3405

5) G.H.W.Milburn, **X-ray Crystallography- An Introduction to the Theory and Practice of Single Crystal Structure Analysis** - Butterworth & Co. Ltd. 1973.

CHAPTER V

COMPOSITION AND STRUCTURAL STUDIES

5.1 Introduction

Solid solutions of $Zn_xCd_{1-x}S$ have been used in a considerable number of commercial applications as stated in chapter 2. By varying the composition of these solid solutions, it is possible to adjust their properties - for example to control the band gap or lattice parameter. The scope to vary the direct band gap, from 2.42 to 3.72 eV is of considerable potential interest for various opto-electronic devices. In some heterojunction solar cells, CdS has been successfully used as a window material. This is because CdS has a sufficiently high energy gap to transmit a large propotion of solar energy and can also be produced with low resistivity in the form of a thin film. $Zn_xCd_{1-x}S$, if it can be prepared with low resistivity, should be a more suitable window material than CdS. In fact if the proper zinc concentration is used, one can match the lattice constant or the electron affinity of the heterojunctions with Cu_2S. Matching the lattice constants of the two materials in a heterojunction is important if interface states are to be avoided.

In this chapter, the results of measurements made to determine the structure and composition of $Zn_xCd_{1-x}S$

solid solutions are presented. The general properties of the crystals grown in this department are described in section 5.2. The following section is devoted to a description of the determination of the composition of these solid solutions using AAS and EDAX. In mounting a study of a solid solution system, it is desirable to be able to determine compositions very quickly and non-destructively. This was possible using EDAX although this had first to be calibrated by comparison with AAS. The structural aspects and lattice parameter determination of the solid solutions are described in section 5.4, followed by band gap determination in 5.5.

5.2 The General Properties of The Crystals

The crystals of $Zn_xCd_{1-x}S$ used in this study were grown from the vapour phase either using the Clark-Woods method (sealed) or Piper-Polich method (open ended) as described in chapter 4 section 2. The colour of the mixed crystals of $Zn_xCd_{1-x}S$ was dependent on the composition of the solid solution. All the crystals were transparent, being colourless when $x>0.5$ and becoming gradually more yellow as the zinc concentration was reduced. Many boules showed a gradation of colour along their length indicating a progressive change in composition during growth. In general more zinc was incorporated in the later stages of growth. Many of the crystals that were zinc rich ($x>0.5$) were found to contain a large density of cracks which

caused optical scattering and consequently a loss of transparency. The crystals grown using the Piper-Polich method are designated by the letter HT followed by the crystal number (eg. HT 160). In some cases the figure in parenthesis under the sample heading indicates the position of the slices in the boules from which the measurements were taken. Crystals grown by the Clark-Woods technique are identified by a number only (i.e no 'HT').

5.3 Determination of Composition

The as-grown boules were normally cut into dice, degreased, etched (as described in chapter 4 section 3) and assessed by EDAX for compositional uniformity. The absolute composition of the mixed crystals was measured by using the AAS technique (chapter 4 section 6). Because of the destructive nature of this technique, this method was deployed after all other measurements on the samples had been completed.

A typical example of an EDAX spectrum can be seen in figure 5.1, which clearly shows the presence of the Cd Ll, the $ZnK\alpha$ and $K\beta$, and the $SK\alpha$ lines. The emission spectra of the elements present in the samples were usually accumulated over a period of several minutes and were displayed on a monitor. The relative intensities of the emission lines were measured directly from the printed spectra, taking care to substract the background levels

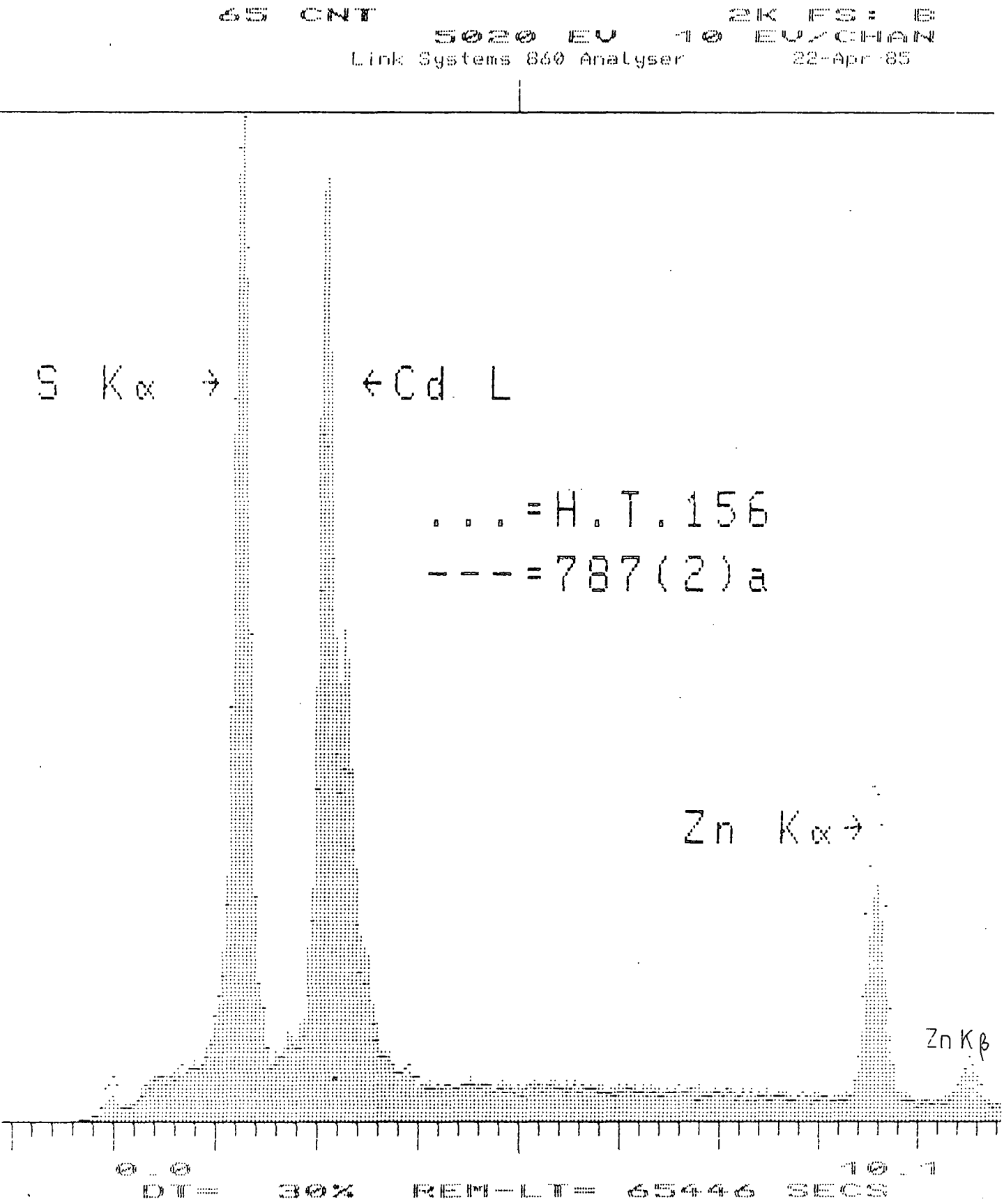

Figure 5.1. Typical EDAX spectra from $Zn_xCd_{1-x}S$ crystal.

from the peaks. The intensity of the $ZnK\alpha$ line cannot be compared directly with that of the CdL1 line to give an indication of the composition of the solid solution because the energies required to produce this characteristic x-ray are very different and this will lead to a difference in the probability of the excitation of the lines. For the samples which contained only a small amount of zinc, the scale could be enlarged so that the calculation of the relative intensities could be measured more accurately.

The use of EDAX to measure composition is very attractive because of the non-destructive and rapid nature of this technique. Normally such determinations are carried out using calibration curves of net intensity against composition derived from known standards. This becomes inappropriate in situations where the sample size, shape and take-off angle are radically different from those of the standard. Furthermore standards of the ternary $Zn_xCd_{1-x}S$ are not readily available. Consequently, it was decided to adopt a prodecure developed for binary systems by Bertin (1).

The prodecure makes use of the fact that the intensity (I) bears the following power law dependence with concentration (C),

$$I_a = K_a C_a^{na} \qquad 5.1a$$

$$I_b = K_b C_b^{nb} \qquad 5.1b$$

where K_a, K_b, na, and nb are constants for elements a and b. By taking the logarithm of the ratio of equation 5.1a and 5.1b, we have

$$\log \frac{I_a}{I_b} = \log \frac{K_a}{K_b} + na \log C_a - nb \log C_b$$

$$= \log K + na \log \frac{C_a}{C_b} - (nb-na)\log C_b \qquad 5.1c$$

if na=nb, the third term can be neglected, and equation 5.1c becomes

$$\log \frac{I_a}{I_b} = \log K + n \log \frac{C_a}{C_b} \qquad 5.1d$$

the third term only is important at large C_b, which introduces non-linearity in that range.

Thus the log-log plot of the intensity ratio and the composition ratio should be linear in a binary compound and independent of sample size, shape, etc. (5.1d). This technique may be extended to ternary compounds such as $Zn_xCd_{1-x}S$ provided that the third element (in this case, sulfur), does not preferentially absorb any of the x-ray fluorescence from either of the other two elements (zinc, and cadmium). In this study, the equation used for

relating the intensities of the x-ray spectra for $Zn_xCd_{1-x}S$ solid solutions is

$$\log \frac{I_{Zn}}{I_{Cd}} = \log K + n\log \frac{C_{ZnS}}{C_{CdS}} \qquad 5.2$$

where

I_{Zn} is the intensity of the ZnKα line

I_{Cd} is the intensity of the CdL1 line

C_{ZnS} and C_{CdS} are the fractional concentrations of ZnS and CdS in the $Zn_xCd_{1-x}S$ ternary respectively.

The ratios of the relative intensities of ZnKα and CdL1 lines are plotted against the composition ratios determined by the AAS technique (chapter 4 section 6) on logarithmic axes as shown in figure 5.2. The plot confirms a linear relationship as predicted by equation 5.1d.

5.4 Structure and Lattice Parameter Determination

The diffractometer traces shown in figure 5.3 were obtained from CdS and $Zn_{0.5}Cd_{0.5}S$. The positions of the peaks in the spectrum for the ternary of this composition indicated that, it had the hexagonal structure with lattice parameters smaller than those of CdS. In fact the structure of all the mixed crystals of $Zn_xCd_{1-x}S$ investigated with zinc composition up to x=0.85 was found to be hexagonal. For each composition studied, the lattice parameters a_o and c_o were calculated and are tabulated in

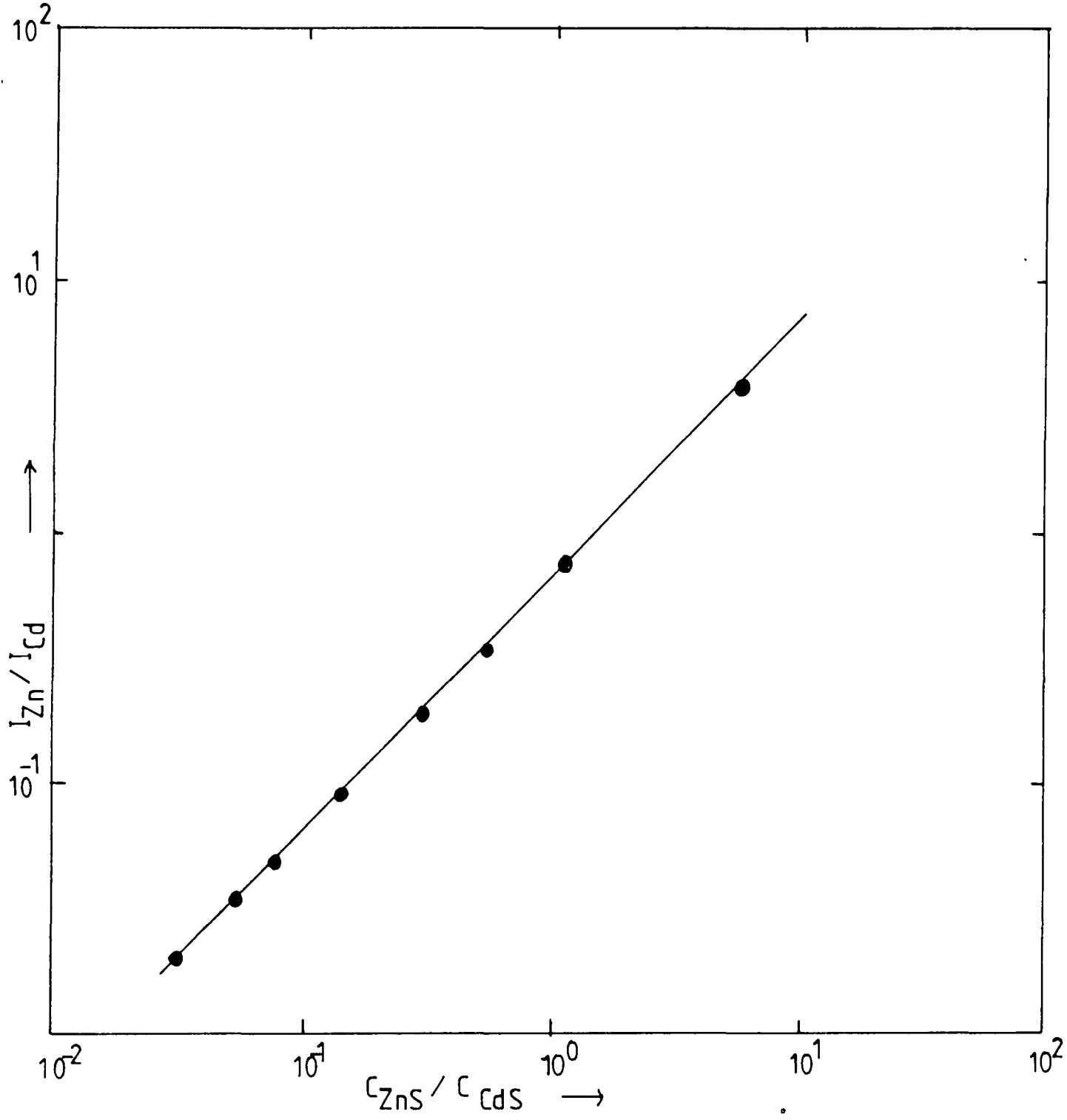

Figure 5.2. Intensity ratio measured from EDAX versus composition ratio measured from AAS.

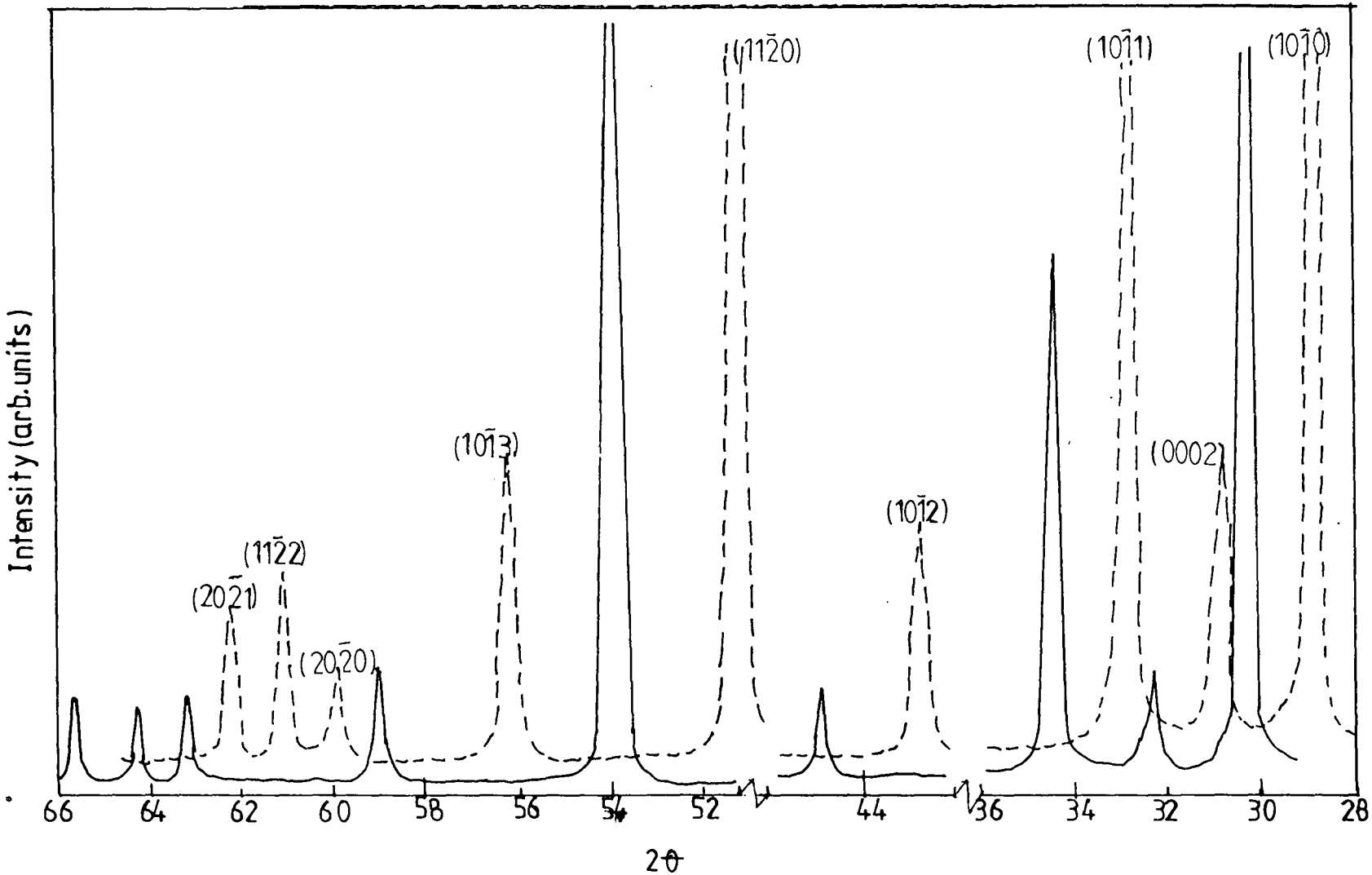

Figure 5.3. X-ray traces for $Zn_xCd_{1-x}S$, x=0 (-----) x=0.5 (——)

table 5.1 where the composition quoted is that determined by AAS. In contrast to the diffractometer traces from CdS and the mixed crystals with zinc content up to x=0.85, the diffractometer trace for ZnS, which is reproduced in figure 5.4, shows that the cubic form was present with a calculated lattice parameter of a=5.41Å. The values of the hexagonal lattice parameters a_o and c_o were then plotted as shown in figure 5.5 as a function of composition. Within the limits of experimental error, the relationship observed follows Vegard's law up to zinc content of x=0.85. The dependence of the lattice parameters of a_o and c_o on composition can be expressed as:

$$a_o = 4.136 - 0.34x$$

$$c_o = 6.705 - 0.46x$$

using a least square fit analysis. x is the mole fraction of zinc in $Zn_xCd_{1-x}S$.

5.5 **Band Gap Measurements**

Schottky diodes were prepared on substrates of different composition by melting indium on one surface to form an ohmic contact and evaporating gold on to the other face to produce a rectfying contact (chapter 4 section 3). These devices were then scanned very slowly especially in the region of the expected value of band gap. This was

x	a_o(Å)	c_o(Å)
0.00	4.139	6.719
0.05	4.127	6.690
0.07	4.113	6.677
0.12	4.093	6.595
0.24	4.052	6.615
0.35	4.009	6.554
0.52	3.955	6.464
0.85	3.853	6.306

Table 5.1. Calculated lattice parameters of hexagonal $Zn_xCd_{1-x}S$ crystals

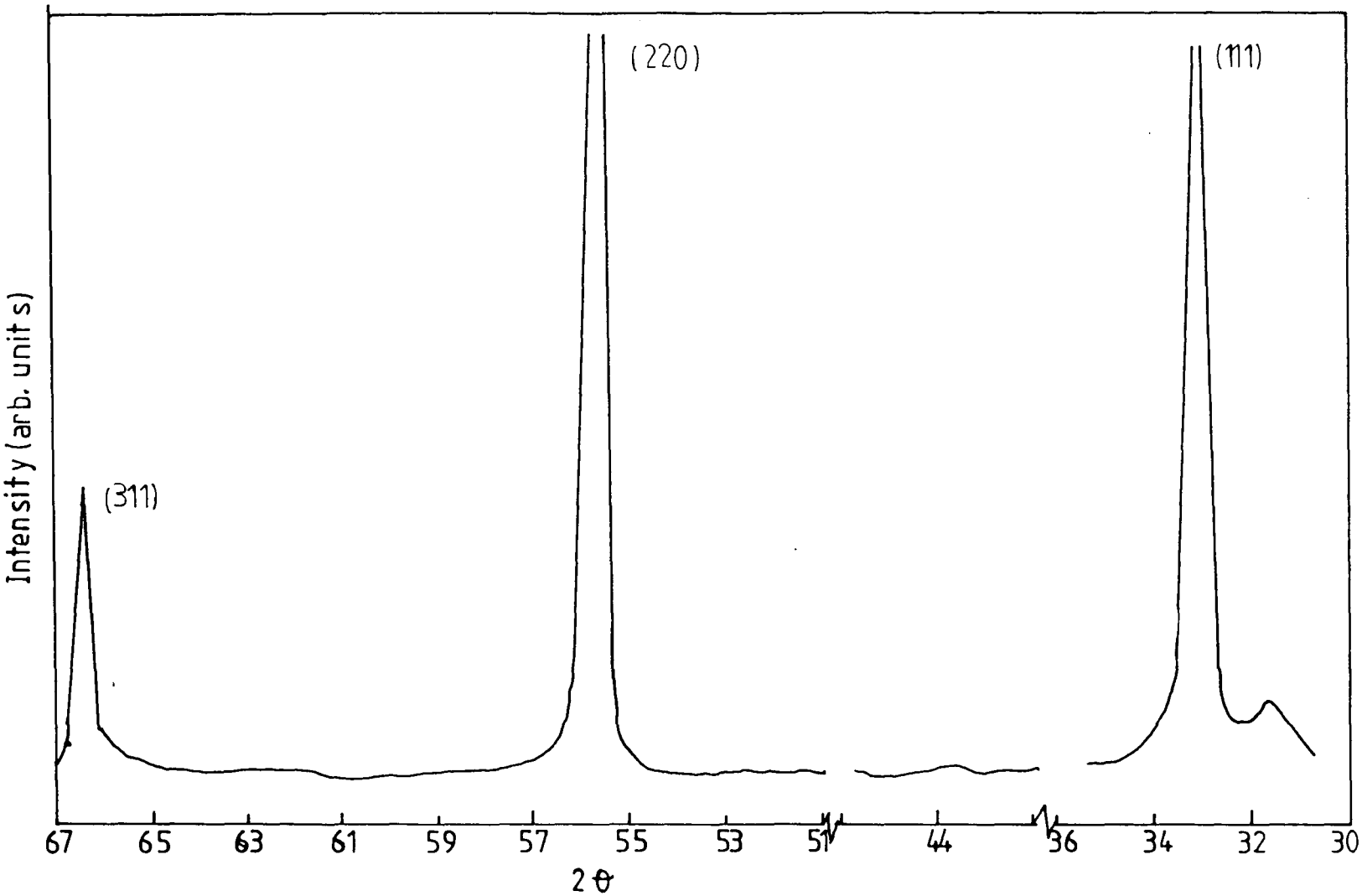

Figure 5.4. X-ray trace for ZnS.

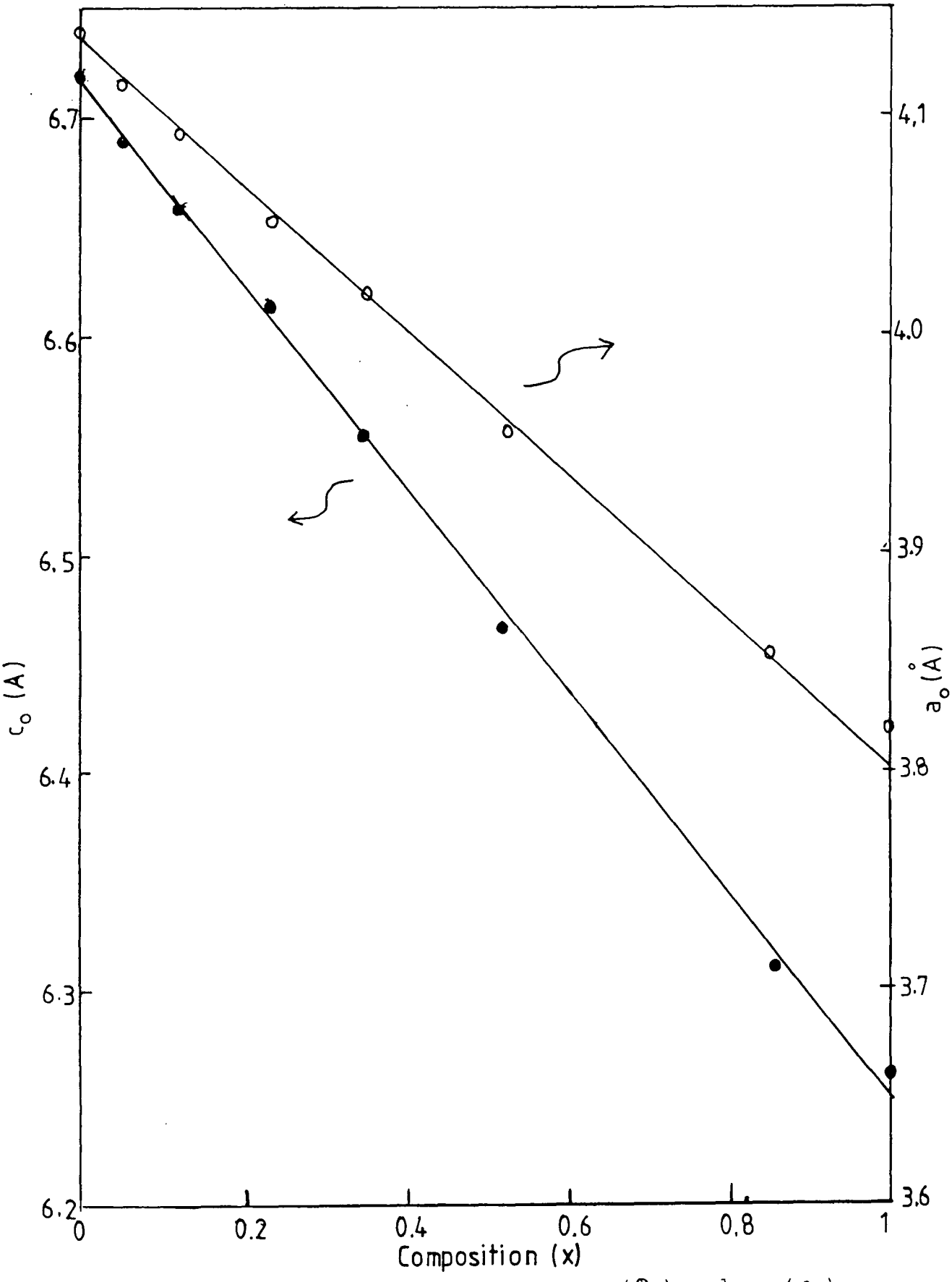

Figure 5.5. Lattice parameters a_o (Θ) and c_o (●) versus composition.

done in the front wall configuration, and the resulting short circuit current was measured at room temperature. Some typical results are shown as a function of photon energy of the incident light in figure 5.6. Generally two peaks were observed in the spectra, corresponding to the emission of the electrons over the metal-semiconductor barrier and generation in the bulk respectively. The barrier height measurements are discussed elsewhere in chapter 7.

This section is concerned with the measurement of the band gap energy, i.e. the high energy peak in the spectral dependence of short circuit current (figure 5.6). When the square root of the short circuit current was plotted against the incident photon energy, good straight lines were obtained for crystals of each composition as shown in figure 5.7. By extrapolating these lines to the energy axis, the values of the band gaps were obtained and these are presented in table 5.2. A nearly linear relationship of band gap with composition was obtained and is shown plotted in figure 5.8. Using a least square fit analysis, the variation of band gap with composition (x) is described as follows

$$E_g(x) = 2.43 + 1.28x$$

In addition it was apparent that the general trend was for the short circuit current of the Schottky diodes to

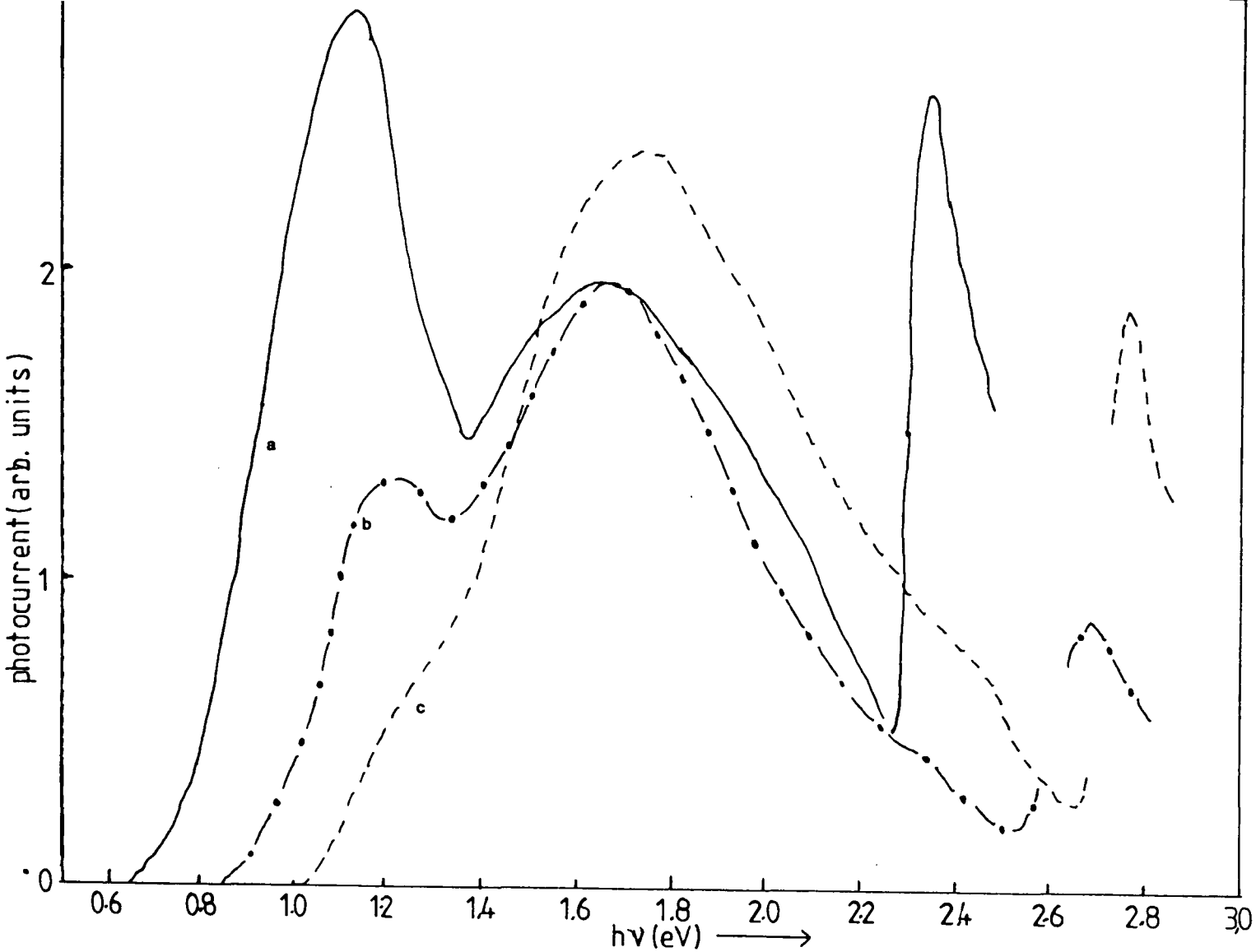

Figure 5.6. Short circuit photocurrent of Schottky diode against photon energy for a) x=0 b) x=0.25 and c) x=0.45.

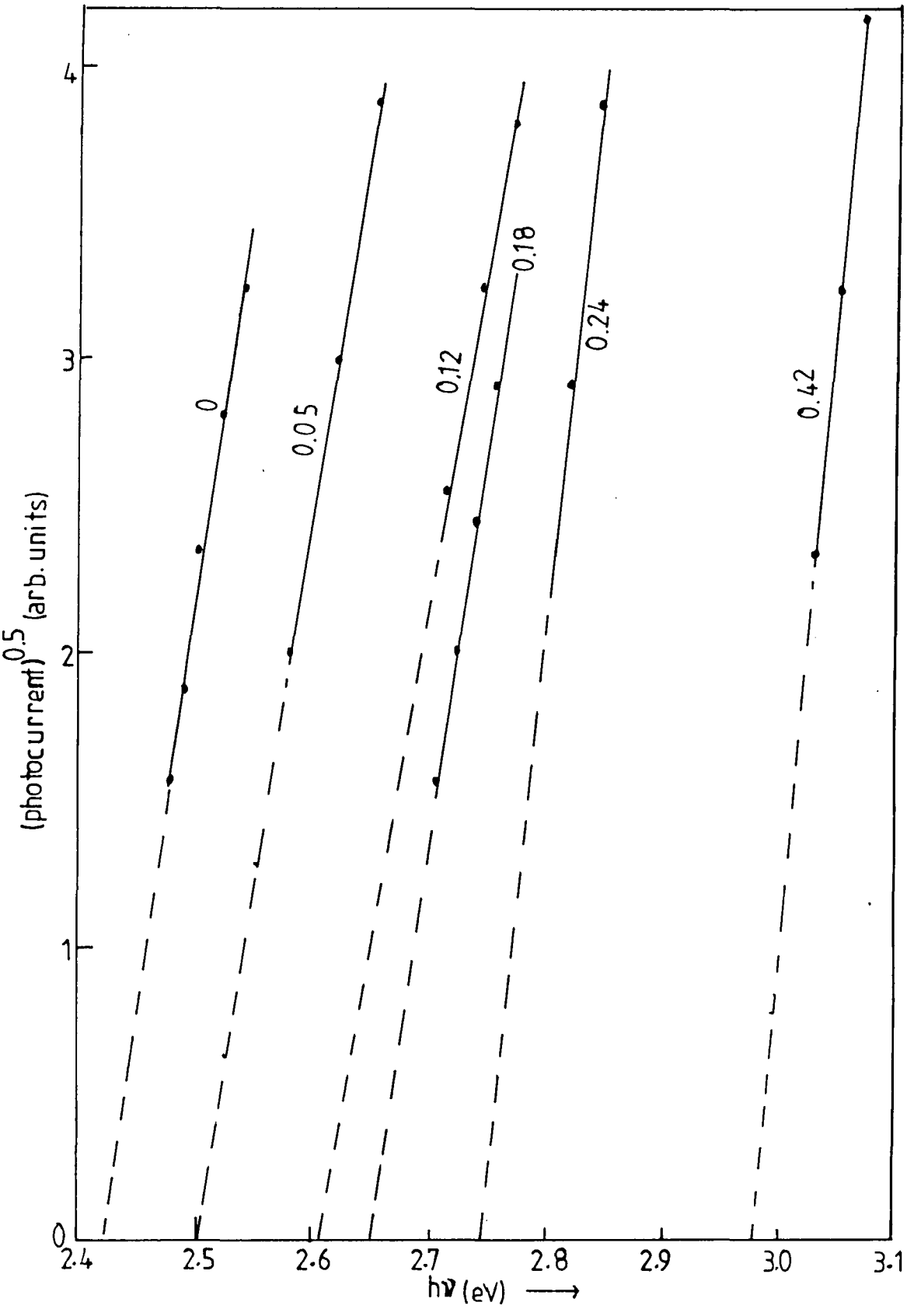

Figure 5.7. Square root of short circuit current against photon energy for different x.

x	E_g(eV)
0.00	2.42
0.05	2.48
0.07	2.50
0.12	2.62
0.18	2.65
0.24	2.75
0.35	2.87
0.42	2.98

Table 5.2. Band gap energy for different composition of $Zn_xCd_{1-x}S$ crystals

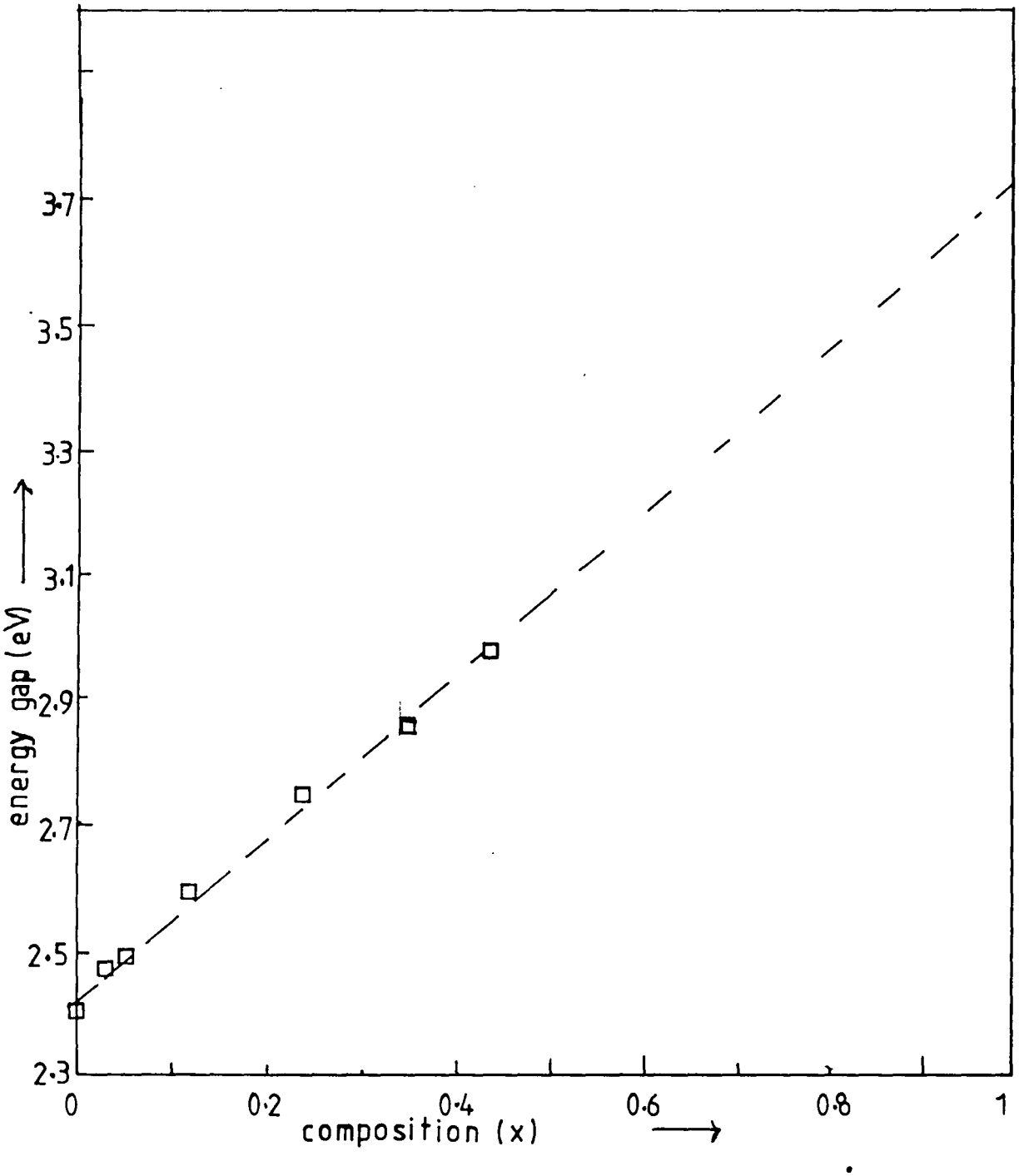

Figure 5.8. Band gap energy against composition.

decrease with increasing zinc content, which is indicative of the higher series resistance associated with these crystals. In fact because of this, it was impossible to prepare satisfactory Schottky diodes on as-grown mixed crystals of $Zn_xCd_{1-x}S$ with $x>0.5$.

5.6 **Discussion**

Good, uniform single crystals of the binary compound CdS have been successfully grown from the vapour phase in this department for some time past (2), using either Piper-Polich (sealed tubes) (3) or Clark-Woods (open ended silica tubes) (4) methods. However as discussed above the mixed crystals of $Zn_xCd_{1-x}S$ grown here were found to be non-uniform. This confirms previous work by Oktik et al (24) who found that a colour gradation along the length of such boules became apparent when the zinc content exceeded a value corresponding to $x=0.4$. The difficulties of growth are due to the fact that the CdS and ZnS starting materials have a large difference in melting point, so that at a given temperature, the vapour pressure of CdS is much greater than that of ZnS (5). Homogeneous crystals of $Zn_xCd_{1-x}S$ have been grown by Cherin et al (5) using chemical vapour transport with iodine. They also claimed that in the presence of iodine, the equilibrium constants for the reaction of ZnS and CdS with iodine are sufficiently similar to result in co-transport.

Difficulties are also ecountered in growing uniform thin films of $Zn_xCd_{1-x}S$. Singh and Jordan (21) found that with zinc compositions with x>0.7, films deposited by spray pyrolysis began to show signs of surface cracking. Epitaxial layers of $Zn_xCd_{1-x}S$ grown on ZnS by Sakurai et al (18) were only found to be smooth when the zinc content was low. With increasing zinc content, various disorder features including pits and facets were observed on the surface of the grown layer. In a recent publication, Duchemin et al (25) also reported difficulty in maintaining the crystallinity of $Zn_xCd_{1-x}S$ films prepared by spray pyrolysis as the zinc content was increased.

Since the crystals of $Zn_xCd_{1-x}S$ grown from the vapour phase are not homogeneous, a quick and non-destructive method to determine the composition of each piece of crystal studied was required. The methods normally used to determine the composition of solid solutions are x-ray powder diffraction and chemical analysis, both of which are destructive techniques (12,13,14). The method of energy dispersive analysis by x-rays (EDAX) described here demonstrates that the log-log plot of intensity ratios of x-ray emission lines of the ZnKα to CdL1 lines against the concentration ratio determined by the AAS technique gives a consistent relationship between the measurements made by the two independent techniques. Consequently, after establishing this relationship, it was possible to determine the composition of solid solutions

directly by non-destructive examination using EDAX. The CdL1 lines were chosen instead of the CdK_{α} line to compare with ZnK_{α} line because the electron beam energy was insufficient to excite the CdK_{α} line, and in any case the CdL1 and ZnK_{α} lines are closer in energy.

The advantages of this technique are its speed and independence of sample shape and size. Measurements made on $Zn_xCd_{1-x}Se$ (23) have been found to show a similar relationship between the ratio of the CdL1 and SeK_{α} lines with the concentration ratio of ZnSe and CdSe. The straight line dependence obtained for the $Zn_xCd_{1-x}S$ ternary in the log-log plot of figure 5.2 also indicated that selective absorption of the zinc or cadmium x-ray flourescence by the sulfur did not appear to be significant and the values of the constant n (see equation 5.1) for CdS and ZnS are quite similar.

CdS and ZnS can crystallise in either the cubic (sphalerite) or hexagonal (wurtzite) forms (6). CdS crystallises in a stable manner only in the hexagonal form (17). However single crystal films of cubic CdS have been reported to grow from the vapour phase by constraining their growth to specific planes of particular substrate crystals, for example on the {111} "P" face of GaP (24). With ZnS, wurtzite is the stable form for high temperature growth while sphalerite is the stable modification at lower temperatures. Temperatures of $1020^{o}C$ (7) and $1150^{o}C$

(8) have been reported for the transformatiom from the wurtzite to the sphalerite phase. However according to Vitrikhovskii and Mizetskaya (12), heating to temperatures at which sphalerite ZnS is supposed to transform into the wurtzite modification does not ensure complete transformation of cubic to hexagonal form.

From x-ray studies, the CdS crystals grown and used in this work were hexagonal with lattice parameters of a_o=4.139Å and c_o=6.719Å, in good agreement with values reported by Ibuki (9).

When working with ternary compounds, it is important to determine the relationship between the two binary components (i.e whether it is linear, sub linear, follows a particular equation or whether a gap occurs at certain compositions). For the mixed $Zn_xCd_{1-x}S$ crystals, the hexagonal phase was the only phase present in the samples which contained up to 85% zinc. This is consistent with the work of Cherin et al (5) on crystals of $Zn_xCd_{1-x}S$ grown using the iodine transport technique. These workers found that the structure did not become completely sphalerite until the zinc concentration had been increased to 95%. Samples with 85-95% zinc were found to contain mixed phases of both wurtzite and sphalerite. In another study of $Zn_xCd_{1-x}S$ crystals ($x<0.5$), Oktik et al (22) found from x-ray diffraction that their crystals were always wurtzite. Crystals of $Zn_xCd_{1-x}S$ grown by Ballentyne and

Ray (13) were also hexagonal up to 65% zinc, but the transition to sphalerite occurred between 65-85% zinc, while the crystals containing more than 85% zinc were completely sphalerite. For thin films of $Zn_xCd_{1-x}S$, Kane et al (14) reported that the change from hexagonal to cubic form occurred between 65-85% zinc for their vacuum evporated samples, while Agnihotri and Gupta (11) observed the presence of some sphalerite phase material in films containing up to 80% zinc. The wurtzite structure was also reported by Uchida (19) for $Zn_xCd_{1-x}S$ powdered samples across the whole range of composition.

In this investigation ZnS was found to exhibit the sphalerite phase with a value of lattice parameter a=5.41Å. This is in agreement with the value reported by Czyzak (10). Since the hexagonal lattice parameters of ZnS were not observed in this study, the values of the hexagonal lattice parameters of ZnS were estimated using the two following methods:

i) From a simple consideration of the close packing of atoms in face centred cubic and hexagonal structures, the relationships between the a_o and c_o lattice parameters of the hexagonal, and the a parameter of the cubic structure are given by,

$$c_o = \frac{2\sqrt{3}}{3} a \quad \text{and} \quad a_o = \frac{1\sqrt{2}}{2} a$$

Taking the value of a=5.41Å for ZnS, as was determined from the x-ray diffraction measurements, the corresponding values of a_o and c_o for hexagonal ZnS turn out to be 3.825Å and 6.247Å respectively.

ii) From the graph of lattice parameters against composition in figure 5.5, extrapolation of the straight line to the axis corresponding to 100% ZnS yields values of 3.80Å and 6.25Å for a_o and c_o respectively.

Both sets of values are in good agreement with each other and also with the values reported by Roth (6).

Previous measurements of the dependence of lattice parameters on composition for $Zn_xCd_{1-x}S$ single crystals (5,12), thin films (11,14) and powders (19), have suggested different behaviour from that reported here. For instance, the early measurements by Vitrikhoski and Mizetskaya (12) suggested that Vegard´s law did not hold but there was considerable scattering of the experimental points especially with the c_o parameter. Ballentyne and Ray (13) and Kane et al (14) found that the values of a_o and c_o deviated sublinearly from Vegard´s law for crystals and thin film material respectively. However measurements made by Cherin et al (5) on single crystals and Uchida (19) on powder samples indicated that the relationship did follow Vegard´s law as it does in the present work.

The nearly linear relationship of the band gap energy with composition observed for our $Zn_xCd_{1-x}S$ crystals containing up to 50% zinc is in agreement with a number of workers (11,14,16,20). Since the band gaps of our as-grown sample were measured from the short circuit currents of Schottky diodes as a function of incident photon energy, the measurements were limited to samples with zinc compositions not exceeding 50%. Samples containing more than 50% zinc were highly resistive, thus making it impossible to fabricate acceptable Schottky diodes. However extrapolation of the line in figure 5.8 to 100% zinc composition yielded a value for the band gap of hexagonal ZnS of 3.7eV. This is good agreement with the value given by Piper (26). Measurements by Kwok et al (20) on their chemically sprayed $Zn_xCd_{1-x}S$ thin films, show that the band gap varied linearly with zinc composition up to 50%. They estimated the band gap by making an extrapolation to the energy axis on the plot of relative photocurrent versus photon energy. Using band gap measurements derived from the maximum peak of photoconductivity, Vitrikhovskii and Mizetskaya (12) and Davis and Lind (15) found that the band gap varied monotonically with increasing zinc content.

Because of the compositional variation within some of the boules of $Zn_xCd_{1-x}S$, care had to be taken to ensure that the same samples were used for all of the measurements (i.e to establish the calibration curve). In this

investigation the measurements were usually taken in the following sequence.

i) EDAX

ii) Band gap from the Schottky diode study

iii)Lattice parameter from x-ray diffractometry

iv) Composition from AAS technique

In some of the published work (16,21), Vegard's law has been assumed to hold in order to determine the composition. Other workers (12,13) have used chemical methods to measure the composition but they have not clearly defined the technique used. In the work of Kane et al (14), compositions were determined indirectly by monitoring the amount of CdS and ZnS that evaporated from separate boats. Similarly with films of $Zn_xCd_{1-x}S$ produced by spray pyrolysis, the composition was assumed to refer to the varying composition of the spray solutions. According to Dachraoui and Vedel (27), the composition of the solid phase contained relatively more zinc than the liquid phase for films produced by spray pyrolysis.

5.7 Conclusion

A non-destructive method for the determination of the composition of mixed crystals of $Zn_xCd_{1-x}S$ grown from the vapour phase has been established. By using the relationship between the intensity of EDAX peaks and

composition determined by AAS, as shown in figure 5.2, the composition of zinc in the solid solutions can be estimated very quickly by simply measuring the ratio of intensities of Zn Kα to Cd L1 lines in the EDAX spectra.

The lattice parameters (both a_o and c_o) of the hexagonal crystals were found to show a linear dependence with zinc composition. From this behaviour, it may be concluded that the crystals grown were substitutional solid solutions. Also from x-ray diffraction studies, CdS and $Zn_xCd_{1-x}S$ for $x < 0.85$ were all found to exhibit the hexagonal form. The structure of $Zn_xCd_{1-x}S$ for x=0.86 to x=1 has not been determined because of the difficulty in growing crystals in this range.

The energy gaps which were determined by extrapolating the straight line plot of the square root of the short circuit current as a function of energy to intersect the energy axis, were linearly dependent of x. The short circuit current was also found to decrease with increasing x. Measurements of the energy gap by this method were limited to compositions up to $x<0.5$ because of the moderately high resistivity of the material containing a large proportion of zinc ($x>0.5$).

References for chapter V

1) E.P.Bertin, Anal. Chem., **34** (1964) 326

2) L.Clark and J.Woods, J. Cryst. Growth, **14** (1968) 126

3) G.J.Russell and J.Woods, J. Cryst. Growth, **46** (1979) 323

4) G.J.Russell, N.F. Thompson and J.Woods, J. Cryst. Growth, **71** (1985) 621

5) P.Cherin, E.L.Lind and E.A.Davis, J. Electro. Chem. Soc., **117** (1970) 233

6) W.L.Roth in **Physics and Chemistry of II-VI compounds**, edited by M.Aven and J.S.Prener. ch.3 (North-Holland pubilshing Co. 1967

7) E.T.Allen and J.L.Crenshaw, Z. Anorg. Chem., **79** (1913) 125

8) A.Addamiano and M.Aven, J. Appl. Phys., **31** (1960) 36

9) S.Ibuki, J. Phys. Soc. Jpn., **14** (1959) 1959

10) S.J.Czyzak, D.C. Reynolds, R.C. Allen and C.C. Reynolds, J. Opt. Soc. Am., **44** (1954) 864

11) O.P.Agnihotri and B.K.Gupta, Jpn. J. Appl. Phys., **18** (1979) 317

12) N.I.Vitrikhovskii and I.B.Mizetskaya, Soviet Phys., Solid-state, **2** (1961) 2301

13) D.G.W.Ballentyne and B.Ray, Physica, **27** (1961) 337

14) W.M.Kane, J.P.Spratt, L.W.Hershinger and I.H.Khan, J. Electro. Chem. Soc., **113** (1966) 136

15) E.A.Davis and E.L.Lind, J. Phys. Chem. Solids, **29** (1968) 79

16) N.Romeo, G.Sberveglieri and L.Tarricone, Appl. Phys. Lett., **32** (1978) 867

17) E.S.Rittner and J.H.Schulman, J. Phys. Chem., **47** (1943) 537

18) Y.Sakurai, Y.Kokubun, H.Watanabe and M.Kaka, Jpn. J. Appl. Phys., **16** (1977) 2115

19) W.Uchida, Phys. Stat. Sol(a)., **80** (1983) K199

20) H.H.L.Kwok, M.Y.Leung and Y.W.Lam, J. Cryst. Growth, **59** (1982) 421

21) V.P.Singh and J.F.Jordan, IEEE Elec. Dev. Lett., **EDL 2(6)** (1981) 137

22) S.Oktik, G.J.Russell and J.Woods, J. Cryst. Growth, **59** (1982) 414

23) A.Al.Bassam, A.W.Brinkman, G.J.Russell and J.Woods, **British Association For Crystal Growth**, Sussex Univ., Brighton, Sept. 1985

24) M.Weinstein, G.A.Wolf and B.N.Das, Apply.Phys. Lett., **6** (1965) 73

25) S.Duchemin, M.Kaka, J.Bougnot and M.Cadene, Thin Soild Film **136** (1986) 289

26) W.W.Piper, Phys. Rev., **92** (1953) 23

27) M.Dachraoui and J.Vedel, Solar Cells, **15** (1985) 319

CHAPTER VI

BULK PROPERTIES

6.1 Introduction

This chapter is devoted to the bulk electrical properties of crystals of $Zn_xCd_{1-x}S$ grown in this department. Measurements on the conductivity and Hall effect were carried out as a function of temperature on some samples. Results and discussions are presented in three sub-sections for a) x=0, b) $0<x<0.5$ and c) $x>0.5$. Conclusions are given in section 6.3.

6.2 Measurements of The Electrical Conductivity and Hall Coefficient

Measurements of electrical conductivity and Hall coefficient of $Zn_xCd_{1-x}S$ crystals for $x<0.45$ were made using the conventional d.c. method as described in chapter 4. The crystals used were found to have a room temperature conductivity in the range from 1.6×10^{1} $ohm^{-1}cm^{-1}$ to 1×10^{-3} $ohm^{-1}cm^{-1}$ depending on the composition ($0<x<0.45$). The conductivity of these samples was independent of illumination. Good ohmic contacts were easily made by brushing In-10% Cd with a fine wire on to the bars, and or by pressing indium dots on to the crystals and heating in an argon athmosphere at $300^{o}C$ for about 10 minutes. Figure

6.1a shows current-voltage curves for two samples taken from boules 820 and 826. The good straight lines obtained indicated that the contacts were ohmic. With samples with higher zinc contentrations it become more difficult to make good ohmic contacts as is clearly demonstrated in figure 6.1b, where the measurements were taken from different slices of boule HT 156 with zinc contentrations of about 45%. As can be seen, a good straight line was obtained up to 4-5 volts after which deviation from linear behaviour occurred as the applied voltage was increased. All measurements were taken at room temperature.

Measurements were also made of the dark conductivity and Hall coefficient as a function of temperature from room temperature down to about 100K. Since the properties were quite different from boule to boule, the results will be presented on a boule to boule basis:

a) **For x=0 (CdS)**

Two different samples of CdS were used in this experiment, one was a bar sample taken from boule 794 and the other was a clover leafed sample taken from boule 780. The room temperature conductivity was about 3.45 and 6.9 $ohm^{-1}cm^{-1}$ for 794 and 780 respectively. The variation of dark conductivity as a function of temperature showed maxima occurring at about 150-160K (figure 6.2a). From the

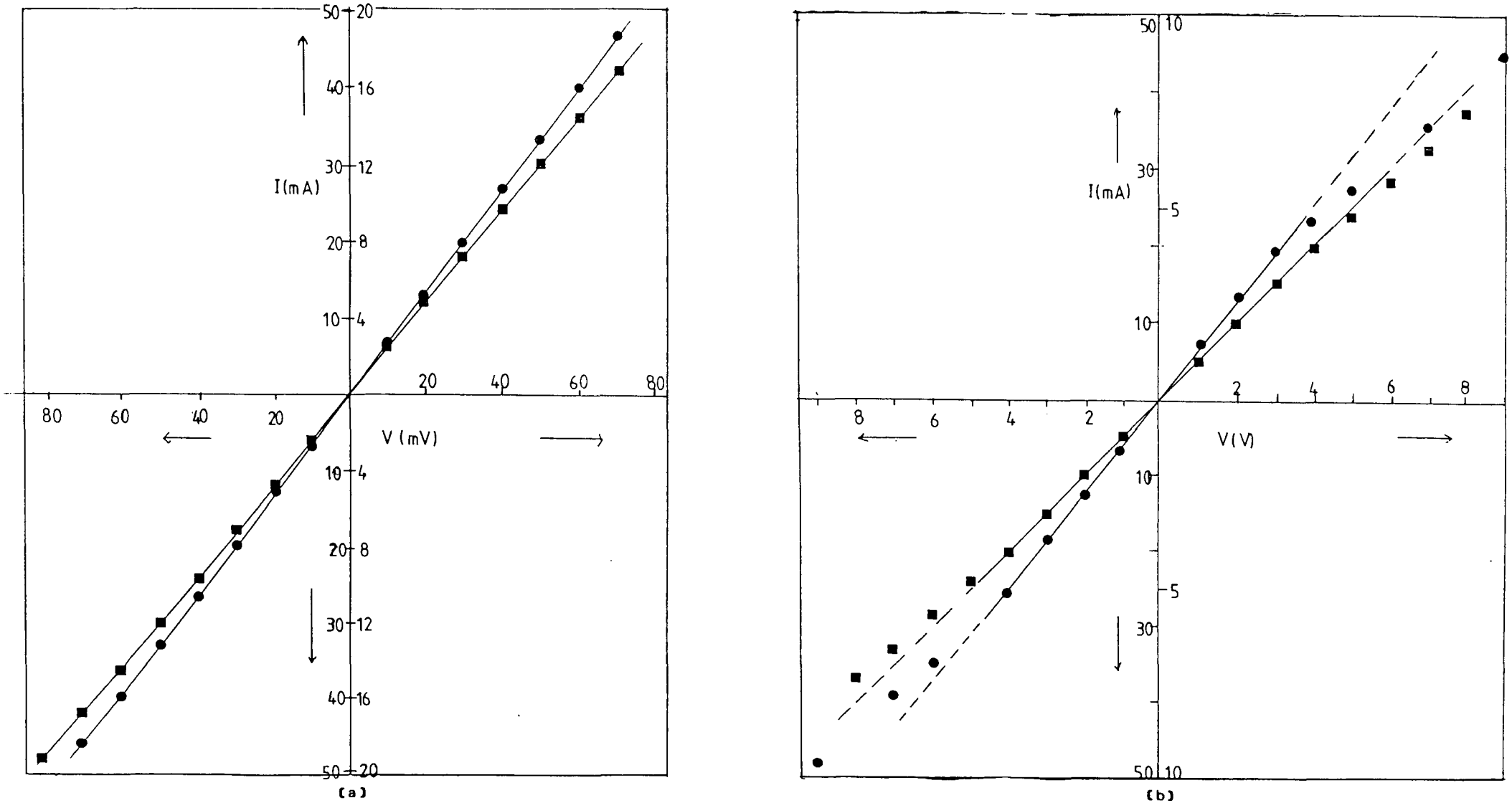

Figure 6.1. Current-Voltage curves for two indium contacts, a) from boule 820 (●) and 826 (■) and b) from two different slices of boule HT 156 {x=0.4 (■) and x=0.45 (●)}.

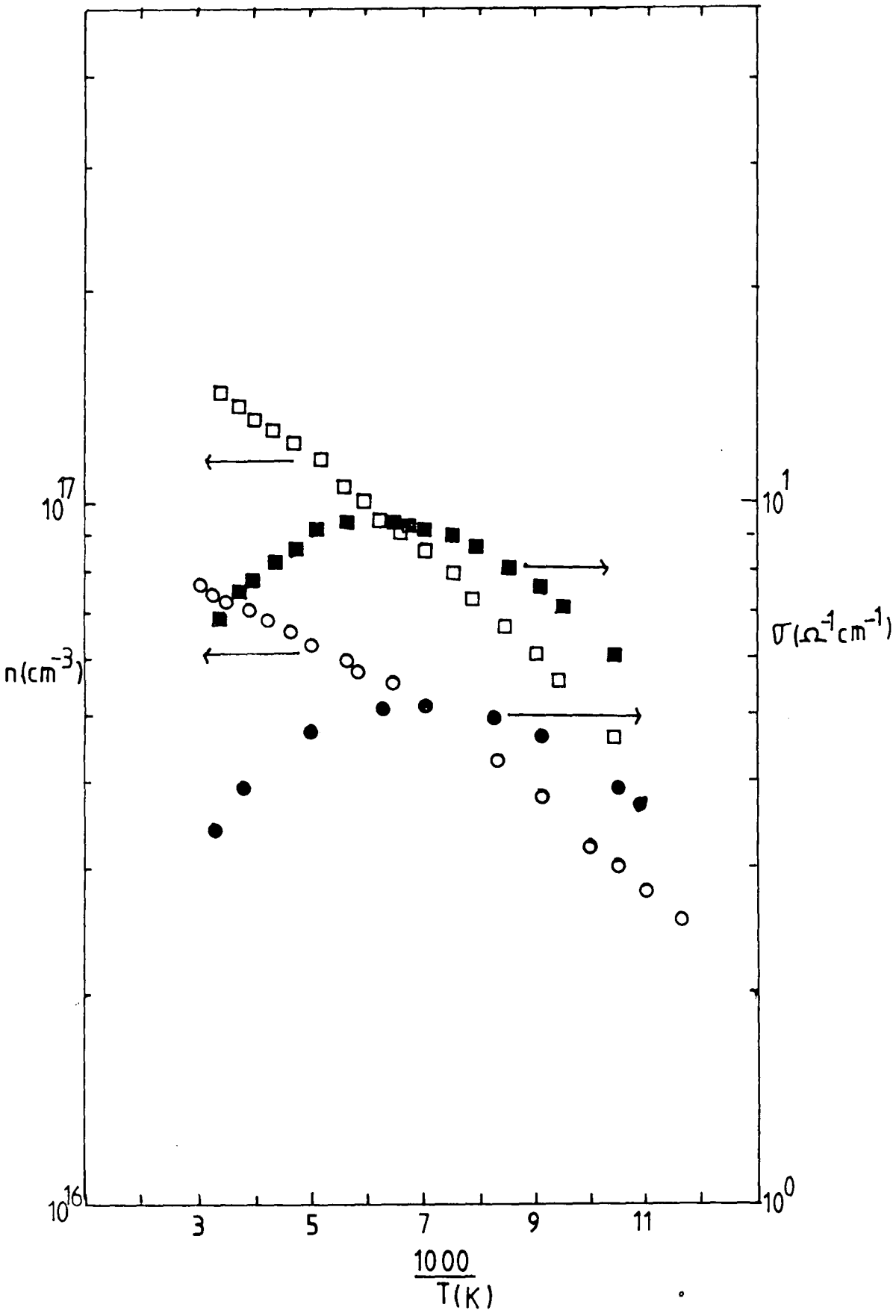

Figure 6.2a. Conductivity and carrier concentration versus reciprocal temperature for CdS (■ and □ for 780, ● and ○ for 794)

same figure, it is also evident that the carrier concentration (n) decreased from 1.45×10^{17} cm^{-3} at room temperature to 4.6×10^{16} cm^{-3} at about 95K for sample 780, and from 7.3×10^{16} cm^{-3} at room temperature to 2.5×10^{16} cm^{-3} at 90K for sample 794. n was calculated using the expression $n = r/R_H q$ where R_H is the Hall coefficient and q is the electron charge. The factor r is the ratio of Hall mobility u_H to drift mobility u which lies between 1 and 2 depending on type of scattering. Since in CdS, the scattering mechanism is limited by different types of scattering over different temperature ranges, the value of r used in this thesis was taken to be unity at all temperatures. The curves of ln n against reciprocal temperature, showed that both samples had two different slopes, corresponding to activation energies of 0.013eV and 0.009eV for 794, and 0.016eV and 0.012eV for 780 (If we neglect the $T^{1.5}$ dependence of N_C compared with the exponential dependence, the plot of ln n versus T^{-1} should give a straight line). The room temperature Hall mobilities calculated from $u_H = R_H \sigma$ were found to be about 300 $cm^2V^{-1}s^{-1}$ and 290 $cm^2V^{-1}s^{-1}$ for 780 and 794 respectively. When the temperature was reduced, the mobility increased to about 800 $cm^2V^{-1}s^{-1}$ at about 100K in both samples (figure 6.2b). The increases in mobility followed a relationship of the form $u_H \sim T^{-1}$ from 300K to about 150K. Below 150K, the Hall mobility seemed to follow a $T^{-0.5}$ trend.

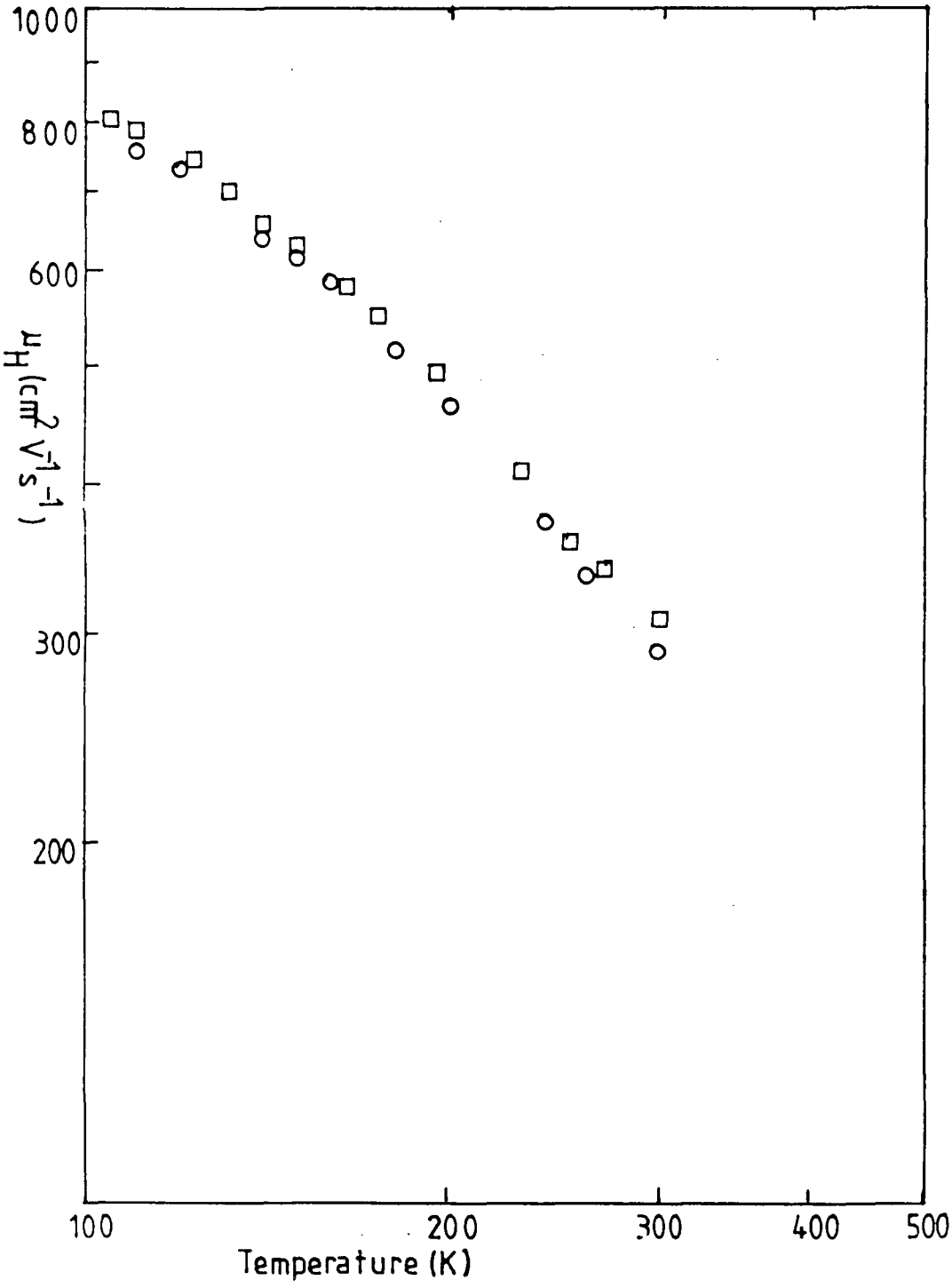

Figure 6.2b. Hall mobility against temperature for CdS (□ 780, ○ 794)

As mentioned earlier, the temperature dependence of the mobility gives some idea about the operative scattering mechanism which limits the carrier mobility. Before going to mixed crystals, an attempt was made to see how measurements on CdS fitted to the calculated values using constants available in the literature for CdS. For this purpose, the mobility limited by each of the scattering mechanisms discussed in chapter III will be given here:

i) **Acoustic mode scattering.** The electron mobility limited by this type of scattering alone (after substituting the parameters in equation 3.32) in $cm^2V^{-1}s^{-1}$ is;

$$u_A = 3.0x10^{-5} \rho C_L^2 [E_1^2 (m^*_e/m)^{2.5} T^{1.5}]^{-1}$$

with values of $\rho C_L^2 = 4.8x8.47x10^{11}$ dyne cm^{-2} (26)

$E_1 = 3.3eV$ (26)

and $m^*_e = 0.2$ m gives

$$u_A = 6.65x10^8 T^{-1.5} cm^2V^{-1}s^{-1}$$

At 300K, the mobility expected from this mode of scattering is $1.8x10^5$ $cm^2V^{-1}s^{-1}$ which is well over the experimental values obtained.

ii) **Polar optical mode scattering.** The mobility due to this type of scattering according to Howarth and

Sondhemier (27) is;

$$u_{OPT} = \frac{1}{2\alpha w_l} \frac{q}{m^*_e} \frac{8}{3\sqrt{\pi}\sqrt{z}} \psi(z) (e^z - 1)$$

where $z = \frac{hw_l}{kT}$ and the coupling constant $\alpha = \frac{q^2}{\hbar} \frac{m^*_e}{2\hbar w_l} \left[\frac{\epsilon_s - \epsilon_\infty}{\epsilon_s \epsilon_\infty}\right]$

Taking values of $w_l = 5.75 \times 10^{13}$ s^{-1} (w_l is the angular frequency of the longitudinal optical phonon), and $\psi(z) = 1$ for $z \ll 1$ and $\psi(z) = 3/8(\pi z)^{1/2}$ when $z \gg 1$,

ϵ_s and ϵ_∞ = 10.33 and 5.24 respectively

$m^*_e = 0.2m$

α is found to be 0.8 and the mobility at 300K due to this scattering alone is about 316 $cm^2V^{-1}s^{-1}$ which is of the same order as the experimental result. The variation of mobility caused by this type of scattering with temperature is also shown in figure 6.2c.

iii) **Piezoelectric scattering.** According to Huston (29), the mobility due to piezoelectric scattering in CdS follows

$$u_{PIE} = 120 (m/m^*_e)^{1.5} (300/T)^{0.5} \text{ cm}^2\text{V}^{-1}\text{s}^{-1}$$

taking $m^*_e = 0.2m$, mobility at 300K limited by this scattering mechanism is about 1.25×10^3 $cm^2V^{-1}s^{-1}$.

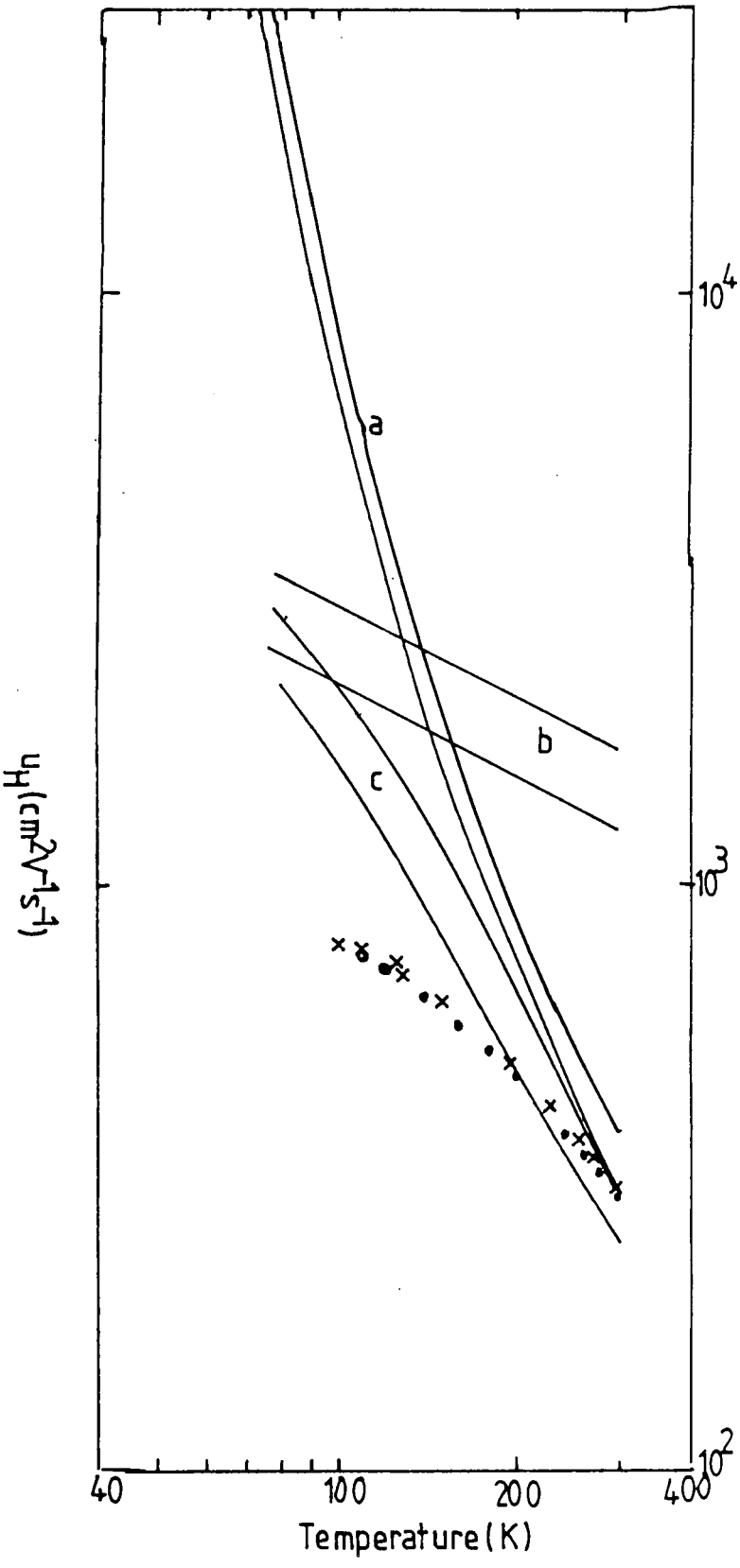

Figure 6.2c. Calculated mobility due to a) optical mode, b) piezoelectric and c) combination of a and b scattering (solid line) together with experimental points.
Upper curve m^*_e=0.17m (for a,b and c).

Lower curve m^*_e=0.21m (for a,b and c).

iv) **Impurity scattering.**

The mobility associated with ionised impurity scattering increases with temperature and also very much depends on the concentration of ionised impurities N_i, while the mobility due to neutral impurity scattering is independent of temperature and normally occurs at very low temperature. In order to estimate the mobility associated with ionised impurity scattering, a knowledge of n, N_d, N_a and N_i at particular temperatures is needed. No attempt was made to estimate those values. However assuming that the calculated values reported by Subhan et al (24) are to be expected because they were using crystals grown by the same method as here, the mobility at 300K would be very much higher than the values obtained here.

Using Mathiessen's rule (15) to combine the effects of polar optical and piezoelectric scattering to give $u^{-1}=u_{opt}{}^{-1}+u_{pie}{}^{-1}$, a mobility of 257 $cm^2V^{-1}s^{-1}$ was obtained assuming $m^*_e=0.2m$. This compares with the values of 290-300 $cm^2V^{-1}s^{-1}$ measured experimentally. If extreme values of $m^*_e=0.17m$ and 0.21m are used, mobilities of 303 and 245 $cm^2V^{-1}s^{-1}$ would be expected which lie in the region of mobility found experimentally. When the temperature variation of mobility is considered assuming $m^*_e=0.17m$ and 0.21m, the calculated mobilities ($u^{-1}=u_{OPT}{}^{-1}+u_{PIE}{}^{-1}$) plotted together with the experimental points agree quite well down to 200K but beyond this point, the measured

mobility fell away quite considerably (figure 6.2c). Clearly ionised impurity scattering was then becoming significant.

Discussion

The excellent photoconductive and luminescent properties of CdS have made it arguably the most thoroughly investigated of II-VI compounds (5,6) but relatively little attention has been paid to its electrical transport properties (7-13). The room temperature conductivity has often been found to vary from boule to boule, and is very much dependent on the growth conditions. The effect of the growth conditions on the conductivity of CdS crystals grown by the same method as that used here has been carried out by Subhan et al (24). Using an ultra high grade purity crystal from Eagle Picher, Morimoto et al (13) showed that the resistivity decreased as the temperature decreased from 300K to about 100K and thereafter increased as the temperature was further reduced. A similar variation was also observed in this work. Other work by Crandall (7), Toyotomi and Morigaki (8) and Subhan et al (24) also showed the same trend with crystals grown from the vapour phase. This is almost entirely due to the changes in mobility ($\sigma = nuq$) while n does not change very much with decreasing temperature in this range.

From the slope of the plots of ln n against

reciprocal temperature, it was found that the Durham crystals apparently had two different shallow donor activation energies with values ranging from 0.009eV to 0.013eV. These values fall well within the range reported in the literature which lie between 0.007eV and 0.021eV (7,8,11,13,14). Crandall (7) reported a value of 0.021eV in his undoped crystals, which he associated with an excess of cadmium, while Itakura and Toyoda (14), in work rather similar to that reported here found two activation energies of 0.007eV and 0.014eV. Clark and Woods (25) also found the shallow donors to have an activation energy of 0.014eV in their crystals grown from the vapour phase. It would appear that the shallow donors present in the Durham crystals are also associated with an excess of cadmium.

The Hall mobility of the Durham CdS crystals was about 290-300 $cm^2V^{-1}s^{-1}$ at room temperature. This value is in reasonable agreement with those reported in the literature. Woodbury (12) and Morimoto et al (13) reported values of about 300 $cm^2V^{-1}s^{-1}$, while Crandall (7) found that a mobility as high as 350 $cm^2V^{-1}s^{-1}$ can be achieved, but in the work of Itakura and Toyoda (14) a mobility as low as 240 $cm^2V^{-1}s^{-1}$ was reported. With CdS crystals grown under different conditions, Subhan et al (24) reported that mobilities ranging between 250-400 $cm^2V^{-1}s^{-1}$ were observed at room temperature.

Work on the temperature dependence of mobility has

been carried out by several authors (7-14). According to Piper and Halsted (11), the Matthiessen's rule explained their results very well, and they concluded that optical phonon and piezoelectric scattering were the two dominant mobility limiting processes in their crystals if m^*_e=0.16m. But if m^*_e=0.2m was used, scattering due to optical phonon alone fitted well with the experimental points. Scattering due to the combination of the optical phonon and piezoelectric mechanism was also supported by Fujita et al (10) using m^*_e=0.19m and by Devlin using m^*_e=0.2m (16). Observations by Itakura and Toyoda (14) suggested that acoustical phonon scattering was more important in their crystals since they found experimentally that $u_H = 6.4 \times 10^4 T^{-1.5}$ from 200K to 50K. Below 50K u_H decreases as temperature decreases. Subhan et al (24) also used Matthiessen's rule and showed that three scattering processes, i.e. polar optical mode, piezoelectric and ionised inpurity scattering fitted well with the calculated values in one of their samples by using m^*_e=0.19m.

As discussed above, m^*_e is used as an adjustable parameter to give a good fit between the experimental and calculated mobilities. When two extreme values of m^*_e are used (m^*_e=0.17m and 0.21m), the calculated Hall mobilities fall within the experimental range of values from 300K to about 200K. This suggests that optical phonon and piezoelectric scattering were the dominant processes in our crystals in that temperature range. Beyond this

temperature, the experimental Hall mobility was rather low compared with the calculated value and this could be attributed to neglecting ionised impurity scattering.

b) **0<x<0.5**

i) **Crystal 789**

This boule was grown in an attempt to produce a crystal with the composition $Zn_{0.2}Cd_{0.8}S$, but after growth, the zinc content was found to vary between x=0.05 to x=0.15 from one end to the other. However it was possible to cut as many as five bars from this boule with x=0.05, 0.06, 0.07, 0.09 and 0.1. Room temperature conductivities were found to vary from 7.2 to 16.5 $ohm^{-1}cm^{-1}$. On cooling, the conductivities reached their maximum values at about 160K and then decreased as the temperature decreased further (figure 6.3a). From the Hall coefficient measurements, the room temperature carrier concentrations were found to vary between 2.5 and $3.7x10^{17}$ cm^{-3}. From the plots of ln n against reciprocal temperature which were fairly linear over the whole range (figure 6.3b), the shallow donor activation energies were found to vary between 0.009eV and 0.011eV. The values of room temperature mobility varied between 200 $cm^2V^{-1}s^{-1}$ and 285 $cm^2V^{-1}s^{-1}$. With decreasing temperature, the mobilities increased steadily as $u_H \sim T^{-1}$ from 300K to about 200K and as $u_H \sim T^{-0.5}$ from 200K to 150K. They then remained pratically unchanged down to 100K

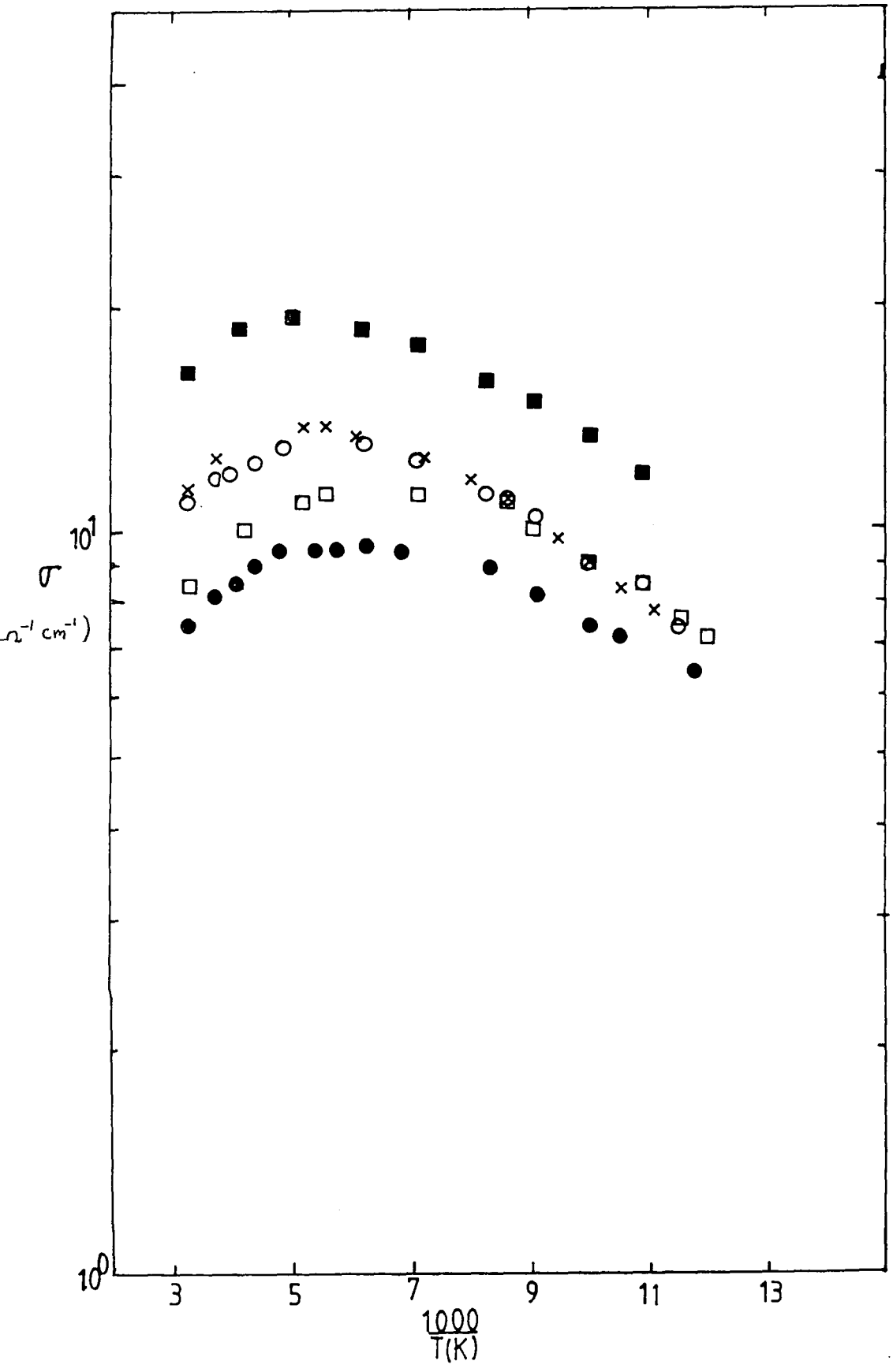

Figure 6.3a. Conductivity against reciprocal temperature for boule no.789 (■ x=0.05, ○ x=0.06, ● x=0.07 X x=0.08 and □ x=0.1).

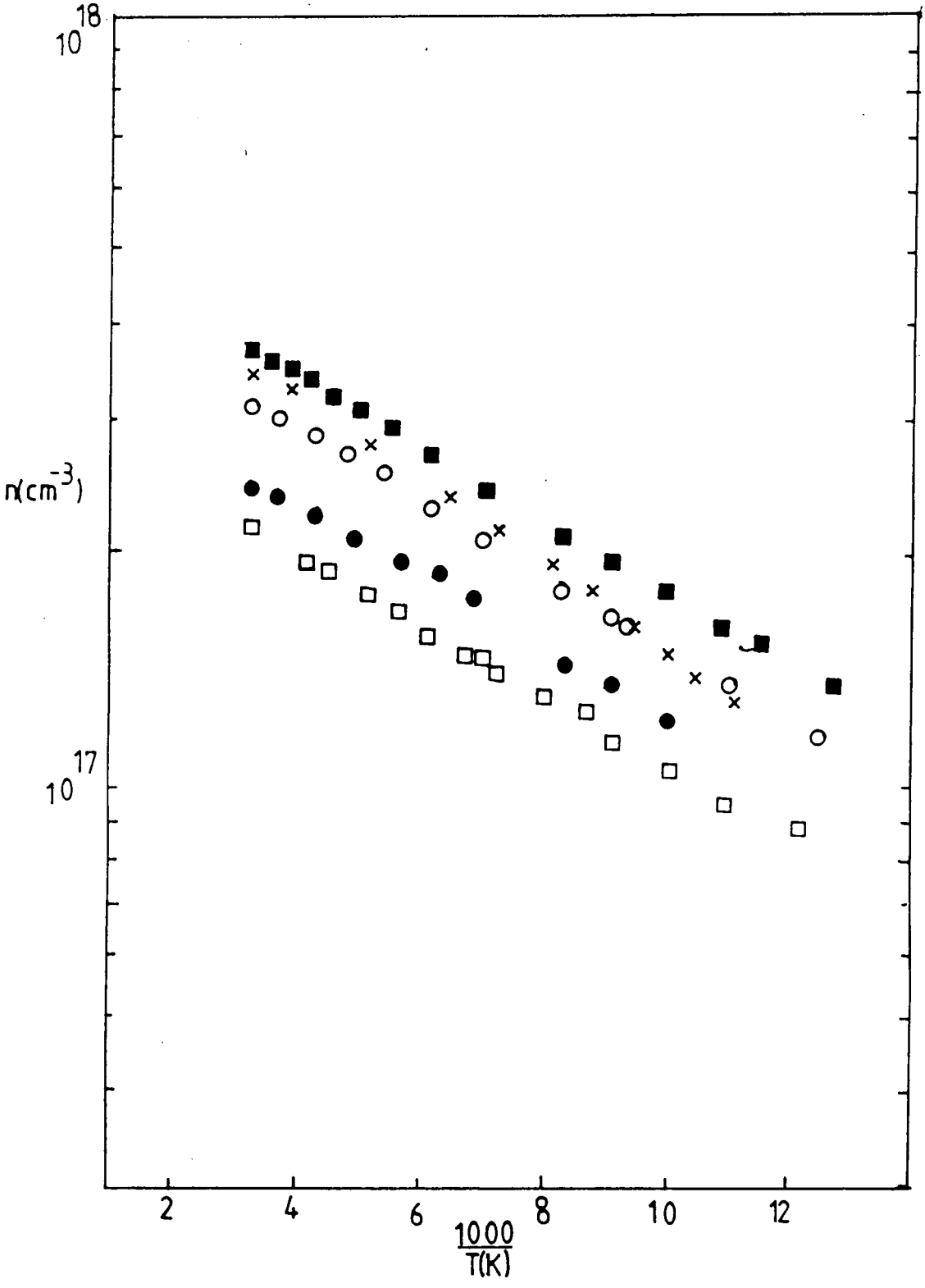

Figure 6.3b. Carrier concentration against reciprocal temperature for boule no. 789
(for key see figure 6.3a)

(figure 6.3c).

ii) **Crystal 826**

The nominal composition of this boule was $Zn_{0.3}Cd_{0.7}S$. Since the boule was of good crystalline quality and quite uniform, it proved possible to cut a clover-leafed sample from it. The zinc content of this particular slice was x=0.12. The room temperature conductivity was about 1.7 $ohm^{-1}cm^{-1}$. As the temperature was decreased the same general trend as for the crystals described earlier was observed (figure 6.4a). The plot of ln n against reciprocal temperature in figure 6.4a indicated an activation energy of 0.013eV. The Hall mobility was about 255 $cm^2V^{-1}s^{-1}$ at room temperature, increasing to its maximum value of about 435 $cm^2V^{-1}s^{-1}$ at 190K. Beyond this temperature it decreased to about 300 $cm^2V^{-1}s^{-1}$ at 100K (figure 6.4b).

iii) **Crystal HT 157**

The composition of the charge from which this crystal was prepared was x=0.4, but after growth the crystal was clearly non-uniform and only one bar with x=0.15 could be obtained. The room temperature conductivity was about 3.4 $ohm^{-1}cm^{-1}$. Once again the conductivity increased to a maximum as the temperature was reduced as shown in figure 6.4a. The plot of ln n against

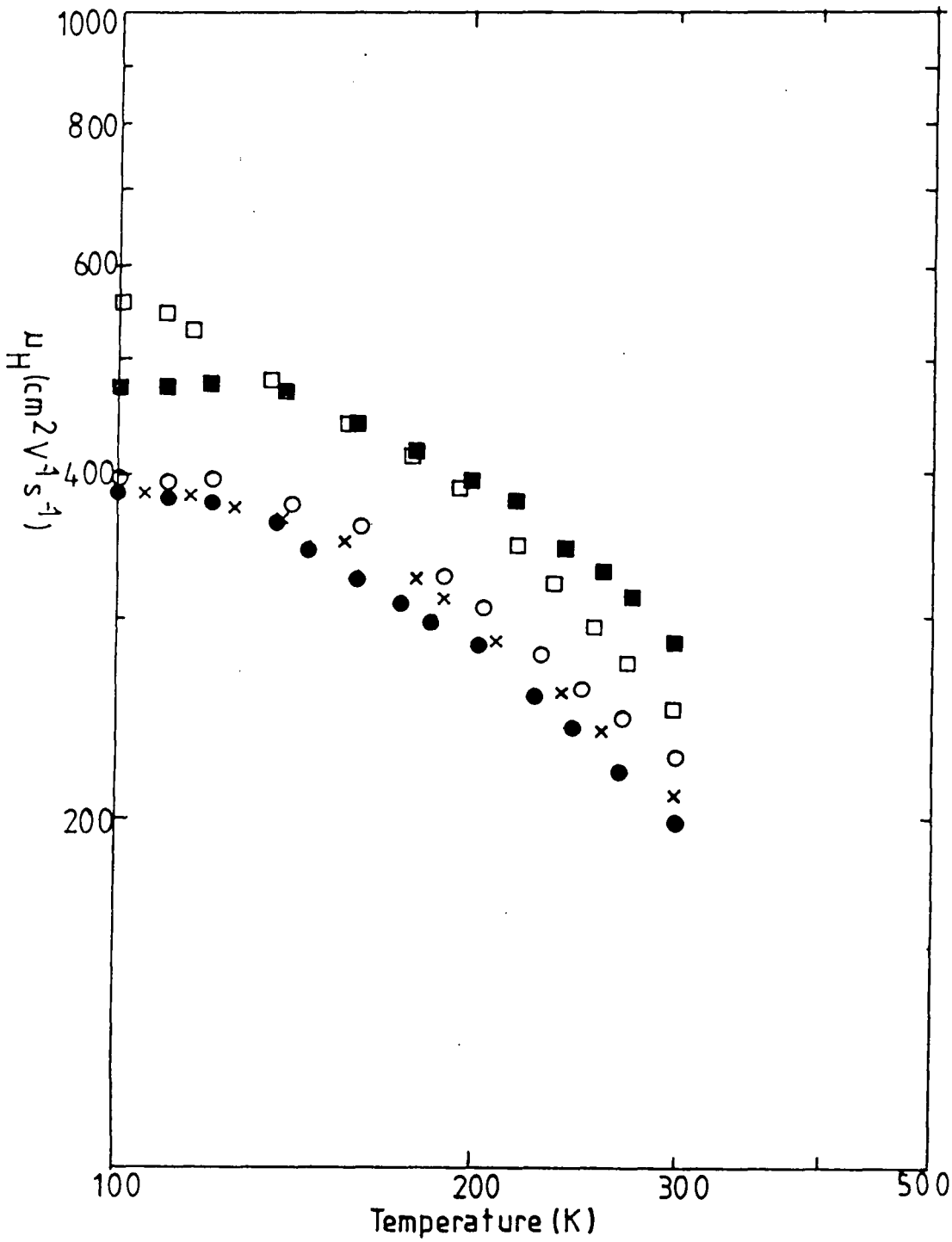

Figure 6.3c. Hall mobility against temperature for boule no.789 (for key see figure 6.3a)

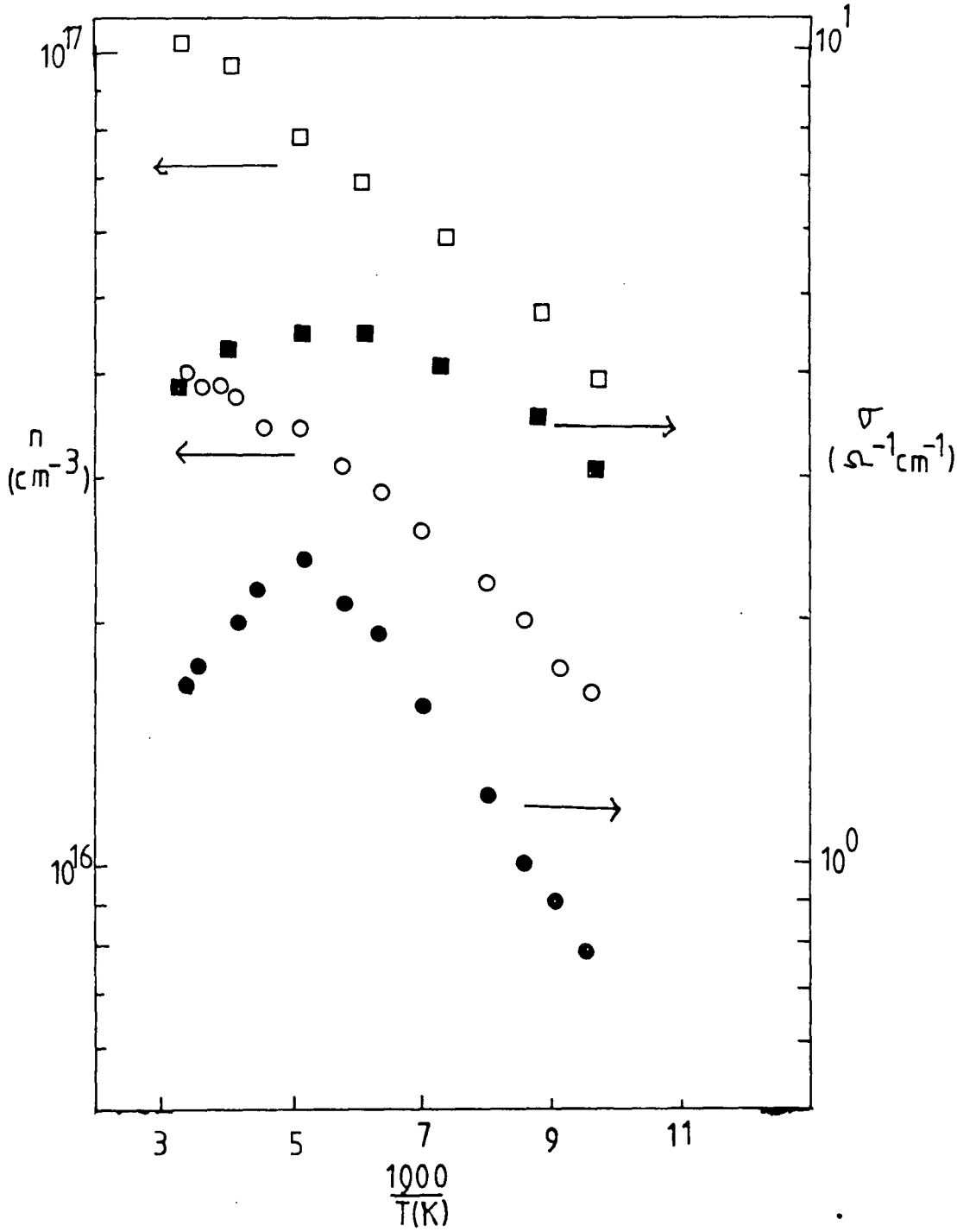

Figure 6.4a. Conductivity and carrier concentration against reciprocal temperature for a) ● ○ x=0.12 (826) and b) ■ □ x=0.15 (HT 157)

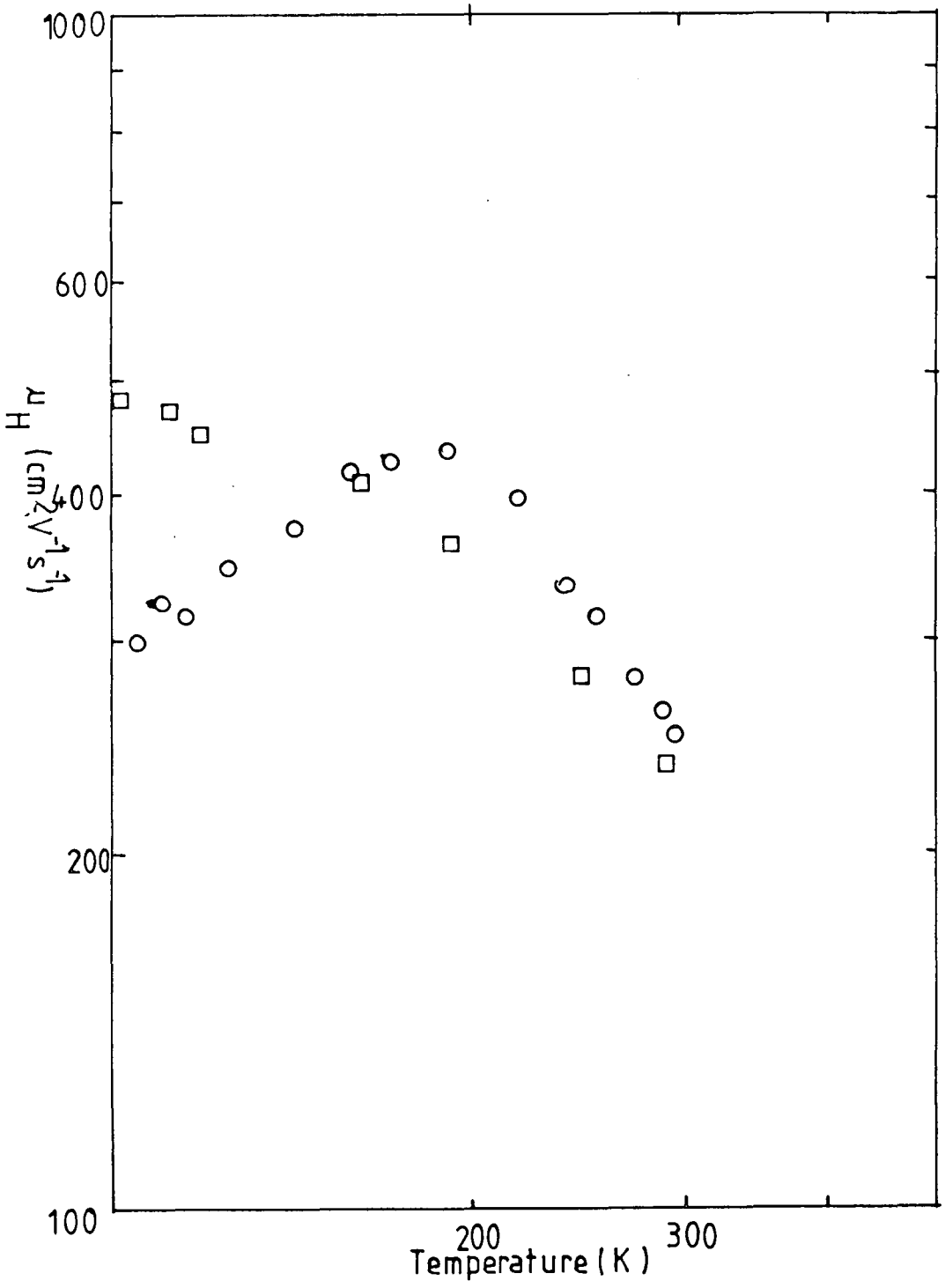

Figure 6.4b. Hall mobility versus temperature for x=0.12, ○ (826), and x=0.15, □ (HT 157).

T^{-1} was linear with an activation energy of 0.013eV. The room temperature mobility was 235 $cm^2V^{-1}s^{-1}$, and the behaviour was similar to that of the other samples with low zinc content, with u_H varying as T^{-1} down to about 190K and as $T^{-0.5}$ down to 100K (figure 6.4b).

iv) **Crystal 787**

The nominal composition of this boule was x=0.3, but after growth, the variation in composition was between x=0.15 and x=0.3. Three bars were cut from this boule with x=0.2, 0.22 and 0.25. In contrast with all other samples the curves in figure 6.5a show that the dark conductivity decreased with decreasing temperature quite rapidly when the temperature was reduced from 300K to 200K, and then more slowly as the temperature fell to about 100K.

Plots of ln n against reciprocal temperature were quite linear (figure 6.5b), with activation energies of 0.01, 0.009 and 0.007eV for x=0.2, 0.22 and 0.25 respectively. Room temperature mobilities varied between 5.5 $cm^2V^{-1}s^{-1}$ and 40 $cm^2V^{-1}s^{-1}$. With decreasing temperature, the Hall mobility decreased, for example for x=0.2, the Hall mobility decreased from 38 $cm^2V^{-1}s^{-1}$ at 300K to about 5 $cm^2V^{-1}s^{-1}$ at 150K. For x=0.22 and 0.25 the slope of the curves following $u_H \sim T^{1.5}$ approximately from 300 to about 200K. In this range a plot of $\ln \sigma T^{-3}$ against T^{-1} give quite a good straight line from which activation

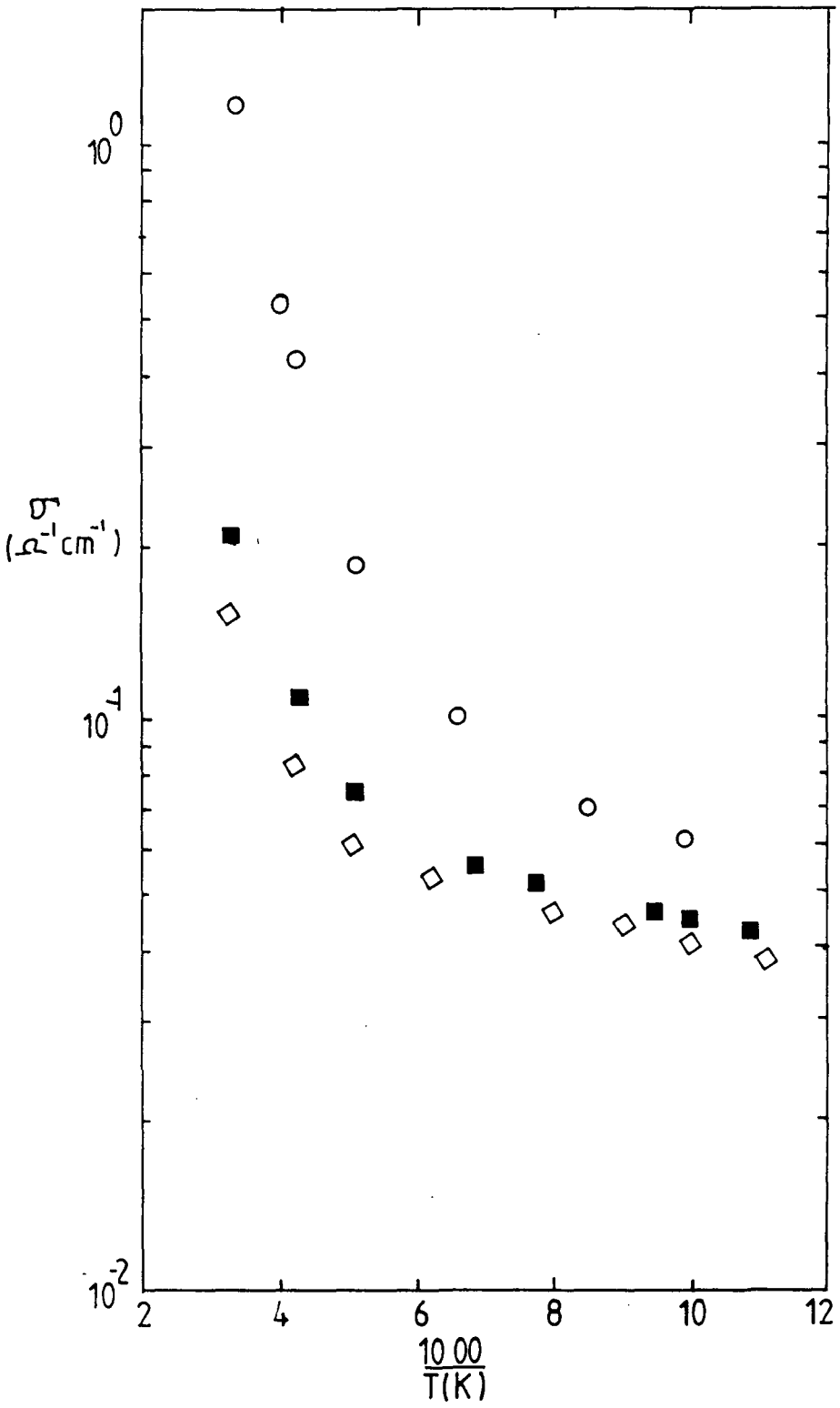

Figure 6.5a. Conductivity against reciprocal temperature for boule 787 (○ x=0.2, ■ x=0.22 and ◇ x=0.25)

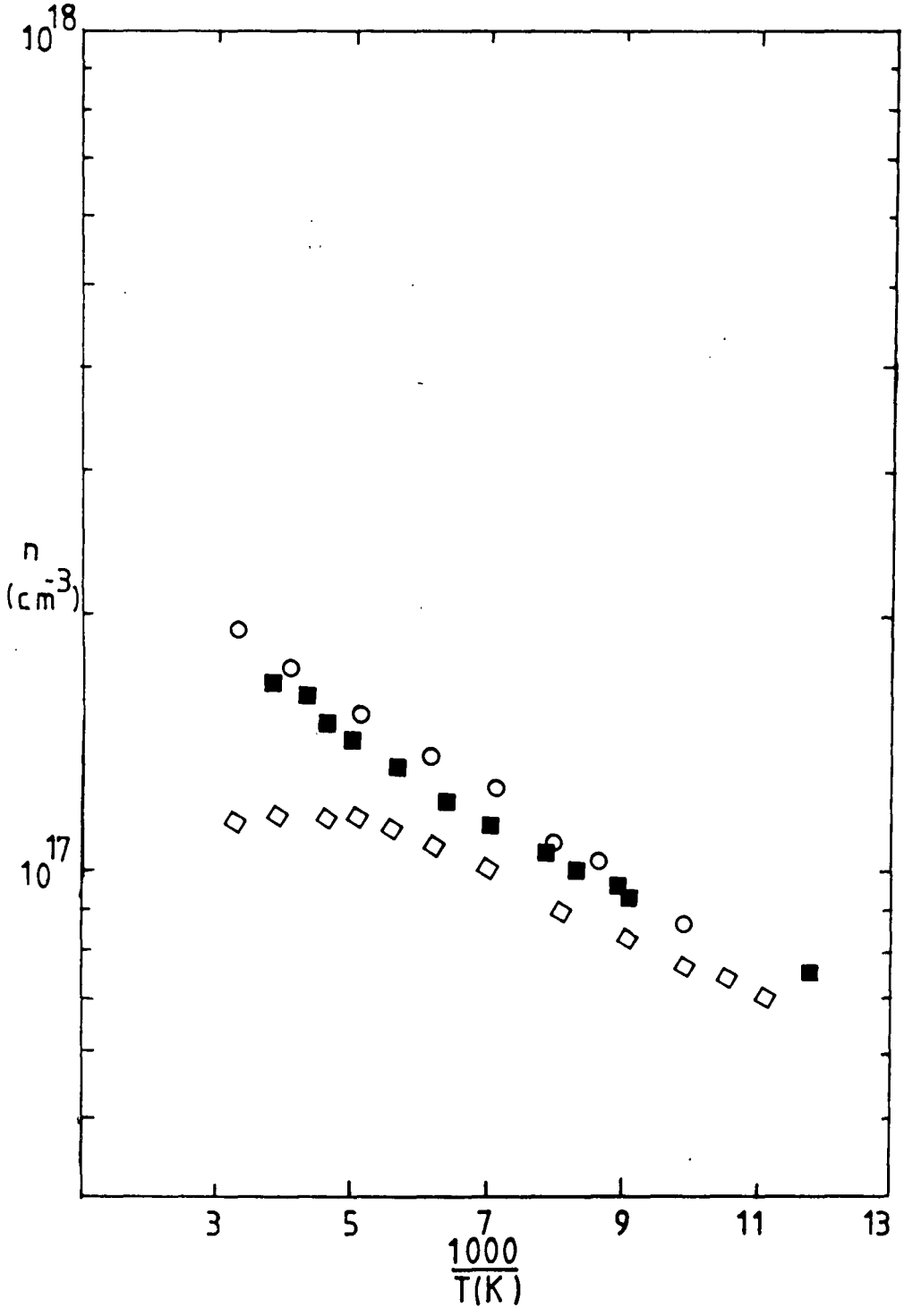

Figure 6.5b. Carrier concentration against reciprocal temperature for boule 787
(for key see figure 6.5a)

energies of 0.032eV and 0.031eV were calculated (figure 6.5d). From 160 to 100K the Hall mobility was practically unchanged with temperature (figure 6.5c).

v) **Crystal HT 156**

This crystal had the highest zinc contentration of all the crystals investigated, unfortunately no measurements of conductivity and Hall coefficient were made on this boule because it was too non-uniform and was heavily cracked making it impossible to cut a good bar. Room temperature conductivity measured on small dice gave values of 2.1×10^{-2} $ohm^{-1}cm^{-1}$ and 3.98×10^{-3} $ohm^{-1}cm^{-1}$ for zinc concentrations of x=0.4 and 0.45 respectively.

Discussion

As far as we are aware, there are very few reports on the transport properties of bulk mixed crystals or films of $Zn_xCd_{1-x}S$. This is mainly due to the difficulty of obtaining good, uniform crystals or films, which in any event are often highly resistive and thus difficult to measure. Observations by Davis and Lind (1) and Vitrikhovskii and Mizetskaya (2) are quite different from those reported in this thesis.

As grown crystals of $Zn_xCd_{1-x}S$ produced in this department using a vapour phase technique with composition

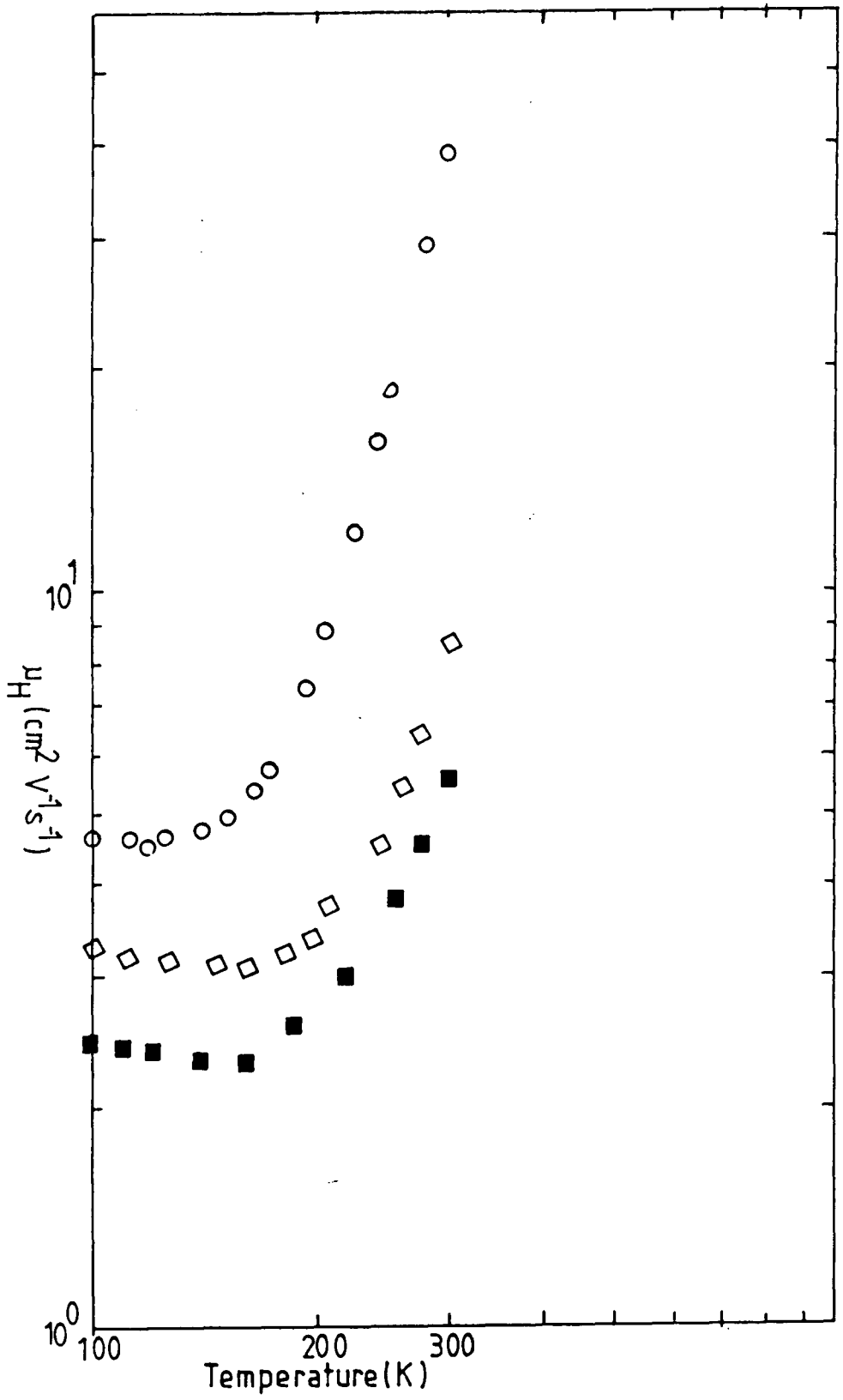

Figure 6.5c. Hall mobility against temperature for boule 787 (for key see figure 6.5a)

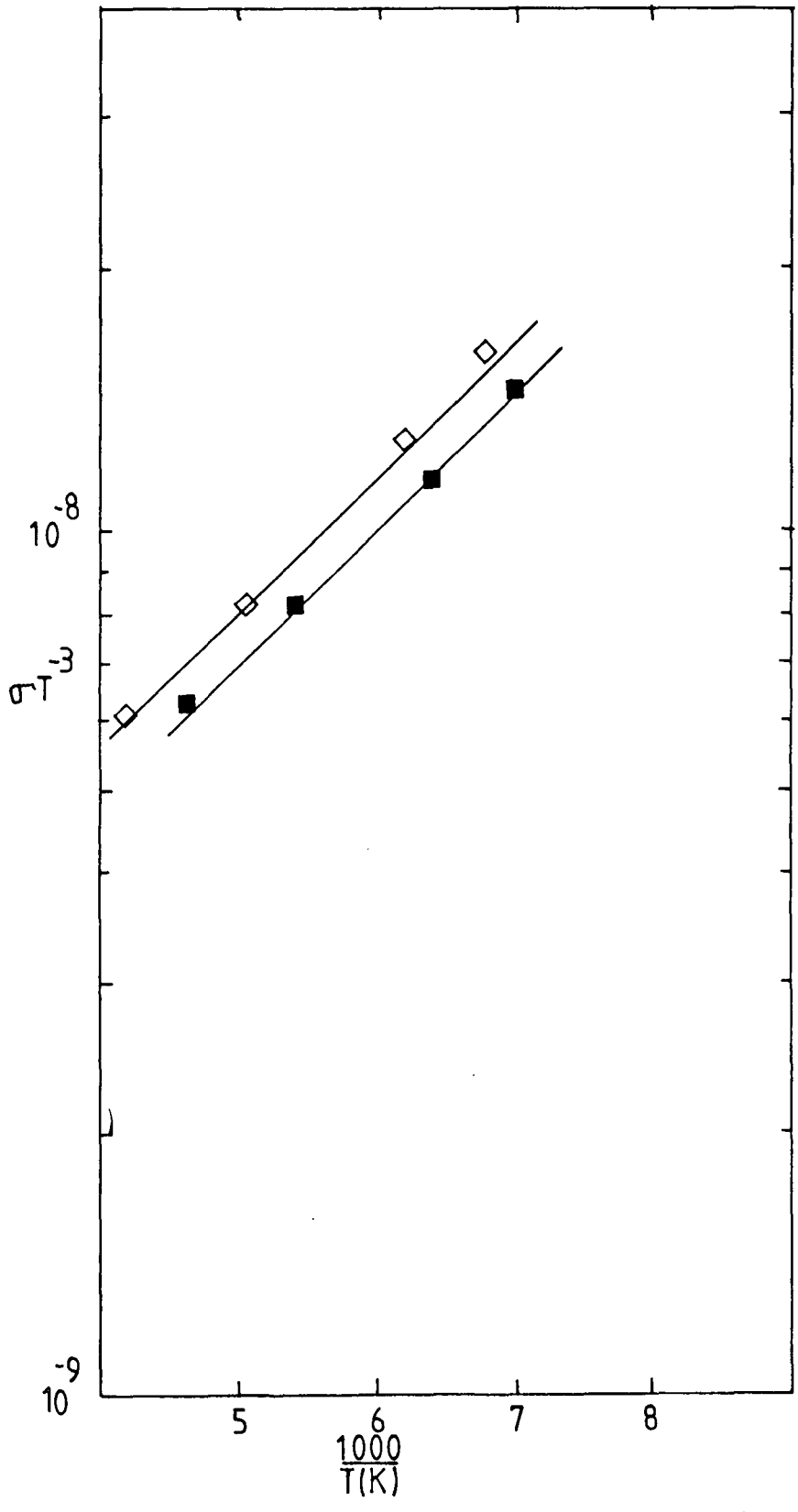

Figure 6.5d. σT^{-3} against reciprocal temperature for a) ■ x=0.22 and b) ◇ x=0.25.

values of $x<0.5$ were found to be quite conductive compared with crystals with the same composition grown by the iodine transport technique (1) and those synthesised directly from streams of zinc, cadmium and sulfur vapours (2). Although the $Zn_xCd_{1-x}S$ boules available were normally non-uniform, the particular bars, dice and clover leafed samples used were more or less quite uniform.

Indium and the alloy of In-10% Cd were found to form good ohmic contacts to samples with $x<0.4$. The difficulties in obtaining good ohmic contact for $x>0.4$ reported by other workers were also experienced here. This is expected because it is well known (3,4) that it is difficult to form good ohmic contact to ZnS.

According to Davis and Lind (1), the dark conductivity of their samples exhibited a sharp decrease in conductivity by 7-8 orders of magnitude when the zinc concentration was increased to about $x\sim0.15$ (conductivity at $x=0.1$ is about $1x10^{-2}$ $ohm^{-1}cm^{-1}$), which is quite different from our experience, where a conductivity as high as $4x10^{-3}$ $ohm^{-1}cm^{-1}$ could still be achieved at $x=0.45$. The curve in figure 6.6a shows a plot of room temperature dark conductivity against composition, where it can be seen that the highest values of conductivity occurred with low zinc content at $x=0.05$. With increasing concentration of zinc the conductivity decreased monotonically from $1x10^{1}$ $ohm^{-1}cm^{-1}$ to about $2x10^{-3}$ $ohm^{-1}cm^{-1}$. Crystals used by

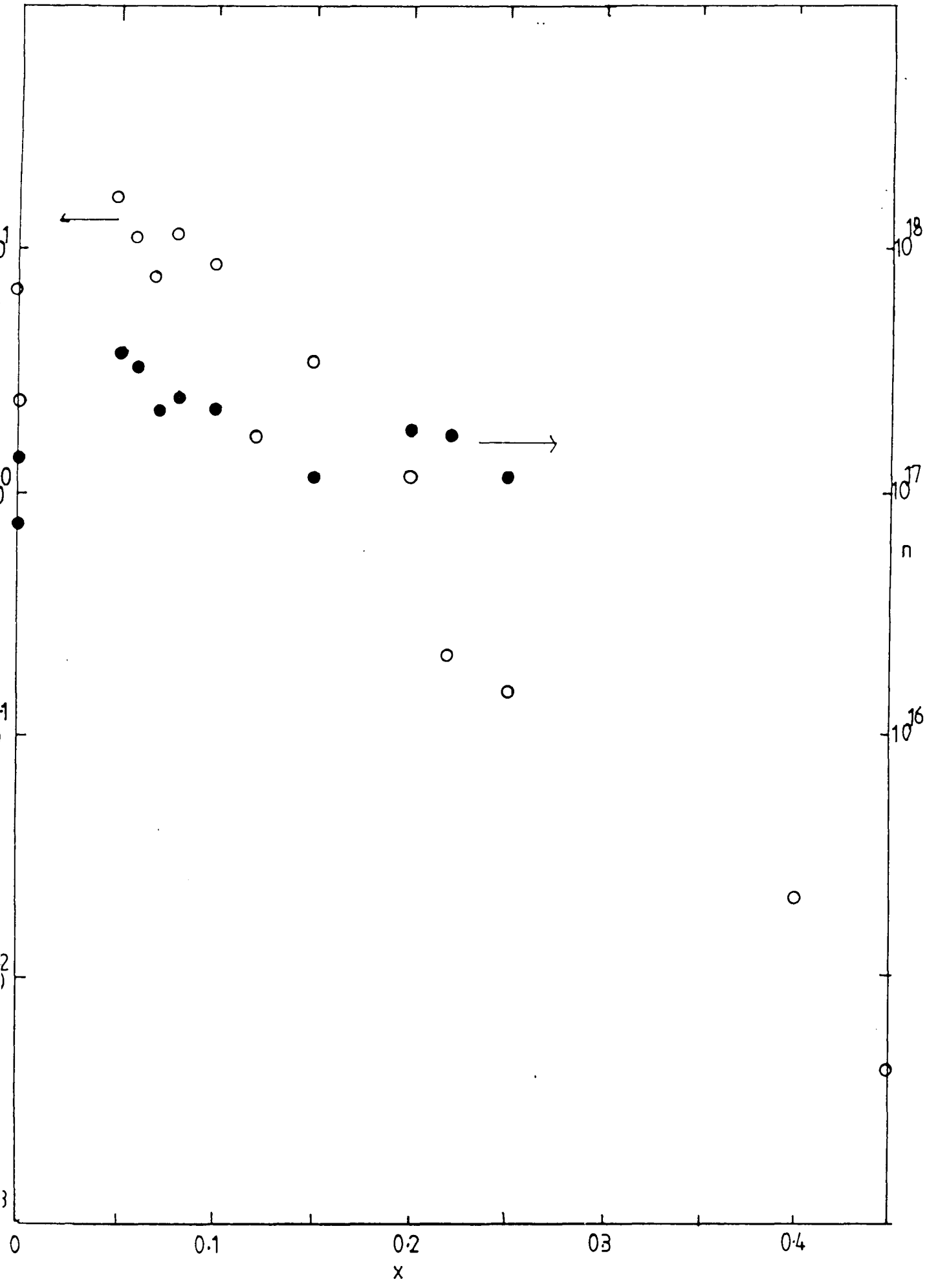

Figure 6.6a. Conductivity ○ and carrier concentration ● against x at 300K.

Vitrikhovskii and Mizetskaya (2) were highly resisitive varying from 10^{10} to 10^{13} ohm-cm. The conductivity of our as grown crystals was independent of illumination which is consistent with the observation of Oktik et al (23).

By plotting $\ln \sigma$ against T^{-1}, Davis and Lind (1) clearly showed that for $x<0.2$, good straight lines were obtained, and the activation energy (calculated from the slope) increased from 0.03eV at x=0 to 0.32eV for x between 0.1 and 0.2. It was suggested that the increase in donor activation energy caused a sharp decrease in conductivity near x=0.15. When our results were plotted in the same way two different curves were obtained. For $0<x<0.2$, the same trend as with CdS was observed with the maximum conductivity occurring in the region of 150-200K. The explanation for this behaviour is the same as for CdS. For $0.2<x<0.3$, the conductivity decreased quite rapidly when temperature was reduced from 300K to 200K and more slowly as the temperature fell to 100K. As mentioned before $\sigma = qun$, and the decrease in mobility in that range caused the conductivity to decrease.

From plots of ln n against T^{-1}, activation energies of shallow donors in our mixed crystals were found to vary between 0.007 to 0.013eV for $x<0.2$ independent of composition. The shallow donors appear in the Durham mixed crystals might be associated with an excess of zinc and cadmium atoms.

As for the Hall mobility of bulk mixed crystals of $Zn_xCd_{1-x}S$, Davis and Lind (1) concluded that the transport was due to electrons and their mobility did not vary significantly over the temperature range used (77-300K), but no values of mobility were quoted. As for the Durham crystals, the room temperature Hall mobility decreased slightly with increasing zinc content from x=0 up to x=0.15 (see figure 6.6b). With x>0.15, the Hall mobility decreased dramatically by 1-2 orders of magnitude to about 6 $cm^2V^{-1}s^{-1}$ at x=0.25 (figure 6.6b). Again for x<0.15 the Hall moblility increased with decreasing temperature as T^{-1} in the range from 300K to about 200K. At low temperature, except for one sample with x=0.12, the mobility was independent of temperature or exhibited the $T^{-0.5}$ trend. In sharp contrast with those crystals containing relatively more zinc with x>0.2, the Hall mobility decreased as the temperature decreased following a $T^{-1.5}$ variation from 300K to 200K and remained unchanged thereafter. The low values of Hall mobility and the $u_H \sim T^{-1.5}$ trend tend to suggest that the ionised impurity scattering had now become the dominant process. As for the first group of the crystals, both polar optical and piezoelectric scattering are probably operative from 180K to 300K. No attempts were made to achieve a fit with theoretical values (Hall mobility versus temperature) since there are too many unknown parameters for $Zn_xCd_{1-x}S$. However the variation of Hall mobility with composition

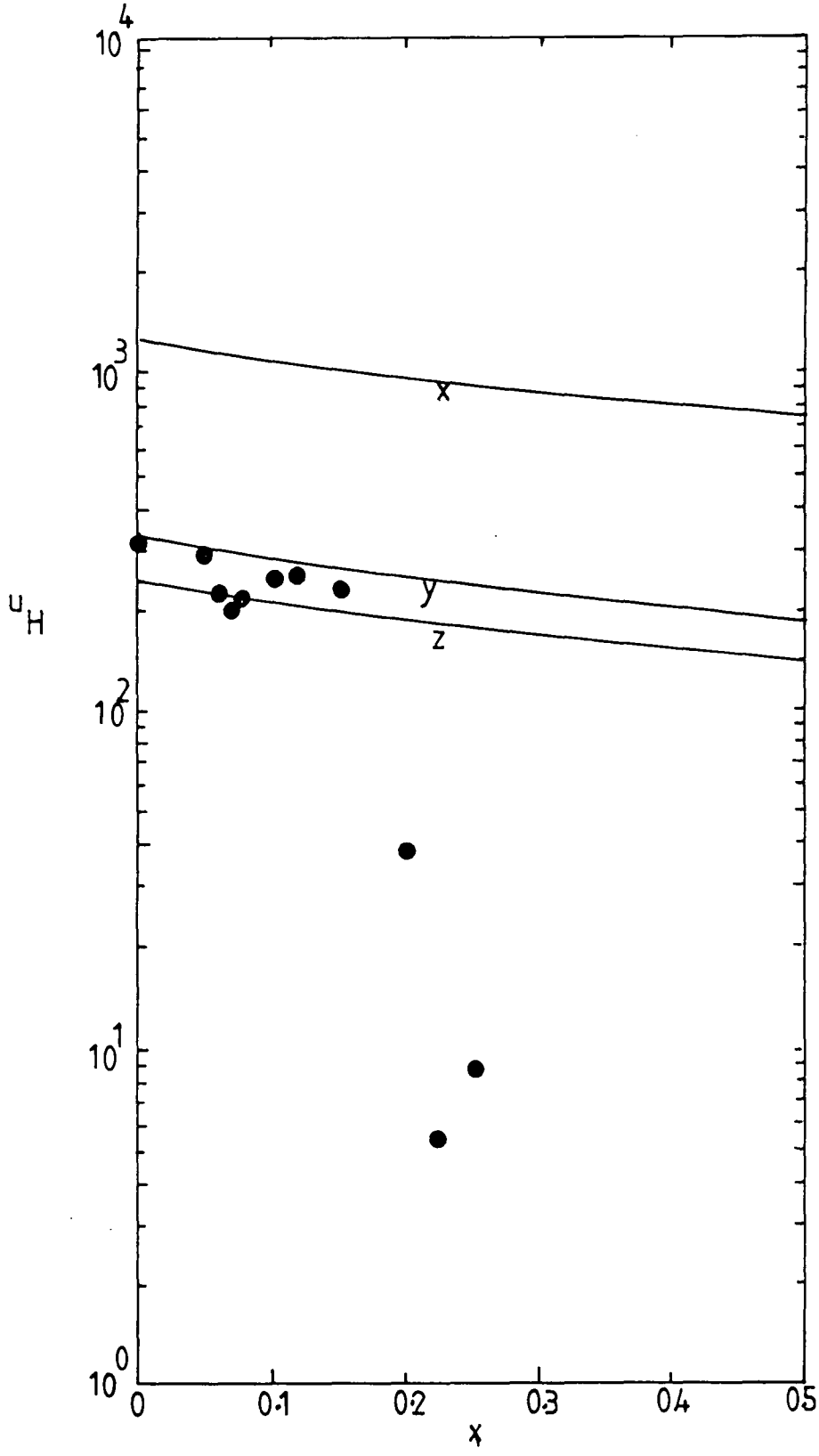

Figure 6.6b. Hall mobility against x at 300K (solid line x, y and z are calculated mobility due to optical, piezoelectric and combination of both respectively and ● experimental point).

($x<0.5$) at room temperature is shown in figure 6.6b together with mobility values calculated by assuming that some parameters are a linear function of x. It is suggested that both optical phonon and piezoelectric scattering are the dominant processes limiting the mobility of our mixed crystals for $x<0.2$. For crystals with $x>0.2$, ionised and neutral impurity scattering is more important.

Low mobilities observed in some materials (about two orders of magnitude lower) have been described by Weisberg (32) as caused by space charge scattering. Inhomogeneous regions due to non-uniform distribution of impurity, and local deviations from stoichiometry especially in compound semiconductors would be expected to occur during growth.

Using the expression proposed by Weisberg, Saxena and Gurumurthy (33) were able to explain their experimental measurements of the electron Hall mobility of $Al_xGa_{1-x}As$ ($0<x<0.78$) quite nicely. The minimum mobility occurring at $x=0.5$ is attributed almost entirely to space chagre scattering, and is given by

$$u_{SC} = \frac{(3.2\times10^{9})T^{-0.5}}{(m^*_e/m)^{0.5}(N_s.A)}$$

where N_s and A are the density and area of the scattering

centres respectively.

Another type of scattering which can be quite important in alloy semiconductors is called alloy scattering. The mobility limited by this type of scattering is given by (34);

$$u_A = \frac{(2\pi)^{0.5} q h^4 N_1}{3(kT)^{0.5} m^*_e{}^{2.5} (E_1-E_2)^2 x(1-x)}$$

where E_1-E_2 is the energy separation between the conduction band edges of unalloyed components, N_1 is the density of lattice sites and x is the composition.

The low mobilities observed in this range of composition may also be responsible for the reduction in short circuit current observed in Cu_2S-$Zn_xCd_{1-x}S$ photovoltaic cells in spite of the better matching of electron affinities and lattice parameters.

The plot of carrier concentration at room temperature against composition (figure 6.6a) shows that the maximum n occurred at about x=0.05. This trend agrees with the calculated values of uncompensated donor density (N_d) from capacitance measurements on Au-$Zn_xCd_{1-x}S$ Schottky diodes which will be discussed eleswhere in chapter seven.

Since there has been some work on transport

properties of thin films of $Zn_xCd_{1-x}S$, it is interesting to see how the results found here compare with those observed in thin films. On the whole, the electrical conductivity decreases with composition. For example, Singh and Jordan (20) showed that the resistivity of their films grown by chemical spray pyrolysis increased exponentially with x from about 10^2 ohm-cm at x=0 to 10^4 at x=0.7. Efforts to reduce the resistivity have been made by Bannergi et al (31), who found that annealing in vacuum at 300°C for about 30 minutes reduced the resistivity by 3-4 orders for small x only. Chynoweth and Bube (21) were able to obtain a resistivity of 4.0×10^2 ohm-cm at x=0.35 following heat treatment in hydrogen. A similar trend was also observed by Sakurai et al (18) who found the maximum conductivity to occur at x~0.15 for epitaxial layers of $Zn_xCd_{1-x}S$ grown on ZnS.

Mobilities reported by Sakurai et al (18), were independent of composition and varied irregularly from sample to sample. The mobility was generally less than 60 $cm^2V^{-1}s^{-1}$ but a maximum of 190 $cm^2V^{-1}s^{-1}$ was observed. Chynoweth and Bube (21) measured the electron mobility at 300K for their spray pyrolysis samples and showed that the mobility decreased from 10 $cm^2V^{-1}s^{-1}$ at x=0 to 1 $cm^2V^{-1}s^{-1}$ at x=0.35. Using similar films, Kwok and Chau (22) also found that the addition of zinc to a CdS film reduced the mobility significantly (from about 1 $cm^2V^{-1}s^{-1}$ at x=0 to 7×10^{-2} $cm^2V^{-1}s^{-1}$ at x=0.1).

The mobility of films produced by multi-source evaporation (19) doped with indium showed that quite high Hall mobilities can be obtained ranging between 100 and 20 $cm^2V^{-1}s^{-1}$ for $0<x<0.3$. Domens et al (28) found a very low Hall mobility in their films ($1x10^{-1}$ $cm^2V^{-1}s^{-1}$ at x=0 and about $5x10^{-3}cm^2V^{-1}s^{-1}$ at x=0.1). A similar decrease in mobility was also reported by Razykov (30) where the films were put down by CVD in a hydrogen flow.

c) **x>0.5**

Numerous attempts were made to grow $Zn_xCd_{1-x}S$ crystals in this range using either the Clark-Woods or Piper-Polich methods, but crystals obtained contained a large number of cracks. Tests carried out on small dice (HT 160) with x=0.85 gave conductivities of the order of 10^{-10} $ohm^{-1}cm^{-1}$. The difficulty of growing crystals with this composition have been discussed in the previous chapter.

6.3 Conclusion

Measurements of conductivity and Hall coefficient have carried out and the results can be summarised as follows;

i) **0<x<0.15**

The behaviour of mixed crystals in this range of composition closely followed that of CdS. The Hall mobility between 300K and 200K was limited by a combination of optical mode and piezoelectric scattering.

ii) **0.15<x<0.25**

A low mobility was found for crystals in this range, quite considerably reduced compared with the mobilities of crystals with a smaller zinc content. The mobility decreased still further with decreasing temperature indicating that ionised impurity scattering dominated in these crystals. It is quite likely that space charge and alloy scattering processes become significant in this range of composition.

iii) **0.25<x<0.45**

No measurement of Hall coefficient could be made because the crystals contained a large number of cracks but conductivities in the range of 10^{-3} $ohm^{-1}cm^{-1}$ could be achieved.

iv) **x>0.45**

No measurements of conductivity or Hall coefficient were carried out because no satisfactory boule could be grown for this range of composition. Conductivities measured on small dice give values of the order of 10^{-10} $ohm^{-1}cm^{-1}$ for x=0.85.

Results obtained at 300K are tabulated in table 6.1.

x	u_H	σ	n
	$cm^2V^{-1}s^{-1}$	$ohm^{-1}cm^{-1}$	cm^{-3}
0	290,300	3.4,6.8	$1.45x10^{17}$, $7.3x10^{16}$
0.05	285	16	$3.6x10^{17}$
0.06	225	11	$3.1x10^{17}$
0.07	200	7.5	$2.15x10^{17}$
0.08	210	1.15	$3.4x10^{17}$
0.1	250	8.5	$2.15x10^{17}$
0.12	255	1.7	$4x10^{16}$
0.15	235	3.4	$1.15x10^{17}$
0.20	38.5	1.15	$1.8x10^{17}$
0.22	5.5	$2.1x10^{-1}$	$1.75x10^{17}$
0.25	8.5	$1.5x10^{-1}$	$1.15x10^{17}$
0.4	-	$2.1x10^{-2}$	-
0.45	-	$3.98x10^{-3}$	-

Table 6.1. Summary of some results obtained for $Zn_xCd_{1-x}S$ crystals at 300K.

References for chapter VI

1) E.A.Davis and E.L.Lind, J. Phys. Chem. Solids, **29** (1968) 79

2) N.I.Vitrikhovskii and I.B.Mietskaya, Soviet Physics-Solid-state, **2** (1961) 2301

3) A.E.Thomas, J.Woods and Z.V.Hauptman, J. Phys. D: Appl. Phys., **16** (1983) 1123

4) G.H.Blount, M.W.Fisher, R.G.Morrison and R.H.Bube, J. Electrochem. Soc., **113** (1966) 690

5) **Physics and Chemistry of II-VI compounds**, edited by M. Aven and J.S.Prener (Wiley, New York 1967)

6) B.Ray, **II-VI** Compounds (Pergamon, New York 1969)

7) R.S.Crandall, Phys. Rev., **169** (1968) 577

8) S.Toyotomi and K.Morigaki, J. Phys. Soc. Jpn., 25 (1968) 807

9) D.L.Rode, Phys. Rev. **2B** (1970) 4036

10) H.Fujita, K.Kobayasi and T.Kawai, J. Phys. Soc. Jpn., **20** (1965) 109

11) W.W.Piper and R.E.Halstead, **Proc. Int. Conference of Semiconductor Physics**, Prague (1960) 1046

12) H.H.Woodbury, Phys. Rev., **9B** (1974) 5188

13) K.Morimoto, M.Kitagawa and T.Yoshida, J. Cryst. Growth, **59** (1982) 254

14) M.Itakura and H.Toyoda, J. Phys. Soc. Jpn., **18** (1982) 150

15) J.M.Ziman, **Electrons and Phonons** (Oxford Univ. Press, London 1967)

16) S.S.Devlin in **Physics and Chemistry of II-VI Compounds**, edited by M.Aven and J.S.Prener (Wiley, New York 1967) chapter 11

17) R.S.Feigelson, A.N.Diaye, S.Y.Yin and R.H.Bube, J. Appl. Phys., **48** (1977) 3162

18) Y.Sakurai, Y.Kokubun, H.Watanabe and M.Wada, Jpn. J. Appl. Phys., **16** (1977) 2115

19) N.Romeo, G.Sberveglieri and L.Tarricone, Appl. Phys. Lett., **32** (1978) 807

20) V.P.Singh and J.F.Jordan, IEEE Elec. Dev. Lett., **EDL2** (1981) 137

21) T.A.Chynoweth and R.H.Bube, J. Appl. Phys., **51** (1980) 1844

22) H.L.Kwok and Y.C.Chau, Thin Solid Films, **66** (1980) 303

23) S.Oktik, G.J.Russell and J.Woods, J. Cryst. Growth, **59** (1982) 414

24) M.A.Subhan, N.M.Islam and J.Woods, J. Phys. Chem. Sol., **33** (1972) 229

25) L.Clark and J.Woods, Brit. J. Appl. Phys., **17** (1966) 319

26) D.L.Rode, Semiconductor and Semimetal **10** (1970) edited by R.K.Willardson and A.C.Beer

27) D.Howarth and E.H.Sondhemier, Proc. Roy. Soc., **A219** (1953) 53

28) P.Domen, M.Cadene, G.W.Cohen Solal, S.Martinuzzi and C.Brouty, Phys. Stat. Sol., **59a** (1980) 201

29) A.R.Hutson, Phys. Rev. Lett., **4** (1960) 505

30) T.M.Razykov, Solar Energy Mat., **12** (1985) 233

31) A.Banerjee, P.Nath, V.D.Vankar and K.L.Chopra, Phys. Stat. Sol(a)., **46** (1978) 723

32) L.R.Weisberg, J. Appl. Phys., **33** (1962) 1817

33) A.K.Saxena and K.S.Gurumurthy, J. Phys. Chem. Sol., **43** (1981) 801

34) G.B.Stringfellow, J. Appl. Phys., **50** (1979) 4147

CHAPTER VII

Au-$Zn_xCd_{1-x}S$ SCHOTTKY DIODES

7.1 Introduction

In this chapter, the properties of Schottky diodes prepared on chemically etched surfaces of crystals of $Zn_xCd_{1-x}S$ are described. The aim of the work is to see how the parameters of the Schottky diodes change with composition (x).

The current-voltage characteristic of the Schottky diodes are described in section 7.2, followed in section 7.3 by capacitance-voltage measurements made on the same devices. In section 7.4, short circuit photocurrent measurements are presented, these were made to determine barrier heights accurately. A discussion of the factors which control barrier heights measured using current-voltage, capacitance-voltage and the photoelectric technique is given in section 7.5. A general discussion and conclusion follow in section 7.6 and 7.7.

7.2 Current-Voltage characteristic

Typical forward current-voltage characteristics of Schottky diodes made on a number of substrates of $Zn_xCd_{1-x}S$ with different values of x are shown in figure 7.1a. The

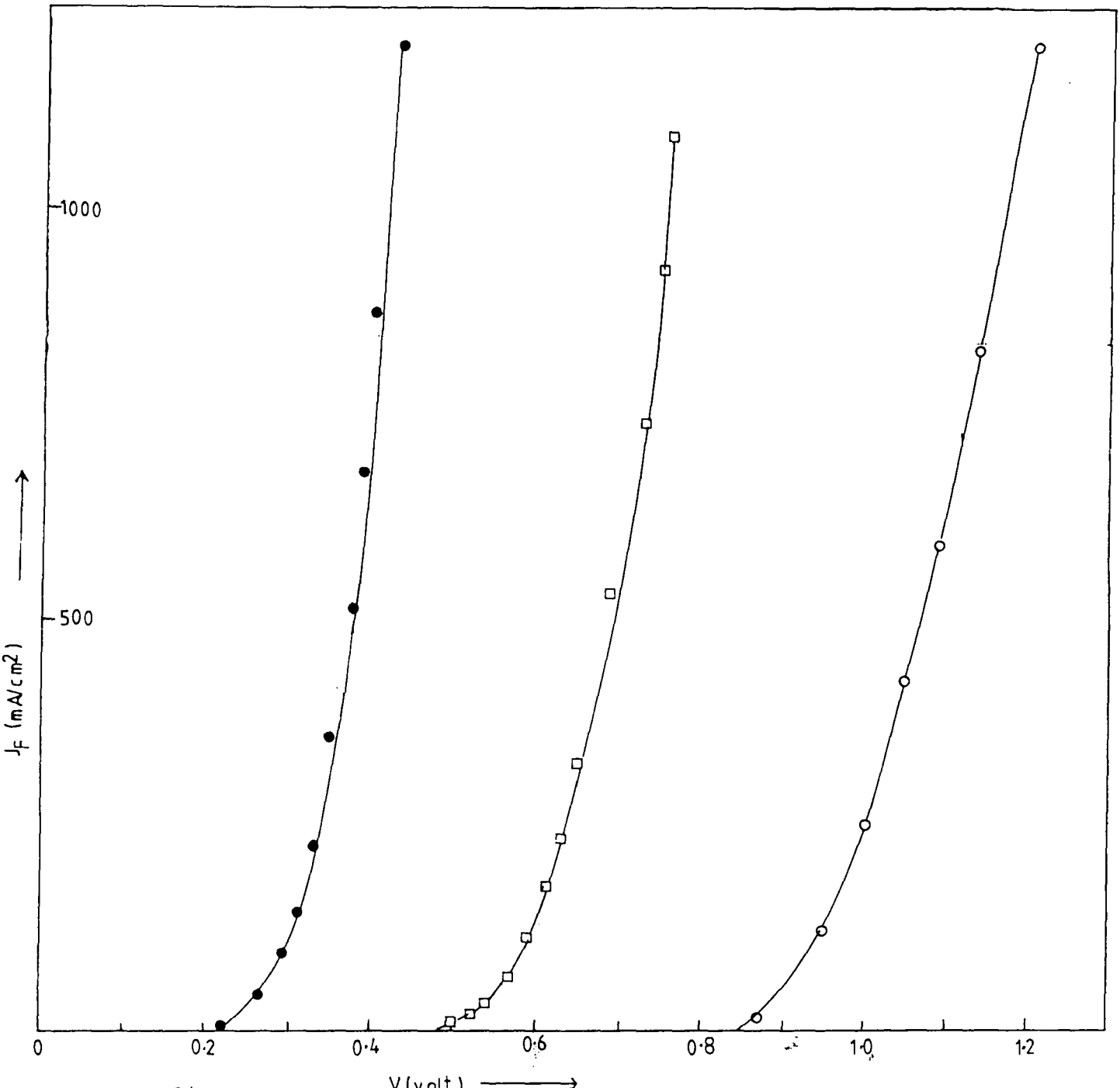

Figure 7.1a. Current-voltage characteristic of Au-$Zn_xCd_{1-x}S$

● x=0, □ x=0.24 and ○ x=0.4.

measurements were made in the dark at room temperature. Details of the experimental procedure have already been given in chapter IV.

Rectifying behaviour was found in all the diodes studied. Assuming that the current flow is controlled by thermionic emission over the barrier, the forward current, J_f is given by $J_f = J_s\{\exp(qV/kT)-1\}$. For $V>3kT/q$, this equation reduces to $J_f \approx J_s\exp(qV/nkT)$, where $J_s=A^*T^2\exp(-q\phi_{bn}/kT)$. By plotting ln J_f against the forward voltage, a straight line should be obtained. If it is, the saturation current density, J_s, can be determined from the intercept of the straight line at V=0. The values of J_s for different composition are presented in table 7.1. The trend is for J_s to decrease with x. Some of the plots of ln J_f against voltage are shown in figure 7.1b.

From the slope of the plot of ln J_f against forward voltage, V, the value of the ideality factor, n of a particular diode can be calculated with the help of equation 3.53; $n = (q/kT)(dV/d\ln(J_f))$. The values of n of all the diodes studied are presented in table 7.1, where they can been seen to vary from 1.03 to 1.736. Knowing the value of J_s, the height of a Au-$Zn_xCd_{1-x}S$ barrier could be calculated from $\phi_{bn} = (kT/q)\ln(R^*T^2/J_s)$ where R^* is the effective Richardson constant which depends on the effective mass (Chapter III): $R^* \sim 120m^*_e/m$. Since the value of m^*_e for $Zn_xCd_{1-x}S$ is not known, it is assumed that

x	J_s(mA-cm^{-2})	n	ϕ_{I-V}(eV)
0.0	1.1×10^{-7}	1.03	0.79
0.05	6.5×10^{-7}	1.54	0.75
0.07	1.9×10^{-8}	1.04	0.84
0.12	3.4×10^{-9}	1.22	0.88
0.23	1.0×10^{-8}	1.04	0.86
0.24	7.8×10^{-9}	1.64	0.86
0.26	1.6×10^{-7}	1.26	0.78
0.35	7.8×10^{-10}	1.73	0.93
0.35	1.1×10^{-9}	1.25	0.92
0.41	9.5×10^{-15}	1.18	1.22
0.42	3.0×10^{-15}	1.12	1.25

Table 7.1: Parameters calculated from current-voltage data at room temperature.

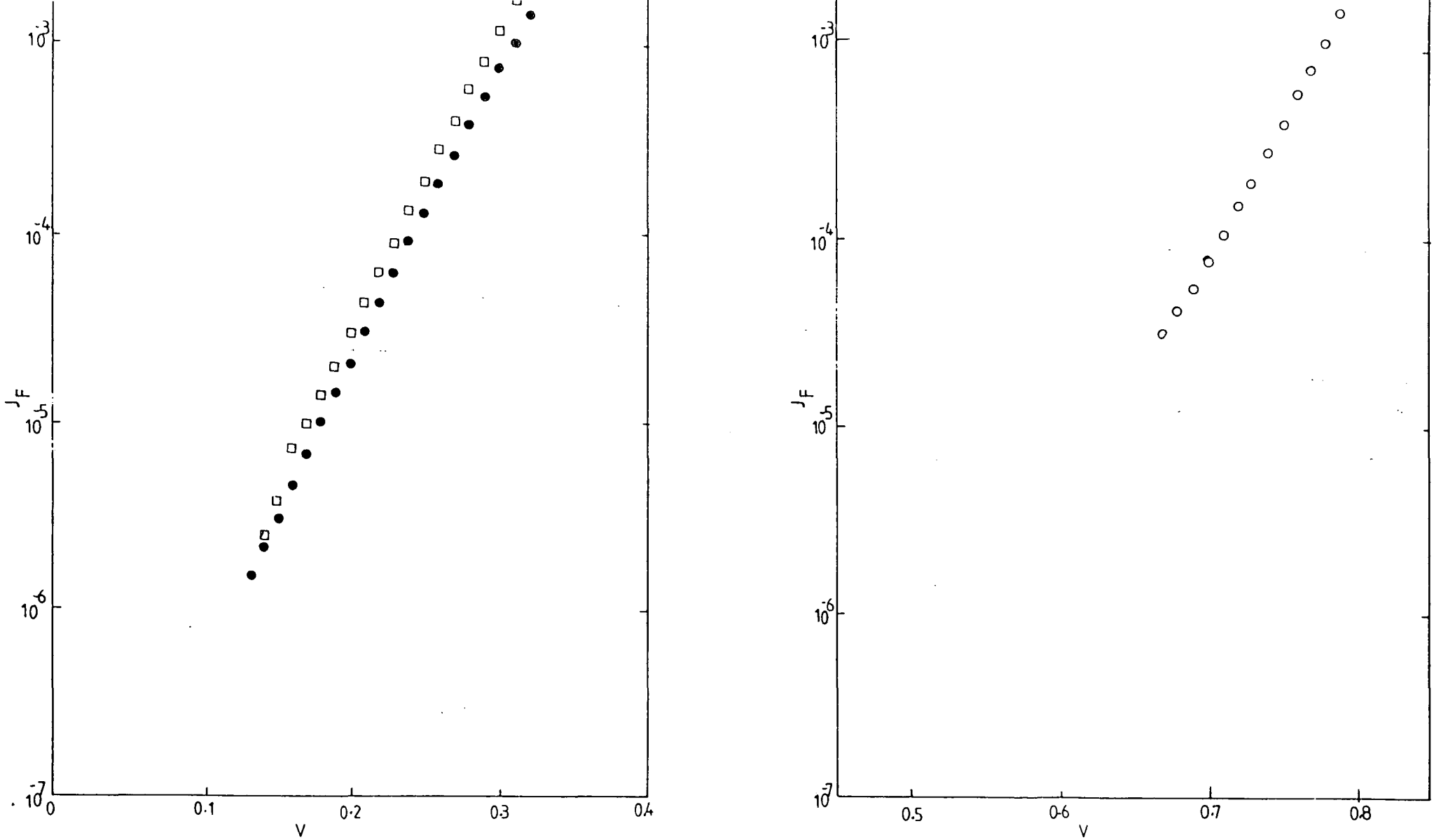

Figure 7.1b. Plot of J_f versus V for sample in figure 7.1a

(for key see figure 7.1a)

m^*_e varies linearly with composition. Barrier heights calculated in this way are also recorded in table 7.1.

Discussion

The problems of correlating the Schottky diode barrier heights and ideality factors measured from forward current-voltage characteristics are quite complex (1,2). Deviation from the ideal situation (n=1) can be due to many reasons (3,4,5,10). In this part of the work, Schottky diodes of Au-$Zn_xCd_{1-x}S$ were fabricated on chemically etched surfaces. Extra care was taken to ensure that all surface preparation was identical for all the samples. As shown in table 7.1, the values of ideality factor were found to vary between 1.03 to 1.73 . With practical Schottky diodes, values of n between 1 and 2 are commonly encounted. According to Card and Rhoderick (4), the ideality factor increases from 1.03 where thin insulating layers 15Å thick are present on the surface of semiconductor, to 1.5 when the i-layer is 22Å thick. This would suggest that insulating layers of different thickness were present after the etching process, prior to the deposition of the gold. The dependence of ideality factor on conductivity has also been demonstrated by Khang (6) where Au-Si Schottky diodes on high conductivity samples gave high n values. High conductivity samples normally give rise to thin barriers and tunnelling through the barrier can than occur. Of course there might have been differences in the surface

properties of the $Zn_xCd_{1-x}S$ crystals themselves. As pointed out in the experimental chapter, the etchant used to clean the $Zn_xCd_{1-x}S$ was concentrated hydrochloric acid. The reaction of hydrochloric acid with CdS (x=0) occurred vigorously, but with increasing x, the reaction slowed down. The difficulty in maintaining the crystallinity of $Zn_xCd_{1-x}S$ films for x>0 has been discussed in chapter V. In a study of the Cu_2S-$Zn_xCd_{1-x}S$ heterojunction, the difficulties in converting the surface layers of $Zn_xCd_{1-x}S$ into Cu_2S by chemical displacement have also been reported and the thickness of the Cu_2S layer was found to be reduced compared with that produced using the same process in Cu_2S-CdS (7). In the dry barrier process, the reaction between CuCl and $Zn_xCd_{1-x}S$ also proceeds slowly compared with CdS (8).

In conclusion however, it is worth mentioning that the value found here for the barrier height of Au-CdS, namely 0.79eV, lies close to values previously reported in the literature.

	ideality factor(n)	barrier height(eV)	surface treatment
present study	1.03	0.79	etched surface
Goodman (17)	1.03-1.18	0.64-0.71	etched surface
Kusaka et al (20)	-	0.73-0.84	etched surface

7.3 Capacitance-Voltage characteristics

Measurements of the dark capacitance of Au-$Zn_xCd_{1-x}S$ diodes at a frequency of 1MHz as a function of small reverse bias will be described in this section. These measurements help to understand more about the junction parameters.

The uncompensated donor densities N_d ($N_d=N_D^+-N_A^-$, where N_D^+ is the concentration of ionised donors, and N_A^- is the concentration of ionised acceptors) for different compositions were determined from plots of C^{-2} versus reverse bias, V_r. In order to obtain correct values of N_d from those plots, equation 3.63 is rewritten in the form $N_d=2/q\epsilon_s A^2 . dV_r/dC^{-2}$, where A is the area of the gold contact. For CdS, with x=0, N_d calculated from the slope is $4.04x10^{16}$ cm^{-3}, while the diode with x=0.1 gave $N_d=1.28x10^{18}$ cm^{-3}, i.e. N_d was higher in devices with 10% zinc. With further increase in zinc composition, the value of N_d decreased. At x=0.41, it had fallen to $1.12x10^{16}$ cm^{-3}. The measured values of N_d for the range of samples with different compositions are shown in table 7.2a and plotted in figure 7.2c. When the temperature was reduced to about 90K, the value of N_d also decreased as can be seen from the C^{-2} versus V_r plots in figure 7.2a. Plots of C^{-2} versus V_r for different slices taken from the same boule (HT 156) are also shown in figure 7.2b.

x	$N_d(cm^{-3})$	E_c-E_f(ev)	V_{int}(volt)
0.0	$4.037x10^{16}$	0.106	0.96
0.05	$3.03x10^{17}$	0.045	1.01
0.10	$1.28x10^{18}$	0.020	0.94
0.24	$3.24x10^{17}$	0.046	1.03
0.26	$4.53x10^{17}$	0.052	0.96
0.35	$3.94x10^{17}$	0.058	1.09
0.38	$1.79x10^{17}$	0.079	1.30
0.41	$1.12x10^{16}$	0.154	1.43
0.42	$1.72x10^{16}$	0.141	1.35
0.50	$1.44x10^{16}$	0.147	1.54

Table 7.2a: Parameters calculated from capacitance-voltage data at room temperature.

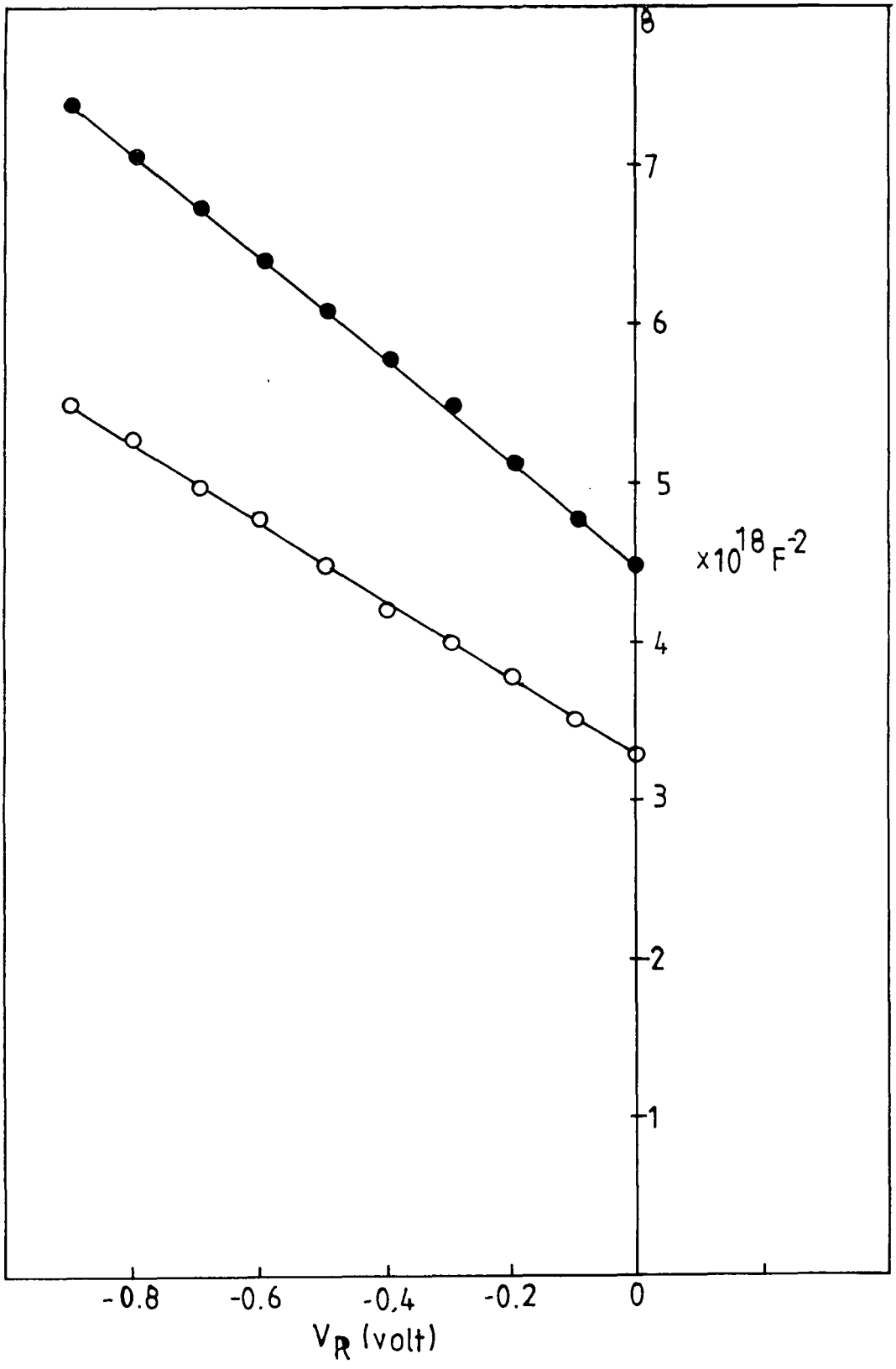

Figure 7.2a. C^{-2} versus V_r plot for Au-$Zn_{0.38}Cd_{0.62}S$ at 300K (●) and 90K (O).

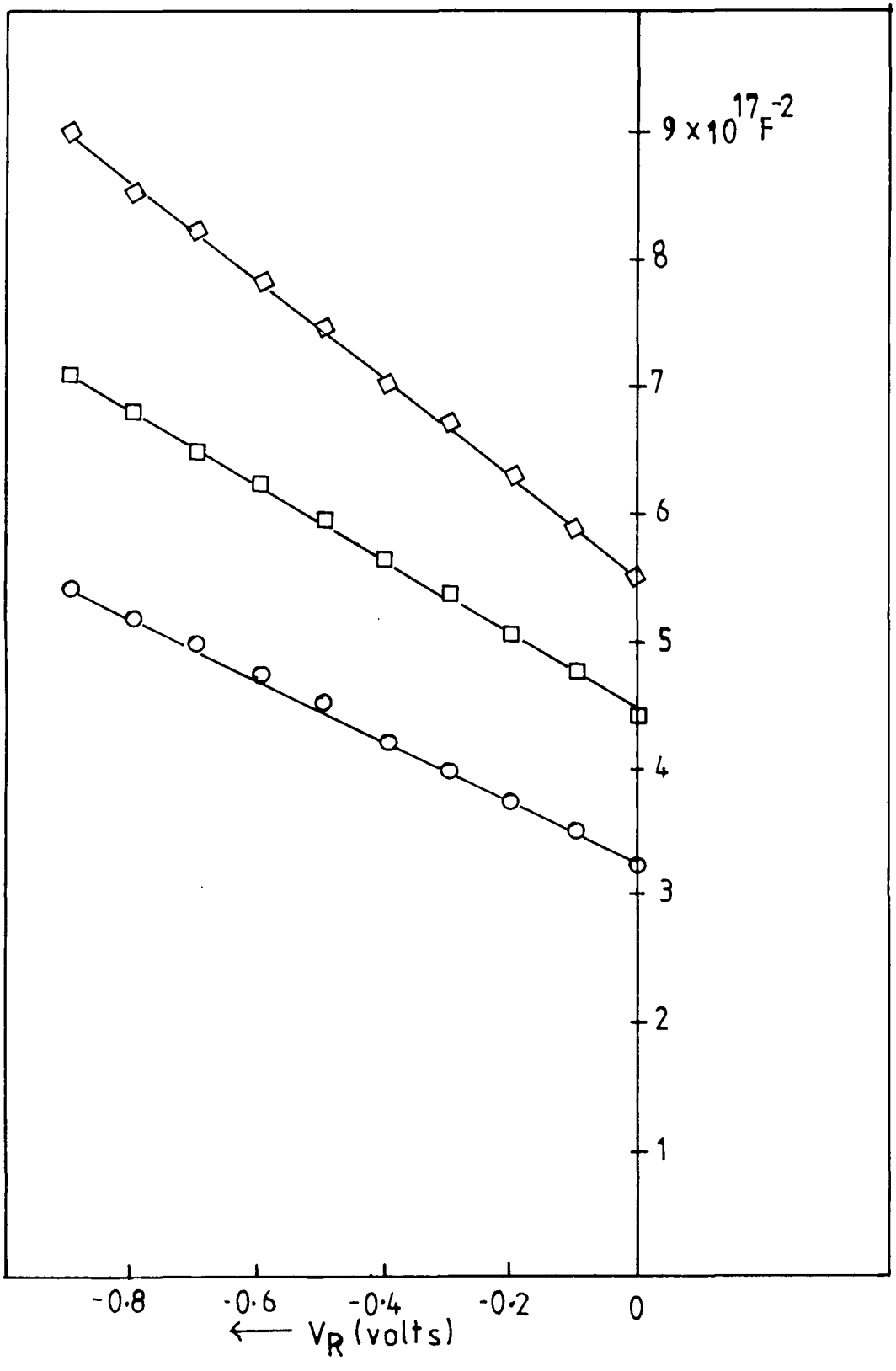

Figure 7.2b. C^{-2} versus V_r taken from different slice of boule HT 156.

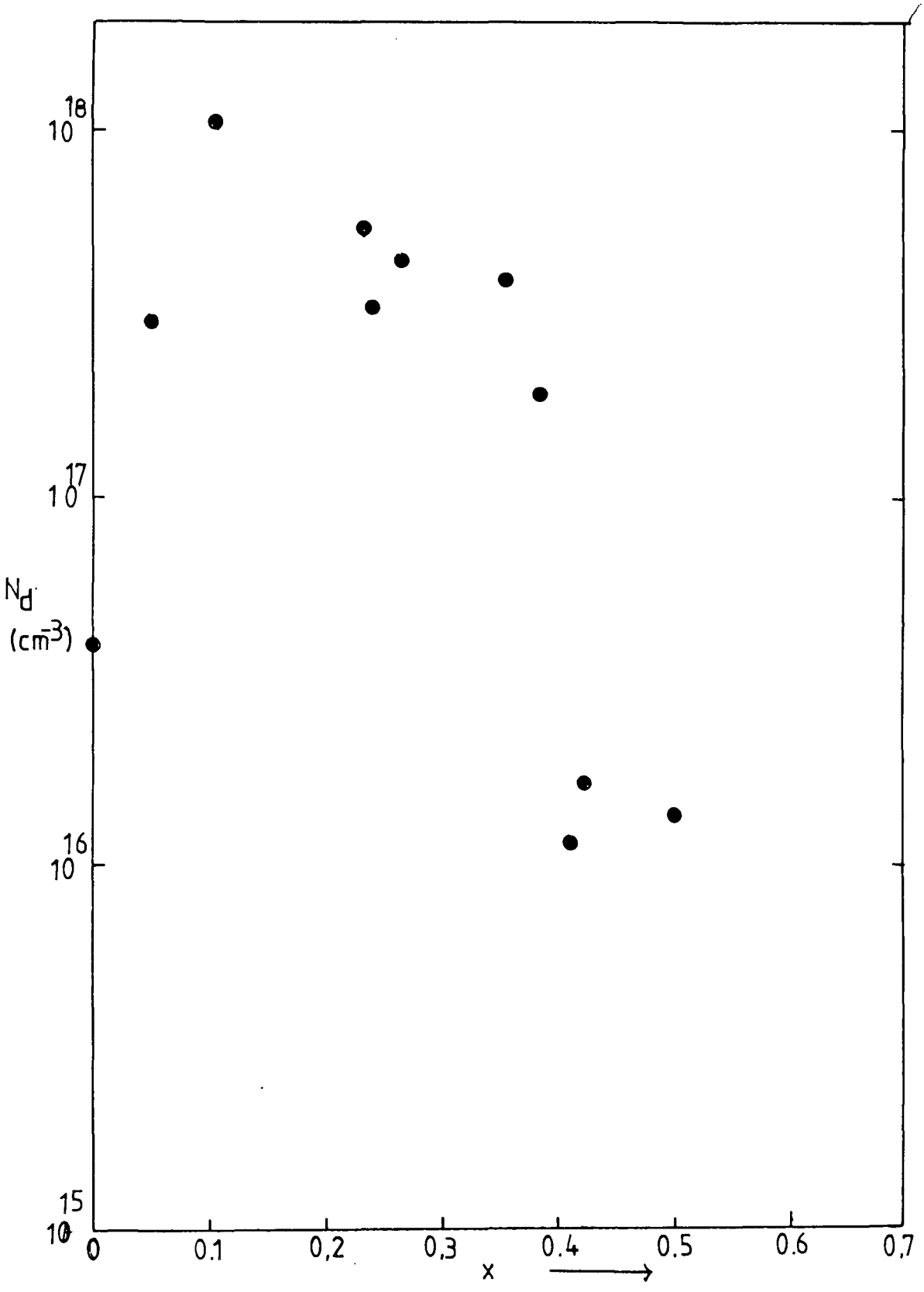

Figure 7.2c. Uncompensated donor density against x at 300K.

The position of the Fermi level, that is the difference between the bottom of the conduction band and Fermi level, E_f, can be calculated with the help of equation 3.66, $E_c-E_f=kT/q \ \ln(N_c/N_d)$. N_c, the effective density of states in the conduction band was calculated by assuming that m^*_e is linearly dependent on composition. The depth of the Fermi level below the conduction band for the various $Zn_xCd_{1-x}S$ compositions is shown in table 7.2a.

As has been described in chapter III, the C^{-2} versus V_r plot can also be used to determine the barrier height of a Schottky diode. According to equation 3.66, $\phi_{C-V}=V_{diff}+(E_c-E_f)$, ϕ_{C-V} is the barrier height determined from the capacitance measurements, and $V_{diff}=V_i+kT/q$ where V_{diff} is the diffusion potential, or band bending in the Schottky barrier. The band bending was determined by observing the intercept on the voltage axis (see for example figure 7.2b). The magnitudes of the intercepts for the various diodes are tabulated in table 7.2a. For compositions with values of x up to 0.2, V_{diff} was almost constant, but then began to increase up to V=1.54V for x=0.5. The corresponding values of ϕ_{C-V} can then be calculated and are listed in table 7.3. The trend was for the barrier height measured by this technique to be fairly constant up to x=0.2, and then to increase up to 1.687eV at x=0.5. The variation of E_f and V_{diff} is also shown graphically in figure 7.2d.

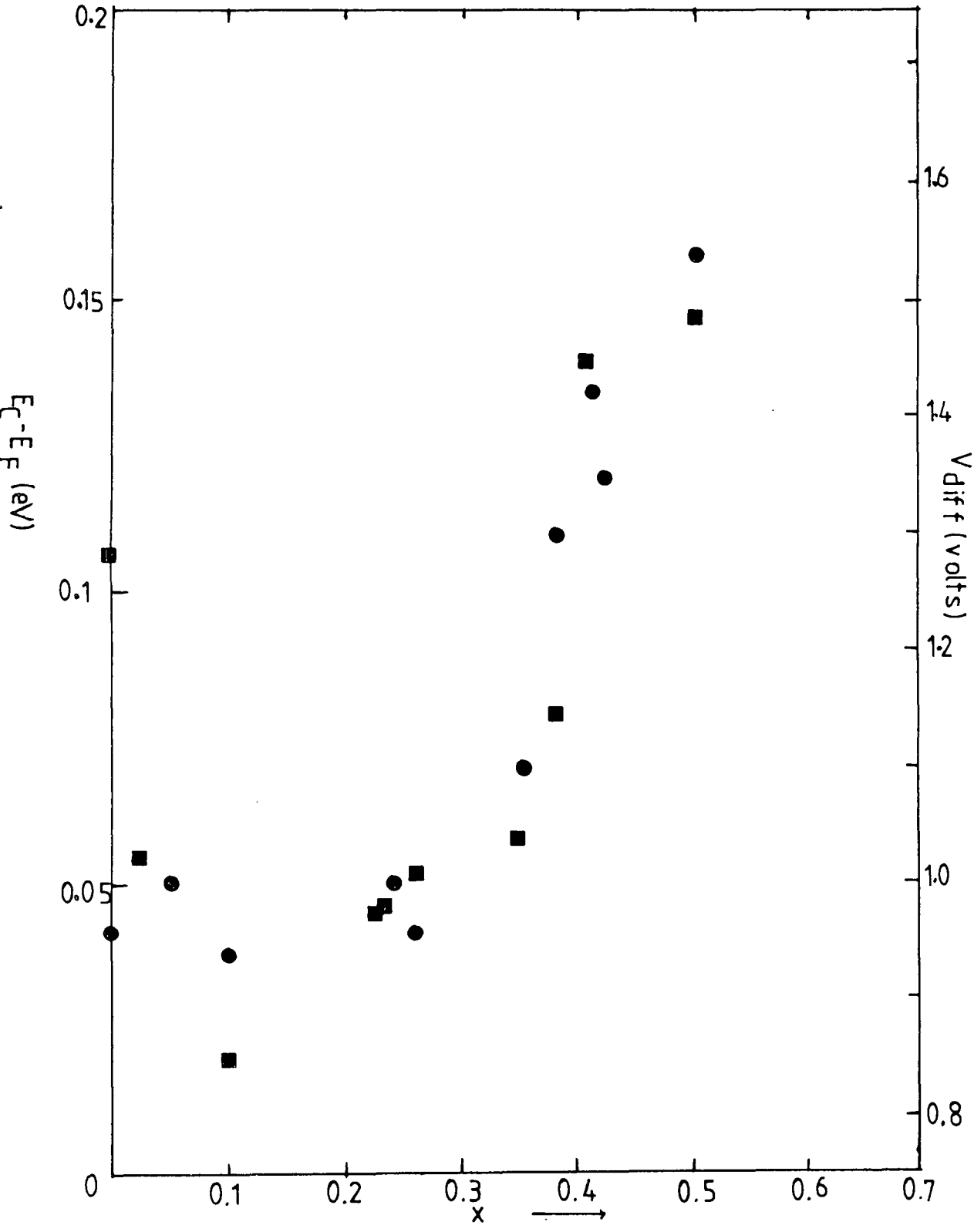

Figure 7.2d. V_{diff}(●) and $E_c - E_f$(■) against x at 300K.

The depletion width (w) of the Schottky diodes should decrease when the reverse bias is increased. The width of the depletion region is calculated from $w=\epsilon_s A/C$, where $\epsilon_s=\epsilon_r x 8.854x10^{-14}$ Fcm^{-1}, A is the area of the diode and C is the capacitance at zero bias. The values of w for different x have been calculated and also recorded in table 7.2b.

The maximum electric field, E_{max} at the interface of the metal and semiconductor under zero bias is given by $E^2_{max}=2qN_d/\epsilon_s.(V_{diff}-kT/q)$, and the lowering of the potential barrier by $\Delta\phi_{bn}$ (also called the Schottky effect) as a result of combining the effects of the image force potential and electric field, is according to Sze (9), $\Delta\phi_{bn}=(qE_{max}/4\pi\epsilon_o)^{0.5}$. The values of E_{max} and $\Delta\phi_{bn}$ calculated from the above equation are also recorded in table 7.2b.

Discussion

From all the diodes studied (with $x<0.5$), straight line plots of C^{-2} versus V_r were obtained, which suggests that the uncompensated donor density was uniformly distributed in the depletion region. A decrease in N_d at lower temperature was also observed in all of the diodes and this can be attributed to incomplete donor ionisation. The uncompensated donor density calculated from the C^{-2}-V_r plot is equivalent to the free carrier concentration (n) determined from Hall coefficient measurements. When the

x	E_{max}	$\Delta\phi_{bn}$(eV)	w(μm)
0.0	1.61×10^5	0.152	0.119
0.05	4.96×10^5	0.267	0.049
0.10	8.99×10^5	0.360	0.023
0.24	4.75×10^5	0.262	0.033
0.26	5.42×10^5	0.279	0.035
0.35	5.40×10^5	0.279	0.040
0.38	3.97×10^5	0.239	0.067
0.41	1.04×10^5	0.122	0.274
0.42	1.25×10^5	0.134	0.274
0.50	1.08×10^5	0.125	0.245

Table 7.2b: Parameters calculated from capacitance-voltage data at room temperature.

uncompensated donor density was plotted against x, a maximum was found at about x~0.1 (figure 7.2c). This increase in uncompensated density for a small admixture of zinc agrees well with the Hall coefficient measurements described in chapter VI (figure 6.6a). Since no such behaviour has previously been reported in crystals of $Zn_xCd_{1-x}S$, it is worth comparing this result with the reported properties of thin films. For instance, a similar trend has also been observed by Sakurai et al (11) on epitaxial layers of $Zn_xCd_{1-x}S$. With films produced by spray pyrolysis, Kwok and Chau (12) and Chow et al (13) showed that the carrier density increased initially with increasing zinc. In contrast, using films produced by the same method, Chynoweth and Bube (14) found that the carrier density decreases as the zinc content increases. In another paper, Kwok et al (15) showed that the carrier concentration increased with increasing zinc concentration initially, but then decreased beyond a certain zinc composition. They also showed that, the inflection point was dependent on the thickness of the film. With films produced by thermal evaporation, an increase in carrier concentration with zinc content was also reported by Domens et al (16) which saturated at about x=0.1. They suggested that the increase is due to an excess of cadmium and zinc atoms dissolving in interstitial sites and acting as donors.

In general, the parameters calculated here were

very much dependent on the resistivity of the samples. To control the growth and pre-determine properties such as resistivity is extremely difficult in many II-VI compounds.

7.4 Short circuit photocurrent

The spectral responses of the short circuit photocurrents of Schottky diodes as a function of photon energy are plotted in figure 5.6 (chapter V) for different compositions. The photocurrent at lower photon energy (less than the band gap energy) is associated with the photoelectric emission of electrons from the gold over the barrier into the $Zn_xCd_{1-x}S$, and the lower energy threshold gives a measure of the barrier height (ϕ_{bn}). It is apparent from figure 5.6 that the threshold and therefore the barrier height increased with increasing zinc content. The threshold is difficult to determine with any accuracy from the spectral distribution curve. However when the square root of the photocurrent per incident photon was plotted against the photon energy in the vicinity of the threshold (also known as Fowler plot (9)), good straight lines were obtained for all junctions studied. Some of these plots are shown in figure 7.3a. With CdS, the barrier height measured by this method was found to be 0.72eV at room temperature. With x>0, the barrier heights were found to increase quite linearly up to x=0.5 at least as

$$\phi_{PH} = 0.72 + 1.06x \text{ eV}$$

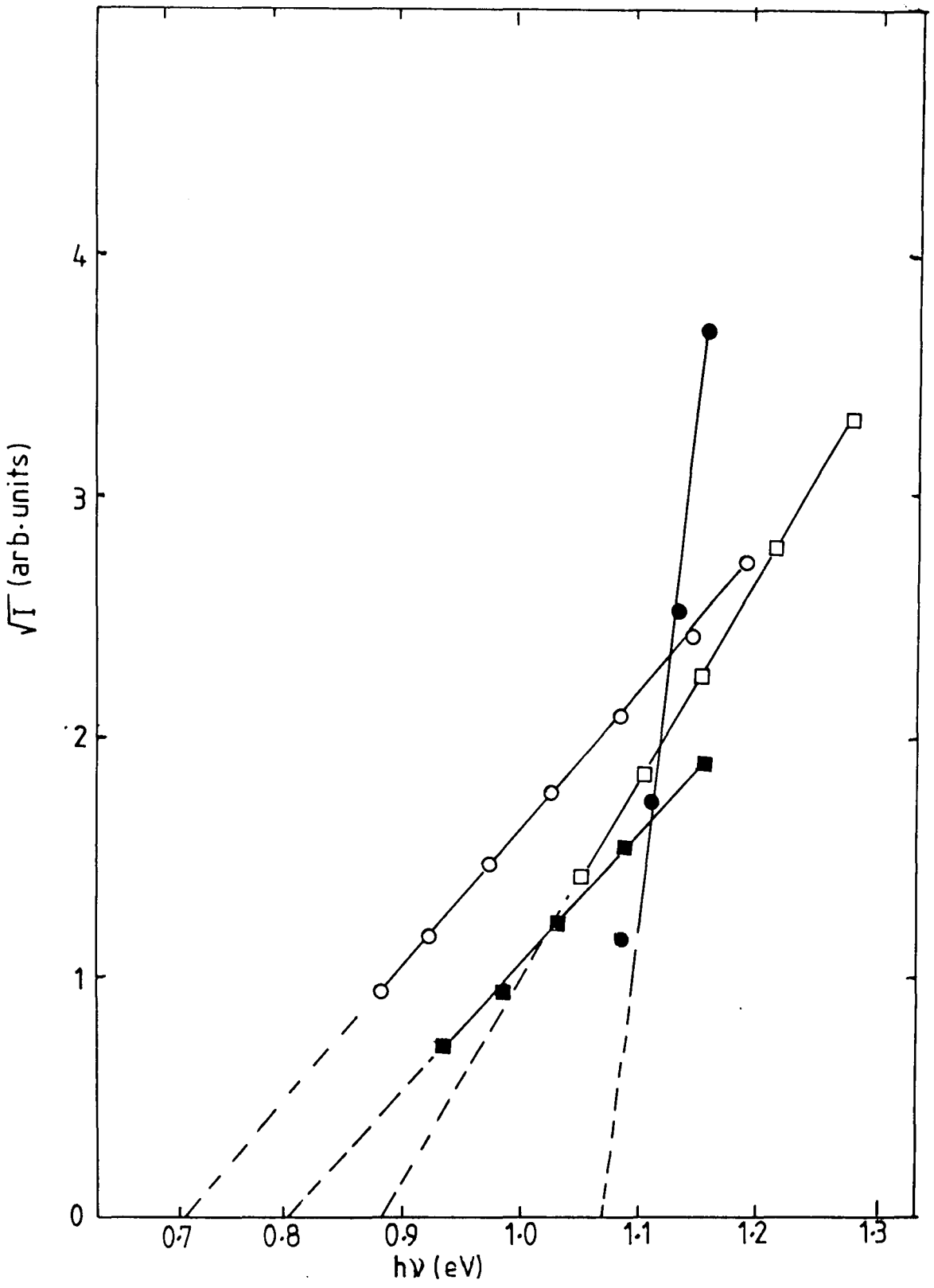

Figure 7.3a. Plot of $\sqrt{I}$ against photon energy for x=0 (○), x=0.07 (■), x=0.12 (□), and x = 0.35(●)

Barrier heights measured by this method are tabulated in table 7.3 and shown graphically in figure 7.3b together with barrier heights measured by other methods. The trend of decreasing short circuit photocurrent as x increases was also observed. A plot of ϕ_{PH} versus band gap is also shown in figure 7.3c where quite a good linear relationship is apparent.

Discussion

The measurement of the short circuit photocurrent of a Schottky diode at photon energies less than the band gap is regarded as the best way to determine the barrier height (10). Most of the work on II-VI compounds using this method has been concentrated on the binaries such as CdS (18) and ZnS (19), where attempts were made to correlate the measured value of the barrier heights with the work functions of the metals used or their electronegativity. As far as we are aware no experimental information has been published concerning the barrier height of Au-$Zn_xCd_{1-x}S$ single crystal diodes. With CdS where the barrier height is strongly dependent on the work function of the metal, it has been reported (18) that the results are sensitive to the surface preparation of the semiconductor. Any attempt to compare the results of different investigators is quite difficult since different methods of surface preparation and metal film deposition

x	ϕ_{PH}	ϕ_{C-V}	ϕ_{I-V}
0.0	0.72	1.06	0.79
0.05	0.80	1.22	0.75
0.07	0.80	-	0.84
0.10	-	0.96	-
0.12	0.89	-	0.88
0.23	-	-	0.86
0.24	0.95	1.07	0.86
0.26	0.97	1.01	0.78
0.35	1.07	1.14	0.93
0.38	-	1.37	0.92
0.41	-	1.58	1.22
0.42	1.15	1.49	1.25
0.50	1.25	1.68	-

Table 7.3: Barrier height calculated from photoelectric, capacitance-voltage and current-voltage

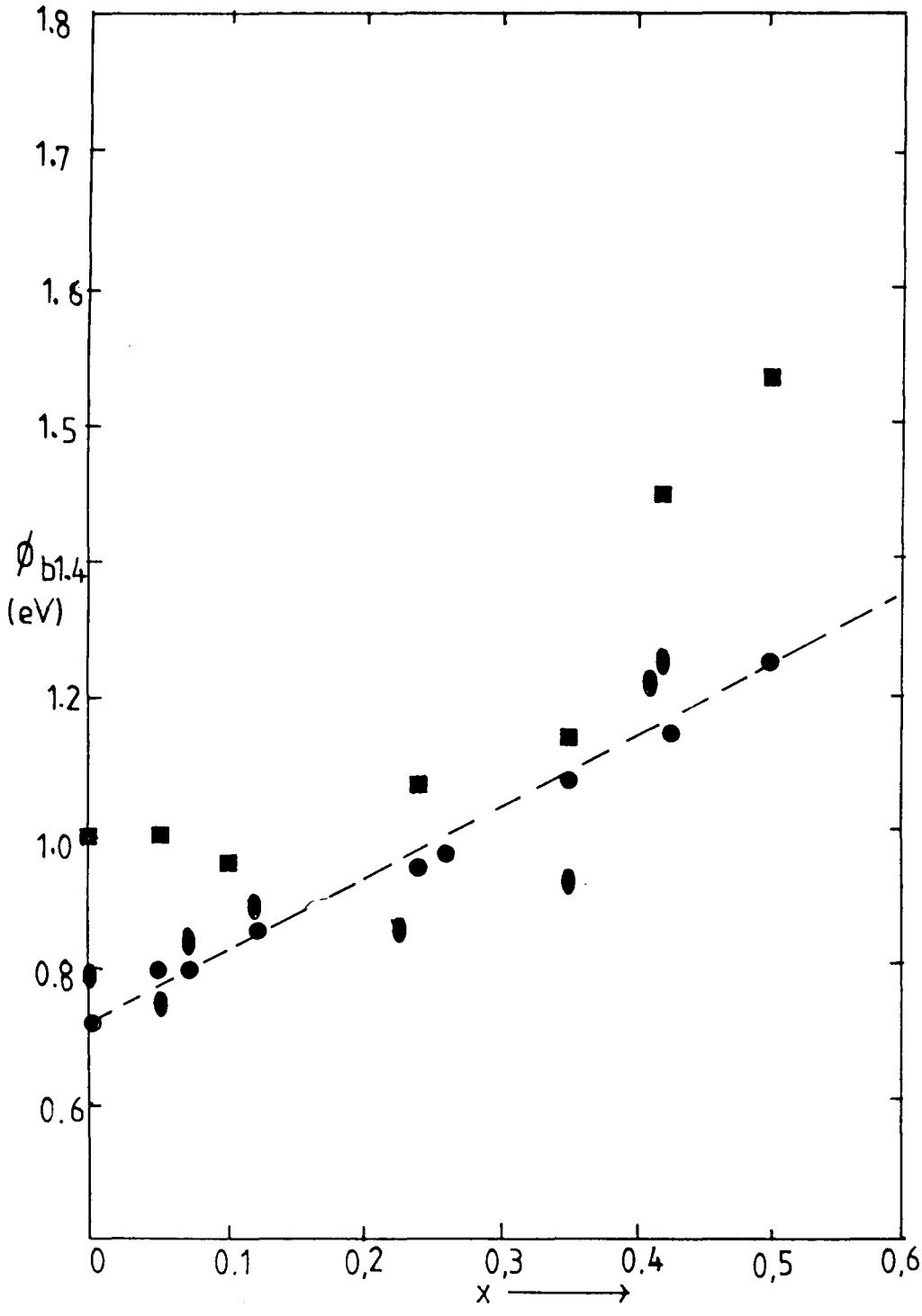

Figure 7.3b. Barrier height against x from photoelectric (●), current-voltage (⬮) and capacitance-voltage (■).

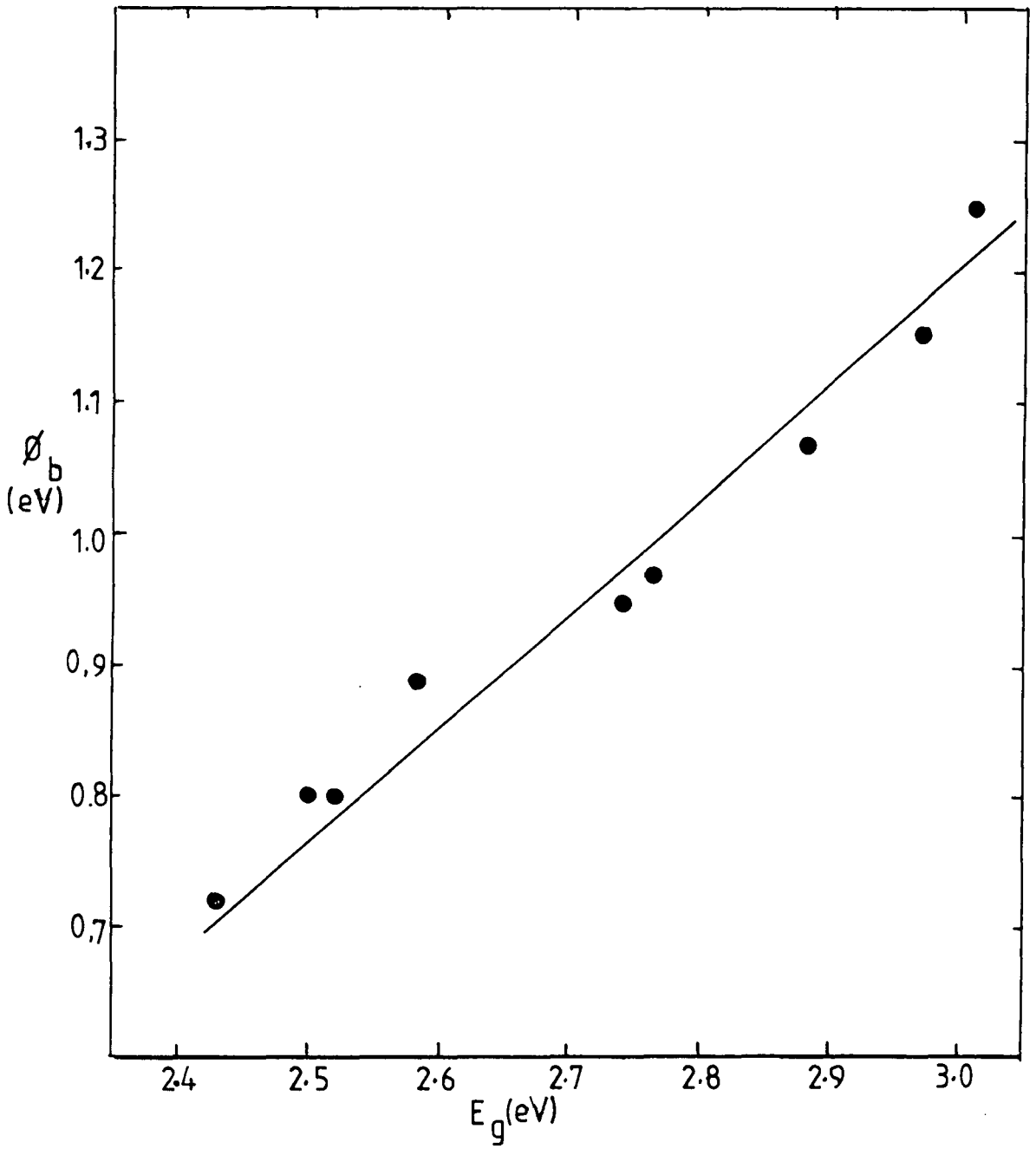

Figure 7.3c. Barrier height measured by photoelectric method versus band gap energy at 300K.

have usually been employed. For example, the barrier height of Au-CdS on vacuum cleaved samples was found to be 0.78eV (21) but the same authors (18) found that the Fowler plot was not linear with air cleaved and etched samples. In contrast, Goodman (22) and Butendeich and Ruppel (23) working on chemical etched surfaces showed that the Fowler plot was linear giving barrier heights of 0.68eV and 0.75eV respectively. The value of 0.72eV found in the present work is in good agreement with these.

Using the photoelectric method, Gol´dberg (24) working on the Au-$Ga_{1-x}Al_xAs$ system with $0<x<0.4$ found a linear relationship between ϕ_{PH} and x. As stated in the preceding section, the barrier height of our Au-$Zn_xCd_{1-x}S$ diodes for $0<x<0.5$, also displayed a linear dependence on x (figure 7.3b). A straight line extrapolation to 100% zinc, suggests that the barrier height for Au-ZnS should be about 1.78eV, but this is rather low compared with the value of 2.0eV reported by Aven and Mead (19) for vacuum cleaved ZnS. There is better agreement with the results on Au-ZnS by Lawther and Woods (25) and Thomas et al (26) who measured barrier heights of (1.85-2.00)eV and 1.9eV respectively.

7.5 Factors which control barrier heights measured by the I-V, C-V and photoelectric methods

The barrier heights of Au-$Zn_xCd_{1-x}S$ diodes

determined from the forward I-V characteristics, the C-V characteristics and the photoelectric method are tabulated in table 7.3, and shown graphically in figure 7.3b. Assuming that the surface preparation prior to depositing the gold contacts to complete the Schottky diodes leaves similar surfaces, the photoelectric barrier height was found to vary linearly with composition. On the other hand the barrier height measured by the C-V method, although still quite linear, was generally larger in magnitude. The following discussion will be focussed on the effects of a) the interfacial layer, b) interface and surface states and c) other effects.

a) **Interfacial layers**

This is a crucial feature when dealing with a chemically etched surface of a semiconductor. In our work, although the surface preparation was the same for all crystals, that is not to say that any i-layer which might have been present afterwards was the same. As discussed in section (7.2), a difference in the thicknesses of i-layers present is quite likely to have occurred. As far as I-V measurements are concerned, the presence of an i-layer at the interface has three major effects (10),

i) Because of the potential drop in the layer, the zero bias barrier height is lower than what it would be in an ideal diode.

ii) The electrons have to tunnel through the barrier presented by the i-layer, so that the current for a given bias is reduced.

iii) When a bias is applied, part of the bias voltage is dropped across the i-layer so that the barrier height ϕ_b is a function of the bias voltage. The effect of the bias dependence of the barrier height is to change the shape of the current-voltage characteristic in a manner which can be described in terms of an ideality factor (n) such that $n^{-1}=1-b$ where $b=d\phi_b/dV$. This relationship shows that n=1, if $d\phi_b/dV=0$, i.e. if ϕ_b is not bias dependent. Even if there is no i-layer present, the Schottky barrier height is lowered by a small amount $\Delta\phi_b$ due to the effects of image force lowering. If we compare, the values of ϕ_b measured by I-V with values obtained by the other methods, especially from C-V, it may be that the values of ϕ_b from I-V are not so much dependent on the i-layer as on the nature of the barrier as described in 7.2. If the barrier at the top is very thin, the electrons could easily tunnel through before emission over the barrier occurred.

The presence of an i-layer will also alter the capacitance of a Schottky barrier because the layer modifies the dependence of the charge in the depletion region on the bias voltage. The capacitance of the i-layer is effectively in series with the capacitance of the depletion region. Because of that, and since the latter is non-linear, the overall capacitance is a rather complicated

function of the parameters involved. The effect of an i-layer on capacitance has been analysed in some detail by Cowley (27) and Robert and Crowell (28). Analysis is easiest if the layer is sufficiently thin for the occupation of any interface states, which may exist at the i-layer-semiconductor interface, to be determined by the Fermi level in the metal (i < 30Å). Cowley's analysis (27) shows that the C^{-2}-V plots remain linear with a slope of $2/q\epsilon_s N_d$ as in the ideal case with no i-layer. The intercept on the voltage axis is modified to

$$V_i = V_{diff} - \left[\frac{kT}{q}\right] + \alpha\left[\frac{2qN_d}{\epsilon_s}\right]^{1/2}\left[V_{diff} - \frac{kT}{q}\right]^{1/2} + \frac{qN_d\alpha^2}{2\epsilon_s}$$

where

$$\alpha = \frac{d\epsilon_s}{\epsilon_i + qdD_s}$$

b) **Interface states**

The effects of surface and interface states on Schottky diodes are always connected with the i-layers present as we can see from the equations derived by Cowley (27). Cowley and Sze (29) and Rhoderick (10) showed that,

$$\phi_b = \beta(\phi_m - X_s) + (1-\beta)(E_g - \phi_o)$$

where $\beta = \epsilon_i/(\epsilon_i + qdD_s)$

Card and Rhoderick (4) divided interface states into two groups, such that all the states in one group (D_{sa}) are in

equilibrium with the metal, while those in the other group (D_{sb}) are in equilibrium with the semiconductor. The general expression is as follows,

$$n = 1 + \frac{(d/\epsilon_i)\{(\epsilon_s/w) + qD_{sb}\}}{1 + (dqD_{sa}/\epsilon_i)}$$

The above equation leads to the following conclusions

i) If the density of states is sufficiently small, $n=1+d\epsilon_s/w\epsilon_i$

ii) If the interface states are in equilibrium with the metal, ($D_{sb}=0$), $n=1+d\epsilon_s/\{w(\epsilon_i+qD_{sa})\}$

iii) If the interface states are in equilibrium with the semiconductor, ($D_{sa}=0$), $n=1+d/\epsilon_i(\epsilon_s/n+qD_{sb})$.

According to Mead (30), semiconductors can be divided into two categories; those in which the barrier height is controlled by surface states, and those in which surface states are not important. This may be too simple a view because some semiconductors (e.g. silicon) may be in either category according to the method of preparation. In a series of papers Mead and his coworker (18,21,30), reported that surface states are unimportant in CdS, but for CdSe the barrier height is effectively locked by surface states. With mixed crystals of CdS_ySe_{1-y} (31) there is apparently a smooth variation from one type of behaviour to the other as the composition is varied from CdS to CdSe. However, in contrast with Mead's statement about CdSe, Ture (32) found that the barrier height of CdSe

is very much dependent on the work function of metal used. As far as other ternary alloys of the II-VI family are concerned very little work has been done to determine how the barrier height depends on composition. Work on ZnS_xSe_{1-x} by Ozsan and Woods (33) showed that the barrier height of Au-ZnS_ySe_{1-y} Schottky diodes varied from 1.6eV (ZnSe) to 1.8eV (ZnS). According to Crowell and Sze (34), an ideality factor near unity does not necessarily imply an extremely thin i-layer since the barrier may also be pinned by a high density of interface states at the semiconductor surface.

c) **Other effects**

If the simple relation for the barrier height at a metal semiconductor contact, equation 3.41a is correct, then $\phi_b(x)=\phi_{Au}-X_x$, where $\phi_b(x)$ is the barrier height for gold on a mixed crystal with an electron affinity X_x. One difficulty is knowing what value of the work function of gold to use because of the wide difference in reported experimental results ranging from 4.86eV to 5.59eV (35-42). Apart from that, the values of the electron affinities of CdS and ZnS are also uncertain. For instance, electron affinities for CdS of 4.5eV (43) and 4.79eV (35) have been used, while for ZnS a value of 3.9eV has been reported (35). Furthermore values of ϕ_m or X determined from the properties of a free metal or semiconductor-vacuum surface are not necessarily the same as for the metal-semiconductor

or semiconductor- semiconductor interface.

7.6 General discussion

In II-VI compounds, 18 ternary alloys can be obtained from the binary systems (44). Work on semiconductor alloys provides a natural means of tuning the material parameters so as to optimise and widen the application of semiconductor devices. For example, the need to provide material for optical applications in the long wavelength range (e.g. infrared detectors), has led to the development of ternary alloys of $Hg_xCd_{1-x}Te$ and a great deal of effort has been put into characterising their properties (45,46). On the other hand, for applications in the short wave length range such as L.E.Ds. particularly in the blue region, work on ZnS_ySe_{1-y} (47) and $Zn_xCd_{1-x}S$ (48) may be quoted.

Before any such application can be made, the preparation and characterisation of the properties of the alloy systems has to be established. In addition to the experimental work, theoretical ideas have also to be developed.

Apart from uncertainty in the values of the work function of gold and the electron affinity for ZnS and CdS, it is generally assumed that the electron affinity of $Zn_xCd_{1-x}S$ decreases as the zinc composition increases (48).

By working on Cu_2S-$Zn_xCd_{1-x}S$ heterojunctions, Oktik et al (49) and Das et al (50) showed that the photoelectric threshold energy increased with increasing zinc content which supports the assumption made earlier. Indeed our measurements of the photothreshold of Au-$Zn_xCd_{1-x}S$ confirm this statement. If we assume that ϕ_{Au} is 5.49eV (35), then $X_{x=0}$, calculated using a simple relation of $X_{x=0}=\phi_{Au}-\phi_b(0)$ is about 4.77eV. If this is correct, a composition with zinc content of about x=0.15 can be used to eliminate the discontinuity at the interface in Cu_2S-$Zn_xCd_{1-x}S$ provided that $X_{x=0} - \Delta E_c \approx 4.65$eV (16) and the linear relationship of X_x with composition holds.

7.7 Conclusions

Schottky diodes of Au-$Zn_xCd_{1-x}S$ ($0<x<0.5$) have been prepared on chemically etched surfaces. The conclusions to be drawn are as follows:-

1) From the I-V characteristics, the values of the ideality factor were found to vary from 1.1 to about 2. In general, the values of saturation current density decreased as the zinc composition increased.

2) From C-V measurements, all the calculated parameters depended on conductivity of the samples. The trend was for the uncompensated donor density to increase as the zinc content increased from x=0 to about x=0.1 and then

decreased as more zinc was added. This is consistent with the Hall coefficient measurements (chapter VI) and with some other published work.

3) The measurements of short circuit photocurrent on Schottky diodes as a function of photon energy, show that the barrier height varies nearly linearly with x ($x<0.5$). On the other hand the barrier height measured by other methods depends to a certain extent on the surface properties and the conductivity of the semiconductor.

4) A mixed crystal with $x\sim0.15$ can be used to eliminate the discontinity at the interface of $Zn_xCd_{1-x}S$-Cu_2S heterojunctions due to the difference in values of X_{CdS} and X_{Cu_2S}.

References for chapter VII

1) L.F.Wagner, R.W.Young and A.Sugerman, IEEE Elec. Dev. Lett., **EDL-4(9)** (1983) 320

2) D.P.Verret, IEEE Elec. Dev. Lett., **EDL-5(5)** (1984) 142

3) E.H.Rhoderick, IEE Proc., **129** (1982) 1

4) H.C.Card and E.H.Rhoderick, J. Phys. D: Appl. Phys., **4** (1971) 1589

5) V.L.Rideout, Thin Solid Films, **48** (1978) 261

6) D.Khang, Sol. State Electr., **6** (1963) 281

7) S.Oktik, G.J.Russell and J.Woods, J. Cryst. Growth, **59** (1982) 414

8) P.C.Pande, **PhD Thesis**, Durham University 1984

9) S.M.Sze, **Physics of Semiconductor Devices**, A Wiley Interscience publication, 2nd. edition, (1981)

10) E.H.Rhoderick, **Metal-Semiconductor Contacts**. Clarendon Press. 1980 Oxford

11) Y.Sakurai, Y.Kokubun, H.Watanabe and M.Kaka, Jpn. J. Appl. Phys., **16** (1977) 2115

12) H.H.L.Kwok and Y.C.Chau, Thin Solid Films, **66** (1980) 1911

13) L.W.Chow, Y.C.Lee and H.H.L.Kwok, Thin Solid Films, **81** (1981) 307

14) T.A.Chynoweth and R.H.Bube, J. Appl. Phys., **51** (1980) 1844

15) H.H.L.Kwok, M.Y.Leung and Y.W.Lam, J. Cryst. Growth, 59 (1982) 421

16) P.Domens, M.Cadene, G.W.Cohen Solal, S.Martinuzzi and

C.Brouty, Phys. Stat. Sol., **59a** (1981) 201

17) A.M.Goodman, J. Appl. Phys., **34** (1963) 329

18) W.G.Spitzer and C.A.Mead, J. Appl. Phys., **34** (1963) 3061

19) M.Aven and C.A.Mead, Appl. Phys. Lett., **7** (1965) 8

20) M.Kusaka,T.Matsui and S.Okazaki, Sur. Science, **41** (1974) 607

21) C.A.Mead and W.G.Spitzer, Phys. Rev.,**143A** (1964) 713

22) A.M.Goodman, J. Appl. Phys., **35** (1964) 573

23) R.Butendeich and W.Ruppel, Phys. Stat. Sol.,**49a** (1978) 169

24) Y.A.Gol´dberg, T.Y.Rafiev, B.V.Tsarenkov and Y.P.Yakovlev, Soviet Phys. Semicond., **6** (1972) 398

25) C.Lawther and J.Woods, Phys. Stat. Sol., **50a** (1978) 491

26) A.E.Thomas, J.Woods and Z.V.Hauptman. J. Phys D: Appl. Phys., **16** (1983) 1123

27) A.M.Cowley, J. Appl. Phys., **37** (1966) 3024

28) G.I.Robert and C.R.Crowell, J. Appl. Phys., **41** (1970) 1767

29) A.M.Cowley and S.M.Sze, J. Appl. Phys., **36** (1965) 3212

30) C.A.Mead, Sol. Stat. Electr., **9** (1966) 1023

31) C.A.Mead, Appl. Phys. Lett., **6** (1965) 103

32) I.E.Ture, **Ph.D Thesis**, Durham University 1984

33) M.E.Ozsan and J.Woods, J. Phys. D:Appl. Phys, **10** (1977) 1335

34) C.R.Crowell and S.M.Sze, Sol. St. Electro., **9** (1966) 1035

35) R.K.Swank, Phys. Rev., **153** (1967) 844

36) E.E.Huber Jr., Appl. Phys. Lett., **8** (1966) 169

37) J.C.Riviere, Proc. Phys. Soc., **70** (1957) 676

38) B.J.Hopkins, C.H.B.Mae and D.Parker, Brit. J. Appl. Phys., **15** (1964) 865

39) J.C.Riviere, Brit. J. Appl. Phys., **15** (1964) 1341

40) P.A.Anderson. Phys. Rev., **115** (1959) 553

41) J.C.Riviere, Appl. Phys. Lett., **8** (1966) 172

42) A.A.Holscher, Sur. Sci., **4** (1966) 89

43) A.L.Fahrenbruch and R.H.Bube, **Fundamentals of Solar Cells-Photovoltaic Solar Energy Conversion.** Academic Press. 1983

44) H.Hartmann, R.Mach and B.Selle, **Current Topics in Material Science,** (North Holland Publ., 1982) edited by E.Kaldis.

45) Proceedings of the 1985 U.S. Workshop on the Physics and Chemistry of Mercury Cadmium Telluride- J. Vac. Sci. Tech., **4a** (1986)

46) Semiconductors and Semimetals, **16** (1981) edited by R.K.Willardson and A.C.Beer.

47) H.E.Gumlich, J. Lumin., **23** (1981) 73

48) L.C.Burton, Solar Cells , (1979/80) 159

49) S.Oktik, G.J.Russell and J.Woods, Solar Cells, 5 (1982) 231

50) R.S.Das, A.Banerjee and K.L.Chopra, Sol. St. Elect., **22** (1979) 533

CHAPTER VIII

PHOTOCAPACITANCE STUDY

8.1 Introduction

In this chapter, steady state photocapacitance (PHCAP) and infra red quenching of photocapacitance (IRQPHCAP) measurements are described. These techniques were employed to see what defect levels, if any, might be present in this material. For this purpose, Schottky diodes were prepared on as-grown undoped, and copper doped samples of Au-$Zn_xCd_{1-x}S$. The methods of preparing the samples, and the experimental procedure and the equipment used have been described in chapter IV. It is very difficult to prepare copper doped samples to make good Schottky diodes which requires a resistivity in the range $10-10^2$ ohm-cm. With $x>0.5$, the as-grown material was highly resistive and measurements were therefore limited to compositions with $x<0.5$.

8.2 CdS

PHCAP and IRQPHCAP measurements were carried out on CdS Schottky diodes prepared on as-grown and intentionally copper doped samples. Figure 8.1a shows a PHCAP spectrum of as-grown CdS (830) at 90K. There was a steady increase in PHCAP as the photon energy increased to the band gap

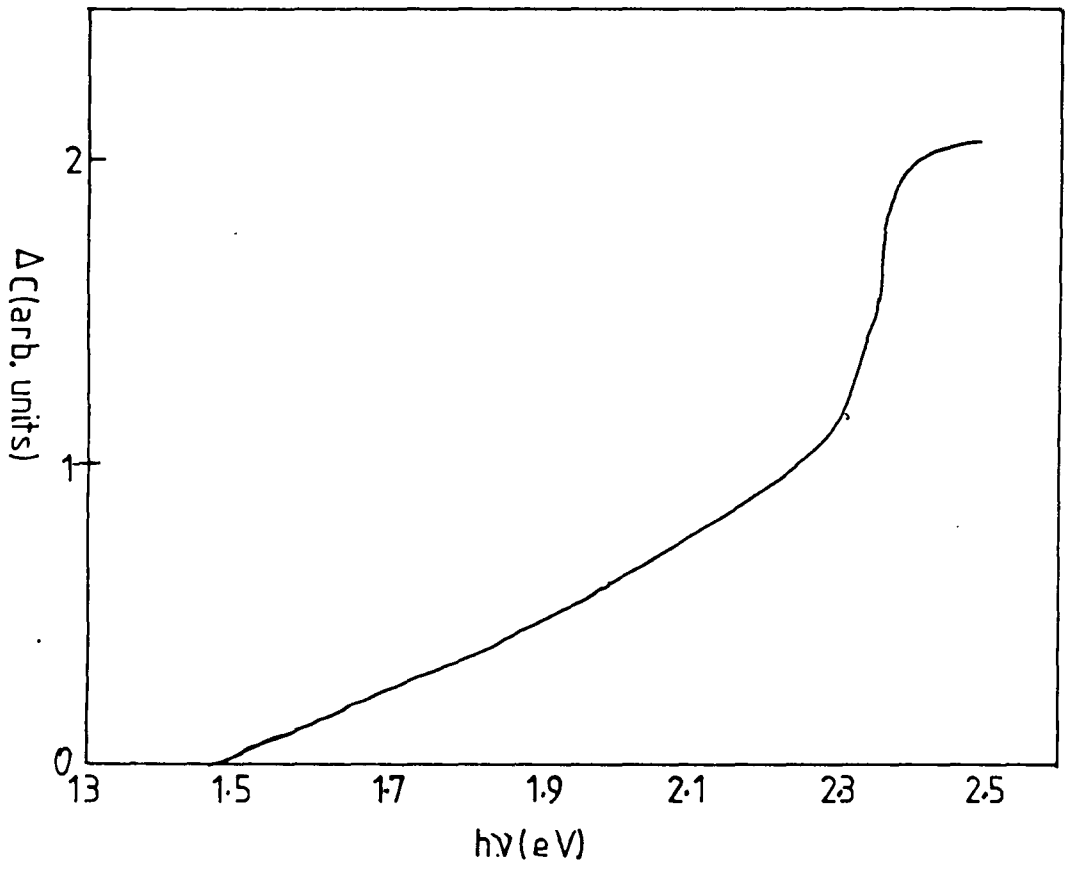

Figure 8.1a. Photocapacitance spectrum of undoped CdS at 90K.

value starting with a threshold at about 1.5eV. This suggests the presence of a level at about 1.0eV above the valence band. The incident light excited electrons from levels 1.5eV below the conduction band leading to a positive charge in the depletion region. A second positive going threshold at a photon energy of 2.25eV indicates that there was also a level some 0.25eV above the valence band.

IRQPHCAP of this sample was also carried out but no quenching was observed.

PHCAP spectra for copper doped CdS at 300K and 90K are shown in figures 8.1b and 8.1c respectively. At 300K, a negative threshold occurred at 0.72eV. As the photon energy was increased, a positive threshold was clearly seen to start at about 1.3eV corresponding to an ionisation energy of the acceptor level of 1.12eV. A sudden decrease occurred at 1.95eV implying that there is a donor level situated at about 0.47eV below the conduction band. Finally another positive threshold at 2.25eV put an acceptor level at 0.17eV. A quite different structure was observed when the scan was made at 90K. The quenching which was apparent at 0.72eV at 300K was not observed; instead there was sharp positive threshold at 0.95eV suggesting that the emptying of a level about 0.95eV below the conduction band was the dominant process. With increasing photon energy a negative going threshold was observed at 1.2eV with an additional positive going

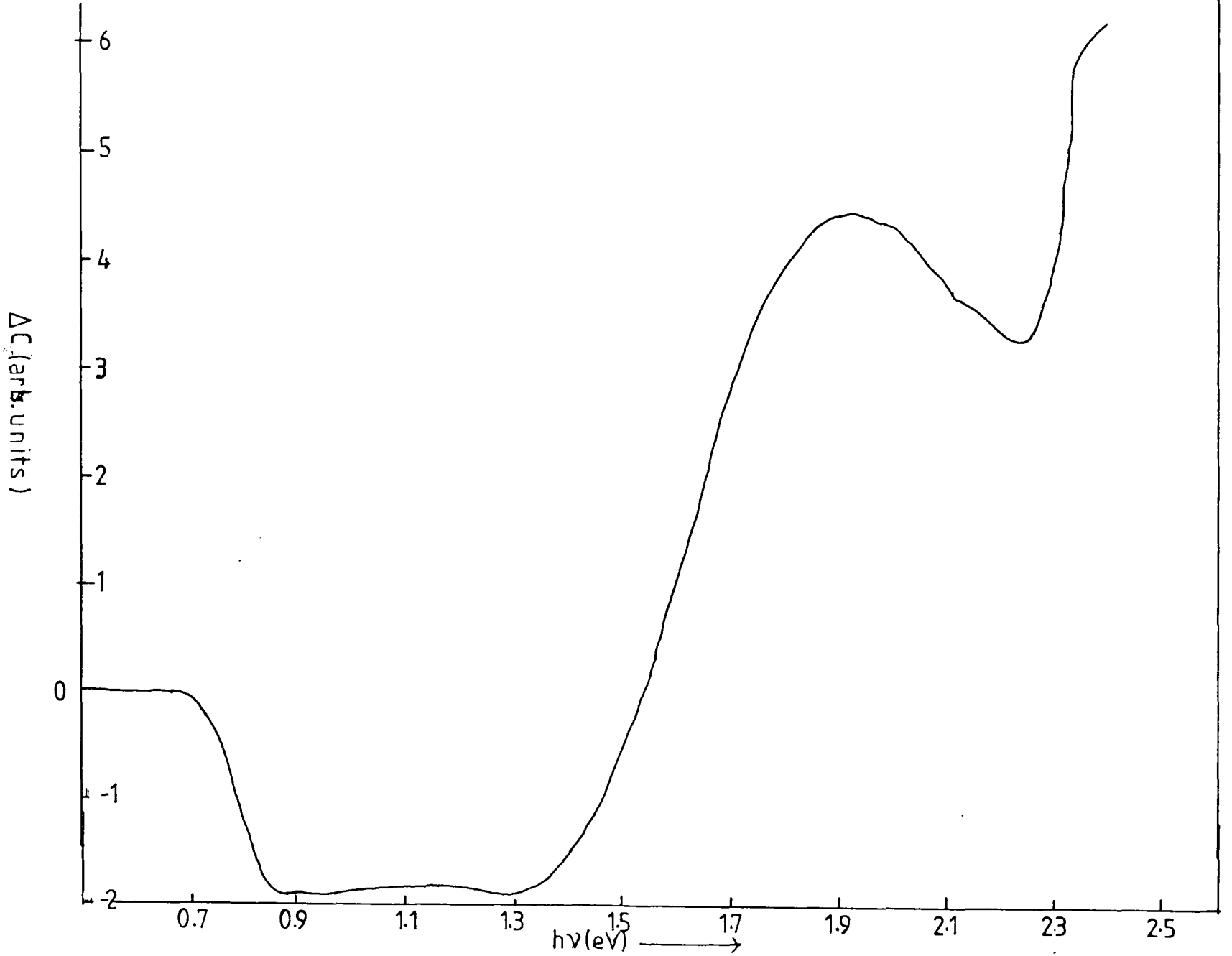

Figure 8.1b. Photocapacitance spectrum of CdS:Cu at 300K.

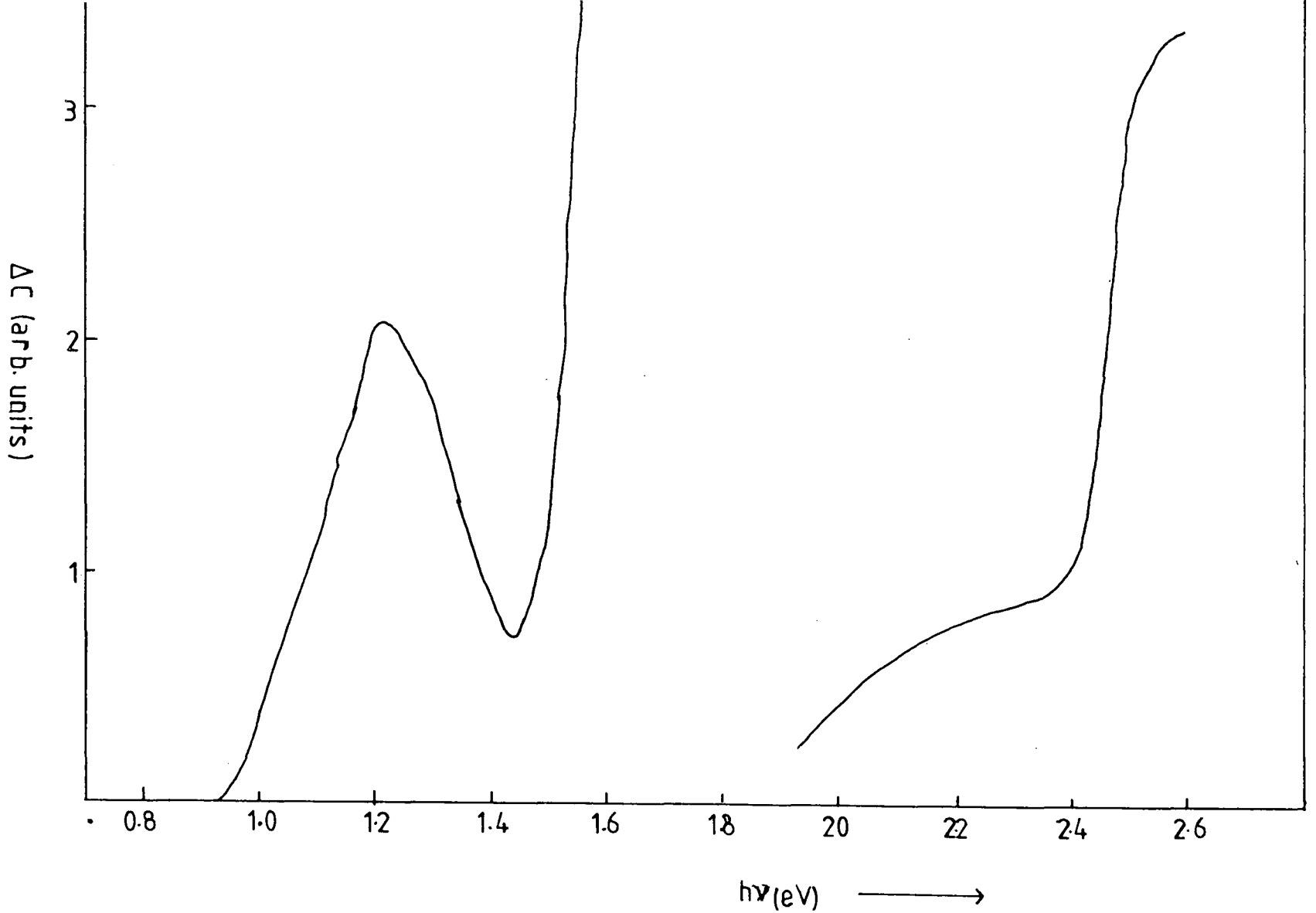

Figure 8.1c. Photocapacitance spectrum of CdS:Cu at 90K.

threshold at 1.43eV. Assuming that the band gap of CdS at 90K is about 2.52eV, the quenching at 1.2eV and enhancement at 1.43eV are probably due to the response of the same centre although the sum of the threshold energies is slightly larger than the band gap.

IRQPHCAP measurements were also carried out for this device. At 300K, two negative thresholds at 0.72eV and 1.15eV were clearly shown (figure8.1d). At 90K, the first threshold disapeared but and the second threshold was still strongly apparent at about 1.17eV.

The photon energies of the PHCAP thresholds are collected together in table 8.1, with plus and minus signs indicating the positive and negative going thresholds respectively.

Discussion

The results obtained on the as-grown and copper doped crystals of CdS, were used as a guide for studying mixed crystals of $Zn_xCd_{1-x}S$. In general the results agree quite well with previously reported work (1,2,3,4,5). The presence of a deep acceptor state at about 1.0eV above the valence band in as-grown undoped crystals prepared using the Clark-Woods growth technique is probably due to a cadmium vacancy as suggested by Pande (1) who also investigated similar samples.

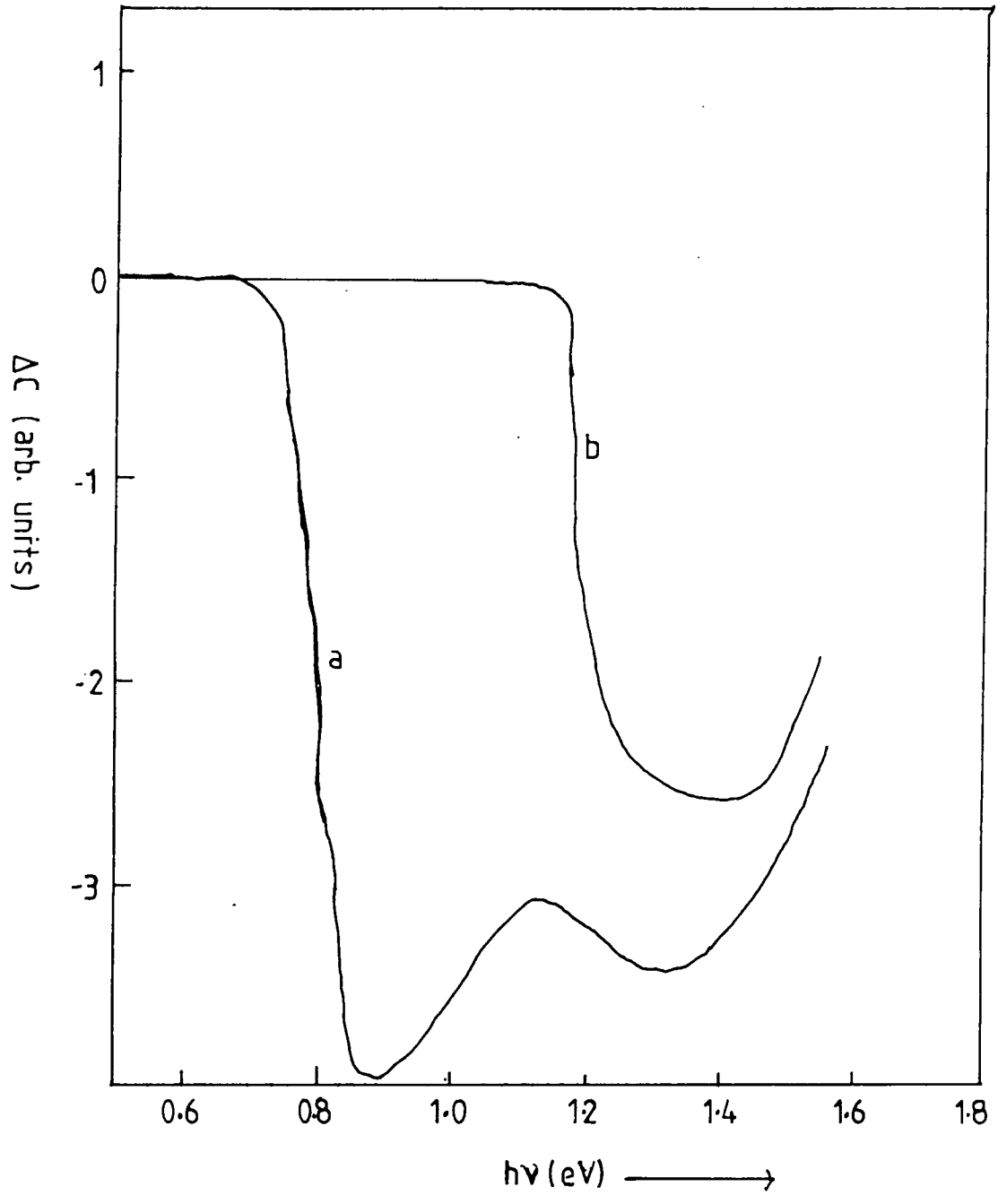

Figure 8.1d. Infra-red quenching of photocapacitance of CdS:Cu a) 300K and b) 90K.

	Measurement	Thresholds (eV)
CdS as-grown	PHCAP 90K	+1.5, +2.25
CdS:Cu	PHCAP 300K	-0.72, +1.3, -1.95, +2.25
	PHCAP 90K	+0.95, -1.2(B) +1.43(A), +2.38
	IRQPHCAP 300K	-0.75, -1.15(B)
	IRQPHCAP 90K	-1.17(B)

Table 8.1: Thresholds obtained from as-grown and copper doped CdS

With copper doped CdS, the dominant feature was the presence of a deep acceptor state at about 1.1-1.2eV above the valence band. This can be attributed directly to the copper level since copper is a well-known impurity which has been investigated by a number of other workers (2,3,4). A wide range of levels varying from 0.93eV to 1.2eV has also been attributed to copper (5,6,7). The differences might be associated with the measurement techniques, although probably the most important fact is the nature of the crystal itself, which depends on the growth method and the doping procedure etc. It has also been suggested that if slightly less cadmium is introduced into the charge then the presence of some of the trapping centres in CdS will be affected (5). In a similar II-VI compound, ZnSe, doped with 5 p.p.m. Ga, an acceptor level was observed at 0.55eV above the valence band, but with increasing gallium content (50 p.p.m.), the concentration of that acceptor decreased while a new shallower acceptor at 0.40eV appeared (8). The method used to introduce copper by evaporating a thin layer of copper on one side and then annealing in vacuum at 800^{o}C for about 10-16 hours (3,5) might well change the native defect centres.

The evidence for the existence of energy levels associated with copper centres at about 1.1-1.2eV and 0.45eV above the valence band is quite apparent from our IRQPHCAP measurements. It has been suggested that copper

acceptors have two states, namely ground and excited states. At 90K infra-red quenching occurs at 1.17eV and is attributed to the excitation of electrons from the valence band to the ground states of the Cu^{2+} acceptors. At 300K, quenching is initiated at lower energy because holes trapped in the ground state of Cu^{2+} can be raised to excited states 0.72eV below the ground states and thermally ionised at 300K. Since the observed thresholds were at 0.72 and 1.15eV at 300K and at 1.17eV at 90K, the hole excited state lies at about 0.45eV above the valence band. This value is in reasonable agreement with that reported by Pande et al (2) and Grimmeiss et al (3).

The presence of an electron trap at about 0.47eV below the conduction band inferred from the threshold at 1.95eV at 300K also been reported by Poulin et al (5) using a DLTS technique, and Patil (9) using TSC measurements.

8.3 $Zn_xCd_{1-x}S$

8.3.1 **As-Grown Undoped Crystals**

PHCAP spectra for mixed crystals grown using the Clark-Woods method (sealed tube technique) are shown in figure 8.2a. All measurements were taken at 90K. With a low zinc content with x=0.05, the first threshold leading to an increased PHCAP was observed at a photon energy of

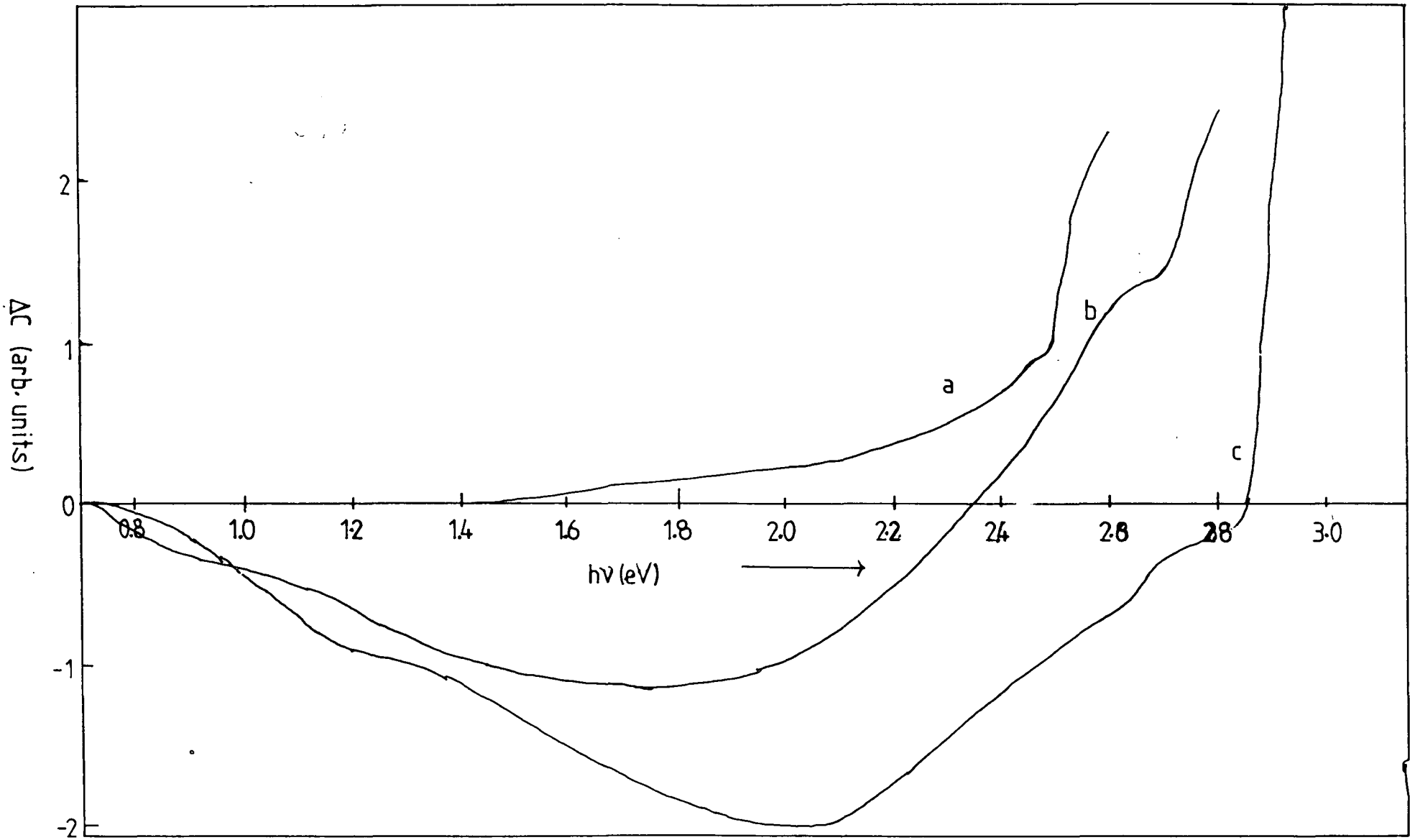

Figure 8.2a. Photocapacitance spectra of as-grown $Zn_xCd_{1-x}S$

a) x=0.05, b) x=0.22 and c) x=0.3 at 90K.

about 1.5eV, indicating that there is a process of excitation of electrons from a level 1.5eV below the conduction band, ~1.1eV above the valence band (E_g =2.6eV for x=0.05 at 90K) as in CdS. As the photon energy was increased, a second threshold was observed at $h\nu$=2.5eV corresponding to the emptying of an acceptor at about 0.1eV above the valence band.

For a sample with much more zinc with x=0.22, two negative going thresholds were observed at $h\nu$=0.75eV and at about 1.15eV. The second negative going threshold at 1.15eV and the positive going threshold at 1.75eV could be associated with the filling and empyting of the same centre, because the sum of these thresholds is the approximate value of the band gap. A threshold at about 2.72eV also indicated the presence an acceptor at about 0.09eV.

In the third sample with slightly more zinc with x=0.3, two negative going thresholds were also observed in similar positions at $h\nu$=0.75eV and about 1.2eV. Three positive going thresholds occurred at $h\nu$=2.1, 2.65 and 2.86eV corresponding to levels 0.81, 0.26 and 0.05eV above the valence band respectively (E_g=2.91eV at 90K).

Figures 8.2b to 8.2e show PHCAP spectra of Schottky diodes fabricated on undoped crystals of $Zn_xCd_{1-x}S$ grown by the Piper-Polich method (open ended technique). Four dice

with different compositions were studied. Two were taken from boule HT 157 (x=0.1 and 0.22), and another two from boule HT 156 (x=0.4 and 0.43). Steady state PHCAP measurements for the sample with x=0.1 measured at 300K and 90K are shown in figure 8.2b. At 300K, a very strong negative going PHCAP was observed at a photon energy of about 0.72eV. Another small negative going threshold was also observed at 1.15eV and can be attributed to a process of promoting electrons from the valence band to levels at about 1.15eV above it. With increasing photon energy a positive going threshold appeared as the photon energy approached 1.40eV. The sum of the negative going threshold (1.15eV) and the positive going threshold (1.4eV) is equal to the band gap energy for crystals with x=0.1 at 300K as demonstrated in chapter V where the width of the energy band gap as a function of composition (x) is described (section 5.5). This suggests that these responses are associated with filling and emptying the same level. The 300K spectrum also reveals the existence of a donor level about 0.23eV and an acceptor at about 0.13eV corresponding to a negative going threshold at 2.32eV and a positive going one at 2.42eV.

In the low temperature spectrum shown in figure 8.2b for x=0.1, a negative going threshold was observed at an incident photon energy of 1.18eV. No negative response at 0.72eV was observed. At a photon energy of 1.58eV, a large positive PHCAP was observed. The sum of the

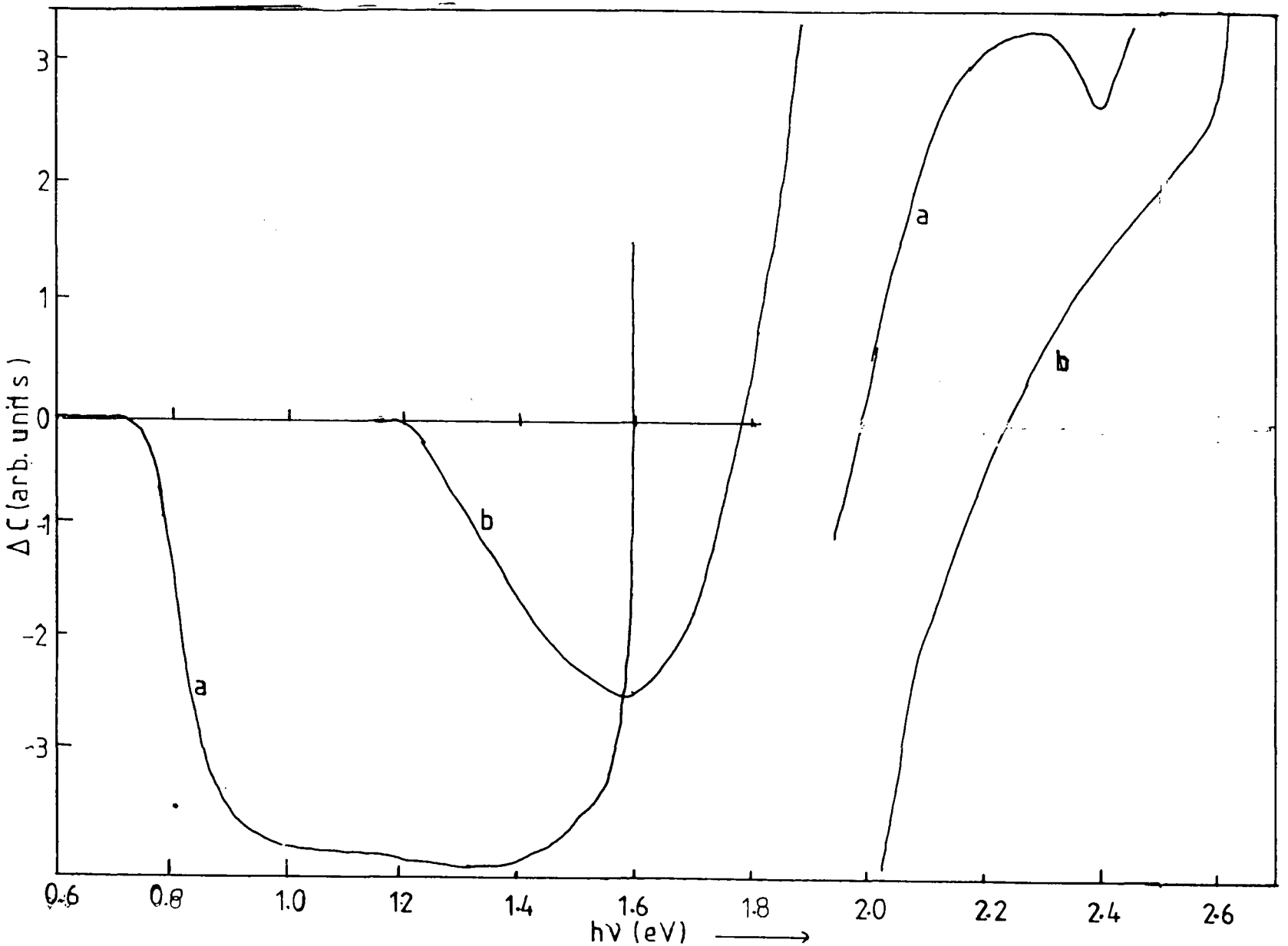

Figure 8.2b. Photocapacitance spectra of as-grown $Zn_{.1}Cd_{.9}S$ at a) 300K and b) 90K.

quenching (1.18eV) and excitation (1.58eV) thresholds was slightly higher than the expected value of the band gap (2.65eV) but no doubt the same centre was being filled and emptied in the two processes. Finally a high energy positive going threshold at $h\nu$=2.56eV indicated the presence of a level at about 0.09eV above the valence band.

Measurements for the diode fabricated in the sample with x=0.22 are shown in figure 8.2c. At 300K the negative threshold at 0.75eV was again observed. As the photon energy was increased a positive going threshold was observed at 1.65eV. No decrease at about 1.1-1.2eV could be seen. However at 90K a quenching threshold appeared at 1.2eV coupled with the enhancment at 1.7eV. Once again the sum of these two values was slightly higher than the band gap energy (figure 8.2c).

The results for the diode on a sample with x=0.4 are shown in figure 8.2d. Once again there is a negative threshold at 0.75eV and this time a second one is resolved at about 1.1-1.2eV at 300K. As the temperature was reduced to 90K, a new feature appeared as an increase in PHCAP at the lower energy of about 0.65eV, indicating that a new donor-like level was present some 0.65eV below the conduction band. Other positive going thresholds were also observed at photon energies of 1.4eV, 2.05eV, 2.2eV, 2.6eV and 2.95eV corresponding to levels at 1.4eV (CB), 1.03eV(VB), 0.88eV (VB) 0.49eV (VB) and 0.13eV (VB)

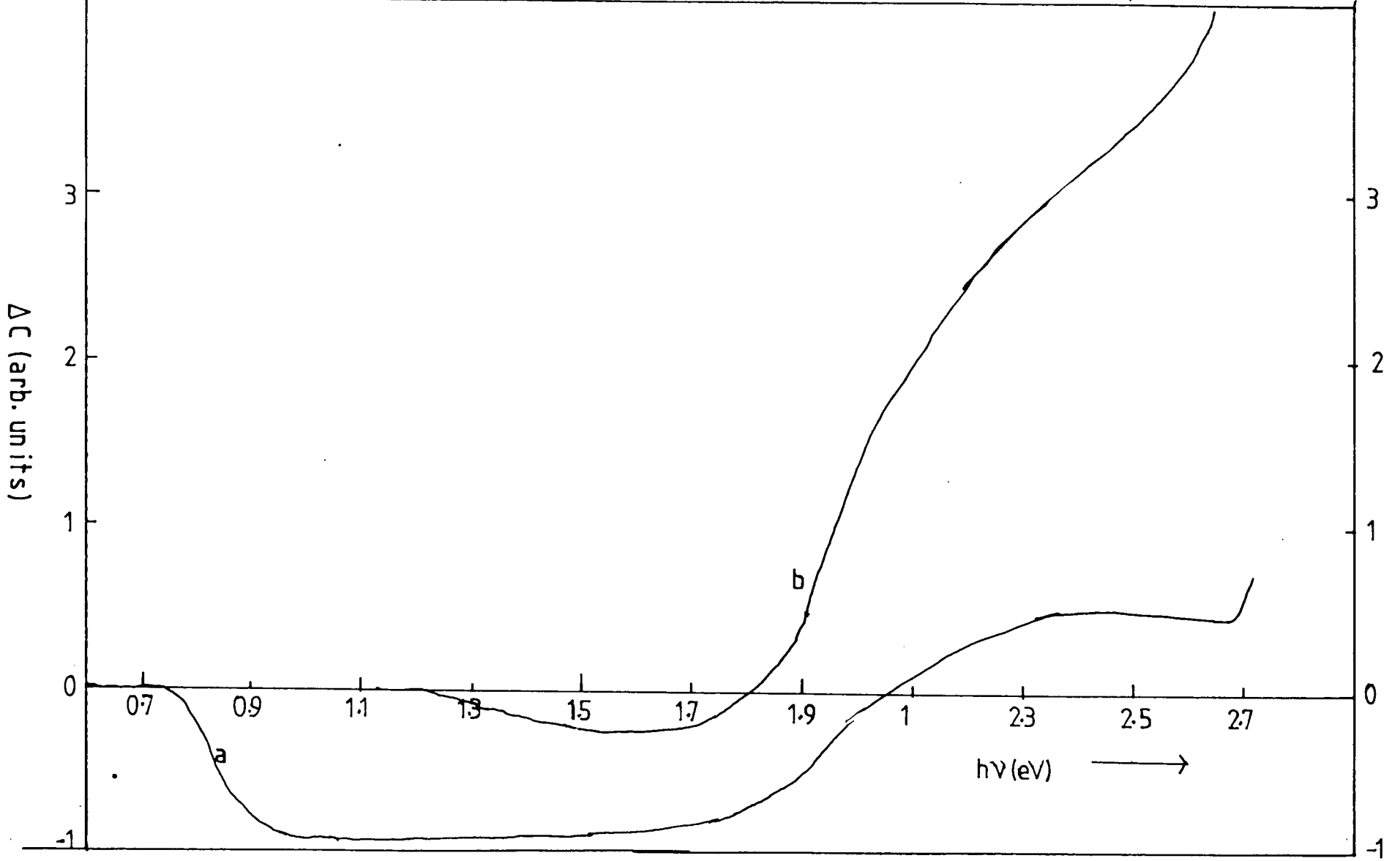

Figure 8.2c. Photocapacitance spectra of as-grown $Zn_{.22}Cd_{.78}S$ at a) 300K and b) 90K.

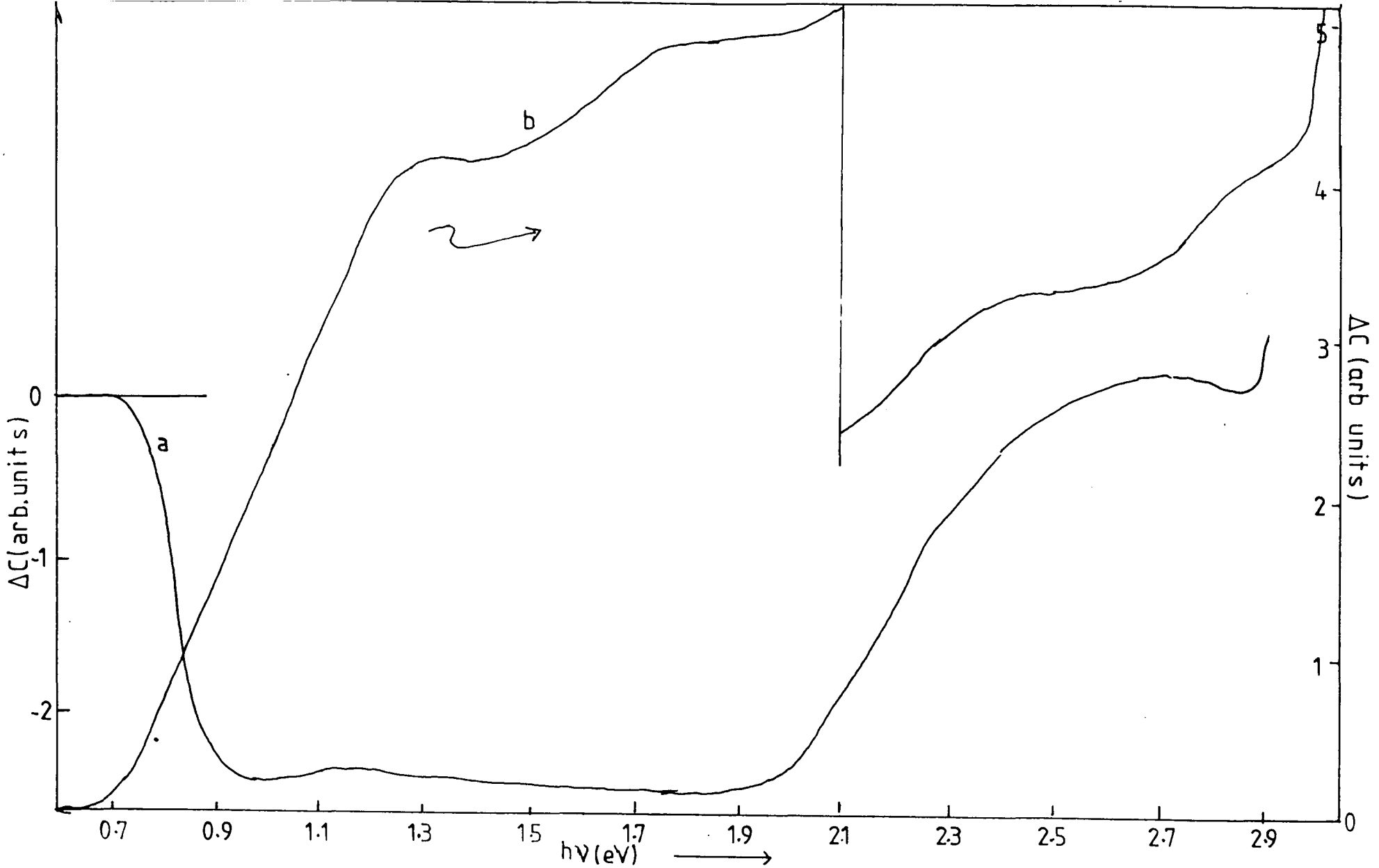

Figure 8.2d. Photocapacitance spectra of as-grown $Zn_{.4}Cd_{.6}S$ at a) 300K and b) 90K.

respectively where (CB) indicates that the energy is measured from the conduction band and (VB) from the valence band.

The PHCAP spectrum at 300K (figure 8.2e) for the diode on the sample with x=0.43 also shows a negative threshold at 0.75eV. As the photon energy was increased, a positive going threshold was observed at about $h\nu$=1.8eV. This corresponds again to a process of emptying a level at about 1.18eV above the valence band. On cooling to 90K, three positive going thresholds at photon energies of 0.85eV, 1.4eV and 2.05eV were observed corresponding to levels 0.85eV (CB), 1.45eV (CB) and 1.03eV (VB) respectively. The three negative going thresholds at photon energies of 1.35eV, 1.85eV and 2.32eV suggest that these are levels at about 1.35eV (VB), 1.23eV (CB) and 0.76eV (CB) respectively. It is understood of course that changes in the shape of the PHCAP spectrum may not be associated with the onset of a new filling or emptying process. There may simply be gradual changes in the transition probabilities.

Measurements were also carried out on these samples using steady state IRQPHCAP. Quenching spectra measured at 300K for diodes on samples with x=0.1, 0.22 and 0.4 illustrated in figures 8.2f and 8.2g show clearly the presence of thresholds at 0.75eV and 1.15-1.2eV. At 90K, these two thresholds were also observed for the diodes with

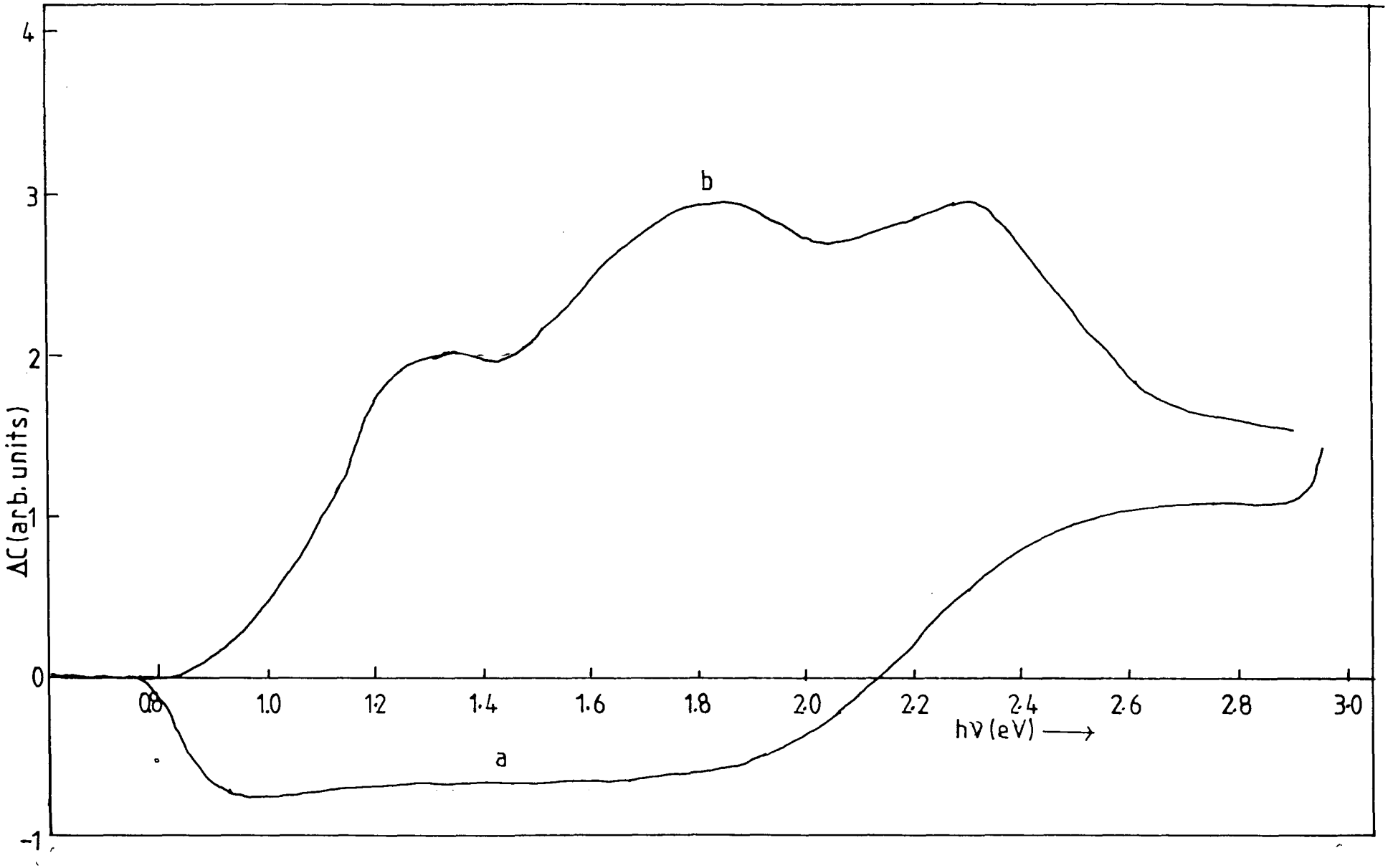

Figure 8.2e. Photocapacitance spectra of as-grown $Zn_{.43}Cd_{.57}S$ at a) 300K and b) 90K.

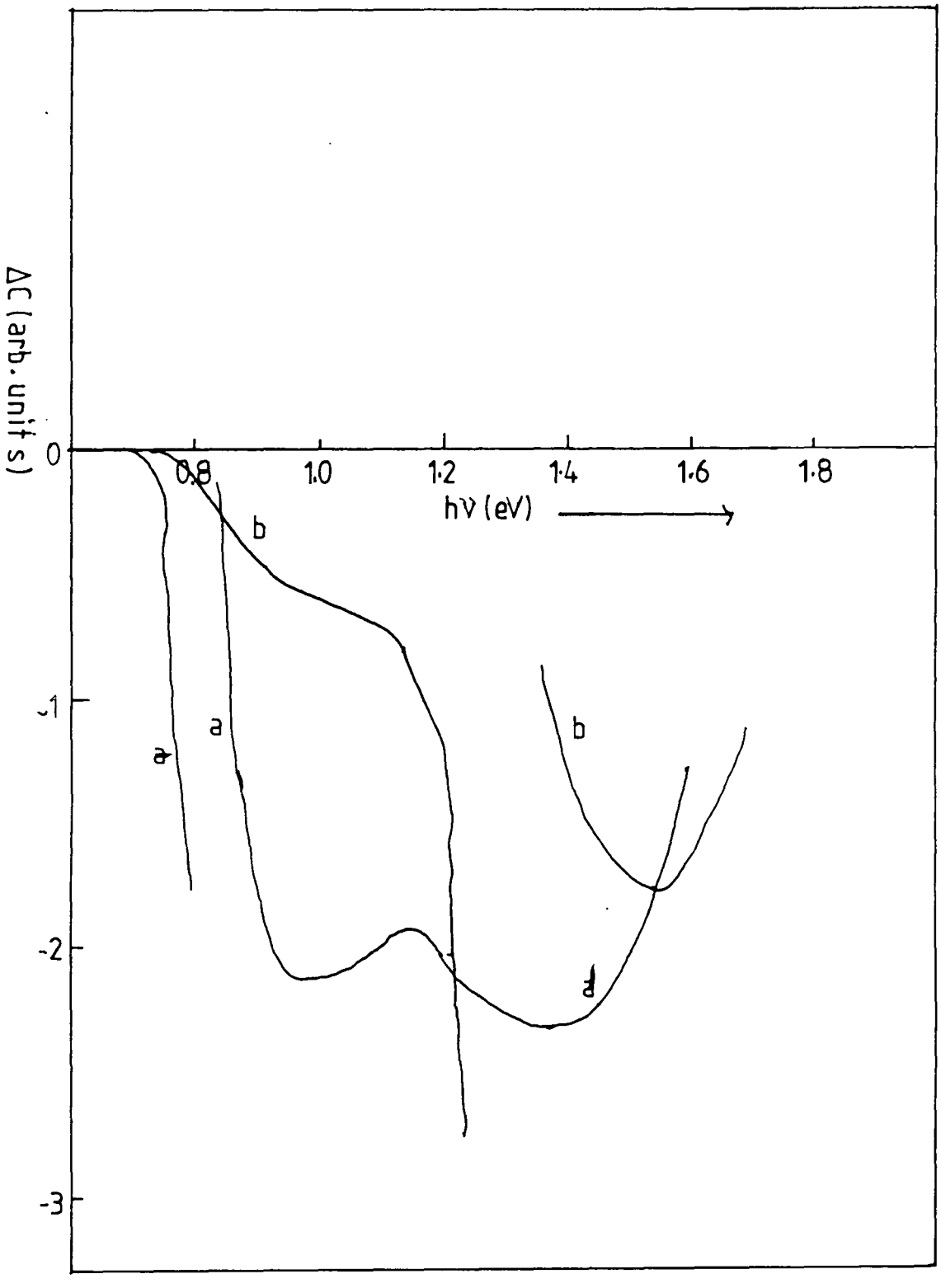

Figure 8.2f. Infra-red quenching of photocapacitance spectra of as-grown $Zn_{.1}Cd_{.9}S$ at a) 300K and b) 90K.

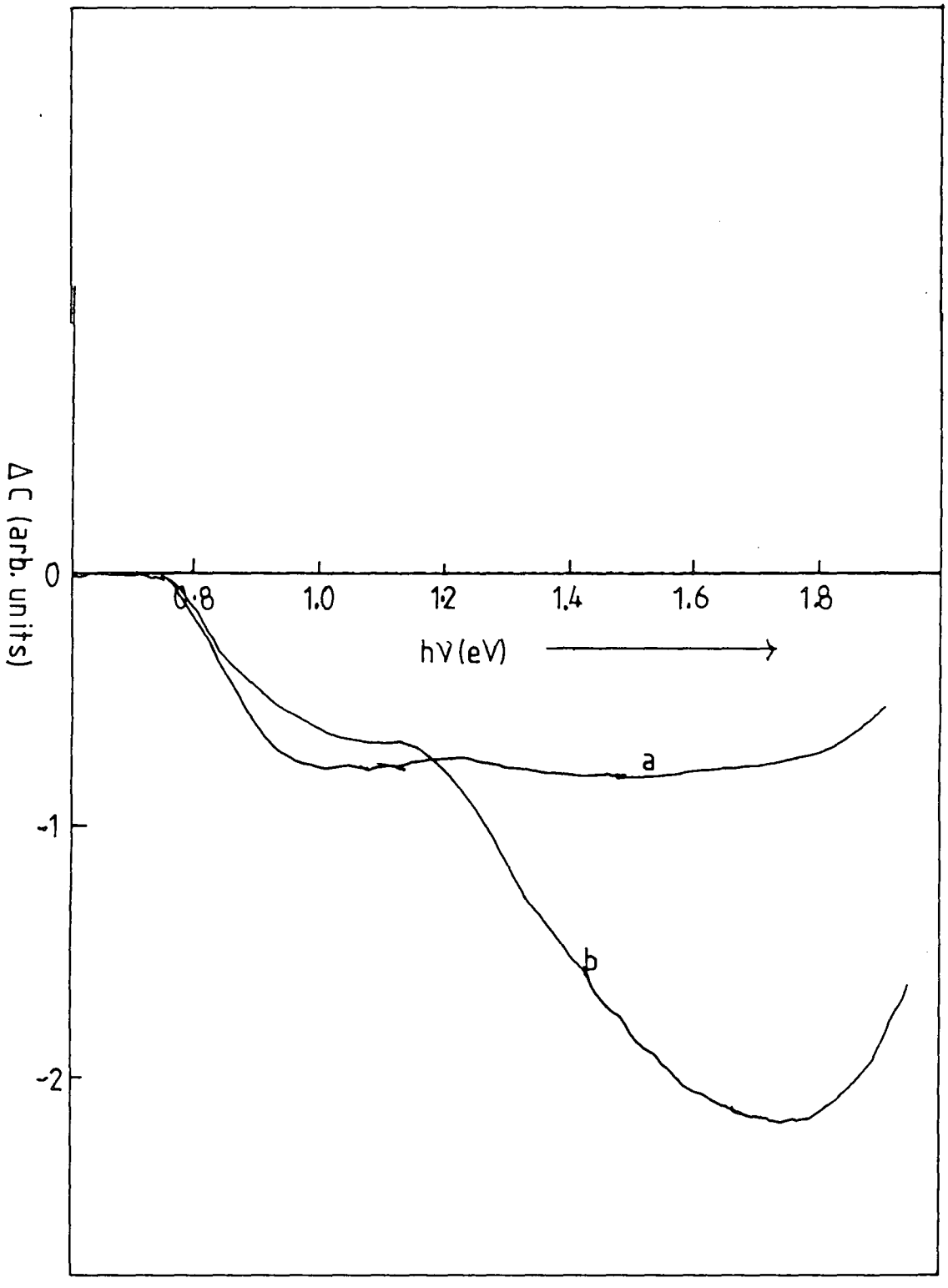

Figure 8.2g. Infra-red quenching of photocapacitance spectra of as-grown $Zn_{.22}Cd_{.78}S$ at a) 300K and b) 90K.

x=0.1 and 0.22 but no measurements were possible on the diode with x=0.4, because of the long time needed to reach equilibrium.

8.3.2 $Zn_xCd_{1-x}S$ deliberately doped with copper.

The PHCAP spectra for a diode on a copper doped Au-$Zn_xCd_{1-x}S$ sample with x=0.1 measured at 300K and 90K are shown in figure 8.2h. At 300K, a sudden decrease in PHCAP was observed at a photon energy of 0.75eV with another small dip at about 1.15eV. As the photon energy increased, a positive going PHCAP was observed at 1.4eV. A second positive going threshold at $h\nu$=2.35eV suggests the presence of a level at about 0.12eV above the valence band (E_g=2.65eV at 300K). In the 90K spectrum a small increase in PHCAP was observed at the relatively low energy of $h\nu$=0.95eV. A sudden decrease occurred at $h\nu$=1.0eV. In addition two positive going thresholds at $h\nu$=1.46eV and 2.25eV were also apparent in the same spectrum.

Similar measurements on a diode with a composition of Au-$Zn_{.25}Cd_{.75}S$:Cu, are shown in figure 8.2i. The spectrum measured at 300K shows two negative thresholds at 0.78eV and 1.18eV, and a positive going one at $h\nu$=1.4eV. In the same spectrum, the decrease in PHCAP at $h\nu$=2.1eV indicates a donor level at 0.65eV while the increase in PHCAP at 2.4eV suggests an acceptor at 0.35eV. At 90K, three positive going thresholds were apparent at $h\nu$=1.08eV,

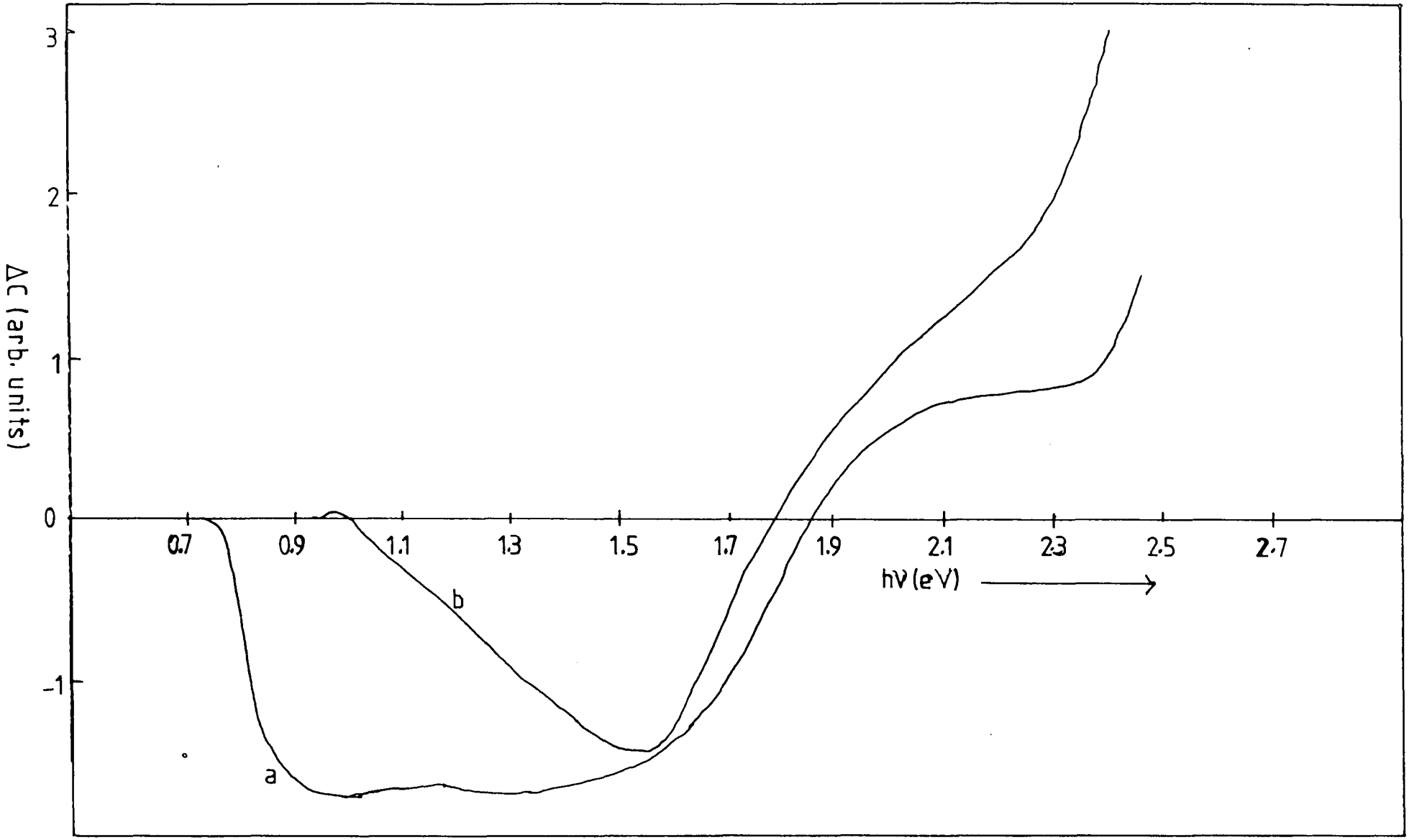

Figure 8.2h. Photocapacitance spectra of copper doped $Zn_{.1}Cd_{.9}S$ at a) 300K and b) 90K.

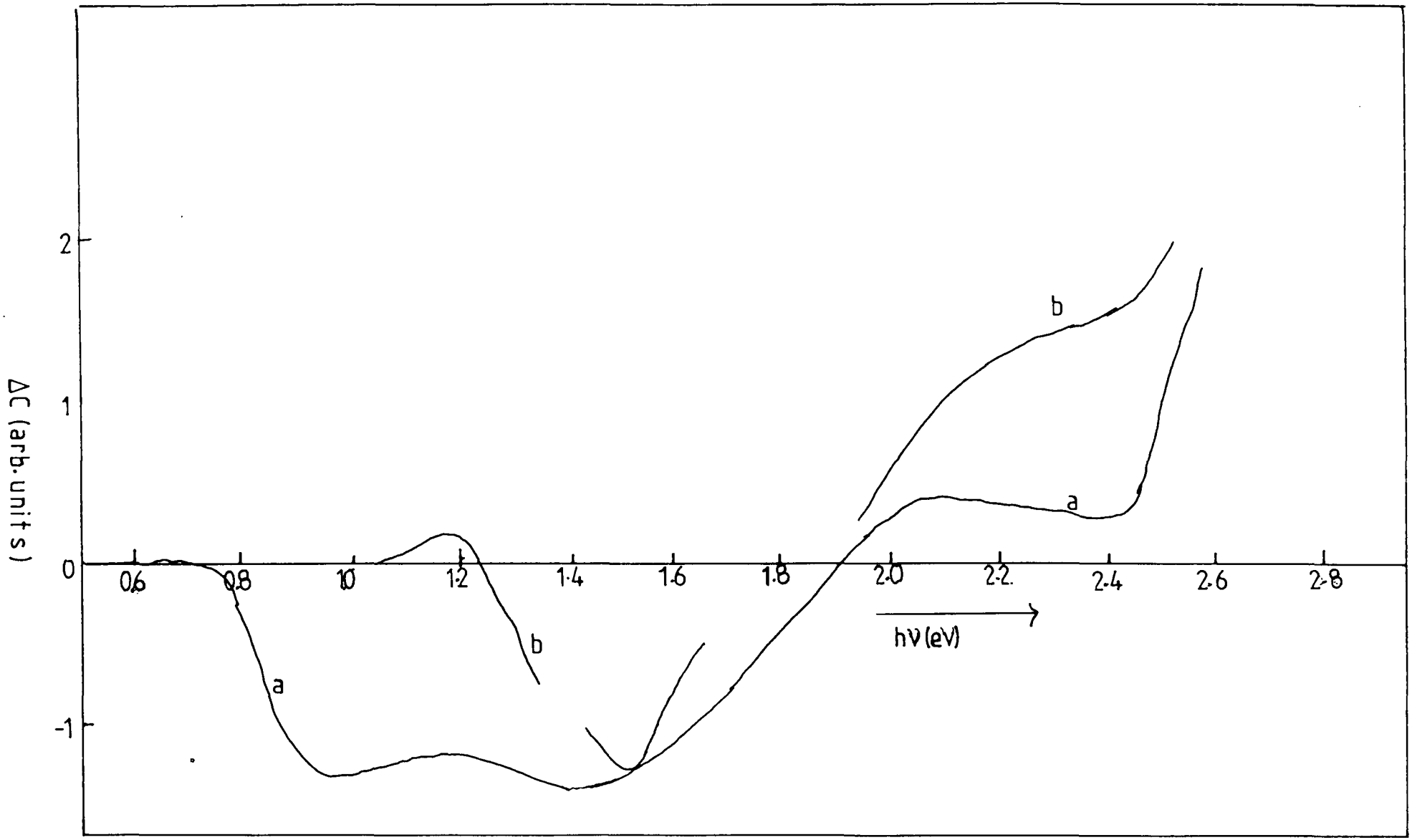

Figure 8.2i. Photocapacitance spectra of copper doped $Zn_{.25}Cd_{.75}S$ at a) 300K and b) 90K.

1.52eV and 2.45eV corresponding to levels at 1.08eV, 1.33eV and 0.4eV below the conduction band. The negative threshold at $h\nu$=1.18eV indicates the presence of an acceptor level at 1.18eV.

For the diode with the composition Au-$Zn_{.4}Cd_{.6}S$:Cu, the 300K spectrum (figure 8.2j) also shows a decrease in PHCAP at $h\nu$=0.75eV. The positive going threshold at $h\nu$=1.75eV indicates the presence of a level at 1.19eV below the conduction band. There is also a sharp decrease in this spectrum at $h\nu$=2.75eV and a positive going threshold at $h\nu$=2.88eV corresponding to a donor level at 0.19eV and an acceptor at 0.06eV (E_g=2.94eV for x=0.4 at 300K).

In the low temperature spectrum (figure 8.2j), positive going thresholds were observed at $h\nu$=1.1eV and 1.58eV corresponding to levels at 1.1eV and 1.46eV below the conduction band. The negative going threshold at $h\nu$=1.22eV can be associated with a level at 1.22eV above the valence band (E_g at 90K = 3.04eV).

IRQPHCAP spectra of copper doped Schottkys on $Zn_xCd_{1-x}S$ for x=0.1 and 0.25 are shown in figures 8.2k and 8.2l respectively. Both spectra have two negative thresholds at about 0.75eV and 1.17eV at both 300K and 90K. For diodes with samples x=0.4, only the 300K spectrum could be measured. It also shows two negative thresholds at 0.75 and 1.2eV.

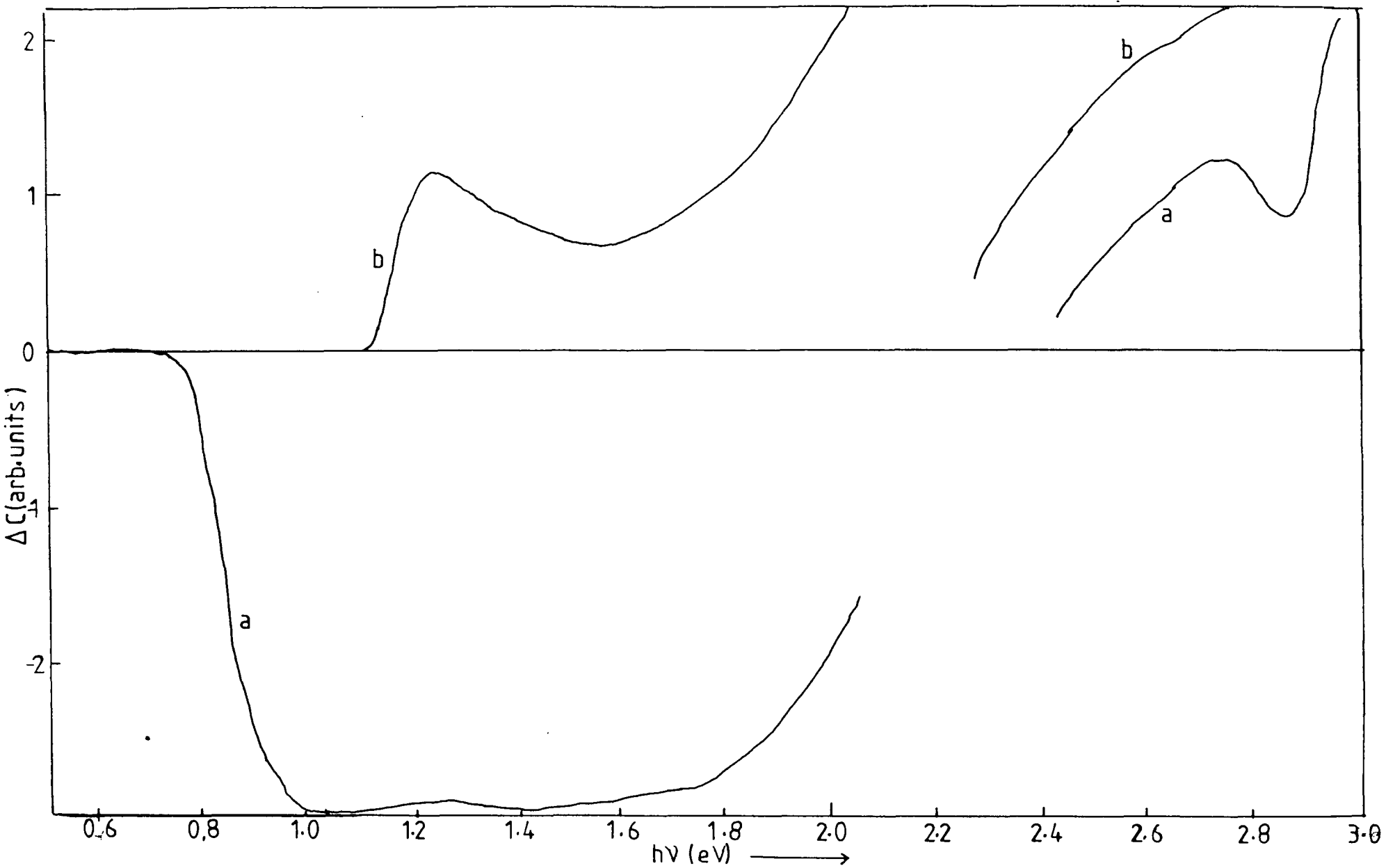

Figure 8.2j. Photocapacitance spectra of copper doped $Zn_{0.4}Cd_{0.6}S$ at a) 300K and b) 90K.

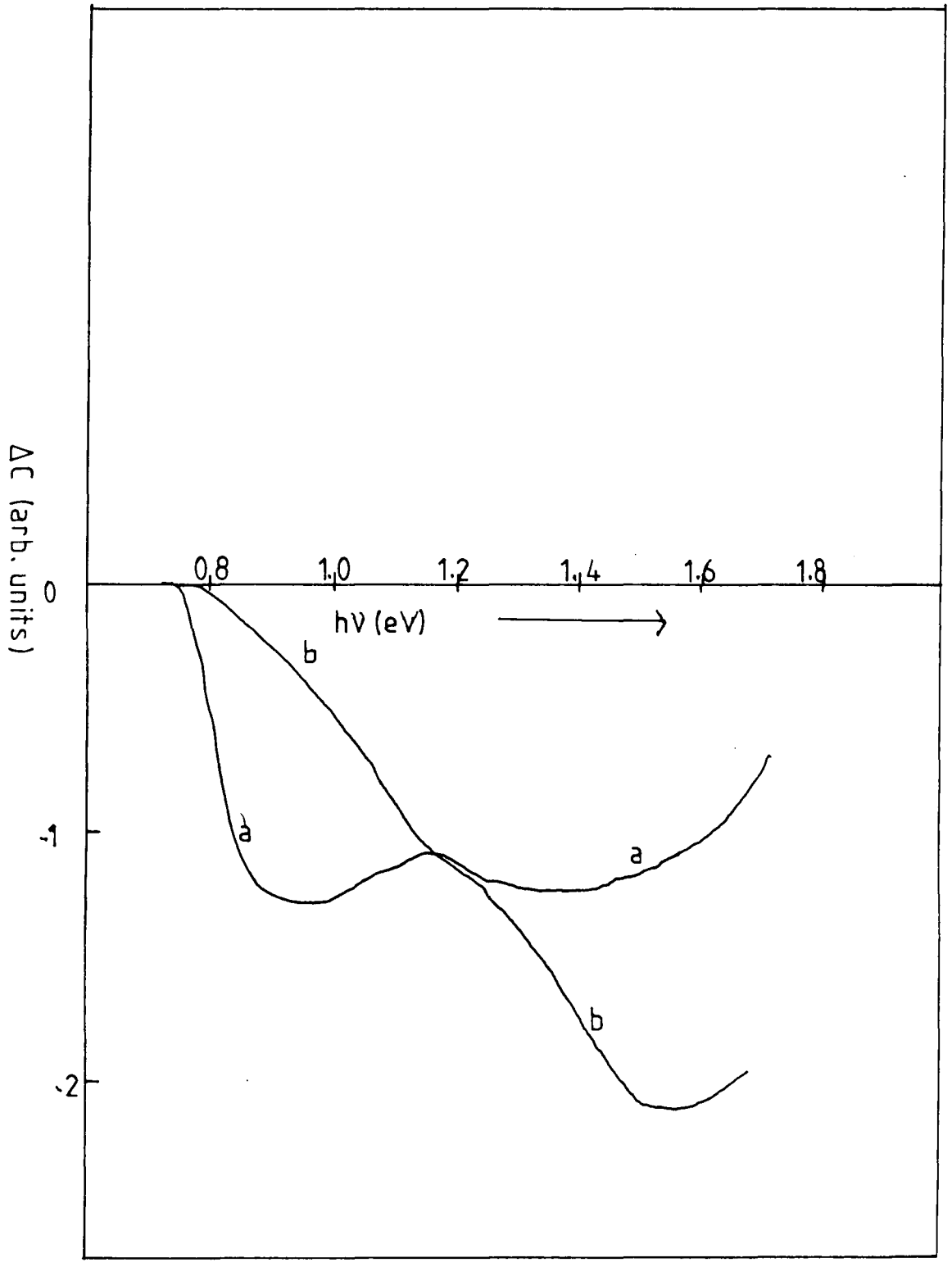

Figure 8.2k. Infra-red quenching of photocapacitance spectra of $Zn_{.1}Cd_{.9}S$:Cu at a) 300K b) 90K.

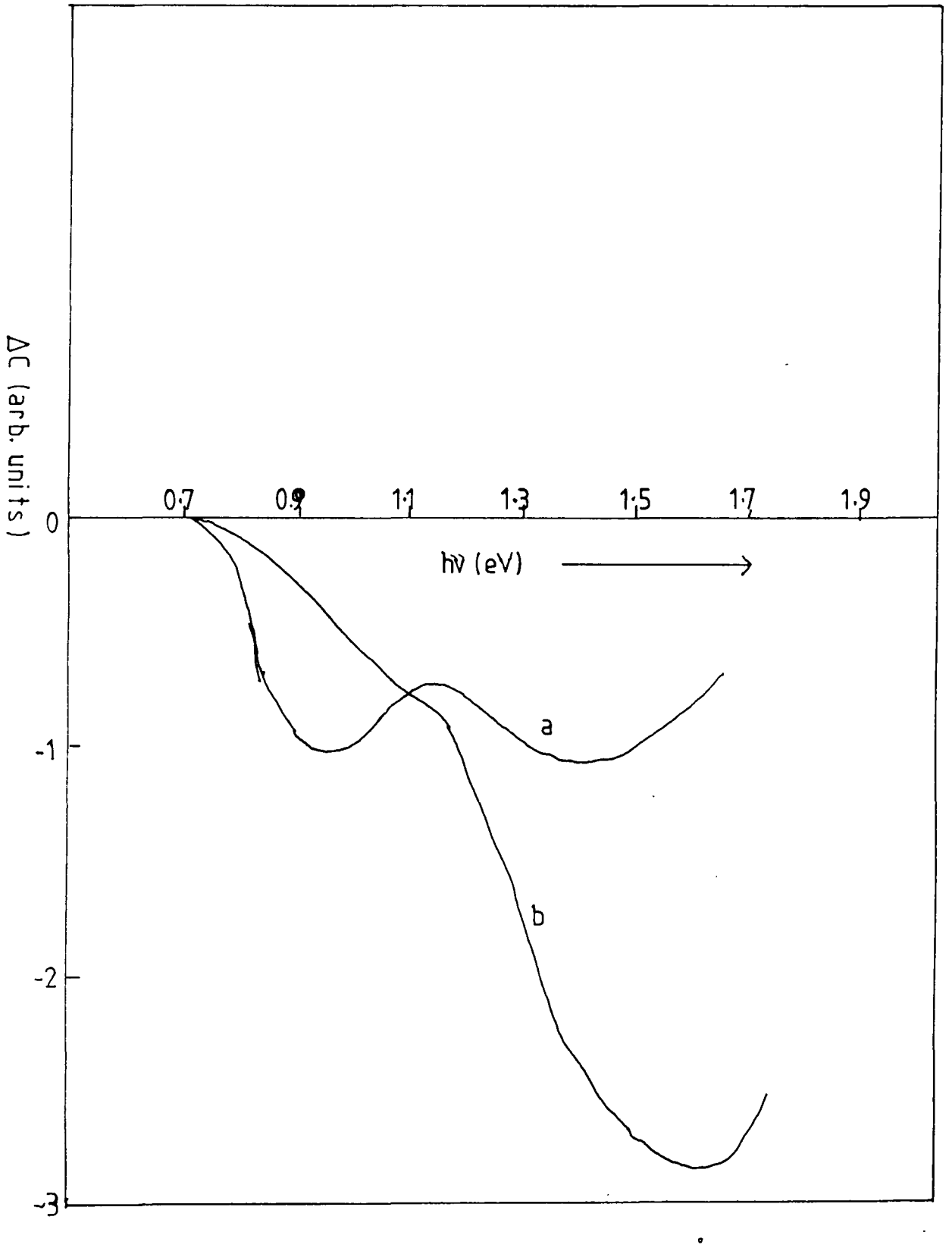

Figure 8.21. Infra-red quenching of photocapacitance spectra of $Zn_{.25}Cd_{.75}S$:Cu at a) 300K b) 90K.

The summary of thresholds obtained is contained in table 8.2 and 8.3.

Discussion

Little work has been done on the detection of deep levels in $Zn_xCd_{1-x}S$ crystals apart from earlier work in Durham using capacitance techniques such as DLTS and photocapacitance (10,11), and the determination of electron and hole traps in $Zn_xCd_{1-x}S$ crystals grown by iodine transport technique using thermally stimulated conductivity and optical quenching of photoconductivity reported by Davis and Lind (12). In general, the results obtained in the present study agree with those reported in the previous work (10,11,12).

The existence of deep electron or hole traps in a material, will up to a point, have undesirable effects on the performance of any device which may be fabricated on it. The present work has revealed that a deep level is situated at about 1.4-1.5eV below the conduction band in $Zn_xCd_{1-x}S$ for all x. This was clearly demonstrated in the crystals grown by the Piper-Polich method and in the copper doped samples. The level was pinned to the conduction band. It follows from this conclusion, that the position of this level is close to that of the copper centre as is well established in CdS, i.e. for x=0. With increasing x the centre moves to the upper half of the band gap and for

x	Measurements	Thresholds (eV)
0.05(a)	PHCAP 90K	+1.5(A) +2.5
0.22(a)	PHCAP 90K	-0.72, -1.15(B) +1.75, +2.72
0.3(a)	PHCAP 90K	-0.75, -1.2(B) +2.1, +2.65, +2.42
0.1(b)	PHCAP 300K	-0.75, -1.15(B) +1.4,-2.32, +2.42
	PHCAP 90K	-1.18, +1.58, +2.56 +2.42
	IRQPHCAP 300K	-0.75, -1.15(B)
	IRQPHCAP 90K	-0.75, -1.15(B)
0.22(b)	PHCAP 300K	-0.75, +1.65
	PHCAP 90K	-1.2, +1.15(B)
	IRQPHCAP 300K	-0.75, -1.15(B)
	IRQPHCAP 90K	-0.75, -1.15(B)
0.4(b)	PHCAP 300K	-0.75, -1.2(B) +1.9, -2.75
	PHCAP 90K	+0.65, +1.4(A) +2.05, +2.2 +2.6, +2.95
	IRQPHCAP 300K	-0.75, -1.2(B)
0.43(b)	PHCAP 300K	-0.75, +1.8
	PHCAP 90K	+0.85, -1.35, +1.42(A) -1.85 +2.05, -2.32
	IRQPHCAP 300K	-0.75, -1.2(B)

Table 8.2. Thresholds obtained from $Zn_xCd_{1-x}S$ crystals, a) Clark-Woods and b) Piper-Polich.

x	Measurements	Thresholds(eV)
0.1	PHCAP 300K	-0.75, -1.15, +1.4(A),+2.35
	PHCAP 90K	-1.0, +1.46(A) +2.25
	IRQPHCAP 300K	-0.75, -1.15(B)
	IRQPHCAP 90K	-0.75, -1.17(B)
0.25	PHCAP 300K	-0.78, -1.18, +1.4(A), -2.1 +2.42
	PHCAP 90K	+1.08, -1.18(B),+1.52(A),+2.45
	IRQPHCAP 300K	-0.75, -1.15(B)
	IRQPHCAP 90K	-0.75, -1.15(B)
0.4(b)	PHCAP 300K	-0.75, -1.28, +1.75, -2.75 +2.88
	PHCAP 90K	+1.1, -1.22, +1.46(A)
	IRQPHCAP 300K	-0.75, -1.2(B)

Table 8.3. Thresholds obtained from copper doped $Zn_xCd_{1-x}S$ crystals

a value of x of about 0.3 its position is exactly at the centre of the gap. For x<0.3 its position is near to the middle of the gap but in the lower half. This centre may well act as a recombination centre and could be responsible for the reduction in the short circuit current in Cu_2S-$Zn_xCd_{1-x}S$ photovoltaic heterojunctions even though the lattices and electron affinities of Cu_2S and $Zn_xCd_{1-x}S$ are well matched at about x=0.2 (21,22). The diagram in figure 8.2m shows how the position of the centre in the band gap varies with composition. The valence band is shown as remaining fixed in energy, since according to the ionic picture, a variation in composition of the host material from CdS to ZnS causes a variation in the conduction band position which is associated with the cation.

The deep donor observed in copper doped samples at 90K (0.95eV-x=0.1, 1.08eV-x=0.25 and 1.1eV-x=0.4) may well be another copper related centre since no such donor was observed in undoped samples.

The presence of an acceptor centre at about 1.1-1.2eV above the valence band was the dominant feature of spectra measured at 300 and 90K in copper doped devices. The energy level of this acceptor was pinned to the valence band, and in agreement with the work of Claybourn (10) and Davis and Lind (12) can be attributed directly to the copper centre. According to Kullendorf et al (13), the copper states in CdS_ySe_{1-y} are composition dependent. The

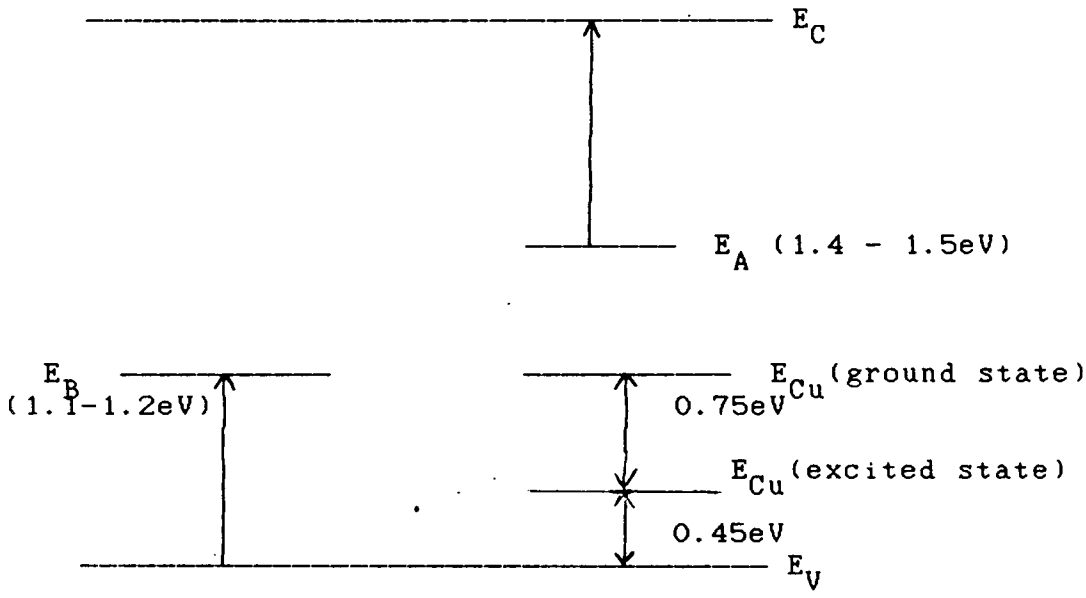

Figure 8.21-a Summary of major levels found in $Zn_xCd_{1-x}S$

x	energy (eV)
0	0.17(VB) 0.95(CB) 1.0(VB) 0.47(CB)
0.05	0.10(VB)
0.1	0.12(VB) 0.95(CB) 0.23(CB)
0.22	1.05(VB)
0.25	0.35(VB) 0.65(CB) 0.4(CB)
0.3	0.26(VB)
0.4	0.13(VB) 0.49(VB) 0.88(VB) 1.03(VB) 1.11(CB) 0.65(CB) 0.19(CB)
0.43	1.03(VB) 1.35(VB) 1.23(CB) 0.85(CB) 0.76(CB)
1	1.35(CB) 0.85(CB) 0.65(CB) 0.35(CB)

Figure 8.21-b Summary of other levels found in $Zn_xCd_{1-x}S$
(CB indicates that the energy is measured from conduction band and VB from valence band)

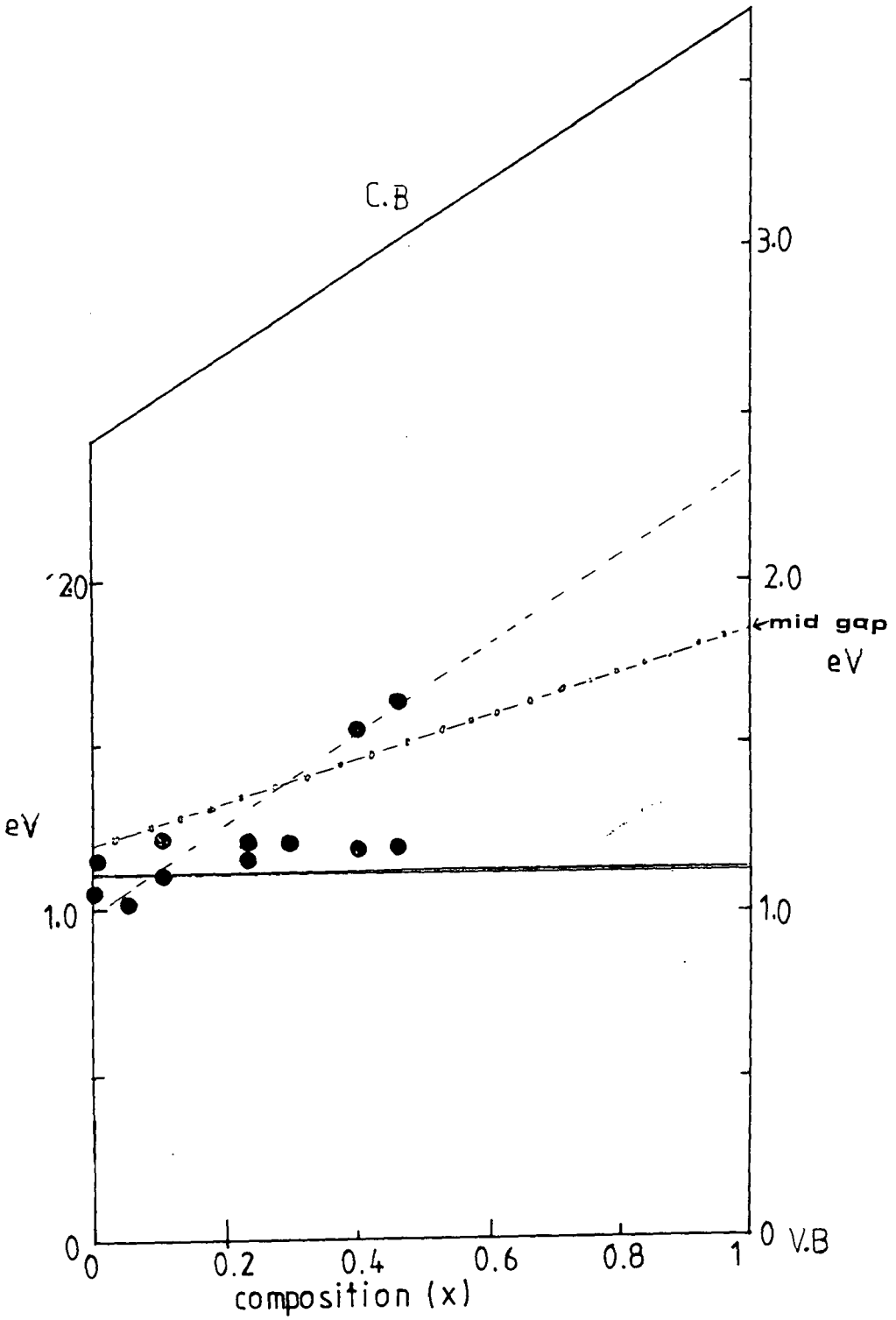

Figure 8.2m. The position of 1.1-1.2eV (——) level above the valence band and 1.4-1.5eV (- - -) level below the conduction band.

shift in the position of the energy level relative to the valence band as the Se content is increased was explained in terms of the symmetry of the defect site. Assuming the defect is a substitutional impurity on the metal site (3), then it is surrounded tetrahedrally by S as well as Se nearest neighbours. Depending on the distribution, the impurity may have T_d symmetry (4S or 4Se), C_{3v} symmetry (3S and 1Se or 1S and 3Se) or C_{2v} symmetry (2S and 2Se). This change in symmetry will affect the degree of crystal field splitting. The replacement of S with Se causes an additional perturbation that alters the covalent bonding between the impurity and its nearest neighbours. This change in the configuration of defect sites would result in a change in activation energy of the copper acceptor states. On the other hand, the replacement of Cd with Zn in $Zn_xCd_{1-x}S$ causes little change in crystal field splitting, and this can also be explained in terms of the symmetry of the defect site. In this case the defect (Cu) is surrounded by sulfur atoms (i.e the nearest neighbours) and not much change in energy position is then expected.

The threshold observed at 0.72-0.78eV at 300K which disappeared when the temperature was reduced to 90K can also be explained as similar to the copper excited hole state found in CdS as discussed previously (CdS section). However the threshold found at 0.72-0.78eV from PHCAP measurements at 90K and also from IRQPHCAP at 90K cannot be explained in the same way. This might be due to another

acceptor at 0.72-0.78eV above the valence band. Measurements on CdS using the DLOS technique (10) also suggest the appearence of such a centre. If this is correct, this centre may also exist in $Zn_xCd_{1-x}S$ and its appearance very much depends on the history of the crystal itself.

It is important to note that the presence of the 1.1-1.2eV centre is more pronounced in as-grown Piper-Polich crystals compared with Clark-Woods crystals. The reason for this is that the Piper-Polich crystals were grown at a much higher temperature and therefore, were more susceptible to accidental contamination with copper.

8.4 ZnS

Polycrystalline ZnS, produced by chemical vapour deposition from zinc vapour and H_2S, was first cut into 4x4x2 mm^3 dice before being etched and heated in Zn + 1%Ga + 0.5%Al at 850^oC for twelve hours to reduce its resistivity (14). The resistivity obtained for these particular dice was about 10^3 ohm-cm. Figure 8.3a shows PHCAP spectra for a Schottky diode on such a dice measured at 300K and 90K. In the 300K spectrum, a positive going threshold at a photon energy of 1.35eV indicated the presence of a donor-like level at 1.35eV below the conduction band. As the photon energy increased another positive going step was observed at about 2.55eV

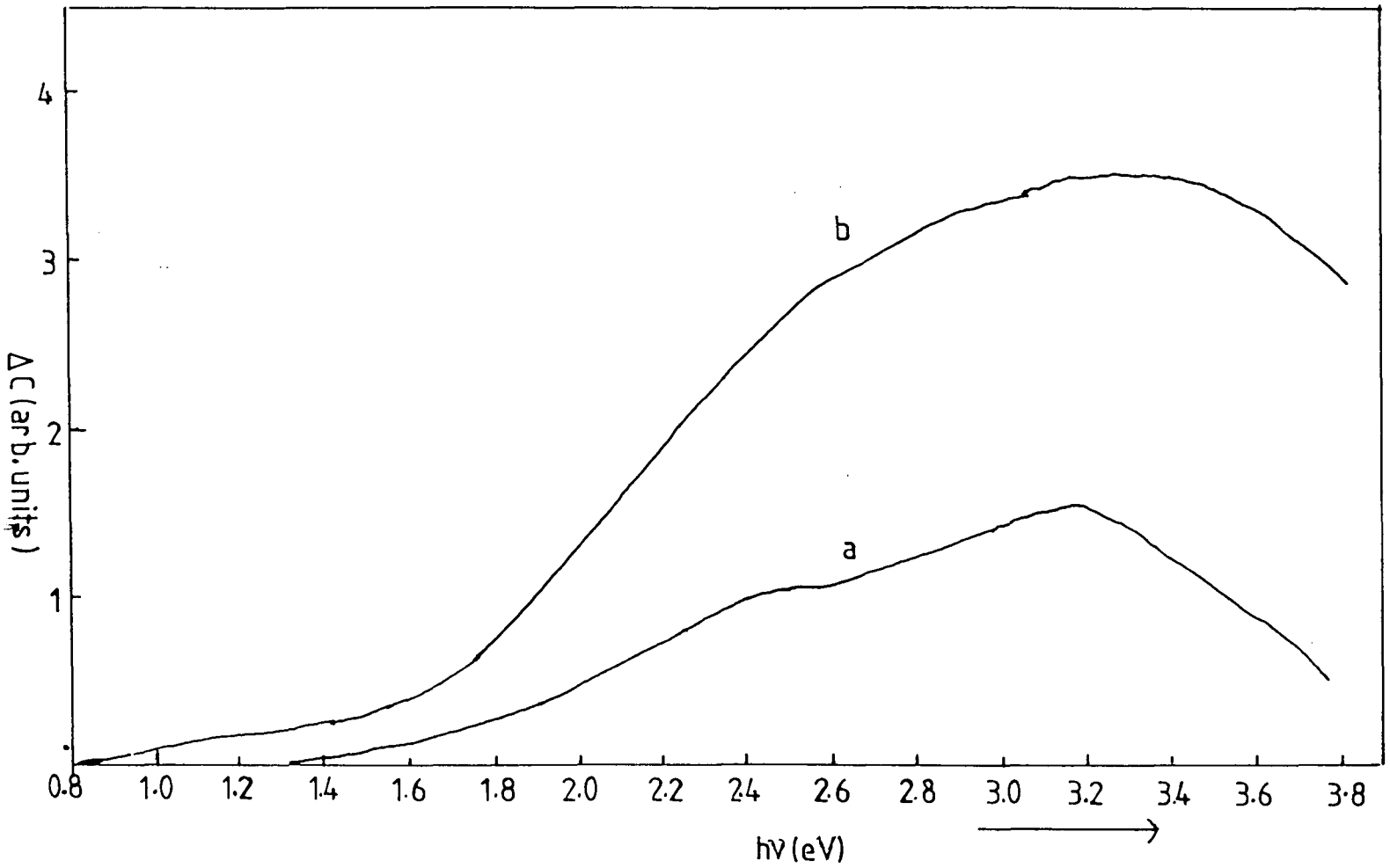

Figure 8.3. Photocapacitance spectra of ZnS: 1%Ga +0.5%Al

a) 300K and b) 90K.

implying that there was a possible acceptor level at about 1.17eV above the valence band. It was estimated that the band gap is 3.72eV at 300K. The sudden decrease in PHCAP at 3.2eV suggests the presence of another donor level at 0.52eV below the conducton band.

In the low temperature spectrum, the first threshold was observed at a lower energy than in the 300K spectrum, i.e. at 0.85eV, indicating the presence of a donor level at 0.85eV below the conduction band. Another positive going threshold at a photon energy of about 1.5eV suggests that there an is emptying proceses of a level at 1.5eV below the conduction band. Finally the decrease in PHCAP at about 3.45eV suggests the presence of another donor level at 0.37eV (E_g at 90K ~3.82eV).

IRQPHCAP was also carried out but no quenching was observed at either temperature.

Thresholds observed are shown in table 8.4

Discussion

The difficulties of producing low resisitivity ZnS make the detection of defect centres using space charge methods (i.e. exploiting the junction capacitance) rather limited. However some work on low resistivity ZnS based on photoluminescence has been reported (14,15). The

	Measurement	Thresholds (eV)
ZnS (C.V.D) Zn+1%Ga +0.5%Al	PHCAP 300K	+1.35, +2.5, -3.2
	PHCAP 90K	+0.85, +1.5(A),-3.45,

Table 8.4: Thresholds obtained from PHCAP measurement

production of low resistivity ZnS in a reproducible manner is also required for the fabrication of devices such as L.E.Ds. so that the emission can be extended to the blue. A series of experiments with the different types of crystal used in this laboratory shows that the production of low resistive ZnS is a complex problem (16). This is in contrast with the published work of Oda and Kukimoto (17) and Kukimoto et al (18) who claimed to reduce the resistivity of ZnS to the region of 10 ohm-cm with no particular difficulty.

In this study, photocapacitance measurements were made at 300K and 90K in an attempt to characterise any form of defect centre present. The existence of a donor at 0.53eV has already been reported by Claybourn (10) using the DLTS technique, this was found in the temperature range from 200-230K. This is almost certainly the same centre found in the present work at 0.52eV. Claybourn (10) also found as many as four other levels at 1.25, 1.37, 1.89 and 2.19eV below the conduction band edge by using the DLOS technique, and another trap at 0.25eV by DLTS. Of these only the 1.35eV donor-like level below the conduction band coincides with those reported by Claybourn.

The existence of a level 1.1-1.2eV above the valence band, has been widely reported (6,19) as associated with the so called sentising centre in ZnS. However it is well known that copper is a residual contiminant in ZnS and

also introduces deep acceptors in ZnS at about 1.2eV above the valence band (20). Indeed it is difficult to distinguish between these two centres. Unfortunately no infra-red quenching was observed to confirm the energy of this centre. Investigations in our laboratory (16) showed that unintentional incorporation of copper impurity is a major contributory factor to the difficulty of preparing low resistivity ZnS. Using the same treatment of heating in molten zinc plus gallium, Thomas et al (14) found two blue emission bands with energies 2.588 and 2.522eV but no corresponding centres have been revealed here.

8.5 **Conclusions**

Steady state PHCAP and IRQPHCAP measurements have been used to characterise the defect centres in undoped $Zn_xCd_{1-x}S$ crystals grown by two different methods. Intentionally copper doped samples have also been examined. The presence of an acceptor centre at about 1.1-1.2eV above the valence band in all samples is due to copper. The level is pinned to the valence band and is composition independent. The excited hole state of this centre at 0.45eV above the valence band has also been observed. The presence of a centre at about 1.4-1.5eV below the conduction band through-out the composition which acts as a recombination centre may be the main reason for the reduction of the short circuit current in Cu_2S-$Zn_xCd_{1-x}S$ solar cells.

References for chapter VIII

1) P.C.Pande, **PhD Thesis**, Durham University 1984

2) P.C.Pande, G.J.Russell and J.Woods, J. Phys. D: Appl. Phys., **16** (1983) 2307

3) H.G.Grimmeiss, N.Kullendorff and R.Brosser, J. Appl. Phys., **52** (1981) 3405

4) T.Suda and R.H.Bube, J. Appl. Phys., **52** (1981) 6281

5) F.Poulin, A.W.Brinkman and J.Woods, J. Cryst. Growth, **59** (1982) 240

6) S.O.Hemila and R.H.Bube, J. Appl. Phys., J. Appl. Phys. **38** (1967) 5258

7) R.H.Bube, Phys. Rev., **99** (1955) 1105

8) A.A.Qidwai and J.Woods, J. Cryst. Growth, **59** (1982), 217

9) S.G.Patil, J. Phys. D: Appl. Phys., **5** (1972) 1692

10) M.Claybourn, **PhD Thesis**, Durham Univewrsity 1986

11) P.C.Pande, M.Claybourn, G.J.Russell, A.W.Brinkman and J.Woods, J. Cryst. Growth, 72 (1985) 174

12) E.A.Davis and E.L.Lind, J. Phys. Chem. Sol., **29** (1968) 79

13) N.Kullendorf, L.Samuelson and G.Grossman, J. Phys. C: Solid State, **17** (1984) 5055

14) A.E.Thomas, G.J.Russell and J.Woods, J. Phys. C: Solid State, **17** (1984) 6219

15) T.Taguchi and T.Yokogawa, J. Phys. D: Appl. Phys., **17** (1984) 1067

16) A.E.Thomas, G.J.Russell and J.Woods, J. Cryst. Growth, **63** (1983) 265

17) S.Oda and H.Kukimoto, IEEE Trans. Elec. Dev., **ED-24** (1977) 956

18) H.Kukimoto, S.Oda and H.Katayama, J. Lumin., **18/19** (1979)

19) G.H.Blount, A.C.Saunderson and R.H.Bube, J. Appl. Phys., **38** (1967) 4409

20) S.S.Devlin in **Physics and Chemistry of II-VI compounds**, edited by M.Aven and J.S.Prener (Wiley, New York 1967)

21) S.Martinuzzi, J.Qualid, D.Sarti and J.Gervais, Thin Solid Films, **51** (1978) 211

22) S.Oktik, G.J.Russell and J.Woods, Solar Cells, 5 (1982) 231

CHAPTER IX

SUMMARY AND CONCLUSIONS

The aim of the work reported in this thesis was to characterise the properties of the crystals of $Zn_xCd_{1-x}S$ grown in this department. Two types of crystals were examined and grown by a) The Clark-Woods and b) The Piper-Polich methods.

Since some of the crystals were not uniform, a non-destructive method of measuring the composition is required. This was done simply by measuring the EDAX spectrum. Before the results could be interpreted the calibration curve had to be established by measuring the composition by the destructive method of Atomic Absorption Spectroscopy (AAS) and then comparing with EDAX. The ratio of the characteristic intensities from EDAX (I_{Zn}/I_{Cd}) plotted against the composition ratio (C_{ZnS}/C_{CdS}) showed that a good linear relationship was followed. The hexagonal structure was found for all crystals with composition up to x=0.85, and Vegard's law was also followed. On the other hand the ZnS crystals were found to exhibit cubic structure. Band gaps measured from the high peak region in the spectral dependence of short circuit photocurrent showed a nearly linear variation with composition for $0<x<0.5$.

Measurements of the electrical conductivity and Hall coefficient were also carried out as a function of temperature (100-300K). The difficulties in preparing uniform bars (8x2x1 mm^3) or clover-leaf samples (1 mm thick and ~10 mm diameter) formed the main obstacles to these measurements. At room temperature, conductivities as high as 10^{-3} $ohm^{-1}cm^{-1}$ could still be obtained at x~0.5. Carrier concentrations calculated from Hall coefficient measurements and from plots of C^{-2} versus V_r on Schottky diodes followed the same trend reaching a maximum at about x~0.05-0.1. Beyond this point, the carrier concentration decreased with x. For x<0.2, the Hall mobility was of the same order as for CdS (x=0) and limited by polar optical and piezoelectric scattering processes. In the range 0.2<x<0.3, the Hall mobility decreased dramatically by two orders of magnitude. Low values of mobility and the trend for the mobility to increase with temperature suggests that ionised impurity scattering is a dominant process in controlling the mobility. Scattering due to localised space charge might be also important in our crystals since region of non-uniformity could exist after growth.

The properties of Au-$Zn_xCd_{1-x}S$ Schottky diodes prepared on chemically etched surfaces were also examined. Parameters calculated depended to some extent on the resistivity of the individual samples. The barrier heights measured by the photoelectric method increased quite

linearly with x, while the barrier heights determined from I-V and C-V plots were dependent on the nature of the barrier and the presence of thin interfacial layers.

The Photocapacitance studies of as-grown and intentionally copper doped samples, showed that the centre at about 1.1-1.2eV above the valence band could be attributed to the copper deliberately added to the samples and obviously present as a contaminant in crystals grown by the Piper-Polich technique. A deep centre at about 1.4-1.5eV below the conduction band was thought to exist in mixed crystals for all x, pinned to the conduction band, but the presence of this centre was dependent on the growth method and the condition or treatments performed on the crystals. This centre which is situated almost at the middle of the gap for $x<0.3$ may act as a recombination centre and might be responsible for reducing the short circuit current in Cu_2S-$Zn_xCd_{1-x}S$ photovoltaic cells even when the matching of electron affinities and lattice parameters between the two limbs of the heterojunction was minimised at about $x\tilde{}0.2$.